Université de Toulouse

THÈSE

En vue de l'obtention du

DOCTORAT DE L'UNIVERSITÉ DE TOULOUSE

Délivré par *l'Université Toulouse III - Paul Sabatier*
Discipline ou spécialité : *Chimie Macromoléculaire et Supramoléculaire*

Présentée et soutenue par

Etienne GIRARD

Le *29 novembre 2012*

Titre :

Macromolecular engineering of CO2-philic (co)polymers through RAFT/MADIX polymerization

---

JURY

Dr. Cyril AYMONIER, Université de Bordeaux 1, examinateur
Pr. Steve HOWDLE, Université de Nottingham, rapporteur
Dr. Jean-François LUTZ, Université de Strasbourg, rapporteur
Pr. Rinaldo POLI, Université de Toulouse, président du jury
Dr. Bruno AMEDURI, Université de Montpellier, invité
Dr. Thierry TASSAING, Université de Bordeaux 1, invité

Ecole doctorale : *Sciences de la Matière*
Unité de recherche :
Laboratoire d'Hétérochimie Fondamentale et Appliquée (UMR 5069)
Laboratoire des Interactions Moléculaires, Réactivité Chimique et Photochimique (UMR 5623)
Directeur(s) de Thèse : *Pr. Mathias DESTARAC & Dr. Jean-Daniel MARTY*
Rapporteurs : *Pr. Steve HOWDLE & Dr. Jean-François LUTZ*

Remerciements

Il y a à peine 5 ans de cela, je n'aurais pas imaginé un jour faire une thèse. Si je ne regrette absolument pas aujourd'hui d'avoir fait les choix qui m'ont amené jusqu'ici, le chemin pour y arriver a parfois été sinueux ! Ce travail est donc quelque part le fruit des gens que j'ai pu rencontrer lors de ces 5 ans et qui ont contribué en tant qu'ami, collègue ou encadrant à cette tranche de vie qu'est la thèse. Ces quelques lignes sont l'expression de ma reconnaissance envers vous tous.

En premier lieu, je voudrais remercier Steve Howdle et Jean-François Lutz d'avoir rapporté mon manuscrit, ainsi que Cyril Aymonier et Rinaldo Poli pour leur participation à mon jury de thèse. Réunir un tel panel d'experts fait certainement partie des réussites de ma thèse !

Je ne garde que de très bons souvenirs de ma thèse et je le dois en grande partie à mon couple de directeurs de thèse, Mathias et Jean-Daniel. En plus d'être des gens biens et détendus, j'ai apprécié plus que tout votre pédagogie, votre exigence scientifique et l'autonomie que vous m'avez laissée pendant ces trois ans. Merci également de m'avoir fait confiance en me confiant ce sujet qui partait de zéro, j'espère vous avoir rendu en partie tout ce que vous m'avez apporté. Vous avez fait de moi un thésard épanoui ! J'aimerais également y associer Patrice Castignolles et Bob Gilbert, qui, à leur époque, ont certainement fait germer en moi l'idée de faire une thèse.

Cette thèse n'aurait pas existé et avancé sans de nombreuses collaborations. Rétrospectivement, je me dis qu'il aurait été peut-être plus malin de demander un financement pour une caravane. Par ordre chronologique, je voudrais d'abord remercier Thierry Tassaing, Stéphanie et Mathilde qui m'ont accueilli à de très nombreuses reprises à Bordeaux. Merci Thierry pour ta disponibilité et les discussions sur la spectroscopie infrarouge, les émulsions et j'en passe !

Un grand merci également à Bruno Ameduri et à son enthousiasme constant, ainsi qu'à son équipe, Guillaume, Yogesh, Nour et Ali qui m'ont mis le pied à l'étrier lors de mes séjours à Montpellier. Merci aussi à Séverine Camy et Jean-Stéphane Condoret pour m'avoir fait profiter de leur installation supercritique au Laboratoire de Génie Chimique, à l'origine de nombreux résultats !

Même si nous n'avons pas directement travaillé ensemble, la réalisation de cette thèse aurait été plus difficile sans la participation des collègues du LHFA et des IMRCP. Je voudrais donc remercier tous les membres de mes 2 équipes d'accueil, PRIAM et IDeAS, pour

l'ambiance de travail et l'entraide quotidienne. Ce fut toujours un grand plaisir de venir au travail, surtout lorsque l'on y vient pour travailler et pour rigoler. Côté LHFA, merci Stéphane, Olivier, Guillaume, Mariana, Aymeric, Aurélie, Aymeric, Manue, Dimitri, Issam, Roland et tous les autres pour les coups de main et tous ces bons moments ! Bon courage à Xuan et Jean-Noël qui reprennent le flambeau du CO_2 ! Côté IMRCP, merci à Christophe(s), Anne-Françoise, Stéphane(s), Juliette, Nancy, Monique, Fabienne, Sar, Sheila, Hanh, Camille, Ophélie, Marion, et tous les autres de s'être intéressé à la RAFT malgré eux et de m'avoir montré autre chose que la chimie des polymères !

Un grand merci à toutes les personnes qui rendent possible le bon fonctionnement du laboratoire et des appareils, les secrétaires toujours disponibles pour les missions de dernière minute, Maryse, Sérah, Nadia, Sandrine, les techniciens et ingénieurs toujours prêts à dépanner, le grand Olivier Volpato, Olivier TDB, Pascale et les personnels techniques de l'Institut de Chimie.

A vrai dire, je regrette déjà l'ambiance au top du labo, et je ne pourrais pas citer tous les bons souvenirs de soirée, d'apéros sur la coursive et de rigolade avec les « collègues ». Venir tous les jours au labo pour discuter du match de la veille avec Thibault, Abder, Olivier, Romain, Nico, Yohan ou Fethi, prendre le café avec Aline, Juliette, Fanny et tout le groupe au soleil à midi, ca fait partie de ces petits moments qui font tout. Merci également à toute l'équipe espagnole, Noël, Ricardo et les autres, à Jérôme, Max, Marc, Feriel, Eric, Chris, Pauline, Damien, Nico L., Audric, Hélène, Norio, David, Hoang, Yannick, Florie, Nico D., Nico T., Faouzi, Lisa, Mohamad, Tibor, Lucian et à tous ceux que je peux oublier en écrivant ces lignes. Ce fut toujours un plaisir de vous croiser dans les couloirs !

Merci aussi à tous ceux qui ont rendu ma vie toulousaine en dehors du labo si agréable : mes colocs, Rosanne, Martin et Emma, les copains de sortie, Camille, Max, Nico, Sam, Stéphanie et les multiples gens que j'ai rencontrés à travers vous !

Cette thèse doit aussi énormément à Audrey Pitt qui y a apporté son regard constructif et critique, et qui a contribué plus que l'on ne pourrait l'imaginer à la réalisation de ce travail par son soutien. Enfin, merci profondément à tous ceux qui me suivent depuis très longtemps maintenant, en premier lieu, ma famille et mes cousins, et tous les potes de Caen, Paris, Lyon et autres.

L'histoire ne s'arrêtant pas là, j'espère avoir l'occasion de tous vous recroiser !

Etienne

Table of contents

Introduction

Faced with simultaneous increasing demand and rarefaction of raw materials, chemistry plays a key role in building a sustainable future. In this regard, intensification of existing chemical processes, minimization of reaction waste and removal of toxic or undesirable materials have been identified by both regulators and the chemical industry as crucial points to minimize environmental impact of human activity and limit exposure to hazardous chemicals while preserving economic competitiveness. The Montreal Protocol and the Stewardship Program are successful examples of such efforts that aimed at either banning ozone-depleting chlorofluorocarbon compounds or persistent long-chain fluorinated surfactants. Yet, greater environmental benefits could be obtained by developing new chemical processes and reactions that drastically reduce chemical waste, energy consumption and hazard, economise atoms and promote the use of renewable feedstocks and low-toxicity substances -including solvents, catalysts and so forth. This constitutes the starting points of the so-called "green chemistry" concept that was introduced by Paul T. Anastas and co-workers in 1998.[1]

From academic research to economic profitability, there still exists certain barriers that slow down the implementation of green innovations in industrial contexts. Apart from financial or regulatory aspects, many scientific challenges are yet to be tackled before imposing green chemistry in industrial workshops. These challenges can be classified in three categories:[2]

1. Finding new synthetic pathways that do not imply protecting or blocking groups and possibly use (bio)catalysts. These green reactions should ideally be quantitative and selective.[3-5]

2. Replacing petroleum-based feedstocks by alternative renewable ones. Bio-based products are strong candidates although their massive use in chemical purposes is to compete with food supply. Alternatively, CO_2 is also an advantageous carbon source to produce basic chemicals. While being extremely thermodynamically stable, recent advances in activation of small molecules have rendered CO_2 a promising pathway to replace traditional carbon sources.[6]

3. Promoting new environmentally acceptable solvents to replace harmful and volatile organic solvents used in chemical synthesis, coatings, inks or adhesives. These green solvents include mostly:

    i. Water (in liquid or supercritical state).
    ii. Ionic liquids that advantageously possess low saturating vapor pressure but the preparation of which require multiple steps.[5,7] In this regard, the use of deep eutectic solvents could be advantageous as they are similar to ionic liquids but readily available from a single reaction. [8]
    iii. Low-waste and energy-saving organic solvents (*e.g.* 2-methyltetrahydrofuran, glycerol, ethyl lactate, methanol, ethanol).[7,9]
    iv. Switchable solvents which can have for example tunable hydrophilic/hydrophobic properties and can allow extraction of compounds without distillation.[10]
    v. CO_2 (in CO_2-expanded liquids[11] (CXLs) or in supercritical state[3,12,13] (sc-CO_2)).

However, the choice of a solvent for a given chemical synthesis is mostly dictated by matters of aprotic or protic nature, basicity, polarizability and polarity. To spread the use of green solvents on a large scale, the availability and range of solvent properties offered by green solvents must cover those of traditional organic solvents (see Figures 1 and 2 for comparison). As a result, a major challenge in this area is the identification of new solvents –and particularly polar aprotic ones which still are scarce– to expand the scope and use of green solvents.

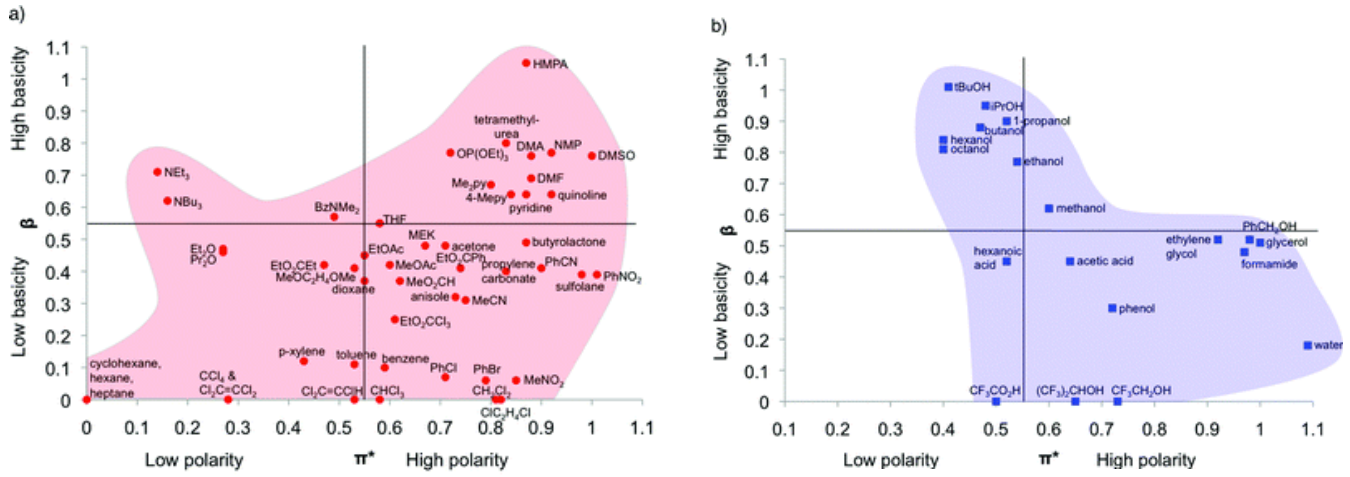

Figure 1. a) Usual aprotic solvents and b) usual protic solvents as a function of their π* (polarity and polarizability) and β (basicity or hydrogen-bond accepting ability) values. Solvents requiring pressure and/or elevated temperatures are shown as hollow symbols. Reprinted from reference 7.

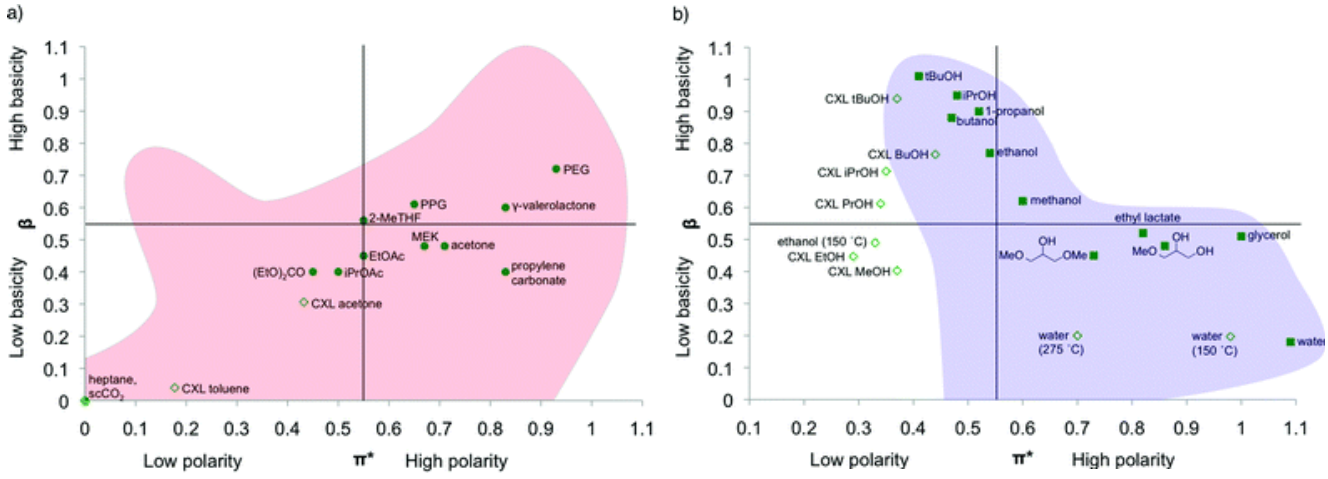

Figure 2. a) Green aprotic solvents and b) Green protic solvents as a function of their *π (polarity and polarizability) and *β* (basicity or hydrogen-bond accepting ability) values. Solvents requiring pressure and/or elevated temperatures are shown as hollow symbols. Reprinted from reference 7.**

An alternative solution to this may lay in the development of CO_2-based homogenous and heterogeneous systems. Carbon dioxide is actually an apolar aprotic solvent which renders it a poor solvent for ionic and polar compounds, catalyst and macromolecules. To circumvent this, several strategies have been suggested:

1. Adding a CO_2-soluble co-solvent such as acetone or ethanol to generate a homogenous medium with increased polarity or proticity.[14]

2. Adding a green polar protic solvent exhibiting low miscibility with CO_2 such as water, glycerol or relevant ionic liquids.

This could consequently act as a universal medium to dissolve polar or ionic compounds in a CO_2-based continuous phase. The stabilization of water/CO_2, CO_2/water, IL/CO_2 emulsions, miniemulsions or microemulsions through efficient (macro)molecular surfactants has thus been attracting considerable attention. However, the intrinsic properties of CO_2 destabilize kinetically-stable macroemulsions and miniemulsions within a few minutes, in the absence of stirring or emulsification process. As a result, thermodynamically-stable microemulsions are of greater interest to perform chemical reactions herein but meanwhile necessitate surfactants able to dramatically decrease the interfacial tension. To do so, a large range of studies have covered the field of molecular surfactants and their ability to stabilize water/CO_2 microemulsions.[15-25] This contrasts with their polymeric counterparts: in this field, most studies focused on the solubility of homopolymers and copolymers in CO_2. However, reports relating to the stabilization of (micro)emulsions in CO_2 by amphiphilic copolymers have scarcely appeared in literature. The relationships between the structure of polymer surfactants and their properties of solubility and interfacial activity still remain unclear. To do so, the emergence of powerful techniques to generate well-defined macromolecules has somewhat rejuvenated this field of research. Reversible deactivation radical polymerization technologies and, in particular, the reversible addition fragmentation transfer (RAFT) process have been proven to be a very efficient chemistry tool to produce polymers with precise macromolecular characteristics. Through the use of such technique, the objective of this present work will be to provide a deeper knowledge on the solubility of polymer amphiphiles in sc-CO_2, given that studies on

their solubility constitute a prerequisite to explore the stabilization of emulsions in sc-CO_2.

1. Chapter 1 will constitute a bibliographic introduction to this matter. Supercritical carbon dioxide and the main classes of polymers exhibiting a substantial CO_2-philicity will be presented. Factors governing their solubility will be clarified for each class of polymers as well as the different strategies that have been considered to improve this property. Then, the self-assembly of amphiphilic block copolymers in sc-CO_2 and their applications as emulsions stabilizers will be covered.

2. Chapter 2 will first introduce reversible deactivation radical polymerization (RDRP)[26] techniques. RAFT/MADIX polymerization will then be applied to provide a complete and detailed study on the solubility of poly(vinyl acetate)-based amphiphilic block copolymers in CO_2. The influence of macromolecular characteristics such as composition, chain length, or chain end will be discussed with the help of infrared spectroscopy.

3. Chapter 3 will present new strategies to improve the solubility of poly(vinyl esters)-based statistical copolymers. A large amount of work will be devoted to describe the polymerization of new vinyl fluorinated monomers by the RAFT/MADIX process. A special attention will be given to understand the factors governing their solubility in CO_2. Their use for the design of amphiphiles will be investigated too.

4. The final chapter of this thesis -Chapter 4- will be devoted to study the use of poly(fluorinated olefins) as new CO_2-philic building blocks. A detailed study on the macromolecular engineering of vinylidene fluoride will be presented. The solubility of innovative poly(fluorinated olefins)-based polymer surfactants will be eventually studied.

References

(1) P.T. Anastas and M.M. Kirchhoff, *Acc. Chem. Res.*, 2002, **35,** 686.
(2) M. Poliakoff, J.M. Fitzpatrick, T.R. Farren and P.T. Anastas, *Science*, 2002, **297,** 807.
(3) H.R. Hobbs and N.R. Thomas, *Chem. Rev.*, 2007, **107,** 2786.
(4) R. Noyori, *Chem. Commun.*, 2005, 1807.
(5) F. van Rantwijk and R.A. Sheldon, *Chem. Rev.*, 2007, **107,** 2757.
(6) C. Das Neves Gomes, O. Jacquet, C. Villiers, P. Thuéry, M. Ephritikhine and T. Cantat, *Angew. Chem. Ed. Int.*, 2012, **51,** 187.
(7) P.G. Jessop, *Green Chem.*, 2011, **13,** 1391.
(8) Q. Zhang, K. De Oliveira Vigier, S. Royer and F. Jerome, *Chem. Soc. Rev.*, 2012,
(9) K. Alfonsi, J. Colberg, P.J. Dunn, T. Fevig, S. Jennings, T.A. Johnson, H.P. Kleine, C. Knight, M.A. Nagy, D.A. Perry and M. Stefaniak, *Green Chem.*, 2008, **10,** 31.
(10) P.G. Jessop, L. Phan, A. Carrier, S. Robinson, C.J. Durr and J.R. Harjani, *Green Chem.*, 2010, **12,** 809.
(11) P.G. Jessop and B. Subramaniam, *Chem. Rev.*, 2007, **107,** 2666.
(12) E.J. Beckman, *J. Supercrit. Fluids*, 2004, **28,** 121.
(13) W. Leitner, *Acc. Chem. Res.*, 2002, **35,** 746.
(14) J.M. Dobbs, J.M. Wong, R.J. Lahiere and K.P. Johnston, *Ind. Eng. Chem. Res.*, 1987, **26,** 56.
(15) D.C. Steytler, E. Rumsey, M. Thorpe, J. Eastoe and A. Paul, *Langmuir*, 2001, **17,** 7948.
(16) J. Eastoe, S. Gold, S. Rogers, P. Wyatt, D.C. Steytler, A. Gurgel, R.K. Heenan, X. Fan, E.J. Beckman and R.M. Enick, *Angew. Chem. Ed. Int.*, 2006, **45,** 3675.
(17) M. Hollamby, K. Trickett, A. Mohamed, S. Cummings, R. Tabor, O. Myakonkaya, S. Gold, S. Rogers, R. Heenan and J. Eastoe, *Angew. Chem. Ed. Int.*, 2009, **48,** 4993.
(18) M. Sagisaka, S. Iwama, S. Hasegawa, A. Yoshizawa, A. Mohamed, S. Cummings, S.E. Rogers, R.K. Heenan and J. Eastoe, *Langmuir*, 2011, **27,** 5772.
(19) M. Sagisaka, S. Iwama, A. Yoshizawa, A. Mohamed, S. Cummings and J. Eastoe, *Langmuir*, 2012, **28,** 10988.
(20) M. Sagisaka, T. Fujii, D. Koike, S. Yoda, Y. Takebayashi, T. Furuya, A. Yoshizawa, H. Sakai, M. Abe and K. Otake, *Langmuir*, 2007, **23,** 2369.
(21) M. Sagisaka, D. Koike, S. Yoda, Y. Takebayashi, T. Furuya, A. Yoshizawa, H. Sakai, M. Abe and K. Otake, *Langmuir*, 2007, **23,** 8784.
(22) Y. Takebayashi, Y. Mashimo, D. Koike, S. Yoda, T. Furuya, M. Sagisaka, K. Otake, H. Sakai and M. Abe, *J. Phys. Chem. B*, 2008, **112,** 8943.
(23) M. Sagisaka, D.K. Oike, Y. Mashimo, S. Yoda, Y. Takebayashi, T. Furuya, A. Yoshizawa, H. Sakai, M. Abe and K. Otake, *Langmuir*, 2008, **24,** 10116.
(24) A. Mohamed, K. Trickett, S.Y. Chin, S. Cummings, M. Sagisaka, L. Hudson, S. Nave, R. Dyer, S.E. Rogers, R.K. Heenan and J. Eastoe, *Langmuir*, 2010, **26,** 13861.
(25) M. Sagisaka, J. Oasa, S. Hasegawa, R. Toyokawa and A. Yoshizawa, *J. Supercrit. Fluids*, 2010, **53,** 131.
(26) A.D. Jenkins, R.G. Jones and G. Moad, *Pure Appl. Chem.*, 2010, **82,** 483.

Abbreviations

A2	Second Virial coefficient
AIBN	2,2-azobisisobutyronitrile
AGET	Activators generated by electron transfer
ARGET	Activators regenerated by electron transfer
ATRP	Atom-transfer radical polymerization
BSSE	Basis Set Superposition Error
CED	Cohesive energy density
CFD	Critical flocculation density
CF_3VAc	1-(trifluoromethyl) vinyl acetate
CMD	Critical micelle density
CMP	Critical micelle pressure
CMT	Critical micelle temperature
CO_2	Carbon dioxide
CMRP	Cobalt-mediated radical polymerization
CSIRO	Commonwealth scientific and industrial research organization
$C_{tr,M}$	Transfer constant to monomer
$C_{tr,PnX}$	Interchain transfer constant
$C_{tr,pol}$	Transfer constant to polymer
$C_{tr,X}$	Transfer constant to agent
C/W	Carbon dioxide/Water
Đ	Dispersity
d	Density
DADMAC	Diallyl dimethyl ammonium chloride
DBM	Dibutyl maleate
DFT	Density functional theory
DLS	Dynamic light scattering
DMA	N,N-dimethylacrylamide
DMF	N,N-dimethylformamide
DP_n	Number-average degree of polymerization
DSC	Differential scanning calorimetry
eATRP	Electrochemically mediated atom transfer polymerization
EtAc	Ethyl acetate
EtTFAc	Ethyl trifluoroacetate
HFP	Hexafluoropropene
ICAR	Initiators for Continuous Activator Regeneration
ITP	Iodine transfer polymerization
IR	Infrared
iPrAc	Isopropyl acetate
k_p	Propagation rate coefficient
k_t	Termination rate coefficient
LA	Lewis acid
LAM	Less-activated monomer
LB	Lewis base
LCSD	Lower critical solution density
LCSP	Lower critical solution pressure
LCST	Lower critical solution temperature
LiBr	Lithium bromide
MADIX	Macromolecular design by interchange of xanthates

MALDI-TOF	Matrix assisted laser desorption/ionization-Time of flight
MALLS	Multi angle laser light scattering
MAM	More-activated monomer
M_n	Number-average molecular weight
$M_{n,exp}$	Experimental number-average molecular weight
$M_{n,theo}$	Theoretical number-average molecular weight
MP2	Second-order Moeller-Plesset
MPa	Megapascal
M_v	Viscosity-average molecular weight
M_w	Mass-average molecular weight
N_{agg}	Aggregation number
NMP	Nitroxide-mediated polymerization
NMR	Nuclear magnetic resonance
OHMRP	Organoheteroatom mediated radical polymerization
OMRP	Organometallic mediated radical polymerization
P	Pressure
PBA	Poly(butyl acrylate)
PBO	Poly(butylene oxide)
PDMA	Poly(N,N-dimethyl acrylamide)
PDMAEMA	Poly(N,N-dimethylaminoethyl methacrylate)
PDMS	Poly(dimethyl siloxane)
PE	Polyethylene
PEA	Poly(ethyl acrylate)
PEC	Poly(ether carbonate)
PEE	Poly(ester ether)
PEHA	Poly(ethyl hexyl acrylate)
PEO	Poly(ethylene oxide)
PFDA	Poly(1,1-dihydroperfluorodecyl acrylate)
PFDMA	Poly(1,1,2,2-tetrahydroperfluorodecyl methacrylate)
PFDS	Poly(perflurooctyl ethyleneoxymethylstyrene)
PFHMA	Poly(1,1,2,2-tetrahydroperfluorohexyl methacrylate)
PFOA	Poly(1,1-dihydroperfluorooctyl acrylate)
PFOMA	Poly(1,1,2,2-tetrahydroperfluorooctyl methacrylate)
PFPO	Poly(hexafluoropropylene oxide)
PHEMA	Poly(hydroxyethyl methacrylate)
PHPMA	Poly(1,1-dihydroperfluorooctyl methacrylate)
PMA	Poly(methyl acrylate)
PMMA	Poly(methyl methacrylate)
PMVE	Perfluoromethyl vinyl ether
PODA	Poly(octadecyl acrylate)
POEGMA	Poly(oligo(ethylene glycol) methacrylate)
PPA	Poly(propyl acrylate)
PPEGA	Poly(poly(ethylene glycol) acrylate)
PPO	Poly(propylene oxide)
PS	Polystyrene
PTAN	Poly(1,1-dihydroperfluorodecyl acrylate)
PtBMA	Poly(tert-butyl methacrylate)
PTFE	Poly(tetrafluoroethylene)

PVAc	Poly(vinyl acetate)
PVEE	Poly(vinyl ethyl ether)
PVME	Poly(vinyl methyl ether)
PVMEE	Poly(vinyl 1-methoxyethyl ether-*co*-acetate)
PVMME	Poly(vinyl 1-methoxymethyl ether-*co*-acetate)
PVPi	Poly(vinyl pivalate)
QELS	Quasi-elastic light scattering
RAFT	Reversible addition-fragmentation transfer
RDRP	Reversible deactivation radical polymerization
R_g	Radius of gyration
R_h	Hydrodynamic radius
RI	Refractive index
RITP	Reverse Iodine Transfer Polymerization
SANS	Small angle neutron scattering
SAXS	Small angle X-ray scattering
SBRP	Stibine-mediated radical polymerization
sc-CO_2	Supercritical carbon dioxide
SCF	Supercritical fluid
SEC	Size exclusion chromatography
SET-LRP	Single electron transfer-Living radical polymerization
T	Temperature
tBPPi	Tert-butyl peroxypivalate
TERP	Tellure-mediated radical polymerization
TFE	Tetrafluoroethylene
TFiPrAc	1,1,1-trifluoropropan-2-yl acetate
T_g	Glass transition temperature
THF	Tetrahydrofuran
T_m	Melting temperature
UCSD	Upper critical solution density
UCSP	Upper critical solution pressure
UCST	Upper critical solution temperature
UV	Ultraviolet
VAc	Vinyl acetate
VDF	Vinylidene fluoride
VPi	Vinyl pivalate
VTFAc	Vinyl trifluoroacetate
W/C	Water/Carbon dioxide
Xa	Xanthate
ZPE	Zero-point Energy

Note

Throughout this thesis, pressures will be given either in bar or megapascal (MPa, 1 MPa = 10 bar).

Chapter 1

- Fundamentals of supercritical CO_2
- State-of-the-art on the solubility of CO_2-philic (co)polymers
- Self-assembly of amphiphilic copolymers in sc-CO_2
- Macromolecular surfactants for water/CO_2 emulsions

Contents

I. Supercritical fluids

A. Historical background[1]

The existence of the supercritical state was discovered by Baron Charles Cagniard de la Tour in 1822. While studying the effects of temperature on liquids such as ether, alcohol or water in a sealed Papin's digester, he observed a discontinuity in the sound of a flint rolling ball located inside the barrel. While hearing the splash generated by the ball upon the liquid-vapour interface at normal temperatures, he reported the disappearance of this noise at temperatures far above the boiling point of the liquid. This state was characterized by the expansion of liquids at several times their original volumes at certain temperatures and the absence of any surface tension above. He thus observed the appearance of a single phase which revealed to be the supercritical state. Interestingly, he could measure the critical temperature of water at 362 °C, not so far from its actual value of 374 °C. In another set of experiments using sealed glass tubes and alcohols, he could also observe the vanishing of the liquid-vapour interface resulting in a transparent phase on heating and the reappearance of a thick cloud on cooling.[2,3] This marked the discovery of the critical point and the critical opacity. However, this concept of supercritical state was first thought particular to the liquids that Cagniard de la Tour studied. The generalization of this concept only started when major scientists such as Michael Faraday and Dimitri Mendeleiev recognized the significance of this work. This particular state was actually referred as its definitive coinage of supercritical state only in 1869 when Thomas Andrews studied the change of states of carbonic acid upon pressure and volume.[4] The concept of supercritical state and its distinctive properties were then explored and formalized by modern physicists such as Joachim Van der Waals and its equation of state for ideal gases.

B. Supercritical fluids: definition and properties

A supercritical fluid is a substance for which the temperature and the pressure are above their critcal values which are defined as the critical point. Similarly to the triple point which defines the zero-variance point for the solid, gas and liquid states, the critical point (P_c) denotes the point where the gas, liquid and supercritical phases

coexist (see Figure I.1.). This point can be experimentally observed through a critical opacity (see Figure I.2). When passing through the coexistence curve, the resulting opacity is usually named a cloud point. Any substance under conditions of pressure and temperature higher than those of P_c is thus called a supercritical fluid.

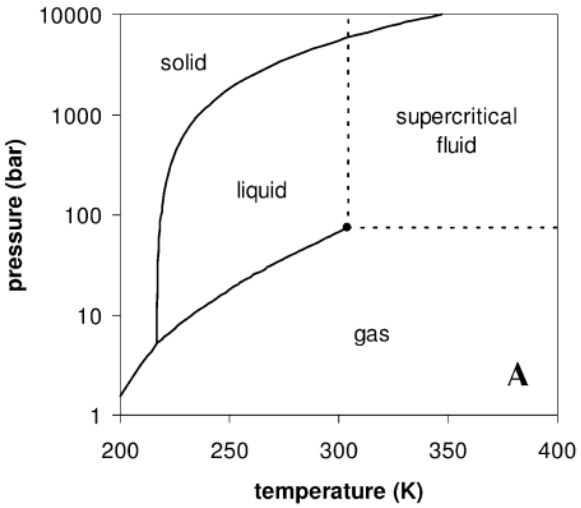

Figure I.1. Pressure-temperature phase diagram for pure CO_2. Reprinted from reference 5.

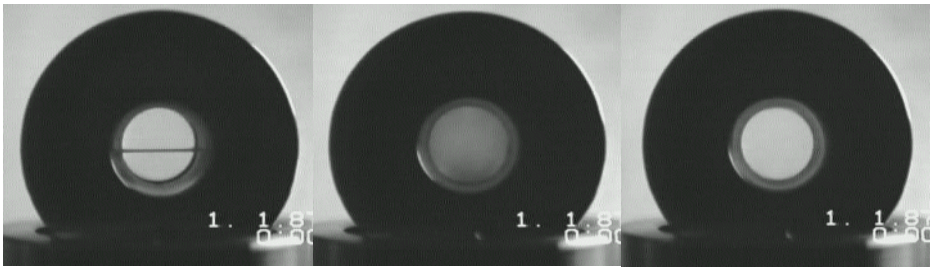

A. B. C.

Figure I.2. Pictures illustrating the different states of CO_2 under varying conditions of pressure and temperature: a) below its critical point with a meniscus denoting the coexistence of gas and liquid phases, b) at its P_c with the characteristic phenomenon of critical opacity, c) above its P_c in the supercritical state.

In the supercritical phase, there is no more coexistence between the gas and the liquid phase, even though this is actually a compressible state similarly to gases. The properties of supercritical fluids (SCFs) both depend on pressure and temperature conditions, which give them properties at the boundary between those of gas and liquids (see Figure I.3). Some important properties such as density,

viscosity or diffusivity are thus intermediate between characteristic values of gas and liquids (see Table I.1.).

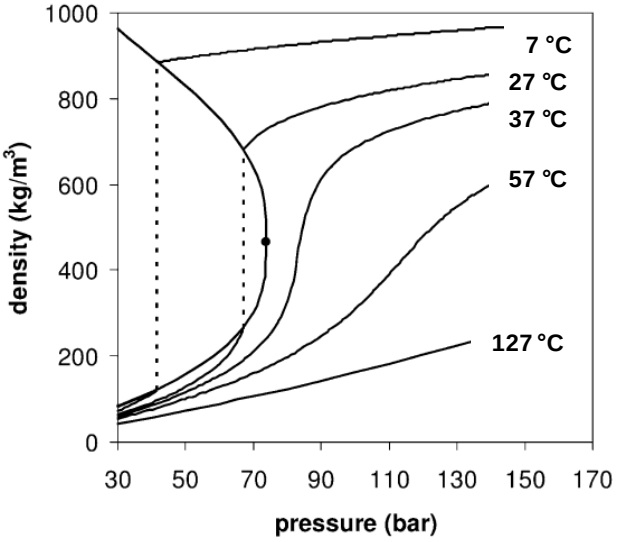

Figure I.3. Pressure-density phase diagram for supercritical CO_2 at different temperatures. The dashed lines indicate the liquid-vapour equilibrium. Adapted from reference 5.

Properties	Gas	Supercritical fluid	Liquid
Density ($g.L^{-1}$)	1	100-800	1000
Viscosity (Pa.s)	10^{-3}	$5\text{-}10.10^{-3}$	0.05-1
Diffusivity ($m^2.s^{-1}$)	10^{-5}	10^{-7}	10^{-9}

Table I.1. Value ranges of density, viscosity and diffusivity for gases, supercritical fluids and liquids. Adapted from reference 5.

C. Examples of supercritical fluids and applications

Although requiring extreme conditions of pressure and temperature, supercritical fluids can occur naturally. Such conditions can be found in submarine volcanoes with supercritical water and the atmosphere of Venus with sc-CO_2. In Table I.2, a comprehensive review of supercritical fluids and their associated critical points is given. Carbon dioxide (31.0 °C, 73.8 bar), ethylene (9.3 °C, 50.4 bar) and propane (96.7 °C, 42.5 bar) are consequently the most current SCFs due to their P_c requiring moderate conditions of pressures and temperature. Singularly, supercritical water has also attracted attention despite harsh supercritical conditions

at 374 °C and 22.1 MPa. In this case, its acid character and oxidation power in supercritical conditions are advantageous enough to overcome limitations arising from both high pressures and corrosion.

Solvent	T_c (°C)	P_c (bar)
CO_2	31	74
Ammonia	132	113
Diethyl ether	194	36
Hexane	234	30
Acetone	235	47
Methanol	239	81
Ethanol	243	64
Toluene	319	411
Water	374	221

Table I.2. Critical conditions of representative supercritical fluids.

The cost of high-pressure equipments at industrial and academic scales represents an economic barrier for the implementation of supercritical technologies. Their major industrial applications deal with the replacement of hazardous solvents such as chlorofluorocarbons and chlorinated solvents including dichloromethane and perchloroethylene. Thus, CO_2 has been widely used to dry cleaning and extracting processes of natural substances, the most striking example being certainly the decaffeination of ground coffee developed in the late 1960s. The use of SCFs has been reported for polymer reaction engineering where carbon dioxide was showed to be a beneficial solvent for the production of fluoropolymers. Polyethylene can also be processed in supercritical ethylene or propane in high-pressure continuous reactors.

II. Supercritical carbon dioxide

A. Comparative advantages of sc-CO_2

Among supercritical fluids, sc-CO_2 certainly possesses the highest potential of practical development. In addition to its low critical conditions, CO_2 is actually a waste of important industrial processes. Thus, the Haber-Bosch process–the main process to produce ammonia from atmospheric nitrogen–generates pure CO_2 which can be commercially used without further purification.[6] Moreover, other factors can explain why CO_2 is perceived as a promising green solvent:

- CO_2 is non-toxic. Its threshold air concentration for working conditions is as high as 5000 ppm. By means of comparison, a daily exposition to 10 ppm of chloroform is considered hazardous.
- CO_2 is non-flammable. This constitutes another very competitive advantage compared to halogenated solvents.
- Its high pressure vapour –superior to 60 bar– allows its complete removal from processed materials. Thus, CO_2 is one of the two solvents fully approved by the Food and Drug Administration (FDA), along with water.
- CO_2 has a low reactivity and is inert towards oxidation. It is also a non-transferring species for radicals.
- Heat and mass transfer are significantly enhanced in sc-CO_2 due to its properties of low viscosity and densities. Its low surface tension allows to wet structured materials better than liquids usually do.

In addition to the cost of high-pressure vessels, CO_2 also has intrinsic physical disadvantages.

- A low cohesive energy density which confers a weak solvent strength to CO_2.
- CO_2 is a Lewis acid through its electron-deficient carbon. It thus reacts reversibly with strong Lewis bases such as primary and secondary amines. However, this can be turned into an advantageous property for the capture of CO_2 by amine-based solvents and surfactants, polymers

and solvents that possess CO_2-responsive moieties such as guanidines and amidines.[7]

- CO_2 is a poison for Ziegler-Natta and palladium-based catalysts due to the formation of CO.

B. Considerations on the nature of CO_2 as solvent

The behaviour of CO_2 as a solvent is of particular complexity although it first appeared as a simple system. At a first glance, CO_2 can be considered an apolar solvent resulting of the centrosymmetry of the molecule. Similarly, its relative permittivity –i.e. its dielectric constant– equals to 1-2 depending on pressure-temperature conditions. By means of comparison, a polar solvent such as water possesses a dielectric constant of 80 at 20 °C. Additionally, it has a low polarizability per volume in the range of 0.012-0.032 at 25 °C, being thus related to alkanes.[8] As a consequence, CO_2 was early perceived as a replacement solvent for hexane. However, the difference of solubility of hydrocarbon-based surfactants between hydrocarbons and CO_2 and the peculiar high solubility of fluorocarbons and carbonyl-based materials both suggest that describing CO_2 as an apolar solvent does not give a full and satisfactory description of its solvation power.[9]

The molecule of CO_2 is actually charge-separated since the partial charges were calculated to have a negative value of -0.36 for the oxygen atoms and a positive value of 0.72 for the central carbon. This induces the existence of bond dipole moments and a consequent quadrupole moment which is estimated at $-4.3.10^{26}$ $erg^{1/2}.cm^{5/2}$.[10] Thanks to its quadrupolar nature, CO_2 is able to solvate polar substances through dipole-quadrupole interactions, which hydrocarbons cannot do. CO_2 should therefore be classified as a nondipolar solvent, along with benzene and dioxane.[11] Interestingly, most studies published in literature do no refer to these quadrupolar-polar interactions but to the existence of basic and acid Lewis sites. Due to the separation of charges, the oxygen atoms can be actually considered weak Lewis bases whereas the carbon atom a Lewis acid. Lewis-type interactions of CO_2 and solutes will be discussed in the following section.

C. Lewis-type interactions of solutes with CO_2

By virtue of these Lewis sites, CO_2 can act either as a Lewis acid or a Lewis base. A great amount of research was devoted to evaluate the strength of these interactions and the identification of CO_2-Lewis complexes able to promote the solubility of (macro)molecules in CO_2. The following paragraphs aim at describing such Lewis complexes and summarizing the possibilities that have been studied so far. This description will not consider interactions with sp3-type oxygen or nitrogen donating atoms that are involved in alcohol, water and primary or secondary amines which are out of scope. Their reactivity with CO_2 actually makes them poorly useful for the macromolecular engineering of polymers. The following sections will rely mainly on results obtained by infrared spectroscopy and computational calculations which are the typical techniques in use for the theoretical and experimental studies of Lewis adducts. However, it should be noted that recent progress in computational chemistry and the development of new levels of theory which take the dispersion forces into better account, prompt to consider older results with cautiousness. To set a comprehensive basis of comparison, the reported energies for the various Lewis complexes will focus mainly on *ab initio* calculations using the aug-cc-pVDZ basis set[12-15] at the second-order Moller-Plesset (MP2) level which explicitly includes the effects of electron correlation.[16] Preferably, the stabilization energy will be corrected for the basis set superposition errors (BSSE) using the full counter-poise method (CP)[17] and the zero-point energy contribution (ZPE).

1. Interactions of CO_2 with sp3 or sp2 N-donating atoms

Ammonia, alkyl amines and pyridine are common strong Lewis bases. However, primary and secondary amines are known to react with CO_2 to form carbamates. In literature, the study of interactions of CO_2 is restricted to tertiary amines for sp3 N-donating atoms whereas pyridine is the most representative compound with a sp2 N-donating atom. Meredith *et al.* performed DFT calculations using CAM/B3LYP on the CO_2-triethylamine interactions and found a low equilibrium constant value of 0.0463 for the Lewis complex.[18] Although the pKa of triethylamine is higher than that of pyridine –respectively 10.65 and 5.25– the equilibrium constant of pyridine was stronger by a factor of three and estimated at

0.133. It apparently resulted from the stronger steric hindrance around the lone pair of the nitrogen of triethylamine while the planar geometry of the pyridine-CO_2 complex concomitantly favored the formation of the Lewis complex. However, these results were criticized by Kilic *et al.* who reproached the lack of an accurate description of electron correlation effects to integrate dispersion forces.[19] In their own *ab initio* calculations on a MP2 level, they computed an interaction energy of -5.64 kcal.mol^{-1} for a triethylamine/CO_2 complex whereas 2-methyl pyridine or 4-methyl pyridine respectively exhibited lower interaction energies of -5.07 and -4.56 kcal.mol^{-1}. Inversely, a difference of 1.34 kcal.mol^{-1} in favor of the pyridine/CO_2 complex had been calculated by Meredith et al without taking into account the Van der Waals forces.[18] Finally, Kilic *et al.* also investigated the self-interactions of trimethylamine and 4-methyl pyridine by *ab initio* calculations. In both cases, the self-binding energies were calculated to be either equivalent or at higher levels of energy compared to their interaction energies with CO_2. This was related to the immiscibility of poly(vinyl 4-pyridine) and the decreasing miscibility of polysiloxanes functionalized with increasing propyl dimethylamine pendant groups in sc-CO_2. As a conclusion on the interactions of CO_2 with sp2 or sp3 N-donating atoms, the self-interactions of such compounds are predominant over the interaction energies with CO_2 even though they are of high energy.

2. Interactions of CO_2 with sp3 O-donating atoms

Functionalities that possess sp3-donating atoms such as ethers are of greater promise as they are known to exhibit lower self-interactions. While studying the swelling of polymers by CO_2, Vitoux *et al.* performed *ab initio* calculations at a MP2/aug-cc-VDZ level of theory.[20] The interactions of propylmethylether with CO_2 were of Lewis-type as the molecule of CO_2 was found above the oxygen of the ether compound in the optimized geometry. This was in accordance with previous results obtained by Van Ginderen et al.[21] The C•••O distance was computed to 2.739 Å while the interaction energy was -3.43 kcal.mol^{-1}. These results also agreed with previous MP2/aug-cc-VTZ calculations on a methylbutylether/CO_2 complex where the interaction energy was -3.49 kcal.mol^{-1}.[22]

In the case of ether oxygens involved in ester functionalities, this energy was lower. For instance, this value was computed to -2.60 kcal.mol^{-1} for isopropyl acetate, -2.49 kcal.mol^{-1} for methyl isobutyrate and -2.52 kcal.mol^{-1} for methyl acetate.[22] By means of comparison, the interaction energies between CO_2 and sp3 O-donating atoms are thus lower compared to those presented for the N-donating atoms.

Another interesting case is the siloxane functionality (i.e. Si-O). The lower electronegativity of silicium actually gives a higher polarity to the Si-O bond compared to the C-O one. Similarly to the case of methylbutyl ether, the carbon of the molecule of CO_2 was located above the silane oxygen, which revealed a LA-LB interaction.[20] The binding energy was slightly lower with a value of -3.59 kcal.mol^{-1}.

3. Interactions of CO_2 with sp2 O-donating atoms

Compared to their sp3 analogs, compounds possessing sp2 O-donating atoms have attracted greater interest as Lewis base, especially as model compounds for commodity polymers such as poly(vinyl methyl ketone) or poly(vinyl acetate). Using DFT calculations at a MP2/aug-cc-pVDZ level of theory, the formation of a Lewis complex between CO_2 and acetone with a planar geometry was proven.[23] The binding energy of this complex was evaluated at -2.63 kcal.mol^{-1} with a C•••O distance of 2.845 Å. Compared to the isolated molecule of acetone, the stretching of the C=O bond was also higher while the torsion angle of CO_2 was 1.9°.[23] This consequently changes the geometry of the molecule of CO_2. Whereas free CO_2 possesses a $D_{\infty h}$ symmetry, the formation of Lewis interactions results in a complex with a C_{2v} or C_s geometry.[24] In parallel, the interactions of CO_2 with carbonyl groups have been also extensively studied using vibrational spectroscopy including infrared and Raman techniques. The formation of an electron donor-acceptor complex between the electron-deficient carbon of CO_2 and the lone pairs of the oxygen of the carbonyl could be demonstrated by the lifted degeneracy of the bending vibrational mode of the CO_2 molecule in the case of acetone-CO_2 complexes.[18,25] The frequency splitting of this band was 18.0 cm^{-1}.

In ester compounds such as methyl acetate, the binding energies computed with a MP2/aug-cc-pVDZ level of theory were slightly higher compared to acetone. The energy of the complex was evaluated to -2.72 kcal.mol^{-1} with CO_2 oriented

towards the methyl side and -2.53 kcal.mol^{-1} towards the ester side.[22] Interestingly, similar results on methylacetate-CO_2 complexes were obtained by Raveendran and Wallen.[26] The strength of these LA-LB interactions were calculated to be half of that measured between two water dimers.[24]

Considering the case of macromolecules, the splitting of the bending mode of CO_2 can partially explain the difference of solubility or swelling that are generally observed for these polymers. Complexes of greater strength were thus evidenced with carbonyl-containing polymers such as poly(vinyl methyl ketone), poly(vinyl acetate) and poly(ethyl methacrylate).[25] Besides, the quantification of the strength of these interactions from the bending mode of CO_2 –located at low wavenumbers in the 640-660 cm^{-1} region– can be operated from the half width of this band and the integration of the IR signal corresponding to the polymer-CO_2 complex. Thus, enthalpies of complex formation were calculated to be respectively -2.22 and -1.91 kcal.mol^{-1} for samples of poly(vinyl acetate) and poly(methyl methacrylate) which qualitatively agrees with their relative solubilities in sc-CO_2.[27] This could be related to the bond length of the C=O band and the negative charge on the oxygen of the carbonyl group calculated through computational studies.[28] A qualitative way to estimate the strength of the complex is also the stretching band of the carbonyl group located at 1700-1800 cm^{-1}. The formation of a complex usually results in the red-shifting of this band.[23] Additionally, DFT calculations and Raman spectroscopy are complementary tools for the study of such complexes.[23,29,30] The existence of CO_2 homodimers and heterodimers could thus be revealed by Raman spectroscopy in binary mixtures of CO_2 and acetone.[30]

Adding to this C=O bond, other Lewis bases possessing a sp2 oxygen-donating atom such as P=O and S=O moieties can also interact with CO_2 through Lewis-type interactions. Thus, *ab initio* calculations and IR spectroscopy evidenced strong interactions in tributyl phosphate-CO_2 complexes resulting from LA-LB interactions. However, their strength was evidenced to depend on concentration, which resulted from self- competitive interactions between tributyl phosphate groups, thus leading to the formation of dimers.[18] Using DFT-B3LYP computational levels with BSSE corrections , the binding energy of tributyl phosphate and CO_2 were calculated to be -4.22 kcal.mol^{-1}.[31] Interestingly, this value was higher than those calculated for trimethyl and triethyl phosphate –respectively -2.40 and -2.47 kcal.mol^{-1}. This

particular fact demonstrates that the steric hindrance around the Lewis base site and its accessibility for the molecule of CO_2 greatly influences the binding energy of the complexes. However, the authors observed a strong competition with the self-interactions of highly polar phosphoric groups.

Finally, sulfoxide groups have also been studied through the prism of dimethylsulfoxide-CO_2 complexes. Using MP2 computational levels, Raveendran and Wallen revealed that dimethylsulfoxide-CO_2 complexes exhibited higher corrected interaction energies than methyl acetate-CO_2 ones.[26] The optimized geometry of the DMSO-CO_2 was also different from the carbonyl-CO_2 ones, which was thought to result from the intermediate sp2-sp3 hybridization of the oxygen of the sulfoxide group. Thus, the molecule of CO_2 exhibited a torsion angle of 3° while interacting with the sulfoxide group. In a few words, the higher polarity of the S=O bond resulted in higher LA-LB interactions.

4. Cooperative hydrogen bonds with CO_2

A common particularity of ether, carbonyl and sulfoxide groups is the existence of non-conventional hydrogen bonds between the lone pairs of the oxygen atom of CO_2 and a hydrogen atom located on a carbon at the alpha position of the C=O (see Figure I.4).[26] This was evidenced by the shortening of the C-H bond– contrasting with classical O-H•••O hydrogen bonding –and the difference of lengths of the C=O bonds in CO_2. By comparing the charges on the oxygen and carbon of CO_2 resulting from H-bonding, it was concluded that this C-H•••O hydrogen bond was actually cooperative and reinforced the strength of the LB-LA interactions.

However, the additional stabilization energy of this hydrogen bond was negligible compared to the energy arising from the LA-LB interactions. [32] Thus, this energy was estimated at 0.2 kcal.mol^{-1} in an acetaldehyde/CO_2 complex using a MP2/aug-cc-pVDZ level of theory. Interestingly, a higher energy of 0.6-1.3 kcal.mol^{-1} for a dimethylether/CO_2 complex was observed.

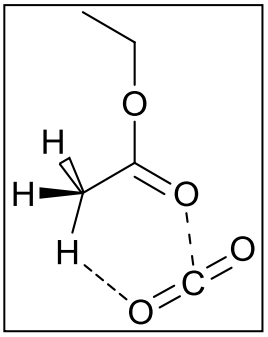

Figure I.4. Typical interaction geometry of CO_2 complexes involving a cooperative C-H•••O hydrogen bond associated with a typical LA-LB interaction between CO_2 and a Lewis base system (e.g., a carbonyl functionality of ethyl acetate).

5. Interactions of CO_2 with fluorine atoms

The interactions of CO_2 with carbonyl functionalities or other groups are central questions to understand the solvation of molecules in CO_2 and to design highly-CO_2-philic polymer materials. While the interactions with C=O seem qualitatively well-understood in the literature, a persistent question concerning CO_2 has been whether it interacts or not with fluorinated substituents which are known to induce significant solubility in CO_2.

Using high-pressure NMR spectroscopy, Dardin *et al.* studied solute-solvent interactions between fluorinated compounds and CO_2.[33] While the absence of site-specific interactions between n-hexane and CO_2 through ^{1}H NMR experiments was noted, excess chemical shifts effects in ^{19}F NMR that were independent of magnetic susceptibility were evidenced in the case of n-perfluorohexane. This was attributed to site-specific Van der Waals interactions with CO_2.[34] However, in a conflicting paper, Yonker *et al.* could not find any specific interactions between fluoromethane, trifluoromethane and CO_2 through ^{1}H, ^{19}F NMR experiments and molecular dynamics simulations.[35] This work supported previous *ab initio* calculations performed by Diep e*t al.*[36] In their simulations performed at a MP2/aug-cc-pVDZ level of theory, the binding energies of methane/CO_2 and tetrafluoromethane/CO_2 were respectively computed to -0.88 and -0.79 kcal.mol^{-1}, thus suggesting no specific interaction between the fluorinated compound and CO_2. To conceal these

contradictory results, Raveendran *et al.* studied the effects of stepwise fluorination on methane.[37] Comparing the partial charges on the hydrogen atoms of methane and the fluorine atoms of tetrafluoromethane at a MP2/aug-cc-pVDZ level of theory, they computed charges of opposite signs for each molecule. Methane with positively charged hydrogen atoms was thus thought to interact with the negatively-charged oxygen of CO_2 through LA-LB interactions while repulsive interactions would be expected with the negatively charged fluorine atoms of tetrafluoromethane. However, the dissociation energies were of same magnitude, i.e. 0.63 kcal.mol^{-1} for the CH_4/CO_2 dimer and 0.58 kcal.mol^{-1} for the CF_4/CO_2 one. By means of comparison, these interactions are weaker than the interaction of a CO_2 dimer which energy was estimated at 1.10 kcal.mol^{-1} with a similar level of theory.[26] As for the partially fluorinated compounds, the dissociation energies of the complexes were evaluated at 1.87, 1.78 and 1.43 kcal.mol^{-1} for respectively CH_3F, CH_2CF_2 and CHF_3. In CH_3F, the carbon-fluorine bond was more polarized resulting in enhanced LA-LB interactions and hydrogen atoms with increased positive charges. Upon increasing fluorination, the interactions between hydrogen atoms and the oxygen atom of CO_2 were increasingly stronger and their distances decreased. However, the dissociation energies decreased as a result of the increasing competition between fluorine atoms and the weakening of their Lewis basicity. This study thus revealed that fluorine atoms can actually interact with CO_2 in specific cases.

In the last paragraphs, the specific interactions that CO_2 can exhibit with various groups were covered. This provides partial guidelines for the macromolecular engineering of CO_2-philic polymers. As stated earlier, the self-interactions of molecules actually play a great role too, especially for a low cohesive energy density solvent like CO_2.

III. Phase behaviour of (co)polymers in CO_2

Before describing the different families of (co)polymers that present substantial solubility in sc-CO_2, a short background regarding the thermodynamics of polymer-CO_2 mixtures and the influence of macromolecular characteristics on the solubility in sc-CO_2 will be presented.

A. Thermodynamic foreword[38-40]

1. Solubility criteria

A solution of polymer and solvent is monophasic and stable at a given temperature and pressure only if the Gibbs free energy is negative. No spontaneous mixing occurs if this energy is superior or equal to zero. The Gibbs free energy is described by the following equation:

$$\Delta G_{mixing} = \Delta H_{mixing} - T\Delta S_{mixing}$$

where ΔH_{mixing} and ΔS_{mixing} are the change on respectively enthalpy of mixing and entropy of mixing, and T is defined as the absolute temperature. The formation of a single phase is obtained only if:

$$\Delta H_{mixing} < T\Delta S_{mixing}$$

The entropy of mixing is commonly defined as the increase of entropy resulting from the mixing of two inert chemicals. It can be divided into two main contributions: the combinatorial entropy –defined as the number of rearrangements during mixing– and the non-combinatorial entropy– defined as the change on specific volume during mixing. On one hand, the combinatorial term is usually described by the following equation:

$$\Delta S_{combinatorial} = -R[\frac{\varphi 1}{r1}\ln(\varphi 1) + \frac{\varphi 2}{r2}\ln(\varphi 2)]$$

where φ_i is the volume fraction of the component I, r_i the number of polymer segments and R the perfect gas constant. R_i being proportional to the degree of polymerization, the combinatorial entropy tends to zero for a polymer chain of infinite molecular weight. On the other hand, the non-combinatorial entropy is closely related to the flexibility of the polymer chain and thus to its glass transition temperature (T_g). Although it seems rather difficult to evaluate its contribution, the depression of T_g induced by the solubilization of polymers in CO_2 may evidence its importance.[41-44]

However, the dissolution of a polymer is globally governed by the enthalpic term. The enthalpy of mixing results from the interplay between solvent-solvent, solvent-polymer and polymer-polymer interactions. Regarding CO_2, the low cohesive energy density of this solvent renders solvent-solvent interactions minor compared to the two other interactions. The balance between polymer-polymer and polymer-CO_2 contributions determines the contribution of enthalpy of mixing, especially when the polymer chain contains Lewis base sites that can promote solute-solvent or intramolecular interactions. This balance is expressed by the interchange energy:

$$\omega = z[\Gamma_{ij}(r,T) - \frac{1}{2}\Big(\Gamma_{ii}(r,T) + \Gamma_{jj}(r,T)\Big)]$$

where z is the coordination number, Γ is the intermolecular pair potential energy, i and j represent solute and solvent molecules, respectively. An approximate form of Γ_{ij} for small molecules is:

$$\Gamma_{ij}(r,T) \approx -[C_1 \frac{\alpha_i \alpha_j}{r^6} + C_2 \frac{\mu_i^2 \mu_j^2}{r^6 kT} + C_3 \frac{\mu_i^2 Q_j^2}{r^8 kT} + C_4 \frac{\mu_j^2 Q_i^2}{r^8 kT} + C_5 \frac{Q_i^2 Q_j^2}{r^{10} kT} + \text{Complex Formation}]$$

where α is the polarizability, μ is the dipole moment, Q represents the quadrupole moment, $C_{1\text{-}5}$ are constants, *r* is the distance between the molecules, *k* is Boltzmann's constant, and T is absolute temperature. However, this equation does not fully describe the interactions of a polymer segment since polymers have chain

connectivity. Qualitatively, the temperature dependence of dipolar and quadrupolar interactions suggests that dispersion forces should be prominent at low temperatures and, inversely, negligible at high temperatures.

Solubility parameters have been developed by Hildebrand and thermodynamics researchers to describe the enthalpy of mixing. To do so, the concept of cohesive energy (E) has been introduced and defined as the increase in the internal energy per mole by breaking the intermolecular forces. This actually corresponds to the internal energy of vaporization. In a volume unit (V), E translates to the cohesive energy density (CED). From these notions, the Hildebrand solubility parameters were defined as:

$$\delta = (\frac{E}{V})^{1/2} = (CED)^{1/2}$$

The enthalpy change on mixing during the dissolution of a polymer has been described as:

$$\Delta H_m = (\delta_1 - \delta_2)^2 \varphi_1 \varphi_2 V$$

where φ_i and δ_i are respectively the volume fraction of I in the mixture and the Hildebrand parameter of i. The Hildebrand parameters of polymer and solvent must be close to ensure the dissolution of the polymer.

Interestingly, the intermolecular forces in a liquid can be related to the work required to increase the surface of the liquid, i.e. its surface tension (γ). In parallel to its definition arising from the energy of vaporization, the CED could be related to the surface tension in the following formula:

$$CED = \frac{\gamma . \Sigma}{V} = \frac{\gamma . N_a^{1/3}}{V^{1/3}}$$

where Σ, V and N_a respectively stand for the surface per mole, the molar volume and the Avogadro constant. As a result, qualitative information on the CED of a material can be gained from the determination of the surface tension. This parameter can be

probed by sessile drop, osmotic pressure, vapor sorption or inverse gas chromatography measurements.

Finally, a useful parameter to determine the overall quality of the solvent towards the polymer chain is the second Virial coefficient (A2). Depending on molecular weight, temperature, pressure or density, the value of A2 indicates either bad ($A_2 < 0$) or good solvent conditions ($A_2 > 0$). For these latter conditions, the polymer will behave as a random coil. The so-called theta conditions correspond to the case where A2 equals to zero. The determination of A2 for a polymer chain is usually achieved through light or neutron scattering experiments.

2. Effects of external parameters on the phase behaviour

Upon decreasing temperature at a constant pressure, the heat of mixing for the solution of polymer is exothermic ($\Delta H_{mixing} < 0$) and the solubilization of the polymer chain is promoted until the increases of the dipole-dipole self-interactions of either solute or solvent outweigh the solute-solvent interactions. This leads to an enthalpically-driven collapse of the polymer chain at an upper-critical solution temperature (UCST) (see Figure I.5).[38] On the opposite, a lower-critical solution temperature (LCST) may appear upon an increase in T and is associated with an endothermic heat of mixing ($\Delta H_{mixing} > 0$) (see Figure I.5). The phase separation is then caused by a free volume difference between the polymer chains and the solvent. It is driven by a negative entropic effect. Additionally, the positions of both UCST and LCST curves depend on pressure. An increase in pressure is actually expected to shift the UCST curves to lower temperatures, and concomitantly the LCST curves to higher ones (see Figure I.6).

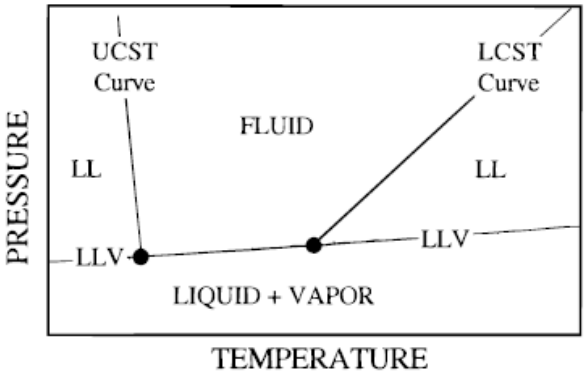

Figure I.5. Schematic pressure-temperature phase diagram for binary mixtures of a high molecular weight polymer. LL represents a liquid-liquid region, LV a liquid-vapor one and LLV a liquid-liquid-vapor line. Reproduced from reference 45.

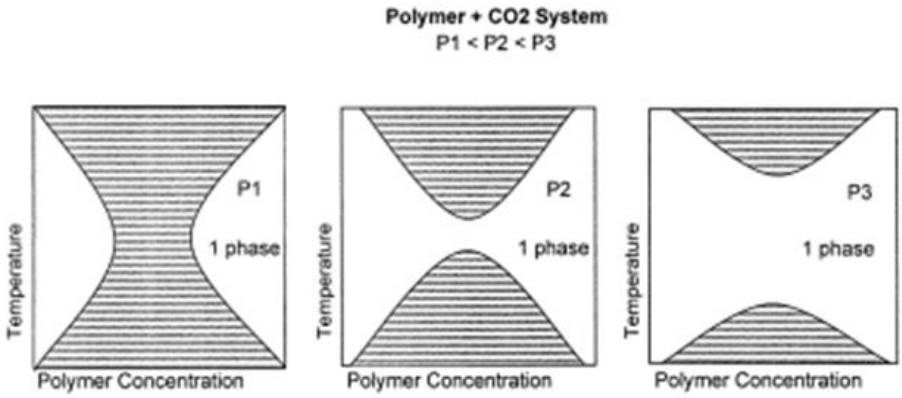

Figure I.6 Theoretical temperature-composition phase diagrams for a pseudo-binary mixture of a polymer in CO_2. Adapted from reference 46.

Similarly, a decrease in pressure at a constant temperature decreases the solvent density and the solubility of polymers until crossing an upper-critical solution pressure (UCSP) boundary which is the same as the LCST one. In this case, the enthalpic factor is thus responsible. A global consequence of these LCST and UCSP phenomena is the existence of an upper-critical solution density (UCSD) which depends on pressure and temperature for supercritical fluids.[46] For a polymer of infinite molecular weight, a theta density which corresponds to this UCSD can be defined. Inversely, the existence of a lower critical solution density (LCSD) was also demonstrated.[47]

As underlined in the previous paragraph dealing with the interactions of CO_2 with Lewis bases such as tertiary amines and phosphates, the polymer-solvent

interactions have to overcome polymer self-interactions. This is of particular importance for polar polymers as quadripolar-polar interactions, such as LA-LB interactions, scale inversely with the distance between molecules to the power of eight whereas dipole-dipole interactions do to the power of six.[38] This results in a higher solubility of polymers having either strong polymer-CO_2 interactions or weak polymer-polymer interactions or both. This will be exemplified in the following paragraphs describing the various CO_2-philic polymers.

B. Predictive influence of macromolecular characteristics[38]

A distinctive feature between small molecules and macromolecules is the influence of characteristics inherent to polymers. Although the phase diagram of a mixture of a small molecule with a supercritical fluid exhibits two critical points, the higher molecular weight of polymers as well as the dispersity in molecular weight somehow complicates the phase diagram of polymers. Higher molecular weights result in the absence of a critical point but in the appearance of UCST, LCST, UCSP phenomena for a polymeric substance. Their respective positions depend on the chemical composition of the polymer chains–the enthalpic lever–but also on the composition of the binary mixture, and the molecular weight and dispersity of the polymer chains. While it seems impossible to draw general conclusions as for the influence of enthalpic interactions on the positioning of the aforementioned curves, predictions can be made concerning the respective roles of polymer content, molecular weight and dispersity in the phase diagrams.

Concerning the influence of polymer content, a global minimum for the P-T curve (and possibly also a global maximum) is expected in the vicinity of 3-15 % wt of polymer in solution (see Figure I.7.a)). Cloud point curves are to superimpose in between. However, the molecular weight of the polymer chain has much more impact on its solubility. Higher molecular weights actually result in an increase of the cloud point pressures–as represented in Figure I.7.b). At a specific molecular weight, the dispersity of the molecular weight distribution has no influence on the cloud point pressure but broadens the pressure transition. Thus, a transition of 5-7 bar is usually observed for polymers samples of dispersity smaller than 3.0. Due to the

polydisperse nature of synthetic polymers, the phase diagrams of CO_2 and polymers are pseudo-binary.

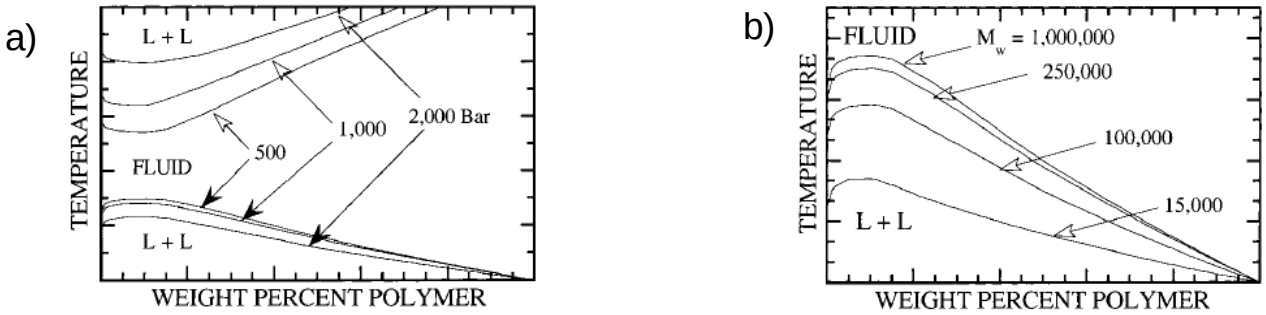

Figure I.7. Schematic representation of T-Composition curves with a) varying pressures for a polymer of given molecular weight and b) varying mass-average molecular weights. Reproduced from reference 38.

Finally, other macromolecular factors such as the nature of end groups, branching and semi-cristallinity can influence the solubility of polymers in compressible solvents. The effects of end groups and branching are case-by-case discussions as they are expected to affect both polymer-polymer and polymer-CO_2 interactions especially for polymer of lower molecular weights. They will be consequently not discussed herein. The existence of semi-crystalline domains in polymer chains requires higher temperatures to outweigh the subsequent enthalpy of fusion and to allow the solubilization of such materials.

C. Solubility of (co)polymers in sc-CO_2

After these general considerations about the phase behaviour of polymers in compressible solvents and sc-CO_2 in particular, the next sections will be dedicated to describe the main family of CO_2-philic polymers. The discussion will start from a specific polymer backbone including:

- organic polymers such as polyethylene, polyethylene oxide and polymers with pendant groups (poly(vinyl ethers), poly(vinyl esters) poly((meth)acrylates), and miscellaneous ones).

- inorganic polymers such as polysiloxanes and polyphosphazenes.

Their solubility in sc-CO_2, the underlying physical reasons, as well as the existing strategies of improvement will be presented. As a conclusion, heuristics will be made to provide guidelines for the macromolecular engineering of CO_2-philic polymers.

1. From polyethylene to fluorinated polyolefins

a) Solubility of homopolymers

Polyethylene (PE) is a semi-cristalline and non-polar hydrocarbon polymer. Because of its apolarity, this polymer is practically insoluble in sc-CO_2 in conditions as harsh as 270 °C and 2750 bar.[48] The interchange energy is then dominated by quadrupolar-quadrupolar interactions of CO_2. To promote dipole-quadrupole interactions, the progressive introduction of fluorine atoms onto the polymer backbone has been studied through poly(vinyl fluoride) (-(CH_2-CHF)$_n$-), poly(vinylidene fluoride) (-(CH_2-CF_2)$_n$-), and polytetrafluoroethylene (-(CF_2-CF_2)$_n$-) (see Figure I.8).

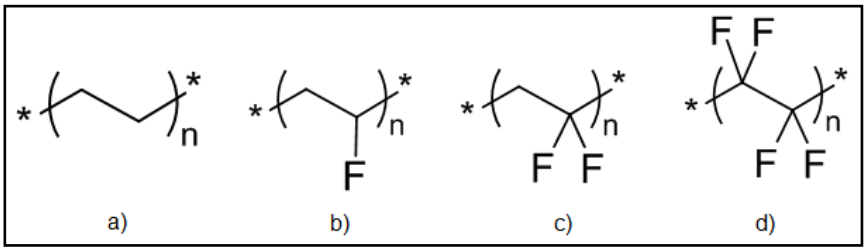

Figure I.8. Molecular structure of a) polyethylene, b) poly(vinyl fluoride), c) poly(vinylidene fluoride) and d) polytetrafluoroethylene.

Due to a high melting temperature of 187 °C and strong polymer-polymer interactions, a high-molecular weight poly(vinyl fluoride) having a M_w of 125000 g.mol^{-1} was found insoluble at temperatures up to 300 °C and pressures of 2750 bar.[48,49] Poly(vinylidene fluoride) (PVDF) exhibited enhanced solubilities in sc-CO_2 as 5 % wt of a sample with a M_w of 181000 g.mol^{-1} was fully soluble at 1650 bar and 140 °C.[50] Investigations on the effect of higher molecular weights showed little effects on the cloud point pressures (see Figure I.9). However, the pressure cloud point was

lowered by 200 bar upon decreasing molecular weight (i.e. for a M_n around 3000 g.mol^{-1}).[51] Under milder conditions of 150 bar and 65 °C, only PVDF oligomers having a number of repeating units less than approximately 20 (i.e. a M_n close to 1300 g.mol^{-1}) exhibited high solubility in sc-CO_2.[52] The maximum DP_n for soluble PVDF was determined to be 35 (i.e. around 2200 g.mol^{-1}). Finally, a high molecular weight poly(tetrafluoroethylene) (PTFE) was insoluble at 207 bar and 35 °C, probably due to its high cristallinity.[53]

These results demonstrate that an optimal polarity exists through partial fluorination of the polyethylene backbone. In PVDF, this creates a dipolar moment that promotes favorable dipolar-quadrupolar interactions with CO_2.

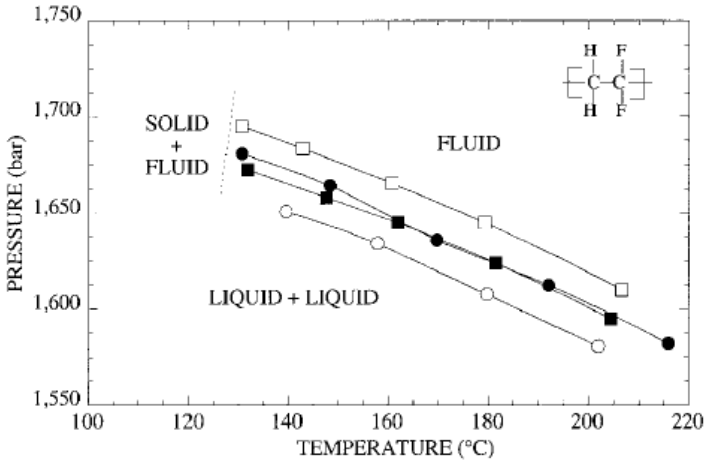

Figure I.9. Pressure-temperature phase diagrams of binary mixtures of sc-CO_2 and PVDF with increasing M_w: (◦) 181000 (▪) 269000 g.mol^{-1} (•) 275000, and (▫) 329000 g.mol^{-1}. Reproduced from reference 50.

However, the solubility of homopoly(fluorinated olefins) is extremely limited as a result of strong polymer-polymer interactions which are experimentally evidenced by their high melting points, degrees of cristallinity and high surface tensions (in the range of 30-33 mN.m^{-1}). [53]

b) Solubility of copolymers

A usual strategy to enhance the solubility of PVDF or PTFE-based polymers in sc-CO_2 is the copolymerization of VDF (or TFE) with a comonomer such as

hexafluoropropylene (HFP),[48] dioxole monomers,[48] or vinyl acetate (VAc).[54,55] The microstructure of the resulting copolymer is affected to decrease or suppress the crystalline domains and incorporate strong Lewis base sites to promote interactions with CO_2.

Hexafluoropropylene is undoubtedly the most studied comonomer for this purpose. The incorporation of 22 % mol of HFP into a VDF-HFP fluoropolymer dramatically affects its microstructure and renders the materials amorphous. A copolymer with a M_w of 85000 g.mol^{-1} gets soluble in milder conditions of approximately 750 bar and 100 °C (see Figure I.10).[48,56] However, this effect is less pronounced with copolymers of TFE and HFP. An equivalent amount of HFP only decreases the melting temperature of the copolymer to 147 °C, which makes the copolymer (M_w equal to 210000 g.mol^{-1}) soluble at temperatures and pressures higher than 185 °C and 1000 bar. The different shape of the curves was attributed to the stronger dipole moment of VDF units and the favored quadrupole-dipole interactions at lower temperatures. Similar remarks can be made from the phase behaviour of a Teflon AF fluoropolymer synthesized from TFE and a perfluorinated cyclooxyaliphatic substituted ethylenic monomer.[48] The presence of this bulky comonomer –incorporated at 65 % mol– suppressed the crystalline domains of PTFE, which lowered the cloud points of this PTFE-based copolymer to approximately 500 bar at 100 °C (see Figure I.10). In this case, the sharp increase at lower temperatures was thought to result from the dipole interactions of Teflon AF.

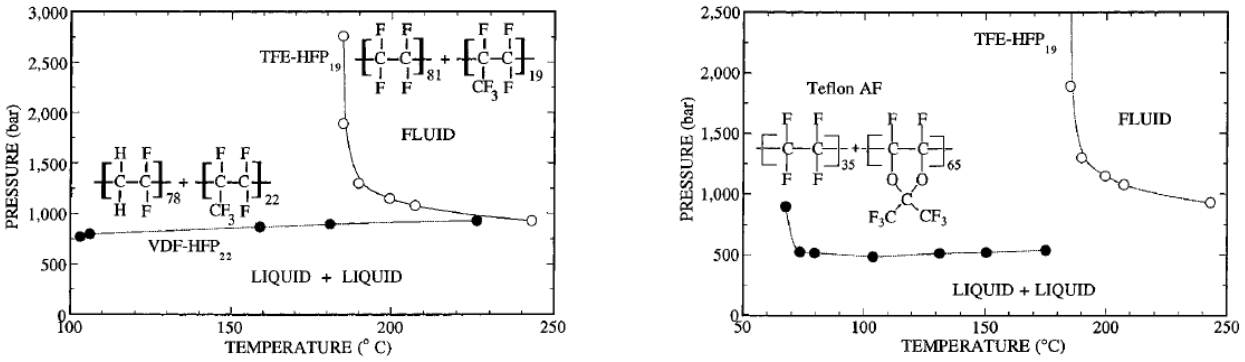

Figure I.10. Pressure-temperature phase diagrams for the VDF-*co*-HFP, TFE-*co*-HFP and Teflon AF copolymers. Reprinted from reference 48.

In addition to affecting the microstructure, the incorporation of vinyl acetate into PTFE or PVDF chains through free-radical copolymerization is expected to promote LA-LB interactions with CO_2. Baradie *et al.* investigated the influence of TFE % mol in TFE-*co*-VAc copolymers.[55] A copolymer having 63.3 % mol of TFE (M_w = 290000 g.mol^{-1}) was insoluble even at 2100 bar and 144 °C. A reduced mole fraction of TFE resulted in the solubility of the copolymers due to the likely partial or total disappearance of crystalline domains and the enhancement of polymer-CO_2 interactions. Thus, a VAc-*co*-TFE copolymer with 46.7 % mol of TFE and a M_w equal to 180000 g.mol^{-1} exhibited a cloud point at 740 bar and 75 °C for a polymer content of 5 % wt. Then, different copolymers with 26.5, 19.3 and 11.6 % mol of TFE and M_w ranging between 140000 and 160000 g.mol^{-1} were fully soluble at around 550 bar and 25 °C for equivalent polymer contents in CO_2. The enhanced solubilities were thought to arise from higher interactions due to quadridentate interactions of the polymer backbone with CO_2 and the enhanced acidity of protons compared to hydrocarbon analogs. In another study, the same authors built on the enhanced solubility of such fluorocarbon-VAc copolymers to copolymerize VAc with vinylidene fluoride, chlorotrifluoroethylene or tetrafluoroethylene in a surfactant-free polymerization process under mild pressure conditions of 200-230 bar.[54]

A new strategy to enhance the solubility of PVDF-based copolymers will be introduced in Chapter 3.

2. From poly(ethylene oxide) to perfluoropolyethers

a) Poly(ethylene oxide)

The incorporation of oxygen atoms –and thus ether linkages- into the polyethylene backbone induces an enhanced but limited solubility of polyethylene oxide in sc-CO_2. A diol-terminated PEO sample (0.92 % wt and M_n = 600 g.mol^{-1}) exhibited a cloud point pressure around 330 bar at 40 °C.[53] By means of comparison, single phases for a binary mixture of CO_2 and squalane –a hydrocarbon linear chain with 30 carbon atoms and a molecular weight of 422 g.mol^{-1} –could not be observed before reaching 400 bar and 80 °C. Several factors are to explain this enhanced solubility of PEO. Adding to the suppression of crystalline domains, the ether

linkages create favorable Lewis base sites through the non-bonding doublets of oxygen and additional hydrogen bonding through the hydrogen atom placed in alpha position. However, the strong polymer-polymer interactions of PEO –illustrated by a high surface tension of 42.9 $mN.m^{-1}$- dramatically decrease its CO_2-philicity.[53]

b) Poly(propylene oxide)

A decrease in the cohesive energy density–and likely an increase in the free volume– can be achieved with the introduction of a methyl group as such in poly(propylene oxide) (PPO). The surface tension is then decreased to 31.5 $mN.m^{-1}$, which greatly enhances the solubility of PPO in contrast to PEO.[53,57] The cloud point pressure at 22 °C of a diol-terminated PPO (M_n = 725 $g.mol^{-1}$) could indeed be observed at pressures lower than 100 bar.[57] Further investigations on poly(butylene oxide) (with an ethyl pendant group) and linear poly(*n*-butylene oxide) did not evidence any enhancement of solubility compared to PPO.[53] As a result of the limitation in chain lengths of CO_2-philic poly(alkylene oxides), the nature of their chain end groups is of special importance. The modification of terminal hydroxyl groups into ether or acetate moieties represents another way of improvement as these groups have been proven to provide favorable LA-LB interactions with CO_2.[57,58] Thus, PPO capped with a butyl ether and an acetate group showed increasing solubilities compared to a diol-terminated PPO in neat CO_2 at 22 °C (see Figure I.11).[58] However, the chain-end modification with trimethyl silyl groups proved to be an even more efficient strategy in this regard.[59] The critical role of the terminal groups is of further importance for the solubility of hyperbranched poly(glycidols). Interestingly, ester groups –either acetate or heptanoate– significantly enhanced the CO_2-philicity of such hyperbranched copolymers in moderately mild conditions (T < 100 °C and P < 1000 bar) and induced LCST or UCST behaviors.[60]

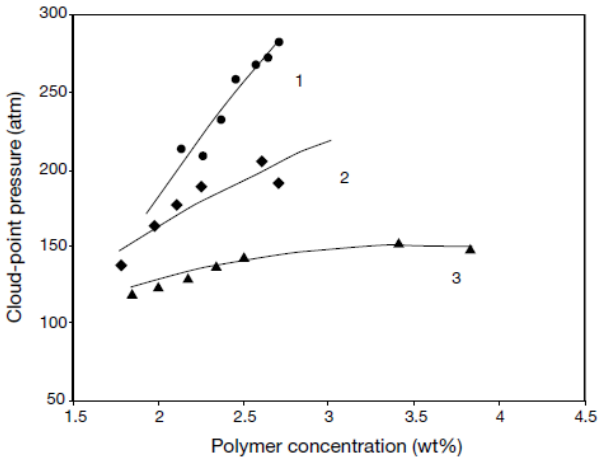

Figure I.11. Pressure-polymer content phase diagram for (1) a PPO diol (2) a PPO monobutyl ether and (3) a PPO acetate with 21 repeat units (M_n ≈ 1250 g.mol^{-1}). at 22 °C (1 atm ≈ 1.01 bar). Reproduced from reference 58.

Although the solubility of PPO is extremely limited for high molecular weight samples, the use of PPO-based amphiphilic statistical, diblock and triblock copolymers in sc-CO_2 has attracted considerable attention due to their commercial availability under the Pluronics trademark.

c) Perfluoropolyethers

Similarly to fluorinated olefins, the introduction of fluorine atoms onto the PEO backbone has been explored through the family of perfluoropolyethers (sometimes coined perfluoropolyalkylethers). Functionalized poly(hexafluoropropylene oxides) are representative perfluoropolyethers that actually attracted early attention for their solubility in sc-CO_2 (see Figure I.12). These polymers are produced by anionic ring-opening polymerization of hexafluoropropylene oxide and commercialized as industrial lubricants by Dupont™ under the name of Krytox®.

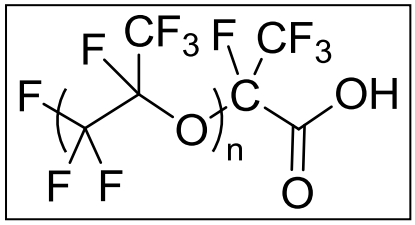

Figure I.12. Schematic representation of a Krytox polymer.

In their pioneering work on CO_2 thickeners, Hoefling *et al.* studied the solubility of different Krytox-class compounds.[61] At a constant temperature of 295 K (i.e. 22 °C), a Krytox polymer having a M_w of 13000 g.mol^{-1} exhibited cloud points at around 75, 125 and 150 bar for respective polymer contents of 1, 5 and 10 % wt. Another Krytox polymer having a carboxylic acid chain end and a M_w of 2500 g.mol^{-1} (also known as Krytox 157 FSL) was also evaluated. This polymer surfactant was fully soluble at 110 bar and 40 °C for polymer contents up to 20 % wt. The carboxylate version of this polymer was also studied with varying molecular weights.[62] A notable increase in pressure with increasing M_w was observed since 3 % wt of polymers of 5000 and 7500 g.mol^{-1} were roughly soluble at respectively 210 and 300 bar (see Figure I.13) while around 4 % wt of polymer with a M_w of 2500 g.mol^{-1} was soluble at 150 bar and 40 °C.

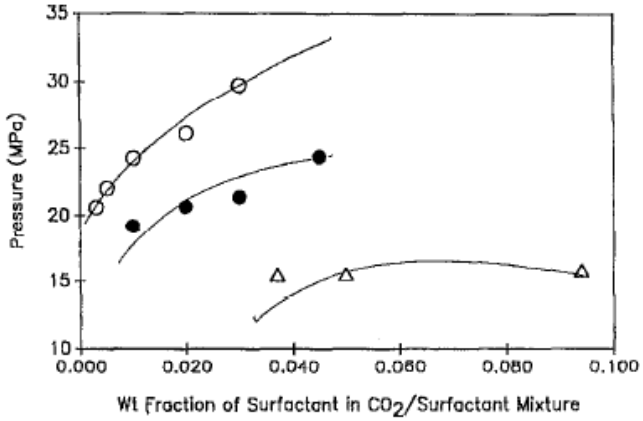

Figure I.13. Pressure-composition phase diagram at 40 °C for binary mixtures of CO_2 and carboxylate-capped Krytox polymers with a M_w of (Δ) 2500, (•) 5000 and (◦) 7500 g.mol^{-1}. Reproduced from reference 62.

The high solubility of Krytox polymers in sc-CO_2 was attributed to their weak polymer-polymer interactions, which is illustrated by their low surface tension in the range of 16-20 mN.m^{-1}.[63] Interestingly, the second virial coefficient was also determined by neutron scattering experiments for a Krytox polymer with a M_w of 16000 g.mol^{-1}.[64] A value of 0 ± 0.2.10^{-4} mol.cm^3.g^{-2} was found, which suggested that the polymer chain adopted an unperturbed chain dimension in sc-CO_2.

As a consequence of their high solubility, perfluoropolyethers could be used to synthesize highly soluble amphiphilic copolymers. This includes various polymeric architectures such as poly(lactide)-*b*-*poly*(hexafluoropropylene oxide) block

copolymers[65] and Krytox-based copolymers grafted from either a poly(methyl methacrylate-*co*-hydroxyethyl methacrylate) backbone[66] or a hyperbranched poly(ethylene imine) core.[67]

3. From polycarbonates to poly(ester ethers)

a) Poly(carbonates) and poly(ether carbonates)

Poly(carbonates) are practically insoluble in CO_2. Poly(5-(4-benzyloxybutyl)-1,3-dioxan-2-one) (M_n = 34000 g.mol^{-1}) was insoluble even at pressures up to 1500 bar and temperatures up 150 °C.[68] However, aliquots of hyperbranched poly(carbonates) modified with trifluoroacetate end groups could be solubilized under such conditions.

In spite of the insolubility of poly(carbonates), Sarbu *et al.* copolymerized epoxides with CO_2 using sterically hindered aluminium catalysts to form statistical poly(ether carbonates) (PECs, see Figure I.14).[58] Through the association of a low cohesive energy density monomer -propylene oxide- and Lewis base carbonyl sites in the main chain, the cloud point pressures of the resulting copolymers revealed to be extremely low. Thus, 1 % wt of a poly(ether carbonate) with 250 repeating units (i.e. a M_n around 16000 g.mol^{-1}) and 15.4 % mol of carbonate were soluble at 22 °C and pressures down to around 130 bar.[69] The versatility of the ether oxide/CO_2 platform was demonstrated with other monomers such as ethylene oxide and cyclohexene oxide (see Figure I.14). A triblock copolymer with an inner poly(ethylene oxide) block of 7 repeating units and two outer blocks comprising 25 units of cyclohexene oxide and CO_2 was also synthesized. This amphiphilic copolymer exhibited

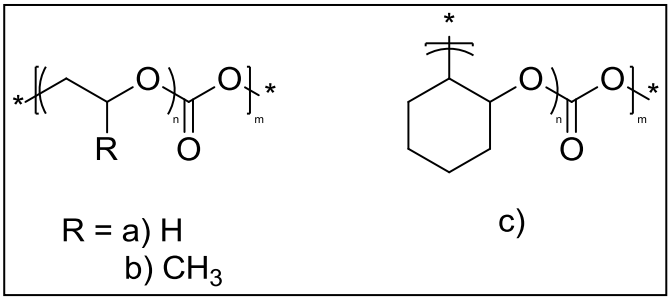

Figure I.14. Molecular structure of statistical poly(ether carbonates) with a) ethylene oxide, b) propylene oxide and c) cyclohexene oxide repeating units.

a cloud point pressure at around 100 bar for a polymer content of 0.7 % wt. In their work, Tan *et al.* explored the solubility of PECs that were synthesized by step-growth polymerization with oligomeric diol-terminated PPO and carbonyl diimidazole as the coupling agent.[70] Surprisingly, 0.17 % wt of a resulting PEC with 12.4 % mol of carbonate and a M_n of 3680 g.mol^{-1} was only soluble at 35 °C and 263 bar. A higher temperature of 45 °C resulted in the non-solubility of this material at pressures below 380 bar. Differences in the molar percentages of carbonate and in microstructure -resulting from the synthetic methodologies- were thought to explain these discrepancies.

Even though PECs were a notable advance in the field of CO_2-philic polymers, CO_2-soluble poly(ether carbonate)-based amphiphilic copolymers are notably restricted to a single example -mentioned above-.[58]

A comparison was also made with PPO incorporating Lewis base sites in the side chain. For this purpose, poly(epichlorhydrin) samples were synthesized and partially functionalized with acetate groups (see Figure I.15).[69] However, the enhancement of solubility was limited as the solubility of a sample with 25 repeating units and 45 % mol of acetate groups was close to that of a PPO with the same number of repeating units. An optimum of acetate-functionalization was also revealed suggesting that a molar percentage in acetate higher than 45 % induced increasing polymer-polymer interactions and thus decreased the solubility in CO_2. A similar approach was followed by Wang et al. who synthesized acetate-terminated oligomers of 3-acetoxy acetate (see Figure I.15).[71] Unfortunately, these materials exhibited elevated cloud point pressures around 700 bar at 25 °C.

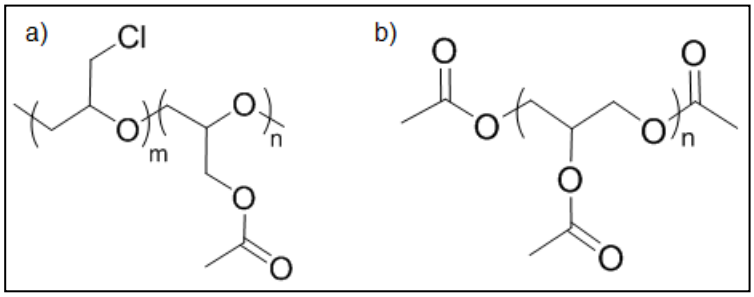

Figure I.15. Molecular structures of acetate-functionalized poly(epichlorhydrins) and oligo(3-acetoxy acetates).

b) Poly(esters) and poly(ester ethers)

Similarly to poly(carbonates), the introduction of an ester linkage disfavored the CO_2-philicity of the polymer, likely due to a lower flexibility of the chain. As a consequence, the solubility of polyesters including poly(lactic acid) and hyperbranched poly(2,2-bis(hydroxymethyl) propionic acid) is extremely limited.[60,72]

Following the same strategy as poly(ether carbonates), poly(ester ethers) (PEE) (see Figure I.16) were also studied as CO_2-philic copolymers. These materials can be synthesized by step-growth polymerization between oligomeric diol-terminated PPO and diglycoyl chloride.[70] Extraction studies performed on a sample with a M_n of 4530 g.mol^{-1}, PPO units of 725 g.mol^{-1} and a carbonyl content of 14.3 % mol revealed that this sample was less soluble than a poly(ether carbonate) counterpart possessing a M_n of 3520 g.mol^{-1}and a carbonyl content of 8.75 % mol.

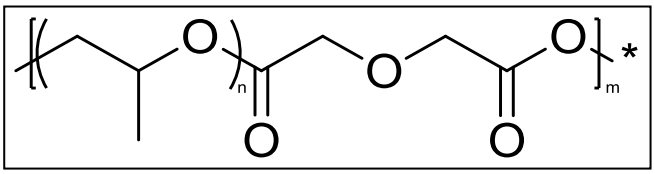

Figure I.16. Molecular structure of statistical poly(ester carbonates).

4. Organic polymers with pendant groups

a) Poly(vinyl ethers)

As a result of their low T_g and the lone pairs of oxygen which should give both favorable entropy of mixing and enthalpic interactions with CO_2, the solubility of poly(vinyl ethers) in sc-CO_2 has also been investigated. Compared to a monomethylether-terminated PPO sample (M_n equal to 1200 g.mol^{-1}) , the solubility of a poly(vinyl ethyl ether) (PVEE) having a M_n of 1500 g.mol^{-1} was rather limited as 1.5 % wt of this material were soluble at 22 °C and pressures as high as 350 bar.[57] However, the effect of molecular weight on the solubility of PVEE appeared less dramatic than for PPO polymers. A PVEE having a higher M_n of 3800 g.mol^{-1} and a T_g of -60 °C actually exhibited a cloud point pressure around 330 bar in similar

conditions of temperature and polymer content.[73] Singularly, PVEE was more CO_2-philic than dimethyl ether-terminated PPO (M_n equal to 3500 g.mol^{-1}) and, to a lesser extent, poly(vinyl methyl ether) (PVME, M_n equal to 3850 g.mol^{-1}, T_g = -31 °C) whilst the surface tension of PVEE, PPO and PVME were respectively 31, 29 and 36 mN.m^{-1} (see Figure I.17). As a consequence, PVME was more CO_2-philic than PPO due to lower self-interactions, but inferior to PVEE due to a lower entropy of mixing.

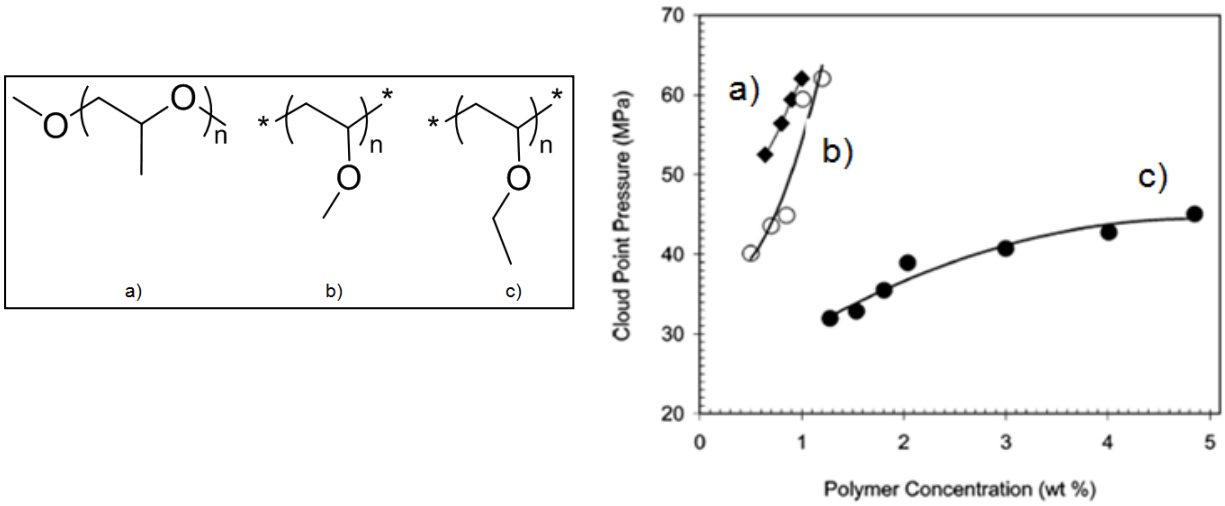

Figure I.17. Molecular structures of a) dimethyl ether-terminated polypropylene oxide, b) poly(vinyl methyl ether) and c) poly(vinyl ethyl ether) and their pressure-concentration phase diagram at 22 °C. Reproduced from reference 73.

To improve the solubility of poly(vinyl ethers), Wang *et al.* suggested the incorporation of diethyl ether-type functionalities in random poly(vinyl alcohol)-*co*-poly(vinyl acetate), thus aiming at increasing the acidity of nearby hydrogens and providing multidentate points for the LA-LB interactions.[71] The two oxygen atoms were actually expected to interact simultaneously with CO_2. From the etherification of a random poly(vinyl alcohol)-*co*-poly(vinyl acetate), poly(vinyl 1-methoxyethyl ether-*co*-acetate) (PVMEE) and poly(vinyl 1-methoxymethyl ether-*co*-acetate) (PVMME) with 9 acetate units, 30 ether repeating units and M_n equal to respectively 3400 and 3600 g.mol^{-1} were synthesized (see Figure I.18). 5 % wt of the PVMME sample were soluble around 700 bar at 25 °C which was roughly twice the pressure needed to solubilize a poly(vinyl acetate) of equivalent M_n. The PVMEE sample was even less soluble since it was only soluble at 3 % wt and exhibited higher cloud point

pressures than its methyl counterpart. This difference was explained by the reduction of the chain flexibility coming from the 1-methoxyethyl group as evidenced by the respective T_g values of the copolymers.

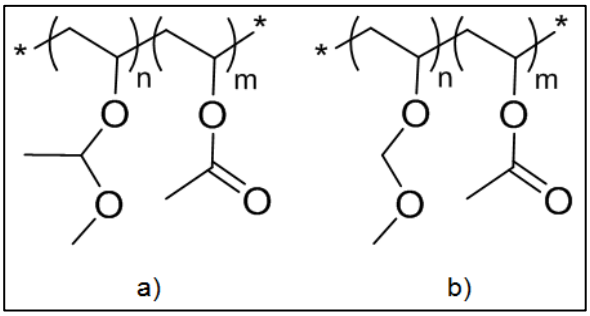

Figure I.18. Molecular structures of a) poly(vinyl 1-methoxyethyl ether-*co*-acetate) (PVMEE) and b) poly(vinyl 1-methoxymethyl ether-*co*-acetate) (PVMME) with 9 acetate units, 30 ether repeating units and M_n equal to respectively 3400 and 3600 g.mol^{-1}.

b) Poly(vinyl esters)

Due to its strong and multidentate LA-LB interactions with CO_2[25] and the existence of a cooperative hydrogen bond,[26] poly(vinyl acetate) (PVAc) constitutes a reference model among hydrogenated CO_2-philic polymers.

In their pioneering work, Rindfleisch *et al.* observed, at approximately 35 °C, a cloud point pressure around 700 bar for 5 % wt of PVAc (M_n = 125000 g.mol^{-1}) in sc-CO_2.[48,74] In further works, this polymer content of 5 % wt was also identified as the cloud point pressure maximum.[48] The following table gives a comprehensive overview on the influence of chain length on the cloud point pressures of PVAc at 25 °C. A high molecular weight PVAc of 193000 g.mol^{-1} was found soluble at 676 bar (67.6 MPa). The strength of the acetate-CO_2 interactions is high enough to outweigh the strong polymer-polymer interactions of PVAc –which has a surface tension close to 36 mN.m^{-1}- and the entropic penalty caused by the polymer conformation.[53] As a general rule, PVAc samples of equivalent number of repeating units or M_n exhibited lower cloud point pressure than PPO at this temperature whilst the surface tension of PPO was 31 mN.m^{-1} (see Figure I.19).[53] A reasonable explanation is a better accessibility of the CO_2 molecule to the lone pair of oxygen in the case of PVAc, the

multidentate interactions provided by the acetate group and subsequent higher polymer-CO_2 interactions.[74]

Polymer	M_n	M_w	M_w/M_n	P_{cp} (MPa)
PVAc	780	980	1.25	13.6
	850	1700	2.00	20.8
	2060	4150	2.01	37.4
	5680	8380	1.47	42.0
	7700	12,500	1.62	43.6
	13,000	17,000	1.31	45.7
	61,600	182,000	2.95	63.7
	193,000	585,000	3.02	67.6
PPO	1640	2030	1.24	43.6

Figure I.19 Cloud point pressures at 25 °C for 5 % wt for PVAc and PPO samples with varying molecular weights. Adapted from reference 74.

Although the solubility of PVAc in CO_2 seems essentially induced by its high solvent-solute interactions, the role of weak polymer-polymer interactions was also highlighted by Bulher *et al.*[75] A PVAc having a M_w of 16600 g.mol^{-1} was fractionated in sc-CO_2 at 45 °C with increasing density. The polymer/CO_2 surface tension of the supernatant solution was measured through static light-scattering experiments at various densities and the collected fractions were analyzed by size-exclusion chromatography (see Figure I.20). It appeared that the collected fractions were smaller as the surface tension increased.

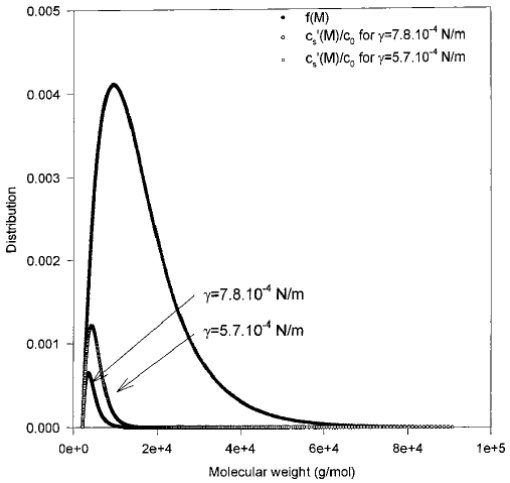

Figure I.20. Normalized molecular weight distribution of collected fractions from a PVAc homopolymer (M_w = 16600 g.mol^{-1}) solubilized in sc-CO_2 with increasing densities. Reproduced from reference 75.

Given that the solubility of PVAc in mild conditions is substantial only at lower molecular weights, the role of the chain end group on the CO_2-philicity of PVAc was also addressed by Cooper and coworkers with a high-throughput gravimetric extraction method.[76,77] Surprisingly, a hydroxyl-terminated PVAc of low molecular weight (M_n = 1620 g.mol^{-1}) was more soluble than PVAc samples modified with acetate or other ester end groups. At higher molecular weights, these differences were less marked as the influence of the terminal group was weaker. Additionally, topology effects were studied and revealed its negative impact as the solubility of branched PVAc was a decreasing function of branching.[77]

Although the possibly important role of weak polymer-polymer interactions in the CO_2-philicity of PVAc has been suggested, strategies to enhance its solubility focused mostly on increasing the entropy of mixing of PVAc-based copolymers. For this matter, vinyl acetate was copolymerized with sterically-hindered comonomers including other vinyl ester and maleate monomers (see Figure I.21). Using vinyl butyrate, the cloud point pressure of a 50:50 copolymer of vinyl acetate and vinyl butyrate (M_n = 2400 g.mol^{-1}) at 40 °C and 0.2 % wt was observed at 172 bar, which was 14 bar lower compared to a PVAc of equivalent M_n.[78] In a ternary mixture of polymer (5 % wt), CO_2 and *N*-vinyl pyrrolidone (15 % wt) at 35 °C, the decrease in pressure was even in the order of 53 bar between a PVAc (M_n = 9600 g.mol^{-1}) and 25:75 copolymer (M_n = 9900 g.mol^{-1}).[79] These enhancements of solubility were attributed to a higher free volume as a result of the lower T_g of the copolymer (-6 °C against 23 °C for the PVAc sample). At equivalent M_n, increasing the side chain length from vinyl butyrate to vinyl octanoate even shifted the cloud point pressure to 182 bar for a 75:25 copolymer of vinyl acetate and vinyl octanoate.[79] Using the same heuristics, the solubility of a 50-50 alternated copolymer of vinyl acetate and dibutyl maleate (M_n = 2400 g.mol^{-1}) was evaluated.[80] The cloud point pressure at 35 °C and 0.2 % wt was observed around 190 bar which was quite close to the aforementioned equivalent PVAc sample.

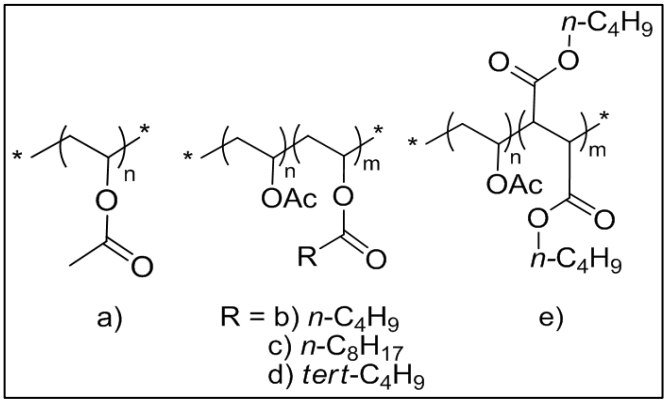

Figure I.21. Molecular structure of a) PVAc and copolymers of vinyl acetate and b) vinyl butyrate c) vinyl octanoate d) vinyl pivalate and e) dibutyl maleate.

It is worth underlining that the attribution of these enhanced solubilities to the solely entropy of mixing can be controversial in most cases. It is difficult to decouple the effects arising from the entropy of mixing and from lower polymer-polymer interactions induced by steric hindrance. A good example of this is provided by the case of vinyl pivalate. In their study on the solubility of copolymers of vinyl acetate and vinyl pivalate, Birkin *et al.* demonstrated that a 10:90 copolymer with a M_n of 8900 g.mol^{-1} showed a phase transition around 134 bar and 35 °C, which represents the lowest cloud point pressure for this kind of copolymers.[81] This was related to enhanced entropy of mixing whilst the reported T_g was in the order of 65 °C –i.e. higher than the T_g of PVAc itself. In this case, it is thus clear that entropy of mixing does not provide a sufficient explanation. Interestingly, a poly(vinyl pivalate) homopolymer of equivalent M_n was more CO_2-soluble than PVAc, contrary to poly(vinyl butyrate and poly(vinyl octanoate) homopolymers.[79] This will be further investigated in Chapter 3 while exploring the solubility of original fluorinated poly(vinyl esters).

As poly(vinyl esters) exhibited moderate solubilities under mild conditions in sc-CO_2, their use as CO_2-philic building blocks in macromolecular engineering has scarcely been reported. To date, the only examples are restricted to PEO-based amphiphilic diblock or triblock PVAc copolymers.[82-84] The synthesis and the CO_2-solubility of a new generation of PVAc-based amphiphilic block copolymers are described in Chapter 2.

c) Poly((meth)acrylates)

Due to their structural similarity with poly(vinyl esters), poly(acrylates) offer an interesting perspective to understand the solubility of PVAc-based copolymers.

Although it is a regioisomer of PVAc, poly(methyl acrylate) is far less soluble in sc-CO_2. At 30°C, the cloud point pressure of a poly(methyl acrylate) (M_n = 31000 g.mol^{-1}) was observed at 2250 bar and was 1500 bar higher compared to a PVAc of 125000 g.mol^{-1}.[48] Since the T_g of PVAc is higher, it was hypothesized that polymer-CO_2 interactions were higher with PVAc due to the better accessibility of the carbonyl group. However, the higher polymer-polymer interactions of poly(methyl acrylate) – with a surface tension of 41 mN.m^{-1}-could also explain this. As for poly(vinyl esters), increasing the side chain length from methyl to ethyl, propyl and butyl resulted in the lowering of T_g but in the shift to higher temperatures required to achieve a single phase transition at a constant pressure (see Figure I.22 a). At low temperatures, the bulkiness of the side chain is likely to diminish the strength of the carbonyl-CO_2 interactions (see Figure I.22.b). At temperatures higher than 100 °C, cloud point pressures were inversely lower for the polymers with increasing free volumes. This can be seen as a result of the domination of dispersion forces at high temperatures.

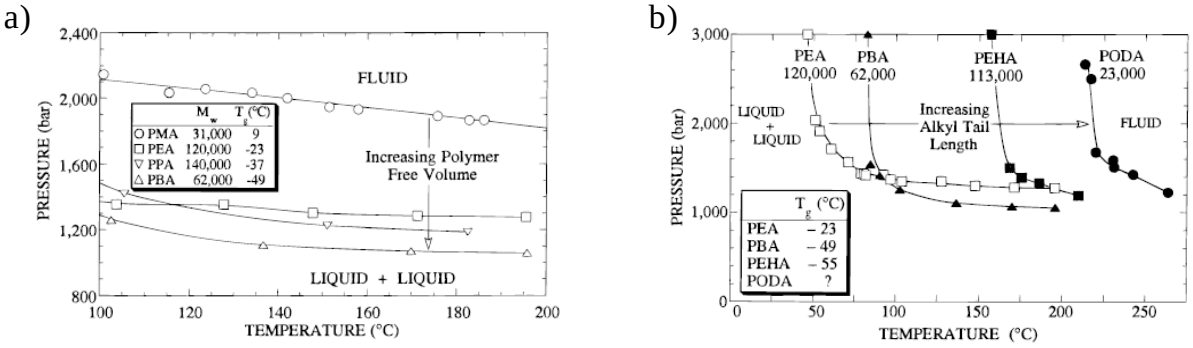

Figure I.22. Pressure-temperature phase diagram of high molecular weight sterically-hindered poly(acrylates) (undetailed polymer content): poly(methyl acrylate) (PMA), poly(ethyl acrylate) (PEA), poly(propyl acrylate) (PPA), poly(butyl acrylate) (PBA), poly(ethyl hexyl acrylate) (PEHA) and poly(octadecyl acrylate) (PODA). Reproduced from reference 48.

The addition of a methyl group to the polymer backbone of poly(methyl acrylate) and poly(ethyl acrylate) renders poly(methyl methacrylate) and poly(ethyl methacrylate) insoluble even in conditions as harsh as 255 °C and 2550 bar.[48] However, a side chain of butyl actually allows to overcome this as poly(butyl methacrylate) (M_n = 62000 g.mol^{-1}) shows a cloud point pressure at 2500 bar and 116 °C, i.e. 33 °C higher than an equivalent poly(butyl acrylate). The overall smaller solubility of poly(methacrylates) was attributed to the decreased entropy of mixing and the lesser flexibility of the polymer chains.

d) Fluorinated poly(meth)acrylates

Adding to their weaker interactions with CO_2, a limiting factor for the solubility of poly(meth)acrylates is their relatively high self-interactions. The surface tension of poly(*n*-butyl acrylate) and poly(methyl methacrylate) are respectively 33.7 and 41.1 mN.m^{-1}. A general strategy to outweigh this is the grafting of low self-interactions moieties such as long perfluorinated chains or poly(siloxane) macromonomers.

Comparing fluorinated and hydrogenated poly(methacrylates), McHugh *et al.* studied the solubility of poly(1,1,2,2-tetrahydroperfluorohexyl methacrylate) (PFHMA, M_n = 200000 g.mol^{-1}), poly(1,1,2,2-tetrahydroperfluorooctyl methacrylate) (PFOMA, M_n = 292000 g.mol^{-1}) and poly(1,1,2,2-tetrahydroperfluorodecyl methacrylate) (PFDMA, M_n = 196000 g.mol^{-1}) in sc-CO_2.[85] They observed a dramatic drop in the pressures and temperatures required to solubilize the fluorinated materials (see Figure I.23). The reduction to a shorter fluorinated side chain –as such in poly(2,2,2-trifluoroethyl methacrylate)– gave equivalent cloud point pressures (M_n = 268000 g.mol^{-1}). For a polymer content of 3.9 % wt, the single phase transition was thus observed at 323 bar and 60 °C.[86]

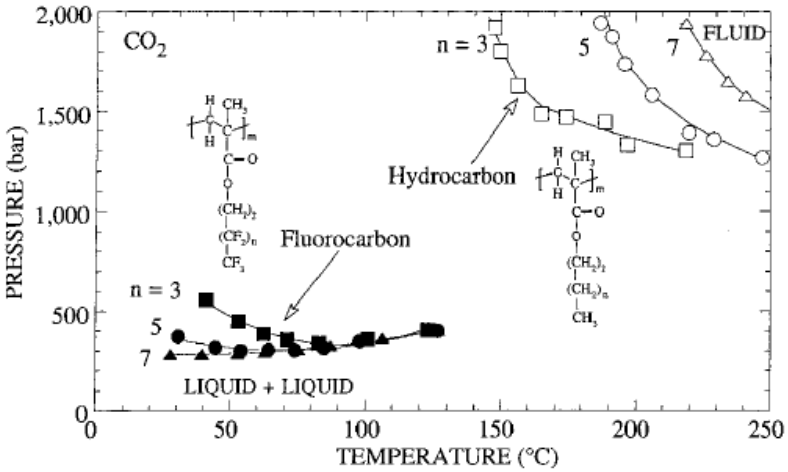

Figure I.23. Pressure-temperature diagram comparing the solubility of fluorinated poly(methacrylates) and their non-fluorous analogous (polymer content of 4 % wt). Reproduced from reference 85.

In this family of fluorinated poly((meth)acrylates), investigations on sc-CO_2 solubility mostly focused on poly(1,1-dihydroperfluorooctyl acrylate) (PFOA), poly(1,1,2,2-tetrahydroperfluorodecyl acrylate) (PFDA) or poly(1,1,2,2-tetrahydroperfluorodecyl acrylate) with an average value of fluorinated carbon equal to 8 (PTAN) (see Figure I.24).

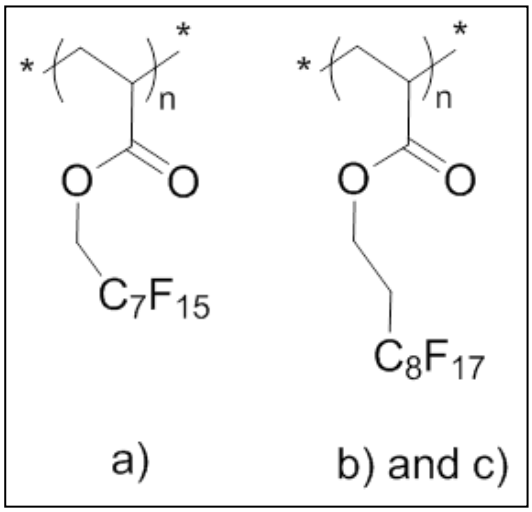

Figure I.24. Molecular structure of a) poly(1,1-dihydroperfluorooctyl acrylate) (PFOA) and b) poly(1,1,2,2-tetrahydroperfluorodecyl acrylate) (PFDA). Poly(1,1,2,2-tetrahydroperfluorodecyl acrylate) (PTAN) is a PFDA analog with an average number of fluorinated carbons equal to 8.

Hsiao *et al.* reported a cloud point pressure at approximately 150-170 bar and 40 °C for 4 % wt of a PFOA sample (M_w = 1000000 g.mol^{-1}).[87] A LCST-type behavior was also noted as a result of the positive dependency of pressure upon increasing temperatures. Through neutron scattering experiments, this high solubility of PFOA could be related to a positive second virial coefficient (A_2) in conditions as mild as 207 bar and 45 °C in the case of a sample with a M_w equal to 36500 g.mol^{-1}.[75] However, the theta pressure was not determined. In another set of experiments, the positive A_2 was found to be a decreasing function of molecular weight, as expected from the case of polymer solutions in incompressible solvents.[88] A_2 was also estimated to be proportional to M_w at the power of -0.4.

Although PFDA has a longer side chain, their solubility in sc-CO_2 is equivalent to amorphous PFOA.[85] Thus, 4 % wt of a PFDA (M_w = 254000 g.mol^{-1}) was fully soluble at pressures around 110 and 200 bar at respectively 25 and 50 °C.[89] Lacroix-Desmazes and coworkers even determined lower cloud point pressures of 85 and 160 bar at the same conditions of polymer content and temperature but for a lower M_w of 120000 g.mol^{-1}.[90,91] The influence of decreasing molecular weight on solubility also appeared negligible.[92,93] From static light scattering experiments, the theta pressure of this polymer at 25 °C was determined at 160 bar (i.e. a theta density around 0.89 g.cm^{-3}), which was above the observed cloud point pressure at 85 °C.[91] Above this pressure of 160 bar, the second virial coefficient was positive (see Figure I.25). The difference between the theta pressure and the cloud point ones was attributed to unfavorable interactions with CO_2 originating from the entropic contribution of the smaller chains. The theta pressure is actually the extrapolation of the cloud point pressures at infinite molecular weight. Finally, the length dispersity of the fluorinated chains in PTAN did not affect its solubility compared to those of PFDA and PFOA (see Figure I.26).[85] Thus, 4.9 % wt of a PTAN (unspecified M_w) was fully soluble at 190 bar and 50 °C.[94]

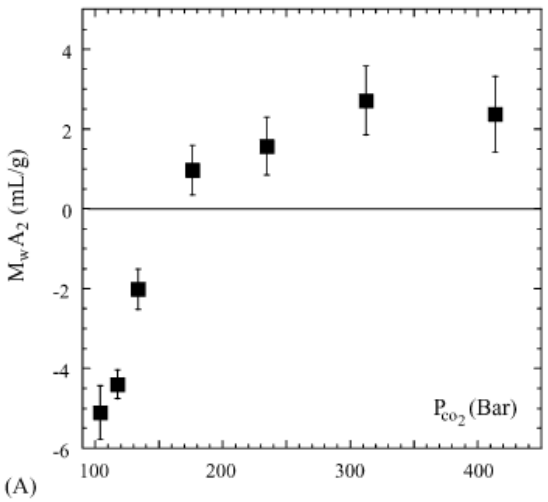

Figure I.25. Weight average molecular weight times second virial coefficient as a function of CO_2 pressure at 25 °C for a PFDA sample (≈ 4 % wt in CO_2). Reproduced from reference 91.

On the contrary, the introduction of a methyl group on the polymer backbone –thus changing acrylates into methacrylates– has a much greater impact on the solubility of fluorinated methacrylates compared to their acrylate analogs. Considering the case of poly(1,1,2,2-tetrahydroperfluorodecyl methacrylate) (PFDMA), the cloud point pressures were approximatively higher of 100 bar at 40 °C (see Figure I.26) compared to PFDA. This was related to the higher steric hindrance and the repulsive interactions provided by the methyl group. However, this effect was less pronounced at higher temperatures. Similarly to PFOA and PFDA, the second virial coefficient could also be evaluated via static light scattering measurements. The theta density at 25 °C was evaluated at 0.88 ± 0.02 g.mL^{-1} for a PFDMA sample having a M_w of 300000 g.mol^{-1}.[95]

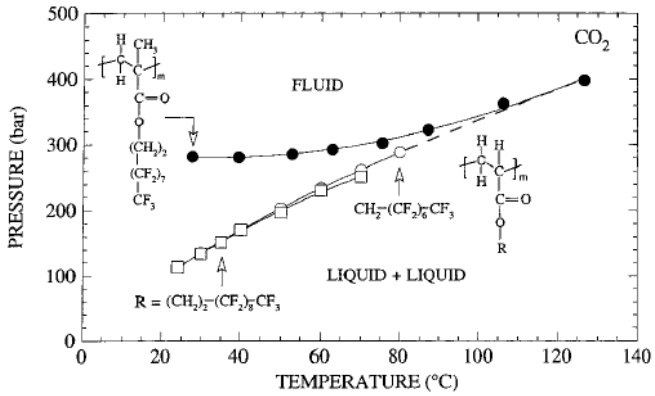

Figure I.26. Pressure-temperature phase diagrams for (▫) PTAN (◦) PFOA and (•) PFDMA samples with polymer contents ranging between 3 and 4 % wt. Reproduced from reference 85.

Similarly to perfluoropolyethers, the widely accepted explanation for the high solubility of fluorinated poly(acrylates) in sc-CO_2 is provided by their low cohesive energy densities and weak self-interactions. Johnston and coworkers reported surface tension values of 10-15 $mN.m^{-1}$, which is actually lower than the values for perfluoropolyethers and poly(vinyl acetate), the other aforementioned CO_2-philic references.

Thanks to their "true" CO_2-philicity, macromolecular engineering using fluorinated poly((meth)acrylates) as CO_2-philic building blocks has been largely investigated by CO_2 researchers.[90,96-98]

e) Poly(perfluorodiitaconates)

Following the high solubility of fluorinated poly((meth)acrylates), McHugh and coworkers investigated the CO_2-philicity of poly(perfluorodiitaconates) which differ from poly((meth)acrylates) by an additional fluorinated acrylate functionality replacing the methyl group (see Figure I.27).[99] Irrespective of the different side chain lengths and polymer content, these polymers (M_w near 150000 $g.mol^{-1}$) exhibited equivalent behaviours at low temperatures. Thus, their cloud point pressures were located near 150 bar at 40 °C, which is somehow comparable to those of fluorinated poly(acrylates) but lower than fluorinated poly(methacrylates).

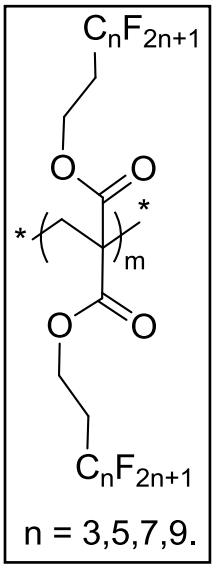

Figure I.27. Molecular structure of poly(perfluorodiitaconates).

f) Miscellaneous polymers with grafted perfluorinated side chains

As a consequence of the high solubility of fluorinated poly((meth)acrylates), the grafting of long perfluorinated chains has been applied to a variety of CO_2-phobic polymers including poly(styrene) and poly(para-phenylenes) to enhance their solubility in sc-CO_2.

Due to strong polymer-polymer interactions and a high T_g, polystyrene is practically insoluble in CO_2.[48] However, the etherification of chloromethylstyrene with 1,1,2,2-tetrahydroperfluorodecanol and the consecutive polymerization of the monomer provided high solubility in sc-CO_2 to the resulting poly(perfluorooctyl-ethyleneoxymethylstyrenes) (PFDS) (see Figure I.28).[90] For a polymer content of 4 % wt at 40 °C, a PFDS having a M_n of 43600 g.mol^{-1} thus exhibited a cloud point around 200 bar. This value was higher of approximately 60 bar compared to a PFDA having a M_n of 52600 g.mol^{-1}.

The same paradigm was applied to poly(para-phenylenes) (see Figure I.28).[100] While samples with fluorous or non-fluorous propyl side chains (unknown M_n) were insoluble in CO_2 even at 190 °C and 2400 bar, the extension to a 1,1,2,2-tetrahydroperfluorohexyl chain allowed the complete solubilization of 1.9 % wt of materials around 140 bar and 40 °C.

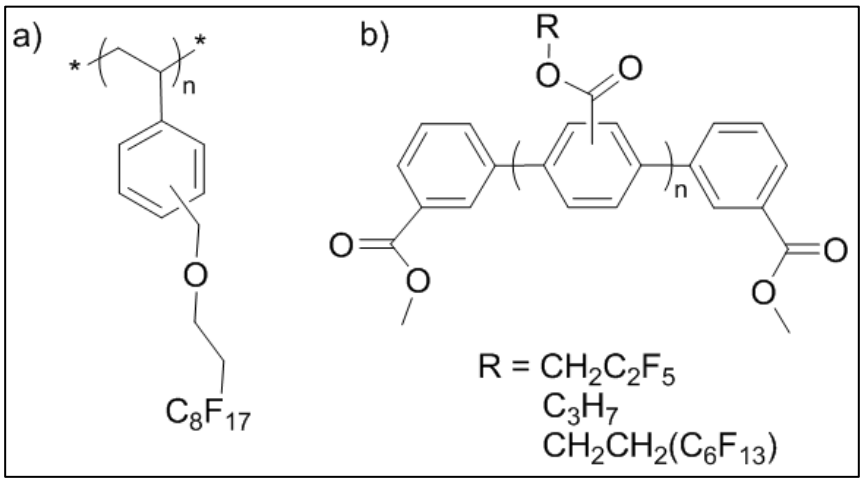

Figure I.28. Molecular structure of a) poly(perfluorooctyl-ethyleneoxymethylstyrene) (PFDS) and b) poly(para-phenylenes).

5. Poly(siloxane)-based copolymers

a) Poly(dimethyl siloxane)

Beside poly(ethers), poly(vinyl esters) and fluorinated poly((meth)acrylates), poly(dimethyl siloxane) (PDMS) has also attracted early attention from CO_2 researchers working on CO_2 thickeners. While studying the viscosity of PDMS solutions in sc-CO_2, Xiong and Kiran reported the phase behaviour of PDMS with increasing molecular weights.[101] For a polymer content of 5 % wt, the lowest M_w PDMS (M_w = 38900 g.mol^{-1}) showed a lowest cloud point pressure at 270 bar and 47 °C (see Figure I.29). Increasing M_w to 93700 and 273500 g.mol^{-1} resulted in the shift to higher pressures and temperatures, i.e. respectively around 300 bar and 49 °C, and 380 bar and 62 °C. The solubility of a PDMS of higher M_w (M_w = 369200 g.mol^{-1}) was then equivalent to that of the latter. Moreover, the shape of the pressure-temperature curves was characteristic of UCST and LCST behaviours of PDMS in sc-CO_2. As a result of an increase in molecular weights, the boundary between the two shifted to higher temperatures. This was confirmed by Melnichenko *et al.* who determined the theta temperature of PDMS to be 65 ± 5 °C through neutron-scattering experiments.[47] This theta temperature was also revealed to be density-dependant.[102] In a following study, Kiran and coworkers further examined the pressure-composition diagrams of a PDMS (M_w = 94300 g.mol^{-1}) in sc-CO_2.[46] While the demixing pressures increased with higher temperatures for T > 50 °C as expected, they also increased for T < 46 °C, which confirmed the UCST behaviour of PDMS.

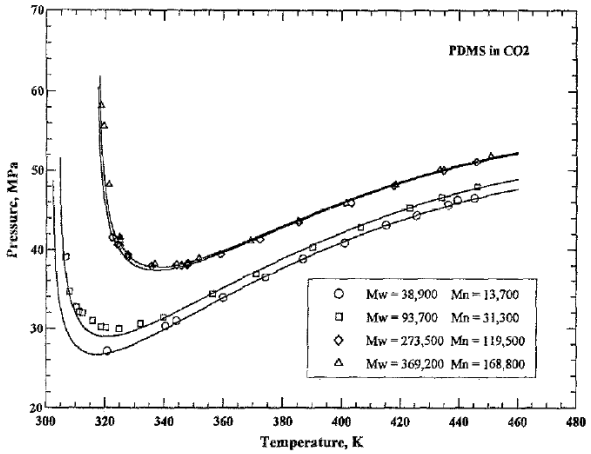

Figure I.29. Pressure-temperature diagrams of poly(dimethyl siloxanes) (5 % wt in sc-CO_2). Reproduced from reference 101.

Temperature-composition diagrams highlighted the influence of pressure on UCST and LCST behaviours (see Figure I.30). Thus, a so-called hourglass-shaped diagram was traced at a lower pressure of 380 bar with a single phase only observed for polymer contents either extremely low or higher than of 3 % wt. Increasing pressure to 440 bar resulted in the appearance of a single phase region between 320 and 360 bar for any polymer content. A further increase to 500 bar broadened the single phase zone.

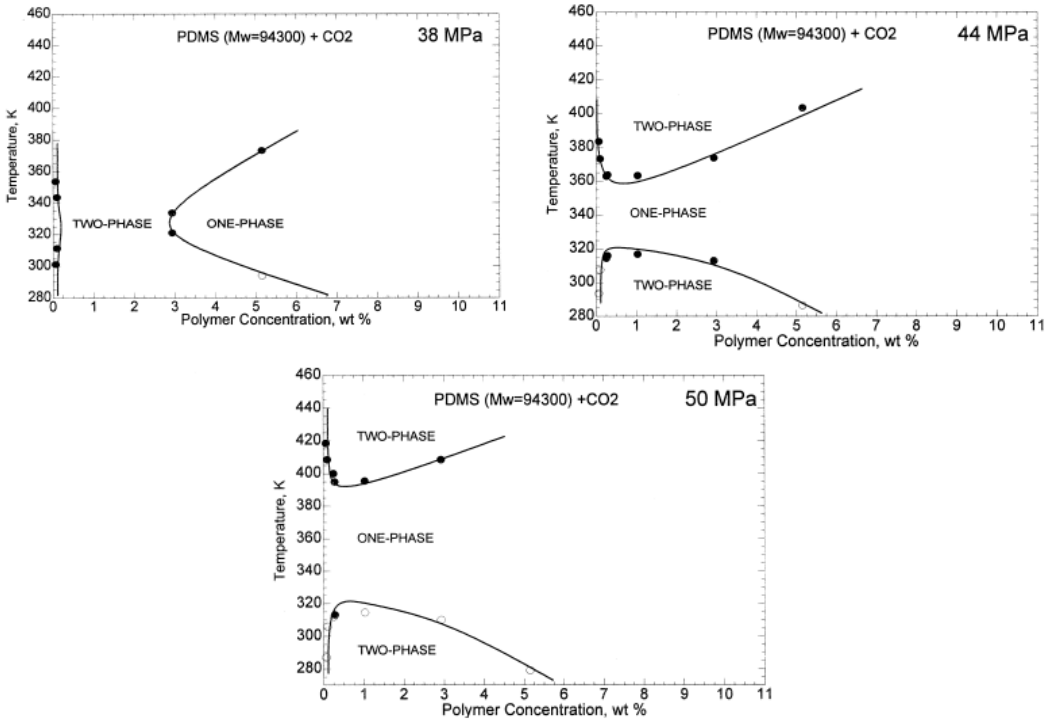

Figure I.30. Temperature-composition phase diagrams for a PDMS (M_w = 94300 g.mol^{-1}) at different pressures. Adapted from reference 46.

The simultaneous UCST and LCST behaviours of this polymer actually revealed the existence of an upper critical solution density (USCD). A representation of the pressure-density diagrams with isotherm curves clearly allows evidencing such phenomenon (see Figure I.31).Lower cloud points were observed for densities close to 1.0 g.cm^{-3}. The existence of a density dependence in the dynamic second virial coefficient for a PDMS (M_w = 75800 g.mol^{-1}) in sc-CO_2 was also reported through dynamic light scattering experiments.[45] However, the second virial coefficient calculated from static light scattering experiments remained negative in a density range of 0.97-1.01 g.cm^{-3}, contrary to perfluoropolyethers and fluorinated poly((meth)acrylates).[91]

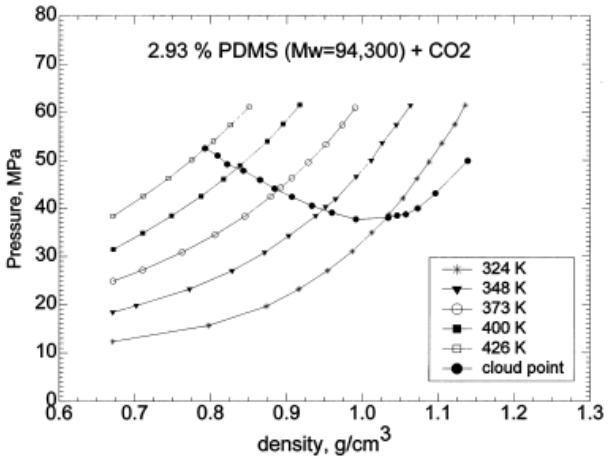

Figure I.31. Pressure-density phase diagrams with isotherm curves for a 2.93 % wt solution of PDMS (M_w = 94300 g.mol^{-1}) in sc-CO_2. Reproduced from reference 46.

Finally, neutron-scattering experiments also revealed a peculiar behaviour of PDMS in sc-CO_2.[47] In the case of a solution of PDMS (M_w = 47700 g.mol^{-1}) heated at a temperature of 32 °C -close to its UCST of 31.8 °C- and prepared at its overlap concentration, the solvent quality of CO_2 gradually increased until reaching a maximum at 520 bar. Beyond this theta pressure, the solvent quality decreased until the polymer chains collapsed at a pressure close to 900 bar. This was related to the existence of a lower critical solution pressure (LSCP). The phase behaviour of a PDMS (M_w = 75800 g.mol^{-1}) in sc-CO_2, as reported by Kostko *et al.*, perfectly illustrates this notion of LCSP (see Figure I.32).[45]

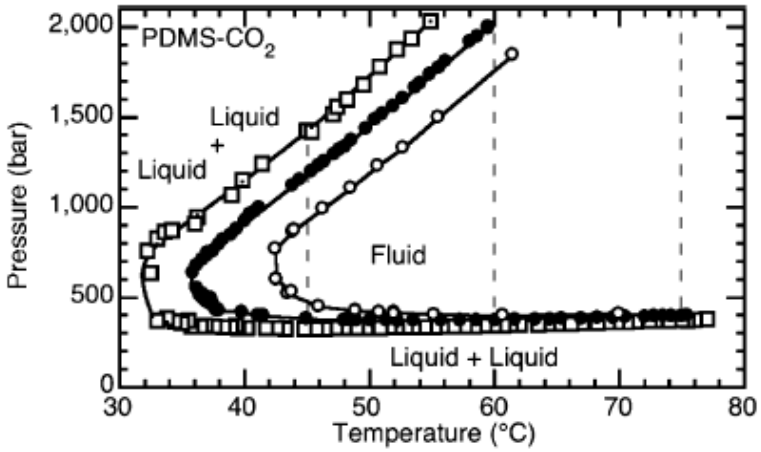

Figure I.32. Pressure-temperature phase diagram for a solution of PDMS in sc-CO_2 with polymer content of 0.077 % wt (open squares), 1.01 % wt (filled circles) and 7.0 % wt (open circles). Reproduced from reference 45.

Even though the Lewis-type interactions between CO_2 and a methoxytrimethylsilane model compound were calculated to be qualitatively high,[20] a widely accepted physical explanation for the high solubility of poly(siloxanes) in sc-CO_2 is both their low cohesive energy density and high chain flexibility, similarly to perfluoropolyethers and fluorinated poly((meth)acrylates). However, poly(siloxanes) exhibited higher cloud points pressures than fluorinated poly(acrylates), which may be explained by their higher surface tension (19-20 $mN.m^{-1}$ against 10-15 $mN.m^{-1}$).[103]

b) Strategies to enhance the CO_2-solubility of poly(siloxanes)

A strategy to decrease the cloud point pressures of poly(siloxanes) was developed with the grafting of side chains on copolymers of methyl hydrosiloxane and dimethylsiloxane. The enhancement of polymer-CO_2 interactions through pendant Lewis base groups was first considered. A statistical copolymer of 25 repeating units with an optimum of 5 units functionalized with propyl acetate (M_w = 2270 $g.mol^{-1}$, see Figure I.33 a)) showed a cloud point pressure at 145 bar and 22 °C for a polymer content of 0.8 % wt. This was lower by approximately 150 bar compared to its non-functionalized analogous.[104] In a following study, Beckman and coworkers investigated the influence of various Lewis bases.[22] At an equivalent substitution degree of 5, the propyl acetate group provided lower cloud point pressures than butyl methyl ketone and propyl ethyl ether. The phase behaviours were opposite yet with a substitution of only 2 units.

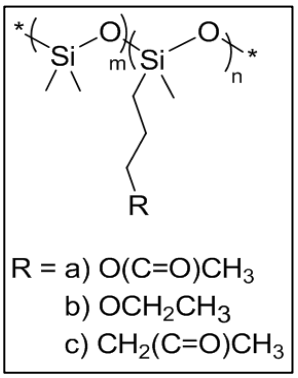

Figure I.33. Molecular structure of functionalized poly(siloxane)-based statistical copolymers.

A decrease in polymer-polymer interactions was also assessed synthesizing homopolymers of methylpropenoxyperfluoroalkyl siloxane.[85] For a polymer content of 3.5 % wt and a temperature of 25 °C, poly(siloxanes) functionalized with chains of either 5 or 7 fluorinated carbons (M_w = 14600 and 17700 g.mol^{-1}, see Figure I.33 b)) exhibited enhanced cloud point pressures around 100 bar while their hydrogenated equivalents could not be solubilized under mild conditions of pressure and temperature (P < 500 bar and T < 100 °C). By means of comparison, equivalent conditions were found for the propyl acetate-functionalized poly(siloxane) of lower molecular weight.[104] Lowering self-interactions thus revealed to be more efficient than increasing polymer-solvent interactions.

Given that PDMS is highly soluble in sc-CO_2, it was used as a CO_2-philic building block to synthesize a large variety of CO_2-soluble statistical, block and triblock amphiphilic copolymers with either hydrophilic or hydrophobic moieties. Interestingly, a hyperbranched amphiphilic copolymer with a poly(dimethyl siloxane) shell also exhibited a significant solubility in sc-CO_2.[67]

To prevent the use of expensive and harmful fluorinated moieties, Lacroix-Desmazes and co-workers suggested the introduction of poly(dimethylsiloxane) pendent groups (M_n = 736 g.mol^{-1}) via the "grafting through" macromonomer route.[105] The copolymerization of alpha-monomethacryloxypropyl PDMS with acetoacetoxyethylmethacrylate gave well-defined amphiphilic comb copolymers with a statistical composition along the polymer backbone. For a polymer content of 0.2 % wt in CO_2 at 40 °C, the cloud point of a sample with a M_n = 9900 g.mol^{-1} and a % mol of 21 % of CO_2-phobic units was observed around 200 bar. While a lower CO_2-phobic molar percentage of 11 % at a constant M_n had virtually no influence on the cloud point pressure, an increase of M_n to 27500 g.mol^{-1} at an equivalent composition gave pressures at 325 bar. A similar strategy implied the use of a 3-[tris(trimethylsilyloxy)silyl] propyl methacrylate monomer.[106]

6. Fluorinated poly(phosphazenes)

Polyphosphazenes are inorganic polymers with a polymer backbone made of phosphorus and nitrogen atoms and a high chain flexibility (see Figure I.34). Like poly(siloxanes), their side chains can be tuned to induce CO_2-philicity. The solubility

of poly[*P*-tris(trifluoroethoxy)-*N*-trimethylsilyl]phosphazene (M_w = 96000 g.mol^{-1}) has been investigated although no data was published on a non-fluorous equivalent .[103] Interestingly, this polymer demonstrated a high solubility in sc-CO_2 at 35 °C since a cloud point was observed around 185 bar for a polymer content of 4 % wt.

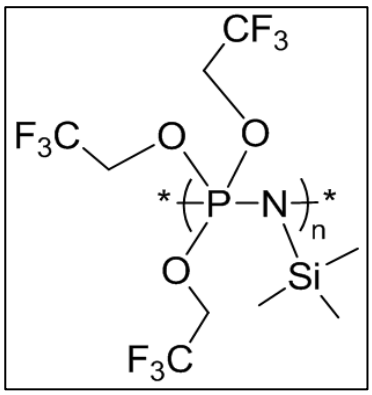

Figure I.34. Molecular structure of poly[*P*-tris(trifluoroethoxy)-*N*-trimethylsilyl]phosphazene.

D. Heuristics on the solubility of (co)polymers in sc-CO_2

As a general overview of the last paragraphs regarding the phase behaviour of polymers in CO_2, the following phase diagram summarizes the solubilities of main CO_2-philic polymers at 22 °C (see Figure I.35).

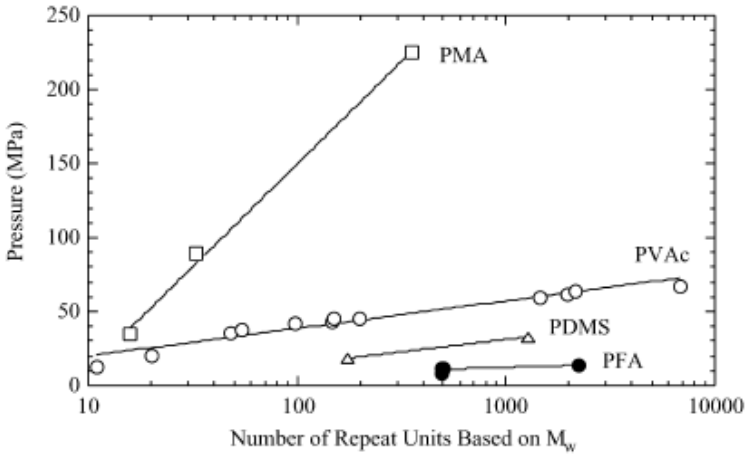

Figure I.35. Pressure versus number of repeat units phase diagrams at polymer contents of 5 % wt and 22 °C for binary mixtures of CO_2 and poly(methyl acrylate) (PMA), poly(vinyl acetate) (PVAc), poly(dimethylsiloxane) (PDMS) and a fluorinated poly(acrylate) (PFA). Adapted from reference 74.

Guidelines on the CO_2-philicity can be drawn from the nature of polymers and their relative solubility in sc-CO_2: the prominent factor is undoubtedly a low cohesive energy density –or weak polymer-polymer interactions– as illustrated by the solubility of fluorinated poly(acrylates), poly(dimethyl siloxane) and poly(vinyl acetate).[103] Moreover, their values of surface tension, respectively in the range of 10-15, 16-20 and 36 $mN.m^{-1}$, fully explain their comparative solubility (see Table I.3).

Although the surface tension of propylene oxide is lower than that of poly(vinyl acetate), the presence of multidentate Lewis base sites in PVAc dramatically enhances the solubility of PVAc in sc-CO_2. Thus, polymer-CO_2 interactions can be considered as a secondary lever to promote CO_2-philicity. From the respective T_g of PVAc and PPO, it appears that these interactions dominate entropy of mixing.

Finally, entropy of mixing appears minor compared to both enthalpic factors. However, it can occasionally play an important role, *e.g.* when comparing the solubilities of poly(methyl acrylate) and poly(methyl methacrylate).

Polymer	M_w ($g.mol^{-1}$)	Solubility	Surface tension ($mN.m^{-1}$)	T_g (°C)
Fluorinated poly(acrylate)	254000	110 bar 25 °C	10-15	-
Poly(dimethylsiloxane)	273500	380 bar 62 °C	19-20	-100
Poly(vinyl acetate)	182000	637 bar 25 °C	36	35
Poly(propylene oxide)	2030	436 bar 30 °C	30-32	-60
Poly(methyl acrylate)	30700	2250 bar 25 °C	41	19
Poly(methyl methacrylate)	3000	Insoluble	41	105

Table I.3. CO_2-philicity and physical properties of some representative homopolymers.

IV. Self-assembly of amphiphilic copolymers in sc-CO_2

Knowing the main parameters that determine the solubility of polymers in sc-CO_2, this part now focuses on the phase behaviour of copolymers that can present amphiphilic properties in CO_2. This class of polymers mainly benefits from the developments of macromolecular engineering –including mainly conjugation, coupling and controlled radical polymerization techniques– which have added another dimension to the study of CO_2-philic polymers. As a result of their high solubility in CO_2, fluorinated poly((meth)acrylates), perfluoropolyethers and poly(siloxanes) have constituted, so far in a quasi-exclusive way, the CO_2-philic building blocks of choice to synthesize amphiphilic materials for sc-CO_2. As it seems a rather exhausting task to describe all examples of CO_2-soluble amphiphilic copolymers, the following parts focus on representative examples of such copolymers, the organization in solution of which was investigated. The assembly of block, gradient and double CO_2-philic copolymers as well as more complex architectures such as comb, triblock, hyperbranched polymers and dendrimers are presented.

A. Block copolymers

Amphiphilic block copolymers that are soluble in CO_2 comprise a CO_2-philic block and a CO_2-phobic one, and are thus prone to form complex structures in solution such as micelle-like aggregates and polymersomes. As a result of their high solubility, fluorinated poly(acrylates) and polysiloxanes mainly constitute the CO_2-philic building blocks of choice to design CO_2-soluble amphiphilic copolymers.

In their seminal work, McClain *et al.* designed a series of poly(styrene)-*b*-poly(1,1-dihydroperfluorooctyl acrylate) (PS-*b*-PFOA) through a photopolymerization process using a tetraethylthiuram disulfide (see Figure I.36 a)).[107] The chain length of each block was varied with regards of their self-assembly behaviour. At 65 °C and 340 bar (i.e. a density of 0.842 g.mL^{-1}), these copolymers self-assembled into polydisperse spherical core-shell structures as evidenced by small-angle neutron scattering (SANS) (see Figure I.36 b)). For a PS block with a constant M_n of 3700 g.mol^{-1}, an increase in the PFOA chain length resulted in an

increase of the radius of the shell and a decrease of the swelling of the core. Inversely, the radius of the core and the aggregation number (N_{agg}) were constant. Increasing the radius of the core could be achieved by an increase of the chain length of the PS block. As a consequence, the scaling laws for block copolymer aggregates were equivalent in CO_2 and usual organic solvents. Finally, the influence of the solvent strength on the self-assembly of PS-*b*-PFOA surfactants was also evaluated. At a lower temperature (i.e. a higher density of 0.934 g.mL^{-1}), the solvation of both blocks was enhanced, which increased the radius of both core and shell, but decreased N_{agg}. The aggregation of PS-*b*-PFOA amphiphilic block copolymers were also corroborated by small-angle X-ray (SAXS)[108] measurements. Finally, the dynamic but slow exchange between unimers and copolymers aggregates was evidenced by DOSY-NMR experiments.[109]

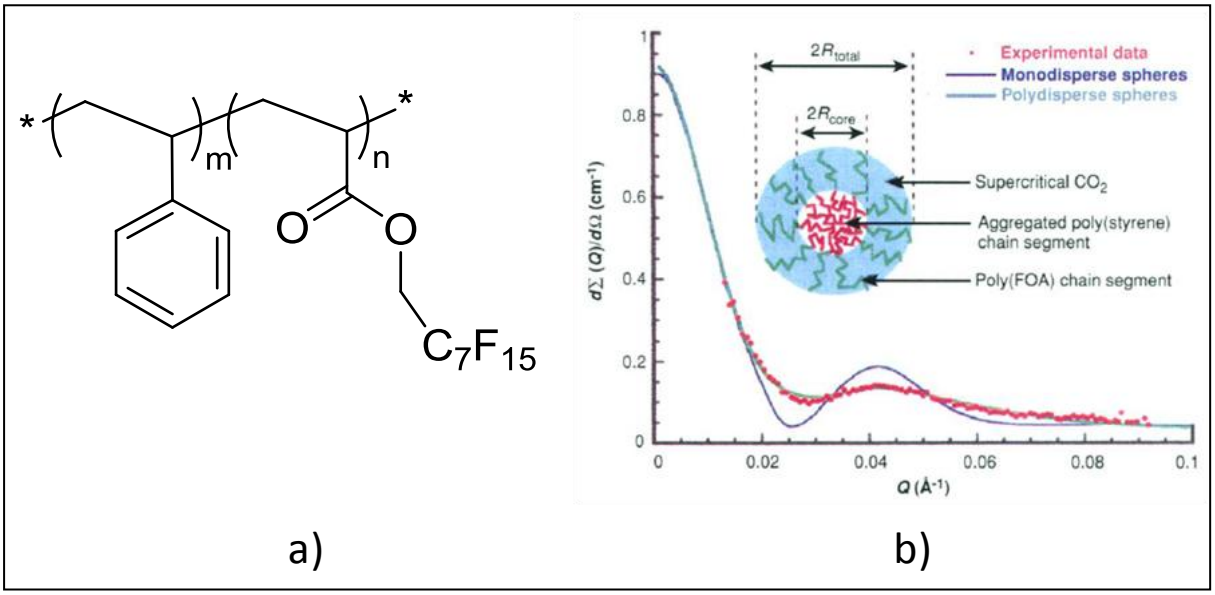

Figure I.36. a) Molecular structure of poly(styrene)-*b*-poly(1,1-dihydroperfluorooctyl acrylate) (PS-*b*-PFOA) b) SANS plot for a solution a PS-*b*-PFOA (with respective M_n of 3700 and 16700 g.mol^{-1}, at 4 % wt) in sc-CO_2 at 65 °C and 340 bar. Reproduced from McClain et al.[107]

Using poly(tert-butyl methacrylate) as the CO_2-phobic block, Lo Celso *et al.* studied the self-assembly of poly(tert-butyl methacrylate)-*b*-poly(1,1-dihydroperfluorooctyl methacrylate) (PtBMA-*b*-PFOMA) in sc-CO_2 at 45 °C (see Figure I.37).[110] Through SAXS and SANS experiments, a transition from a random coil to a polydisperse sphere model was evidenced suggesting the existence of a critical micelle density (CMD) in the range of 0.85–1.05 g.mL^{-1}. From different chain

lengths of both blocks, the CO_2-phobic part appeared to be the major influencing factor concerning the value of the CMD. Note that the CMD was a decreasing function of temperature. This transition was characterized by a two-step process where a phase separation between the solvent and the polymer chain first occurred upon decreasing pressure. Then, the CO_2-philic moiety reoriented towards the solvent-rich domains, which led to the formation of aggregates. The kinetics of the second step was revealed to be slower and depended on the pressure jump.

The unimer-to-aggregates transition was spotted by SAXS experiments on a solution of poly(2-tetrahydropyranyl methacrylate)-*b*-poly(1,1-dihydroperfluorooctyl methacrylate) (PHPMA-*b*-PFOMA) in sc-CO_2 at 52 °C (see Figure I.37).[111] Three distinctive behaviours were identified. While the copolymer was insoluble for pressures lower than 121 bar, the radius of gyration (R_g) gradually increased with pressures increasing from 121 to 220 bar, suggesting the association of unimers into aggregates. The values of R_g were then constant around 3 nm for pressures between 220 and 335 bar, and decreased for higher pressures as the aggregates partially dissolved.

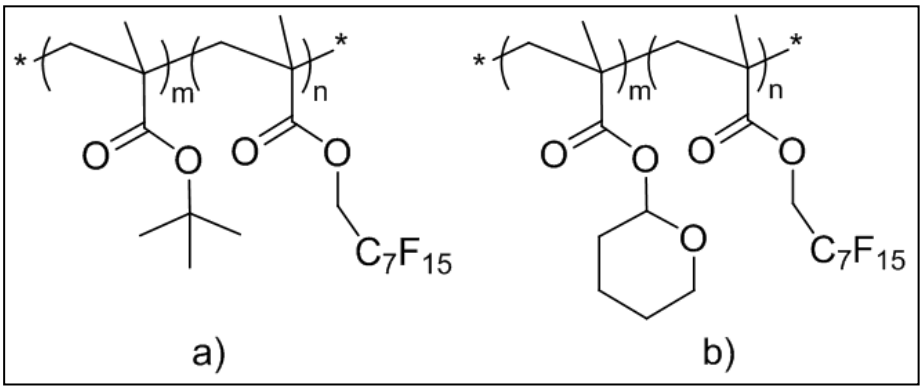

Figure I.37. Molecular structure of a) poly(tert-butyl methacrylate)-*b*-poly(1,1-dihydroperfluorooctyl acrylate) (PtBMA-*b*-PFOMA) and b) poly(2-tetrahydropyranyl methacrylate)-*b*-poly(1,1-dihydroperfluoro-octyl methacrylate) (PHPMA-*b*-PFOMA).

Perfluoropolyethers were also used as CO_2-philic building blocks to design amphiphilic block copolymers. Lodge and coworkers synthesized two examples of poly(lactide)-*block*-poly(hexafluoropropylene oxide) (PLA-*b*-PFPO, M_n around 10000 g.mol^{-1}) with varying CO_2-philic/CO_2-phobic balances (see Figure I.38).[65] The self-assembly of these copolymers in CO_2 at 25 °C and 400 bar was studied by

dynamic light-scattering (DLS). A 1 % wt solution of a copolymer ($M_{n,PLA}$ = 4000 g.mol^{-1}, $M_{n,PFPO}$ = 6000 g.mol^{-1}) was found to self-assemble into spherical aggregates with a hydrodynamic radius (R_h) of 4 nm. Interestingly, the R_h of a copolymer with a lower CO_2-philic/CO_2-phobic balance ($M_{n,PLA}$ = 5000 g.mol^{-1}, $M_{n,PFPO}$ = 4000 g.mol^{-1}) was 135 nm although the maximum chain length was evaluated at 30 nm for this copolymer. Upon freezing of the solution and redispersion in a PFPO selective solvent, observations via transmission electron microscopy (TEM) revealed the formation of polymersomes (i.e. polymer vesicles). To date, this constitutes the unique example of such structures in CO_2.

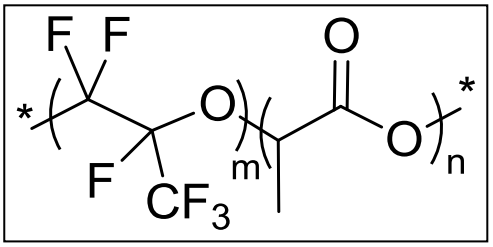

Figure I.38. Molecular structure of poly(hexafluoropropylene oxide)-*block*-poly(lactide) copolymers.

B. Amphiphilic gradient copolymers

Contrary to amphiphilic block copolymers, gradients copolymers exhibit a composition gradient along their chain. They can be synthesized by controlled radical polymerization techniques and all chains have virtually the same composition by virtue of this. They thus differ from statistical copolymers which are mainly produced via free radical polymerization and where each chain has a different composition. As a consequence, the properties of gradient copolymers are expected to be intermediate between those of block and statistical copolymers. Additionally, their kinetics of aggregation and exchange can be faster than in the case of block copolymers.

Building on the lower reactivity ratios of 1,1,2,2-tetrahydroperfluorodecyl acrylate) (PFDA) compared to methacrylates and styrenics, Ribaut *et al.* synthesized amphiphilic gradient copolymers incorporating either acetoacetoxyethyl methacrylate, vinyl benzylphosphonic acid diethylester or vinyl benzylphosphonic acid by controlled radical polymerization (see Figure I.39).[92] The gradient structures

could be confirmed by monitoring the individual conversions of each monomer. At similar conditions of composition, molecular weight and polymer content, these gradient copolymers exhibited enhanced solubilities in CO_2 compared to equivalent block copolymers.[112] Interestingly, the nature of the CO_2-phobic monomer hardly had any effect on the solubility of gradient copolymers contrary to diblock copolymers where it dominated over composition effects.

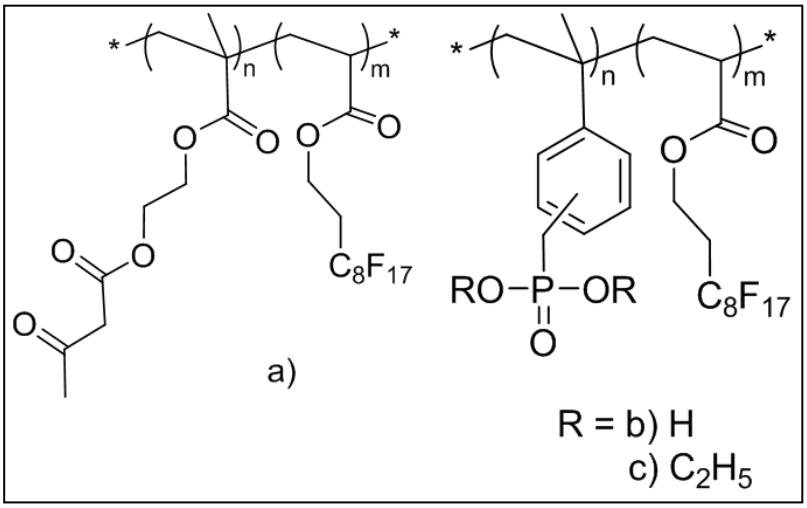

Figure I.39. Molecular structure of gradient copolymers synthesized by Ribaut *et al.*[92]

Their self-assembly behaviour in sc-CO_2 was then revealed by SANS experiments.[112] As a general trend, both composition and molecular weight of the gradient copolymers had little influence of R_g and N_{agg}. Comparing the organization of equivalent block and gradient copolymers above their respective cloud points, R_g was found lower for the block sample whereas N_{agg} was similar. Parallel to the cloud point observations, this suggested the lower solvation of block copolymer aggregates as a result of a better microphase separation. Experimental parameters such as pressure, temperature and density were also investigated (see Figure I.40).[112] In the case of acetoacetoxyethyl methacrylate-based gradient copolymers at 4 % wt in sc-CO_2, an increase of pressure from 140 to 210 bar resulted in N_{agg} and R_g respectively decreasing from 2.9 to 1 and from 3.3 to 2.5 nm. This corresponded to the transition from small aggregates to unimers resulting from the enhancement of solvent strength of CO_2. This evidenced a pressure-induced aggregation. Similarly, a decrease in temperature from 55 to 40 °C at a constant pressure of 210 bar resulted in a better solvent quality –i.e. a higher density and increased R_g. This was

characteristic of a temperature-induced aggregation. However, the existence of hydrogen bonding between poly(acetoacetoxyethyl methacrylate) blocks limited the enhancement of aggregation compared to a purely density-induced phenomenon. The same remark on H-bonds applied when changing both temperature and pressure at a constant CO_2 density of 0.76 $g.mL^{-1}$. The aggregates were actually more swollen due to temperature effects.

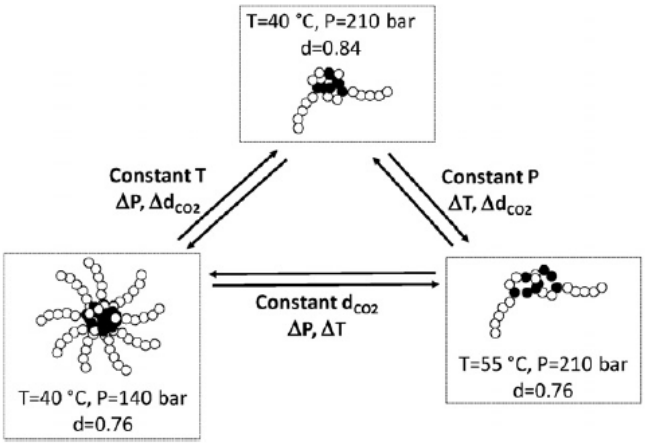

Figure I.40. Experimental parameters investigated for the solubility of gradient amphiphilic copolymers in sc-CO_2. Reproduced from reference 112.

C. Double CO_2-philic block copolymers

Similarly to double hydrophilic block polymers, double CO_2-philic copolymers are made of two chemically different blocks soluble in CO_2. At high pressures, they behave as fully soluble block copolymers. Their amphiphilic behaviour can be induced by a change in pressure or temperature which renders CO_2 a selective solvent for a specific block. The resulting amphiphilic copolymers with a CO_2-philic outer shell and a CO_2-phobic core can be expected to self-assemble into aggregates or polymersomes. To date, the only example of double CO_2-philic copolymers concern block copolymers comprising a fluorinated poly(acrylate) block and a poly(vinyl acetate) one (see Figure I.41).

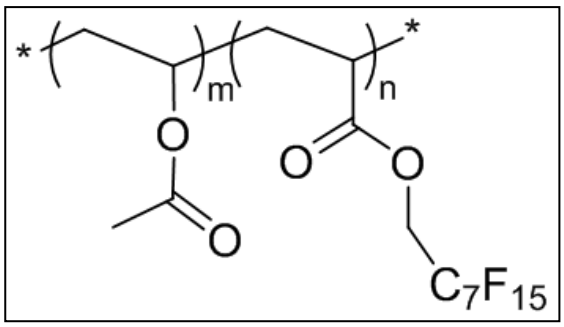

Figure I.41. Schematic molecular structure of a double CO_2-philic block copolymer comprising PFOA (or PTAN) and PVAc blocks.

In their work, Zhou and Chu used dynamic light scattering (DLS) to study the pressure-induced aggregation of a poly(1,1-dihydroperfluorooctyl acrylate)-*b*-poly(vinyl acetate) (PFOA-*b*-PVAc) block copolymer under a isothermal process at 65 °C.[113] The respective molecular weights of the blocks were 43100 and 10300 g.mol^{-1}. The block polymer exhibited distinctive aggregation states depending on pressure and concentration. For a concentration of 0.057 g.mL^{-1}, a first transition was observed at 148 bar, which corresponded to the appearance of well-defined unimers with a hydrodynamic radius of 2.2 nm in solution. Then, a small fraction of polydisperse aggregates with a $<R_h>$ around 500 nm coexisting with unimers were formed at 225 bar. With increasing pressures of 242, 310, 345 and 379 bar, the large aggregates disappeared at the benefit of a high proportion of narrowly distributed micelles with a $<R_h>$ of 23 nm. Within this range of pressure, the micelle-to-unimer intensity ratio and the number aggregation respectively from decreased 30:1 to 11:1, and from 18 to 9. Inversely, the calculated critical micelle concentration increased from 0.021 to 0.033 g.mL^{-1}. At higher pressures, aggregates formed again and the micelles gradually disappeared at the benefit of both aggregates and unimers until reaching a pressure of 552 bar where all micelles disappeared. This value was taken as the critical micelle pressure. The complex behaviour of this copolymer was attributed to the composition heterogeneity of the polymer sample, resulting from its dispersity.

Using the same polymer sample, Chu and coworkers also studied the influence of temperature on the aggregation states under a isobaric process at 225 bar and for

a polymer concentration of 0.024 g.mL^{-1}.[111] At 65 °C, ill-defined aggregates with a $<R_h>$ and unimers were concomitantly observed. With a decrease of solvent quality at 55 °C, the disappearance of unimers was observed while aggregates and micelles having a $<R_h>$ around 20 nm coexisted. Lowering the temperature to 35 °C and 30 °C resulted in the increase of the aggregate:micelle ratio and, finally, the solely existence of large particles. The critical micelle temperature (CMT) was estimated at around 33 °C for these particular conditions of concentration and pressure.

Parallel to CO_2-philic homopolymers and their upper critical solution density, the existence of both CMT and CMP transitions is actually indicative of a critical micelle density (CMD). This concept was introduced by Buhler *et al.*,[75] performing static and dynamic light scattering studies on a poly(1,1-dihydroperfluorooctyl acrylate)-*b*-poly(vinyl acetate) (PTAN-*b*-PVAc) block copolymer (see Figure I.42). The respective molecular weights of the blocks were 43100 and 4400 g.mol^{-1}. Through the examination of aggregation numbers (N_{agg}), this copolymer was found insoluble at densities lower than 0.814 g.cm^{-3} (N = 120) and fully soluble at densities higher than 0.95 g.cm^{-3} (N_{agg} = 1). Although N decreased with increasing density resulting from the better solvation of both blocks, spherical micelles with a constant $<R_h>$ around 15 nm were observed in between. This appeared as a consequence of compensating effects of the excluded volume parameter for the shell chains and the core-shell interfacial tension. Finally, the critical micelle concentration –*i.e.* the transition curve between spherical micelles and free copolymers– was determined to depend on density. The CMD phenomenon was also confirmed through small-angle neutron (SANS) and X-ray scattering (SAXS) studies.[114-116] A transition from a random coil to a polydisperse core-shell could be modeled with either increasing pressures at 40 °C or temperatures at 240 bar.[114]

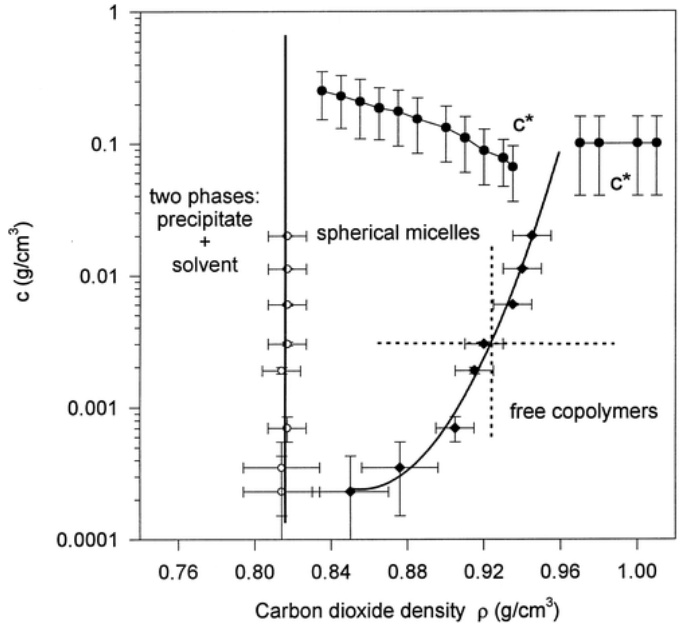

Figure I.42. Polymer concentration-density phase diagram for a binary mixture of CO_2 with poly(1,1-dihydroperfluorooctyl acrylate)-*b*-poly(vinyl acetate) at 45 °C ($M_n \approx 47500$ g.mol^{-1}). Reproduced from reference 75.

D. Amphiphilic graft and comb copolymer

Graft and comb copolymers are another fascinating class of polymers. They are made distinctive by their synthesis pathway. Graft copolymers are obtained through either the grafting on or the grafting from methods. The macromonomer route is used for the synthesis of comb copolymers. Regarding the solubility and self-assembly of graft and comb copolymers, the macromolecular parameters of study are the graft chain length, the graft chain density and the backbone length.

An amphiphilic comb copolymer could be synthesized from the free-radical copolymerization of a 1,1-didydroperfluorooctyl acrylate monomer with a poly(ethylene glycol) styrenic macromonomer (see Figure I.43.a).[117] The self-assembly of this polymer with PEO grafts having a M_n of 5000 g.mol^{-1} and an overall PEG % wt of 15-18 % was investigated through SANS experiments performed at 333 bar and 65 °C.[64] Aggregates with a R_g of 5,6 nm and a N_{agg} of 3 were deduced from a polydisperse core-shell model. The aggregates were demonstrated to swell upon incorporation of water in binary mixtures.

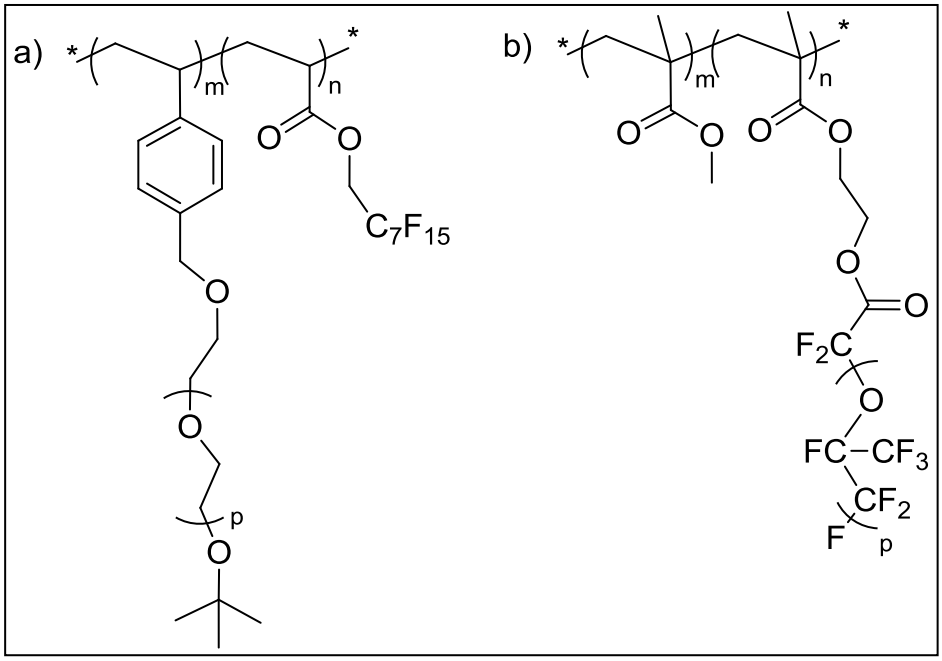

Figure I.43. Molecular structure of amphiphilic comb and graft block copolymers.

Lepilleur *et al.* examined the phase behaviour of a series of statistical perfluoropolyether-grafted poly(methyl methacrylate-*co*-hydroxyethyl methacrylate) in CO_2 (see Figure I.43.b).[66] These copolymers were synthesized via the grafting of a carboxylic acid-terminated perfluoropolyether on a statistical poly(methyl methacrylate-*co*-hydroxyethyl methacrylate[66] backbone. For shorter polymer backbone lengths, the cloud point pressures could be decreased by increasing either graft chain lengths or graft chain density until a minimum in pressure was reached. Beyond this minimum, further increases resulted in higher cloud point pressures and the domination of molecular weight effects over lowered polymer-polymer interactions. As expected, longer polymer backbones and higher CO_2-phobic/CO_2-philic balances resulted in higher cloud point pressures. The best strategy to enhance the solubility of comb polymers was built on a high grafting density with low molecular weights grafts.

E. Amphiphilic hyperbranched polymers and dendrimers

These classes of polymers are of special interest as unimolecular aggregates in sc-CO_2. The CO_2-solubility of hyperbranched polymers and dendrimers having a hydrophilic core is usually achieved via the grafting of either perfluorinated chains[67,118,119] or CO_2-philic polymers (see Figure I.44).[67] Mecking et al. thus functionalized a hyperbranched polyethylene imine core (M_w = 5000 g.mol^{-1}) by imidazole-coupling with a long perfluorinated chain or a poly(hexafluoropropylene oxide) one (see Figure I.44).[67] At a density of 0.88 g.mL^{-1}, 0.3 % wt of a perfluorinated sample with a CO_2-phobic/CO_2-philic balance of 3.2 was soluble. At a constant balance, the solubility was approximately twice as high as the perfluopolyether polymeric chain.

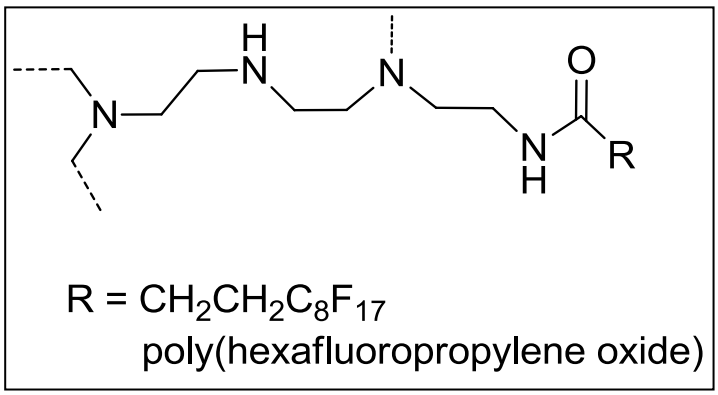

Figure I.44. Molecular structure of hyperbranched polymers and dendrimers grafted with fluorinated moieties.

V. Macromolecular surfactants for water/carbon dioxide emulsions.

Since water is a highly cohesive and polar solvent, its solubility in sc-CO_2 is extremely low. Using a flow method, it was determined to be less than 0.5 % wt at pressures and temperatures up to 450 bar and 75 °C (see Figure I.45).[120] It thus makes water an interesting dispersed phase to solubilize CO_2-phobic polar and ionic solutes in CO_2, provided that an emulsion is formed. This has stimulated the synthesis of macromolecular surfactants specifically designed to stabilize the water-CO_2 (W/C) interface. The next paragraphs focus on the stabilization of such interface with amphiphilic block copolymers and their derived architectures.

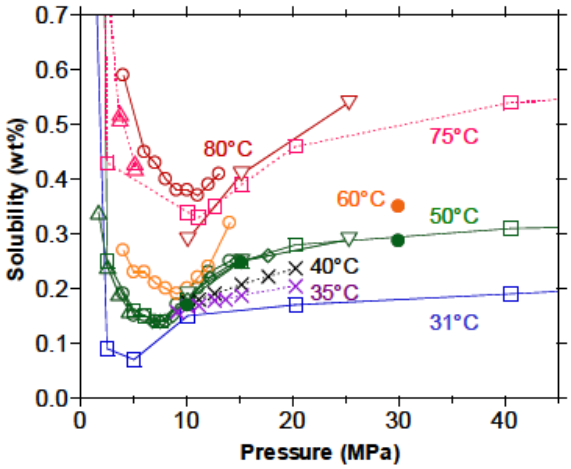

Figure I.45. Solubility of water in sc-CO_2 as a function of pressure and temperature. Reproduced from reference 121.

A. General considerations about emulsions

The creation of an interface surface between two liquids is characterized by a difference in the Gibbs free energy per area, which is defined as the surface tension (γ). In other terms, the cost of energy to create the interface is proportional to the product of the interfacial tension and the surface area. The stability of the interface will be thus related to a low surface tension, which can be achieved through the use of appropriate surfactants. The hydrophiphilic-lipophilic balance (HLB, also called hydrophilic/CO_2-philic balance (HCB) for CO_2 applications) and the surface tension of the surfactant will thus determine the curvature of the interface. According to the

empirical Bancroft's rule, the continuous phase is the prefered phase of the emulsifier. Several cases can be distinguished:

- The surfactant prefers the aqueous phase. Carbon dioxide/water (C/W) emulsions then coexist with a surfactant-poor carbon dioxide phase (so-called Winsor I type emulsions).

- The surfactant prefers the carbon dioxide phase. Water/carbon dioxide (W/C) emulsions then coexist with a surfactant-poor aqueous phase (Winsor II).

- The surfactant has equal affinity for both phases, the curvature is zero and the surface tension is then at a minimum. When the surfactant concentration is low, three phases can coexist, i.e. a intermediate surfactant-rich middle phase, a surfactant-poor carbon dioxide phase and a surfactant-poor aqueous phase (Winsor III). When the surfactant concentration is high, a single-phase emulsion can be obtained (Winsor IV).

The Winsor III and Winsor IV emulsions are usually more difficult to stabilize as the bending of the interface is lower. The gradient in γ which originates from the tangential flow of the continuous phase between dispersed droplets then tends to zero, thus weakening the so-called Marangoni-Gibbs stabilizing effect. Additionally, the bending elasticity of the stabilizing monolayer in Winsor III/IV is higher, which favors its rupture and subsequent coalescence phenomenons.

Phase transitions between Winsor types can be achieved by manipulating the formulation variables such as temperature, pressure, pH, ionic strength and HCB (see Figure I.46). In the case of temperature, this corresponds to the so-called phase-inversion temperature.

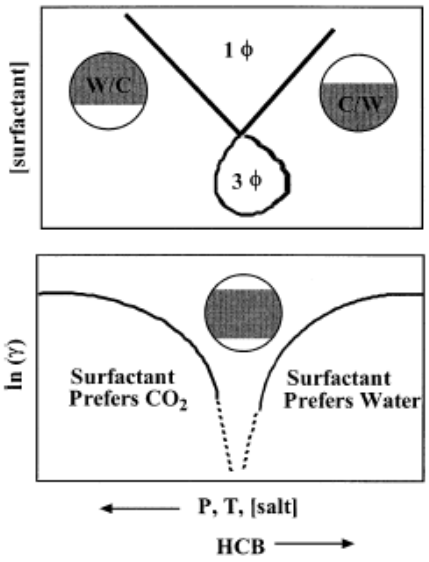

Figure I.46. Schematic diagram indicating the relationship between formulation variables, emulsion morphology, and interfacial tension (γ).

Emulsions can be categorized in three parts. Macroemulsions are large droplets –with a average size above 500 nm– which are only kinetically stable due to a high interfacial free energy. They are formed upon stirring with a low percentage of surfactant, typically less than 5 % wt. Miniemulsions (also called nanoemulsions) which are usually obtained by phase inversion methods, ultrasonification or homogenization at high pressures exhibit a average diameter of 50-500 nm but are only kinetically stable too. Compared to macroemulsions, their resistance to flocculation and sedimentation is enhanced due their lower size.

Because of their thermodynamic unstability, macro- and microemulsions can be destabilized by various mechanisms :

- flocculation (or aggregation), i.e. the clustering of two or more droplets as a result of attractive Van der Waals forces between dispersed droplets. These forces can be overcome by steric repulsion with an appropriate surfactant.

- coalescence, i.e. the merging of two or more droplets to form larger ones. This is caused by the rupture of the thin layer of the continous phase between flocculated droplets.

- Ostwald ripening which is a thermodynamically-driven process characterized by the growth of larger particles to the detriment of smaller ones to reduce the free energy of the system.

- creaming, i.e. the migration of the dispersed to the bottom (or top) of the mixture, depending on relative densities of phases.

- sedimentation, i.e. the settling of particles due to gravity effects.

Thermodynamically-stable emulsions are named microemulsions as a result of their lower diameter below 50 nm, which prevents them from destabilization mechanisms such as Ostwald ripening or flocculation. To achieve so, higher concentrations of surfactant –typically 10 % wt–are necessary, provided that the surfactant decreases the surface tension enough. Contrary to the milky appearance of macroemulsions, microemulsions are translucent and can be thus considered pseudo-monophasic systems.

B. Water/CO_2 interface

Johnston and coworkers investigated the interfacial tension between water and CO_2 by the pendant drop method and its dependence on pressure and temperature.[121] The drop shape was analyzed after 1 hour to get closer to the thermodynamic equilibrium. Upon pressure, two distinctive behaviours were observed (see Figure I.47). Below 70 bar, the interfacial tension decreased with increasing pressures –and consequently higher density of CO_2. Above 70 bar, the decrease in γ was smaller as the compressibility of CO_2 is smaller at higher pressures. In this range of pressures, the value of the W/C interfacial tension was close to 20 $mN.m^{-1}$. This value was lower than the one estimated in previous works where shorter equilibrium times were used. Interestingly, the interfacial tension of W/C is lower than the γ values for water/alkanes interfaces, which both reflects higher interactions between CO_2 and water and a better solubility of CO_2. Note that a local

minimum in the evolution of γ versus pressures was observed around 70 bar. This phenomenon was amplified at temperatures closer to the critical point.

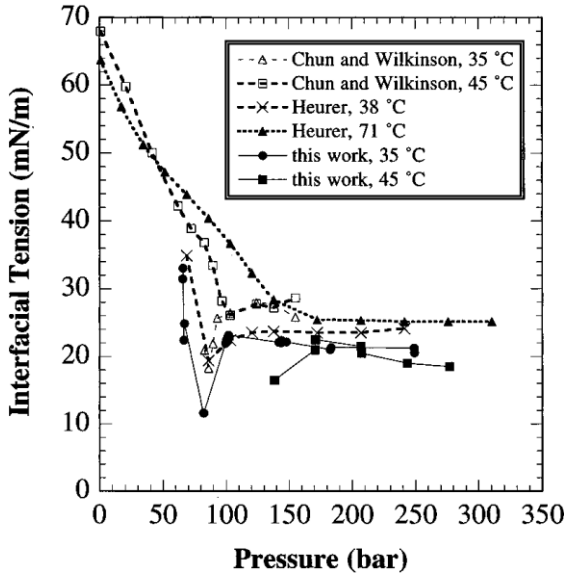

Figure I.47. Surface tension at the water/carbon dioxide interface as a function of temperature and pressure. Reproduced from reference 122.

C. Water/CO_2 macroemulsions

Due to the larger interfacial area of macro- and microemulsions, the requirements for surfactants for lowering the interfacial tension are less stringent than for microemulsions. The range of surfactants conceivable to stabilize W/C macro- and microemulsions is therefore larger. Referring to the design of macromolecular surfactants which both include CO_2-philic and hydrophilic repeating units in block, statistical or more complex structures, the CO_2-philic building block can be selected among polymers having a substantial solubility in sc-CO_2. As exposed in previous paragraphs, the use of perfluoropolyethers, fluorinated poly((meth)acrylates), poly(siloxanes), poly(alkylene oxides) or poly(vinyl esters) as CO_2-philic building block can be therefore considered. Advantageously, the solubility of polymers is somehow primarily related to their surface tension, which translates to the nature of the stabilizable emulsion.

1. Poly(alkylene oxide)-based copolymers

a) Poly(propylene oxide)-based copolymers

Regarding potential applications, the use of non-fluorous moieties in the stabilization of W/C emulsions would be preferable. Adding to the lower values of surface tension required to stabilize W/C emulsions, poly(alkylene oxides) are ideal candidates to do so. In this perspective, Da Rocha *et al.* studied the behaviour of poly(propylene oxide)-*b*-poly(ethylene oxide)-*b*-poly(propylene oxide) (PPO-*b*-PEO-b-PPO) at the W/C interface as a function of their M_w and HCB.[121] Using a high pressure pendant drop tensiometer at 45 °C, 276 bar and 0.1 % wt of polymer content, these triblock copolymers were demonstrated to lower the water /CO_2 interfacial tension to 2.3-5.1 mN.m^{-1}. The lowest γ was found for a symmetric triblock copolymer comprising 30 propylene oxide units and 26 ethylene oxide ones. Although its partitioning between water and CO_2 should favor the formation of C/W emulsions, a slightly turbid W/C emulsion with 0.1 % wt of surfactant/CO_2 and less than 1 % w/w of water could be stabilized for over 10 minutes. Inversely, PEO-*b*-PPO-*b*-PEO surfactants with low HCB only stabilized C/W emulsions, which again constituted an exception to the Bancroft's rule.[122] This was related to the low viscosity of CO_2 which favors the coalescence of the droplets.

b) Poly(butylene oxide)-based copolymers

In the same study, the formation of W/C macroemulsions with a poly(butylene oxide)-*b*-poly(ethylene oxide) (PBO-*b*-PEO) sample was also studied.[121] Even though the change from PPO to PBO resulted in a decreased CO_2-philicity, the absorption of the surfactant at the W/CO_2 interface was stronger than for the PPO-based analogous, as evidenced by a lower γ of 1.4 mN.m^{-1}. While a W/C curvature could be expected upon increasing temperature and adding salts, only C/W macroemulsions were observed with 1 % wt of surfactant. However a Winsor III-type emulsion of low stability (< 1 minute) was observed at a temperature of 65 °C and 2 mol of KBr.

2. Poly(vinyl acetate)-based copolymers

Although poly(vinyl acetate) has a higher solubility in sc-CO_2 than poly(propylene oxide), the formation of W/C macroemulsions using non-ionic poly(vinyl acetate)-based surfactants has not been proved so far. Due to a high tendency to partition into the aqueous phase, they were proven to be efficient surfactants to stabilize C/W emulsions.[82,83,123] The incorporation of a ionic hydrophilic block could overcome this by providing a better adsorption at the W/C interface.[124]

3. Poly(siloxane)-based copolymers

a) Block copolymers with a non-ionic hydrophilic block

The formation of W/C macroemulsions using a PDMS-based amphiphilic copolymer with a pH-neutral poly(hydroxyethyl methacrylate) (PHEMA) hydrophilic block was reported by Psathas *et al.*[125] At densities higher than 0.8 g.mL^{-1}, 1 % wt of a PDMS-*b*-PHEMA (M_n(PDMS)= 10000 g.mol^{-1}, M_n(PHEMA) = 4700 g.mol^{-1}) in a 50:50 (w/w) water/CO_2 mixture was able to form an emulsion stable for at least 90 minutes. This stability could last for over 5 hours when temperature was decreased between 22 and 34 °C at a constant density of 1 g.mL^{-1}.

b) Block copolymers with a pH-sensitive hydrophilic block

The stability of a W/C emulsion stabilized by 1 % wt of a block copolymer comprising a PDMS block (M_n = 10000 g.mol^{-1}) and a poly(acrylic acid) one (1500 g.mol^{-1}) (PDMS-*b*-PMA) was reported to decrease upon decreasing CO_2 densities as a result of a gradual collapse of the PDMS tails.[126] The flocculation of W/C emulsions stabilized by PDMS-based amphiphilic copolymers can be actually related to the CO_2 density. Additionally, the greater difference between the aqueous and CO_2 phase densities accelerates the sedimentation of the flocculated emulsions. Note that an increase in temperature at a constant density furthers stabilized the formed W/C emulsions. An increase in the chain length of the PDMS blocks could not provide sufficient steric stabilization of the W/C emulsions in order to prevent flocculation.

On a series of PDMS-*b*-PAA copolymers with varying CO_2-philic and hydrophilic chain lengths, the tuning of pH allowed to enhance the resistance to flocculation, as a general rule. While the stability was low at a pH of 3, the progressive ionization of the carboxylic groups with an increase of pH from 3 to 5 led to a better adsorption of the surfactant at the W/C interface and enhanced time stabilities. Beyond a pH around 5, a maximum of stability was noted until the balanced state was approached and a Winsor-III emulsion was observed. Furthermore, the pH values corresponding to this maximum in stability increased for surfactants of lower molecular weights while the emulsions were increasingly stable with shorter PDMS chain lengths at this maximal pH. No C/W emulsions were observed in the case of PDMS-*b*-PAA upon increasing pH up to 9.

When changing the nature of the hydrophilic block from PAA to either poly(methacrylic acid) or a statistical block comprising both acrylic acid and tert-butyl acrylate repeat units, similar trends were observed. Additionally, an inversion from W/C to C/W curvatures upon increasing pH was noted for the poly(methacrylic acid)-containing amphiphilic copolymer with the shortest chain length.[125]

c) Amphiphilic comb copolymers with a non-ionic hydrophilic block

Johnston and coworkers investigated the ability of commercial poly(dimethylsiloxane)-based graft copolymers to stabilize W/C macroemulsions.[121] Through the comparison of the nature of the graft chains, a minimum in interfacial tension was observed for 0.1 % wt of a $PDMS_{24}$-*g*-EO_{22} at 45 °C and a density of 0.88 $g.mL^{-1}$. The W/C interfacial tension was lowered to 0.2 $mN.m^{-1}$ while the minimal interfacial tension determined for PBO-based copolymers was only 1.4 $mN.m^{-1}$ as a result of the greater solvation of the PDMS tails in CO_2. Similarly, this $PDMS_{24}$-*g*-EO_{22} copolymer was able to emulsify up to 9.5 % wt of water, i.e. more water than PPO-based copolymers. The resulting emulsion was a C/W emulsion, thus contradicting the Bancroft's rule.[122] Moreover, the steric stabilization provided by this copolymer was not sufficient enough to prevent flocculation and sedimentation after a few seconds, even though the residual emulsion did not coalesce. Moving away from the balanced state, the formation of a W/C emulsion could be achieved at 24 °C and 188 bar with a copolymer of $PDMS_{105}$-*g*-EO_{68} that exhibited a lower

interfacial activity and a slightly lower HCB. However, the resulting emulsion was still extremely sensitive to flocculation.

4. Fluorinated poly((meth)acrylate)-based copolymers

Comparatively to PBO-based copolymers, poly(dimethyl siloxane)-based stabilizers allow to stabilize W/C emulsions in a larger range of pressure and temperature, in addition to a higher water uptake. Though they provide an efficient barrier against coalescence, a major drawback is the fast flocculation of W/C emulsion stabilized by such surfactants resulting from their moderate CO_2-philicity. Amphiphilic polymers comprising a fluorinated CO_2-philic block can thus be expected to be much more efficient stabilizers.

Considering the design of macromolecular surfactants for the stabilization of W/C emulsions, poly(1,1-dihydroperfluorooctyl acrylate) (PFOA) and poly(1,1-dihydroperfluorooctyl methacrylate) (PFOMA) are strong candidates due to their true CO_2-philicity. Lim and coworkers explored the interfacial properties of an amphiphilic block copolymer comprising a PFOMA block (M_n = 7500 g.mol^{-1}) and a PEO (M_n = 5000 g.mol^{-1}) at the W/C interface as a function of salinity, temperature and pressure.[127] At a concentration of 0.05 % wt and a CO_2 density of 0.9755 g.mL^{-1} (T = 25 °C, P = 320 bar), the interfacial tension could be lowered to 4.40 mN.m^{-1}. Increasing the ionic strength with the addition of 0.15 M NaCl then increased γ to 5.11 mN.m^{-1} as the solubility of the surfactant in water was lowered. Similarly, an increase in temperature at a constant pressure of 320 bar and a decrease in pressure to 25 °C resulted in higher values of γ. From this, a W/C emulsion could be formed with 0.05 % wt of surfactant in a 50:50 (w/w) water/CO_2 mixture. After stopping stirring and recirculation, creaming was observed after 30 minutes.

Following the same strategy, the formation and stability of W/C emulsions was assessed in the presence of a PEO-*b*-PFOA copolymer ($M_{n,\ PEO}$= 2000 g.mol^{-1} and $M_{n,PFOA}$ ≈ 31000 g.mol^{-1}).[96] Note that the HCB was lower and the M_n of the copolymer was higher compared to the previous study. The observation of a W/C emulsion was reported from 25 °C and 143 bar while flocculation or coalescence of dispersed water phase slowly occurred upon stopping of the stirrer. Notably, the

formation of a W/C emulsion was reported at the cloud point pressure of the copolymer in a binary polymer/CO_2 mixture.

D. Water/CO_2 miniemulsions

1. Poly(dimethyl siloxane)-based block copolymers

As a general rule, poly(dimethyl siloxane)-based copolymers exhibited lower values of surface tension than poly(alkylene oxides), which makes their use in the stabilization of W/C miniemulsions advantageous. The concept of W/C miniemulsions was first demonstrated by Johnston and coworkers using the point-inversion temperature method (PIT) with a PEO-*b*-PDMS-*b*-PEO triblock copolymer ($M_{n,PEO}$ = 1136 g.mol^{-1} and $M_{n,PDMS}$ = 1095 g.mol^{-1}).[128] The general strategy consisted in putting the water/CO_2/polymer mixture at a balanced state and then apply a quick heating to form nano-sized W/C miniemulsions. The identification of conditions required to reach the balanced state were required as a preliminary work. For a given density of 0.842 g.mL^{-1} with 0.05 % wt of surfactant in the absence of added salt, a balanced state but no W/C emulsions were observed at temperatures higher than 66 °C. The addition of 0.1 M NaCl resulted in the shift of the balanced state to lower temperatures between 38 and 58 °C. A minimum in interfacial tension then appeared around 0.2 mN.m^{-1} and W/C emulsions could be observed at higher temperatures. Under these conditions, the rapid heating from 50 from 65 °C resulted in the formation of W/C miniemulsions which were highly flocculated and heterogeneous. An increase in the shear rate only produced less flocculated miniemulsions.

As a conclusion, the feeble stability of W/C miniemulsions stabilized by PDMS-based amphiphilic block copolymers was related to the low steric stabilization provided by the short PDMS block. To date, no further study on the formation and stabilization of W/C miniemulsions with longer PDMS blocks has been reported.

2. Fluorinated poly(methacrylate)-based block copolymers

The most convincing attempt to stabilize W/C miniemulsions undoubtedly came with the use of poly(fluorinated methacrylate)-based block copolymers. Whereas creaming was observed with W/C macroemulsions stabilized with a PEO-*b*-PFOMA copolymer (see above), its applicability to W/C miniemulsions was successfully demonstrated.[129] Concomitantly with low values of surface tension ranging between 0.19 and 0.50 $mN.m^{-1}$, water droplets sized between 70 and 120 nm were obtained from 1 % wt of a sample of PEO-*b*-PFOMA ($M_{n,PFOMA}$ = 5500 $g.mol^{-1}$ and $M_{n,PEO}$ = 2000 $g.mol^{-1}$) in a mixture of CO_2 and 2-3 % wt of water. Variations in temperature, CO_2 density, shear rate and HCB further allowed tuning the surface tension and the resulting average drop sizes. Remarkably, the droplet size was proportional to surface tension at the power of 2/5 while this factor equals to 3/5 for incompressible fluids. Ultimately, these W/C miniemulsions exhibited an unprecedented stability over 24 hours against flocculation.

E. Critical flocculation density

The concept of critical flocculation density (CFD) gives a comprehensive overview on flocculation and the relative efficiency of macromolecular surfactants. The CFD is defined as the CO_2 density below which flocculation occurs. Interestingly, the CFD of a homopolymer coincided with its UCSD, provided that the chain length was long enough to screen the attractive Van der Waals forces. This qualitatively differs from incompressible solvents where the critical flocculation temperature coincides with the theta temperature. When the attractive forces dominate over steric stabilization, flocculation then occurs at densities higher than the CFD. Regarding block copolymers, the chain of the solvophilic block must be similarly long enough to prevent flocculation above its UCSD.[130]

The critical flocculation density of W/C miniemulsions stabilized by PEO-*b*-PFOMA copolymers and its dependency on molecular weight, temperature, surfactant and water contents were investigated by Johnston and coworkers.[131] As expected, the CFD decreased with either smaller droplet size or increasing molecular weight of the CO_2-philic PFOMA block as a result of enhanced screening of the core-

core attractions. The attractive forces were fully dominated when the molecular weight was higher than 30000 g.mol^{-1}. An increase in temperature also induced a decrease in the CFD since the attractive forces are inversely proportional to temperature. Inversely, when the surfactant content was decreased from 1 to 0.1 % wt, the CFD increased, which resulted from the poorer surface coverage. The W/C miniemulsions were then destabilized.

F. Water/CO_2 microemulsions

Compared to macro- and miniemulsions, the water uptake is lower in microemulsions. By virtue of their smaller sizes and, subsequently, the more efficient packing of the surfactant at the interface, microemulsions are not subject to flocculation effects. In the field of microemulsions, the water uptake is defined as the molar ratio of water to surfactant, W_o. The corrected W_o (called W_o^c) taking account of the solubility of water in CO_2 is defined as:

$$W_0^c = \frac{[water]_0 - [water]_s}{[surfactant]_0}$$

where $[water]_o$ is the number of moles of water in the system, $[water]_s$ the number of moles soluble in the background CO_2 and $[water]_o$ the number of moles of surfactant. W_o^c usually ranges from 10 to 100. When this ratio is lower, microemulsions are preferably referred as hydrated micelles.

While the stabilization of W/C microemulsions with Krytox-type polymers or molecular surfactants has been largely reported,[132,133] examples implying amphiphilic copolymers are scarce in literature. These examples –described below– are exclusively based on fluorinated poly((meth)acrylates) as a consequence of their lower surface tension compared to hydrocarbons and poly(siloxanes).

a) Amphiphilic block copolymers

Lim and coworkers reported the formation of hydrated micelles stabilized by a poly(1,1,,2,2-tetrahydroperfluorooctyl methacrylate)-based copolymers incorporating

either poly(N,N-dimethylaminoethyl methacrylate) (PDMAEMA) or poly(oligo(ethylene glycol) methacrylate) (POEGMA) hydrophilic blocks.

Using 0.5 % wt of a PDMAEMA-*b*-PFOMA sample ($M_{n,PDMAEMA}$ = 2000 g.mol^{-1} and $M_{n,PFOMA}$ = 10000 g.mol^{-1}), the formation of hydrated aggregates could be achieved above 180 bar at 40 °C.[134] However, the corrected water-to-surfactant molar ratio taking account of the intrinsic solubility of water in CO_2 (W_o^c) was only 5 and decreased to 2.4 with a higher polymer content of 1 % wt. Similarly, a W_o^c corrected ratio of 2.7 was determined with 0.25 % wt of a POEGMA-*b*-PFOMA sample ($M_{n,POEGMA}$ = 6500 g.mol^{-1} and $M_{n,PFOMA}$ = 20000 g.mol^{-1}) above 140 bar at 40 °C.[135] By means of comparison, a W_o up to 80 was attained in microemulsions stabilized by molecular surfactants.[136]

b) Amphiphilic gradient copolymers

A greater amount of water could be dispersed in sc-CO_2 using an amphiphilic gradient copolymer made of 1,1,2,2-tetrahydroperfluorodecyl acrylate and vinyl benzoic phosphonic acid (23 % mol) repeat units.[112] From SANS measurements performed at 40 °C and 350 bar with 4.6 % wt of polymer and 0.37 % wt of D_2O, D_2O-swollen aggregates with a R_g of 2.25 nm and a N_{agg} of 8 were observed. This corresponded to a W_o^c of 13. These aggregates were stable for 8 hours as a further indication of the formation of microemulsion. The stabilization of higher water content appeared unfeasible in mild conditions of temperature (T < 65 °C) and pressure (P < 400 bar).

c) Amphiphilic comb copolymers

A single example of hydrated micelles stabilized by a sample of poly(1,1-dihydroperfluorooctyl acrylate)-*graft*-poly(ethylene oxide) (PFOA-*g*-PEO) was published so far.[117] From SAXS experiments, the swelling of an aggregate upon the presence of 0.32 % wt of water and 0.6 % wt of the copolymer was observed at 60 °C. At 300 bar, a shell radius around 12 nm and a N_{agg} of 123 were extracted from the experimental data fitted with a core-shell model. An increase of the polymer content up to 1.9 % wt resulted in an increase of this radius to 12.9 nm at 300 bar. Chillura-

Martino *et al.* performed additional SANS experiments on this same example.[64] Using the same fitting model, they could confirm the swelling of aggregates stabilized by this graft amphiphilic copolymer. A shell radius of 12.8 nm and a slightly lower N_{agg} of 83 were determined too.

VI. Present objectives of this thesis

The quantity of studies dedicated to the solubility of polymers in sc-CO_2 contrasts with the scarceness of publications concerning the self-assembly of amphiphilic copolymers and their use as macromolecular surfactants. Moreover, a large majority of these studies have focused on fluorinated poly((meth)acrylates) and poly(siloxanes) and commercially-available poly(alkylene oxides). As a matter of fact, the possibilities offered by modern techniques of macromolecular techniques have not been fully exploited to develop new amphiphilic copolymers that provide alternatives to the aforementioned ones. In particular, poly(vinyl acetate) and fluorinated poly(olefins) still have a great unexplored potential.

To address such challenges, this work relies on modern techniques of free radical polymerization including RAFT/MADIX polymerization –presented in the next chapter– that provides excellent control both on the architecture and macromolecular characteristics of such copolymers. Throughout this thesis, the extension of RAFT/MADIX polymerization to unprecedentedly controlled monomers –including novel vinyl esters and fluorinated olefins– will be also demonstrated with the finality of studying the solubility of the resulting (co)polymers in sc-CO_2. In addition to the usual cloud point observations, the understanding of factors governing their solubility will be pursued using a large palette of experimental techniques including in-situ infrared spectroscopy, DFT calculations and tensiometry experiments.

VII. References

(1) B. Berche, M. Henkel and R. Kenna, *Journal of Physical Studies*, 2009, **13,** 3001.
(2) C. Cagniard de la Tour, *Ann. Chim. Phys.*, 1822, **21,** 178.
(3) C. Cagniard de la Tour, *Ann. Chim. Phys.*, 1823, **22,** 410.
(4) T. Andrews, *Philosophical Transactions of the Royal Society of London*, 1869, **159,** 575.
(5) M. Kemmere, in *Supercritical carbon dioxide: in Polymer Reaction Engineering*, ed. M. Kemmere and T. Meyer, Wiley-VCH, Weinheim, Wiley-VCH,2005, Chap. 1.
(6) E.J. Beckman, *J. Supercrit. Fluids*, 2004, **28,** 121.
(7) P.G. Jessop, S.M. Mercer and D.J. Heldebrant, *Energy Environ. Sci.*, 2012, **5,** 7240.
(8) K.E. O'Shea, K.M. Kirmse, M.A. Fox and K.P. Johnston, *J. Phys. Chem.*, 1991, **95,** 7863.
(9) K.A. Consan and R.D. Smith, *J. Supercrit. Fluids*, 1990, **3,** 51.
(10) D.E. Stogryn and A.P. Stogryn, *Mol. Phys.*, 1966, **11,** 371.
(11) P. Raveendran, Y. Ikushima and S.L. Wallen, *Acc. Chem. Res.*, 2005, **38,** 478.
(12) T.H. Dunning, *J. Chem. Phys.*, 1989, **90,** 1007.
(13) R.A. Kendall, J. Dunning and R.J. Harrison, *J. Chem. Phys.*, 1992, **96,** 6796.
(14) A.K. Wilson, T. van Mourik and J. Dunning, *J. Mol. Struc. -THEOCHEM*, 1996, **388,** 339.
(15) H. Tatewaki and S. Huzinaga, *J. Comput. Chem.*, 1980, **1,** 205.
(16) C. Moller and M.S. Plesset, *Phys. Rev.*, 1934, **46,** 618.
(17) S.F. Boys and F. Bernardi, *Mol. Phys.*, 1970, **19,** 553.
(18) J.C. Meredith, K.P. Johnston, J.M. Seminario, S.G. Kazarian and C.A. Eckert, *J. Phys. Chem.*, 1996, **100,** 10837.
(19) S. Kilic, Y. Wang, J.K. Johnson, E.J. Beckman and R.M. Enick, *Polymer*, 2009, **50,** 2436.
(20) P. Vitoux, T. Tassaing, F. Cansell, S. Marre and C. Aymonier, *J. Phys. Chem. B*, 2009, **113,** 897.
(21) P. Van Ginderen, W.A. Herrebout and B.J. van der Veken, *J. Phys. Chem. A*, 2003, **107,** 5391.
(22) S. Kilic, S. Michalik, Y. Wang, J.K. Johnson, R.M. Enick and E.J. Beckman, *Ind. Eng. Chem. Res.*, 2003, **42,** 6415.
(23) Y. Danten, T. Tassaing and M. Besnard, *J. Phys. Chem. A*, 2002, **106,** 11831.
(24) M.R. Nelson and R.F. Borkman, *J. Phys. Chem. A*, 1998, **102,** 7860.
(25) S.G. Kazarian, M.F. Vincent, F.V. Bright, C.L. Liotta and C.A. Eckert, *J. Am. Chem. Soc.*, 1996, **118,** 1729.
(26) P. Raveendran and S.L. Wallen, *J. Am. Chem. Soc.*, 2002, **124,** 12590.
(27) Y. Yuan and A.S. Teja, *J. Supercrit. Fluids*, 2011, **56,** 208.
(28) J. Wang, M. Wang, J. Hao, S.i. Fujita, M. Arai, Z. Wu and F. Zhao, *J. Supercrit. Fluids*, 2010, **54,** 9.
(29) M.I. Cabaço, Y. Danten, T. Tassaing, S. Longelin and M. Besnard, *Chemical Physics Letters*, 2005, **413,** 258.
(30) M. Besnard, M.I. Cabaço, S. Longelin, T. Tassaing and Y. Danten, *J. Phys. Chem. A*, 2007, **111,** 13371.
(31) Y. Park, *J. Supercrit. Fluids*, 2005, **36,** 154.
(32) K.H. Kim and Y. Kim, *J. Phys. Chem. A*, 2008, **112,** 1596.

(33) A. Dardin, J.B. Cain, J.M. DeSimone, C.S. Johnson and E.T. Samulski, *Macromolecules*, 1997, **30,** 3593.
(34) A. Dardin, J.M. DeSimone and E.T. Samulski, *J. Phys. Chem. B*, 1998, **102,** 1775.
(35) C.R. Yonker, T.S. Zemanian, S.L. Wallen, J.C. Linehan and J.A. Franz, *J. Magn. Reson. A*, 1995, **113,** 102.
(36) P. Diep, K.D. Jordan, J.K. Johnson and E.J. Beckman, *J. Phys. Chem. A*, 1998, **102,** 2231.
(37) P. Raveendran and S.L. Wallen, *J. Phys. Chem. B*, 2003, **107,** 1473.
(38) C.F. Kirby and M.A. McHugh, *Chem. Rev.*, 1999, **99,** 565.
(39) D. Patterson, *Polym. Eng. Sci.*, 1982, **22,** 64.
(40) B.A. Miller-Chou and J.L. Koenig, *Prog. Polym. Sci.*, 2003, **28,** 1223.
(41) T. Banerjee and G.G. Lipscomb, *J. Appl. Polym. Sci.*, 1998, **68,** 1441.
(42) R.G. Wissinger and M.E. Paulaitis, *J. Polym. Sci. B Polym. Phys.*, 1991, **29,** 631.
(43) R.G. Wissinger and M.E. Paulaitis, *J. Polym. Sci. B Polym. Phys.*, 1987, **25,** 2497.
(44) J.S. Chiou, J.W. Barlow and D.R. Paul, *J. Appl. Polym. Sci.*, 1985, **30,** 2633.
(45) A.F. Kostko, M.A. McHugh and J.H. van Zanten, *Macromolecules*, 2006, **39,** 1657.
(46) Z. Bayraktar and E. Kiran, *J. Appl. Polym. Sci.*, 2000, **75,** 1397.
(47) Y.B. Melnichenko, E. Kiran, G.D. Wignall, K.D. Heath, S. Salaniwal, H.D. Cochran and M. Stamm, *Macromolecules*, 1999, **32,** 5344.
(48) F. Rindfleisch, T.P. DiNoia and M.A. McHugh, *J. Phys. Chem.*, 1996, **100,** 15581.
(49) M. Lora, J.S. Lim and M.A. McHugh, *J. Phys. Chem. B*, 1999, **103,** 2818.
(50) T.P. DiNoia, S.E. Conway, J.S. Lim and M.A. McHugh, *J. Polym. Sci. B Polym. Phys.*, 2000, **38,** 2832.
(51) S. Beuermann and M. Imran-ul-haq, *J. Polym. Sci. A Polym. Chem.*, 2007, **45,** 5626.
(52) B. Bonavoglia, G. Storti and M. Morbidelli, *Macromolecules*, 2005, **38,** 5593.
(53) M.L. O'Neill, Q. Cao, M. Fang, K.P. Johnston, S.P. Wilkinson, C.D. Smith, J.L. Kerschner and S.H. Jureller, *Ind. Eng. Chem. Res.*, 1998, **37,** 3067.
(54) B. Baradie and M.S. Shoichet, *Macromolecules*, 2002, **35,** 3569.
(55) B. Baradie, M.S. Shoichet, Z. Shen, M.A. McHugh, L. Hong, Y. Wang, J.K. Johnson, E.J. Beckman and R.M. Enick, *Macromolecules*, 2004, **37,** 7799.
(56) C.A. Mertdogan, T.P. DiNoia and M.A. McHugh, *Macromolecules*, 1997, **30,** 7511.
(57) C. Drohmann and E.J. Beckman, *J. Supercrit. Fluids*, 2002, **22,** 103.
(58) T. Sarbu, T. Styranec and E.J. Beckman, *Nature*, 2000, **405,** 165.
(59) S. Li, Y. Li and J. Wang, *Fluid Phase Eq.*, 2007, **253,** 54.
(60) J. Gregorowicz, Z. Fras, P. Parzuchowski, G. Rokicki, M. Kusznerczuk and S. Dziewulski, *J. Supercrit. Fluids*, 2010, **55,** 786.
(61) T.A. Hoefling, D. Stofesky, M. Reid, E.J. Beckman and R.M. Enick, *J. Supercrit. Fluids*, 1992, **5,** 237.
(62) D.A. Newman, T.A. Hoefling, R.R. Beitle, E.J. Beckman and R.M. Enick, *J. Supercrit. Fluids*, 1993, **5,** 205.
(63) Dupont Krytox Performance Lubricants: Product Overview, 2012. Available at: http://www2.dupont.com/Lubricants/en_US/assets/downloads/Krytox_Overview_LowRes_H-58505-5.pdf
(64) D. Chillura-Martino, R. Triolo, J.B. McClain, J.R. Combes, D.E. Betts, D.A. Canelas, J.M. DeSimone, E.T. Samulski, H.D. Cochran, J.D. Londono and G.D. Wignall, *J. Mol. Struct.*, 1996, **383,** 3.
(65) W.F. Edmonds, M.A. Hillmyer and T.P. Lodge, *Macromolecules*, 2007, **40,** 4917.

(66) C. Lepilleur, E.J. Beckman, H. Schonemann and V.J. Krukonis, *Fluid Phase Eq.*, 1997, **134,** 285.
(67) V. Martinez, S. Mecking, T. Tassaing, M. Besnard, S. Moisan, F. Cansell and C. Aymonier, *Macromolecules*, 2006, **39,** 3978.
(68) M. Tryznowski, K. Tomczyk, Z. Fras, J. Gregorowicz, G. Rokicki, E. Wawrzynska and P.G. Parzuchowski, *Macromolecules*, 2012, **45,** 6819.
(69) T. Sarbu, T.J. Styranec and E.J. Beckman, *Ind. Eng. Chem. Res.*, 2000, **39,** 4678.
(70) B. Tan, H.M. Woods, P. Licence, S.M. Howdle and A.I. Cooper, *Macromolecules*, 2005, **38,** 1691.
(71) Y. Wang, L. Hong, D. Tapriyal, I.C. Kim, I.H. Paik, J.M. Crosthwaite, A.D. Hamilton, M.C. Thies, E.J. Beckman, R.M. Enick and J.K. Johnson, *J. Phys. Chem. B*, 2009, **113,** 14971.
(72) C.L. Bray, B. Tan, S. Higgins and A.I. Cooper, *Macromolecules*, 2010, **43,** 9426.
(73) S. Kilic, S. Michalik, Y. Wang, J.K. Johnson, R.M. Enick and E.J. Beckman, *Macromolecules*, 2007, **40,** 1332.
(74) Z. Shen, M.A. McHugh, J. Xu, J. Belardi, S. Kilic, A. Mesiano, S. Bane, C. Karnikas, E.J. Beckman and R. Enick, *Polymer*, 2003, **44,** 1491.
(75) E. Buhler, A.V. Dobrynin, J.M. DeSimone and M. Rubinstein, *Macromolecules*, 1998, **31,** 7347.
(76) C.L. Bray, B. Tan, C.D. Wood and A.I. Cooper, *J. Mat. Chem.*, 2005, **15,** 456.
(77) B. Tan, C.L. Bray and A.I. Cooper, *Macromolecules*, 2009, **42,** 7945.
(78) H. Lee, E. Terry, M. Zong, N. Arrowsmith, S. Perrier, K.J. Thurecht and S.M. Howdle, *J. Am. Chem. Soc.*, 2008, **130,** 12242.
(79) E.J. Park, A.P. Richez, N.A. Birkin, H. Lee, N. Arrowsmith, K.J. Thurecht and S.M. Howdle, *Polymer*, 2011, **52,** 5403.
(80) H. Lee, J.W. Pack, W. Wang, K.J. Thurecht and S.M. Howdle, *Macromolecules*, 2010, **43,** 2276.
(81) N.A. Birkin, N.J. Arrowsmith, E.J. Park, A.P. Richez and S.M. Howdle, *Polym. Chem.*, 2011, **2,** 1293.
(82) B. Tan, J.Y. Lee and A.I. Cooper, *Macromolecules*, 2007, **40,** 1945.
(83) J.Y. Lee, B. Tan and A.I. Cooper, *Macromolecules*, 2007, **40,** 1955.
(84) K. Chen, N. Grant, L. Liang, H. Zhang and B. Tan, *Macromolecules*, 2010, **43,** 9355.
(85) M.A. McHugh, A. Garach-Domech, I.H. Park, D. Li, E. Barbu, P. Graham and J. Tsibouklis, *Macromolecules*, 2002, **35,** 6479.
(86) S. Kwon, W. Bae, K. Lee, H.S. Byun and H. Kim, *J. Chem. Eng. Data*, 2006, **52,** 89.
(87) Y.L. Hsiao, E.E. Maury, J.M. DeSimone, S. Mawson and K.P. Johnston, *Macromolecules*, 1995, **28,** 8159.
(88) J.B. McClain, D. Londono, J.R. Combes, T.J. Romack, D.A. Canelas, D.E. Betts, G.D. Wignall, E.T. Samulski and J.M. DeSimone, *J. Am. Chem. Soc.*, 1996, **118,** 917.
(89) A. Blasig, C. Shi, R.M. Enick and M.C. Thies, *Ind. Eng. Chem. Res.*, 2002, **41,** 4976.
(90) P. Lacroix-Desmazes, P. Andre, J.M. DeSimone, A.V. Ruzette and B. Boutevin, *J. Polym. Sci. A Polym. Chem.*, 2004, **42,** 3537.
(91) P. Andre, P. Lacroix-Desmazes, D.K. Taylor and B. Boutevin, *J. Supercrit. Fluids*, 2006, **37,** 263.
(92) T. Ribaut, P. Lacroix-Desmazes, B. Fournel and S. Sarrade, *J. Polym. Sci. A Polym. Chem.*, 2009, **47,** 5448.
(93) T. Ribaut, J. Oberdisse, B. Annighofer, B. Fournel, S. Sarrade, H. Haller and P. Lacroix-Desmazes, *J. Phys. Chem. B*, 2011, **115,** 836.

(94) S. Mawson, K.P. Johnston, J.R. Combes and J.M. DeSimone, *Macromolecules*, 1995, **28,** 3182.
(95) J. Guo, P. Andre, M. Adam, S. Panyukov, M. Rubinstein and J.M. DeSimone, *Macromolecules*, 2006, **39,** 3427.
(96) Z. Ma and P. Lacroix-Desmazes, *J. Polym. Sci. A Polym. Chem.*, 2004, **42,** 2405.
(97) Z. Guan and J.M. DeSimone, *Macromolecules*, 1994, **27,** 5527.
(98) W.J. Ye and J.M. DeSimone, *Macromolecules*, 2005, **38,** 2180.
(99) D. Li, Z. Shen, M.A. McHugh, J. Tsibouklis and E. Barbu, *Ind. Eng. Chem. Res.*, 2003, **42,** 6499.
(100) M.E. Wright, K.M. Lott, M.A. McHugh and Z. Shen, *Macromolecules*, 2003, **36,** 2242.
(101) Y. Xiong and E. Kiran, *Polymer*, 1995, **36,** 4817.
(102) P. Andre, S.L. Folk, M. Adam, M. Rubinstein and J.M. DeSimone, *J. Phys. Chem. A*, 2004, **108,** 9901.
(103)M.L. O'Neill, Q. Cao, M. Fang, K.P. Johnston, S.P. Wilkinson, C.D. Smith, J.L. Kerschner and S.H. Jureller, *Ind. Eng. Chem. Res.*, 1998, **37,** 3067.
(104) R. Fink, D. Hancu, R. Valentine and E.J. Beckman, *J. Phys. Chem. B*, 1999, **103,** 6441.
(105) M.S. Chirat, S. Clerc, d.F. Ganchau, B. Fournel and P. Lacroix-Desmazes, *Abstr. Pap. Am. Chem. Soc.*, 2011, **242,** 197.
(106) H. Yuvaraj, H.S. Hwang, W.S. Kim, H.G. Kim, E.D. Jeong and K.T. Lim, *Eur. Pol. J.*, 2008, **44,** 2253.
(107) J.B. McClain, D.E. Betts, D.A. Canelas, E.T. Samulski, J.M. DeSimone, J.D. Londono, H.D. Cochran, G.D. Wignall, D. ChilluraMartino and R. Triolo, *Science*, 1996, **274,** 2049.
(108) J.D. Londono, R. Dharmapurikar, H.D. Cochran, G.D. Wignall, J.B. McClain, D.E. Betts, D.A. Canelas, J.M. DeSimone, E.T. Samulski, D. Chillura-Martino and R. Triolo, *J. Appl. Cryst.*, 1997, **30,** 690.
(109) J.B. Cain, K. Zhang, D.E. Betts, J.M. DeSimone and C.S. Johnson, *J. Am. Chem. Soc.*, 1998, **120,** 9390.
(110) F. Lo Celso, A. Triolo, F. Triolo, P. Thiyagarajan, H. Amenitsch, M. Steinhart, M. Kriechbaum, J.M. DeSimone and R. Triolo, *J. Appl. Cryst.*, 2003, **36,** 660.
(111) T. Koga, S. Zhou and B. Chu, *Appl. Opt.*, 2001, **40,** 4170.
(112) T. Ribaut, J. Oberdisse, B. Annighofer, I. Stoychev, B. Fournel, S. Sarrade and P. Lacroix-Desmazes, *Soft Matter*, 2009, **5,** 4962.
(113) S. Zhou and B. Chu, *Macromolecules*, 1998, **31,** 5300.
(114) F. Triolo, A. Triolo, R. Triolo, J.D. Londono, G.D. Wignall, J.B. McClain, D.E. Betts, S. Wells, E.T. Samulski and J.M. DeSimone, *Langmuir*, 1999, **16,** 416.
(115) A. Triolo, F. Triolo, F. Lo Celso, D.E. Betts, J.B. McClain, J.M. DeSimone, G.D. Wignall and R. Triolo, *Phys. Rev. E*, 2000, **62,** 5839.
(116) F. Lo Celso, A. Triolo, F. Triolo, D.I. Donato, M. Steinhart, M. Kriechbaum, H. Amenitsch and R. Triolo, *Eur. Phys. J. E*, 2002, **8,** 311.
(117) J.L. Fulton, D.M. Pfund, J.B. McClain, T.J. Romack, E.E. Maury, J.R. Combes, E.T. Samulski, J.M. DeSimone and M. Capel, *Langmuir*, 1995, **11,** 4241.
(118) A.I. Cooper, J.D. Londono, G. Wignall, J.B. McClain, E.T. Samulski, J.S. Lin, A. Dobrynin, M. Rubinstein, A.L.C. Burke, J.M.J. Frechet and J.M. DeSimone, *Nature*, 1997, **389,** 6649.
(119) E.L.V. Goetheer, M.W.P.L. Baars, L.J.P. van den Broeke, E.W. Meijer and J.T.F. Keurentjes, *Ind. Eng. Chem. Res.*, 2000, **39,** 4634.

(120) Y. Takebayashi, Y. Mashimo, D. Koike, S. Yoda, T. Furuya, M. Sagisaka, K. Otake, H. Sakai and M. Abe, *J. Phys. Chem. B*, 2008, **112,** 8943.
(121) S.R.P. da Rocha, K.L. Harrison and K.P. Johnston, *Langmuir*, 1998, **15,** 419.
(122) S.R.P. da Rocha, P.A. Psathas, E. Klein and K.P. Johnston, *J. Coll. Int. Sci.*, 2001, **239,** 241.
(123) B. Tan and A.I. Cooper, *J. Am. Chem. Soc.*, 2005, **127,** 8938.
(124) B. Tan, J.Y. Lee and A.I. Cooper, *Macromolecules*, 2006, **39,** 7471.
(125) P.A. Psathas, E.A. Sander, M.Y. Lee, K.T. Lim and K.P. Johnston, *J. Disp. Sci. Tech.*, 2002, **23,** 65.
(126) P.A. Psathas, S.R.P. da Rocha, C.T. Lee, K.P. Johnston, K.T. Lim and S. Webber, *Ind. Eng. Chem. Res.*, 2000, **39,** 2655.
(127) K.T. Lim, M.Y. Lee, M.J. Moon, G.D. Lee, S.S. Hong, J.L. Dickson and K.P. Johnston, *Polymer*, 2002, **43,** 7043.
(128) P.A. Psathas, M.L. Janowiak, L.H. Garcia-Rubio and K.P. Johnston, *Langmuir*, 2002, **18,** 3039.
(129) J.L. Dickson, P.A. Psathas, B. Salinas, C. Ortiz-Estrada, G. Luna-Barcenas, H.S. Hwang, K.T. Lim and K.P. Johnston, *Langmuir*, 2003, **19,** 4895.
(130) J.C. Meredith and K.P. Johnston, *Macromolecules*, 1998, **31,** 5518.
(131) J.L. Dickson, C. Ortiz-Estrada, J.F.J. Alvarado, H.S. Hwang, I.C. Sanchez, G. Luna-Barcenas, K.T. Lim and K.P. Johnston, *J. Coll. Int. Sci.*, 2004, **272,** 444.
(132) K.P. Johnston, K.L. Harrison, M.J. Clarke, S.M. Howdle, M.P. Heitz, F.V. Bright, C. Carlier and T.W. Randolph, *Science*, 1996, **271,** 624.
(133) M. Sagisaka, S. Iwama, S. Hasegawa, A. Yoshizawa, A. Mohamed, S. Cummings, S.E. Rogers, R.K. Heenan and J. Eastoe, *Langmuir*, 2011, **27,** 5772.
(134) K.T. Lim, H.S. Hwang, W. Ryoo and K.P. Johnston, *Langmuir*, 2004, **20,** 2466.
(135) H.S. Hwang, H.J. Kim, Y.T. Jeong, Y.S. Gal and K.T. Lim, *Macromolecules*, 2004, **37,** 9821.
(136) M. Sagisaka, S. Iwama, A. Yoshizawa, A. Mohamed, S. Cummings and J. Eastoe, *Langmuir*, 2012, **28,** 10988.

Chapter 2

- Reversible deactivation radical polymerization techniques
- RAFT/MADIX synthesis of vinyl acetate-based (co)polymers
- Influence of macromolecular characteristics of poly(vinyl acetate)-based copolymers on their solubility in sc-CO_2

Contents

Due to its specific interactions with CO_2,[1,2] the acetate group has attracted increasing attention as a CO_2-philic moiety and has been, for instance, used to enhance the CO_2 solubility of poly(siloxanes)[3] or sacharrides.[4] As exposed in the first chapter, the solubility of poly(vinyl acetate) in CO_2 has been widely investigated as a function of its molecular weight or chain end groups.[5-7] Although vinyl acetate (VAc) can be considered as a reference building block for CO_2-philic compounds, the examples where PVAc blocks were applied to synthesize macromolecular surfactants are scarce.[8-10] A specific reason of that is related to the synthesis of PVAc which can only be achieved through radical polymerization when poly(siloxanes) and perfluoropolyethers are obtained by anionic polymerization. As a consequence, the macromolecular engineering of PVAc is considerably more challenging. The higher reactivity of the VAc propagating radicals has long been an obstacle to the development of a technique that efficiently controls the polymerization of VAc. However, the emergence of reversible deactivation radical techniques in the mid 1990s has undoubtedly opened new perspectives for the macromolecular engineering of PVAc.

The present chapter aims at describing the synthesis of novel macromolecular surfactants incorporating a CO_2-philic poly(vinyl acetate) block through the application of such techniques. The possibilities offered by RDRP polymerization will be explored to produce a large range of (co)polymers with varying chain lengths, chain end groups and compositions. The solubility of the obtained copolymers will then be determined via infrared spectroscopy where cloud point observations are classically used, which constitutes an additional originality of this study.

I. Macromolecular engineering of vinyl acetate through radical polymerization

A. Free radical polymerization of vinyl acetate

Vinyl acetate is homopolymerized only by radical means. Intriguingly, vinyl acetate can also be copolymerized with carbon monoxide via a coordination-addition mechanism with palladium complexes.[11] In terms of radical polymerization, the polymerization of VAc possesses distinctive features due to the relatively high instability of its radicals, which are summarized below:

- A high propagation rate (k_p) around 10500 $L.mol^{-1}.s^{-1}$ at 60 °C in bulk.[12].
- A non-negligible proportion of inverted adducts comprised between 1 and 2 % mol at 60 °C.[13]
- A non negligible transfer constant to polymer ranging between 1 and $8*10^{-4}$ were reported at 60 °C, leading to the formation of short branchings.[14] Similarly, the constant transfer to monomer ranges between 1.75 and $2.75*10^{-4}$ at 60 °C. In both cases, the preferential sites of transfer are the methyl hydrogens of the acetate group.
- The nature of the solvent can significantly influence the kinetics of polymerization of VAc.[15] Strong solvent effects were reported with aromatic solvents retarding the polymerization. Concerning the transfer events to solvents, ethyl acetate is the preferential low-transferring solvent except benzene. Below are shown some transfer constants to usual solvents (see Table II.1).

	Benzene	Ethyl Acetate	Anisole	Acetone	1,4-Dioxane	Toluene	DMF	2-butan-one	Triethyl amine
$C_{tr,s}$ (10-4) (60 °C)	1.2 - 20	1.7 – 3.4	10	12	20	17.8 - 69	50	74	370

Table II.1. Transfer constants to usual polymerization solvents with vinyl acetate. Figures selected from references [14] and [16].

B. Reversible deactivation radical polymerization of vinyl acetate

1. General principles

By analogy with living ionic polymerization techniques, the turning point to achieve the control of a free radical polymerization process is the minimization of termination and transfer phenomena. Note that these events cannot be completely suppressed in radical processes contrary to ionic ones. For these reasons, IUPAC has officially suggested the term reversible deactivation radical polymerization (RDRP) over former terms such as controlled/living radical polymerizations.[17]

The minimization of transfer and termination events comes from the reduction of the radical lifetime from 1 to $\approx 10^{-4}$ seconds using an appropriate agent that provides reversible capping of the active center. In an ideal RDRP, the creation of chains should be fast to allow all chains to grow simultaneously and ensure a high concentration of growing chains. Meanwhile, the propagating radical concentration at a given time should be kept low. This apparent paradox is fulfilled by the control agent which creates a dynamic exchange between dormant growing chains and propagating free radicals. Roughly speaking, the propagating radicals are continuously regenerated and capped through the overall RDRP process so that the concentration of propagating radical can be kept low. Since termination is second-order with respect to propagating radical concentration, the proportion of dead chains can be reduced below 5 %.

The obtained amount of dead polymers allows the synthesis of polymer chains having controlled molecular weights, lower dispersities and well-defined end groups contrary to polymers obtained through a conventional free radical process. Polymer architectures such as comb, star, nanogel and hyperbranched polymers are also attainable from a RDRP process.

2. Reversible deactivation

To achieve such control on the FRP process, two main mechanisms have been identified so far: reversible deactivation by either coupling or atom transfer, and degenerative chain transfer which will be introduced in the next sections. As a frame for the forthcoming discussion, the different monomers will be classified into two main classes including:

- More-activated monomers (MAMs) which exhibit a more stable radical state. MAMs mainly include (meth)acrylates, styrenics, acrylamido monomers.
- Less-activated monomers (LAMs) which exhibit a less stable radical state. LAMs mainly include vinyl esters, vinyl amides, vinyl carbazoles, vinyl phosphonates and fluorinated olefins.

As the experimental work presented within this thesis mostly concerns the RDRP of LAMs, the applicability of every mechanism and RDRP techniques to these specific monomers–and vinyl acetate in the first place–will briefly be discussed.

a) Reversible deactivation by coupling

This mechanism is based primarily on a persistent radical effect, *i.e.* using stable free radical species (see Scheme II.1).[18] The homolytic cleavage is usually generated upon an increase in temperature to uncap the propagating chain which further propagates. The equilibrium constant of the reaction should be low to favor the deactivation state–and the dormant species–and keep the concentration of macroradicals low.

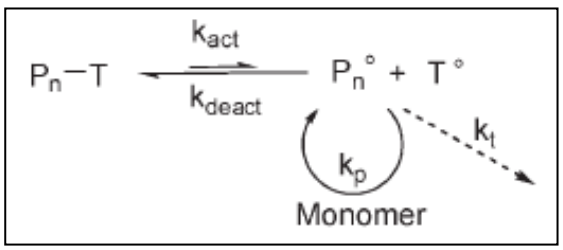

Scheme II.1. General mechanism of a RDRP based on a reversible deactivation by coupling.

Nitroxide-mediated polymerization (NMP) is the most characteristic RDRP technique based on the use of stable free radicals.[19] Examples of NMP control agents mostly include cyclic nitroxides such as TEMPO and acyclic ones such as SG1 (see Scheme II.2). The homolytic decomposition of TEMPO-based alkoxyamines- usually requires high temperatures in the range of 100-130 °C to provide fast initiation and sufficient rates of polymerization. The controlled radical polymerization of styrene, acrylates and some acrylamido monomers could be achieved with TEMPO-based alkoxyamines. A progress came with the development of SG1-based alkoxyamines which require lower decomposition temperatures (see Scheme II.2). The NMP of LAMs and, in particular, vinyl acetate, is of greater challenge as higher temperatures are necessary to cleave the NO-C bond in alkoxyamines. As evidenced for VAc, an additional hyperconjugation effect even strengthened this bond while concomitantly weakening the N-OC bond. The nitroxide-mediated polymerization of LAMs has never been reported to date. The development of photosensitive alkoxyamines (nitroxide-mediated photopolymerization) might constitute a promising perspective to overcome this.

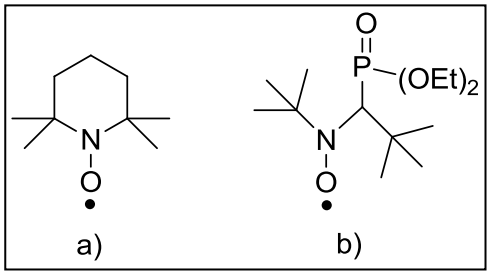

Scheme II.2. Molecular structure of a) TEMPO and b) SG1 nitroxides.

Other examples of stable free radicals able to mediate radical polymerizations include Co(II) with porphiryne ligands and verdazyl radicals even though their efficiency is not as high as that of nitroxides. The use of cobalt control agents will be discussed later.

b) Reversible deactivation by atom transfer

The main RDRP technique based on this mechanism is certainly atom-transfer radical polymerization (ATRP). In an ATRP process, the dormant species is an alkyl halide (*i.e.* a polymer chain capped with a halogen atom, P_n-X) which reacts with a

ligand-stabilized transition metal complex under its lower oxidation state (Mt^n/L) through a redox process (see Scheme II.3). Copper constitutes the most widespread transition metal in ATRP although other examples include iron, osmium or ruthenium. The efficiency of an ATRP reaction can be related to the activity of the catalyst and the associated rate constants, $k_{activation}$, $k_{desactivation}$ and their ratio, K_{ATRP}. Besides the experimental conditions, the rate constants of a Cu-based ATRP process are mainly influenced by the nature of the ligand and the monomer. A further understanding of ATRP and its derivatives -including AGET, ARGET, ICAR, eATRP and SET-LRP- has been given in recent reviews by Matyjazewski and coworkers.[20,21]

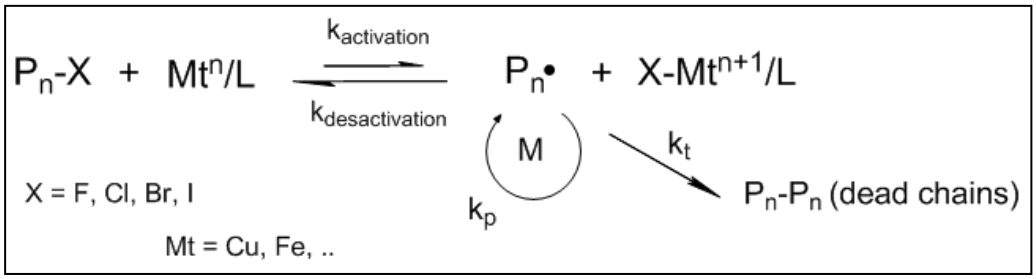

Scheme II.3. General mechanism of a RDRP based on a reversible deactivation by atom transfer.

The reactivity of MAMs and LAMs can be extremely different in ATRP. Under similar experimental conditions, a 90 % conversion can be achieved within 1 second for acrylonitrile, 10 hour for styrene and 15 years for vinyl acetate.[20] As a consequence, the ATRP catalyst must be carefully selected and match the reactivity of the monomer. Thus, the usual deactivating species that are successful for the ATRP of styrenics and acrylates are far too reactive for the VAc radicals, which results in a too high $k_{deactivation}$. An additional difficulty associated to the ATRP of VAc is the stronger energy of the VAc-X bond, which requires a particularly efficient CuX/L to obtain a high $k_{activation}$. Up to date, a single example has been demonstrated using a low active copper complex stabilized by terpyridine ligands.[22] Both first-order kinetics and linear increase of molecular weights with conversion were evidenced. PVAc with M_n weights up to 12000 $g.mol^{-1}$ and moderate dispersities ranging between 1.5 and 1.8 could be obtained. A greater degree of control was demonstrated with iron complexes and a iodoinitiator even if a concomitant iodine-transfer polymerization (*vide infra*) could be thought to compete with ATRP.[23]

Furthermore, the competing transformation of the halogen chain end into an aldehyde group is a severe drawback for the macromolecular engineering based on the ATRP of vinyl acetate.[22]

c) Degenerative chain transfer

(1) Definition and kinetics

In a degenerative transfer-based process, the equilibrium is generated by a direct and continuous exchange between dormant species and propagating chains (see Scheme II.4).

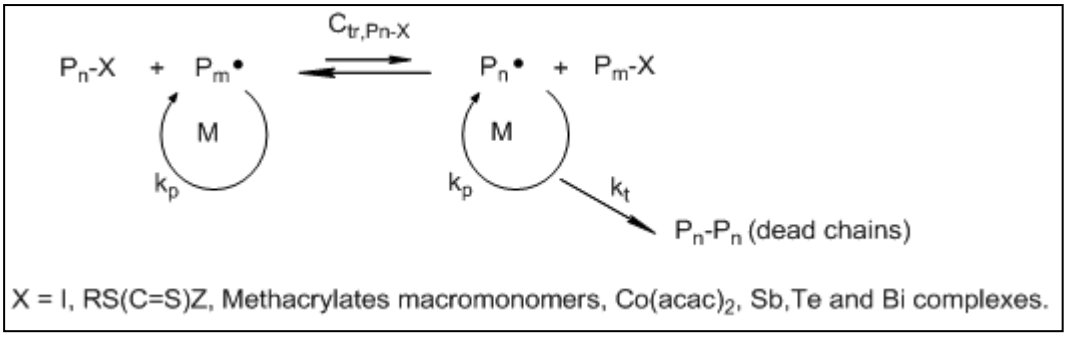

Scheme.II.4. General mechanism of a RDRP based on a degenerative transfer.

Regardless of its anionic or radical nature, the kinetics of a degenerative transfer process can be roughly modeled through two main constants, namely the interchain transfer agent ($C_{tr,PnX}$) and the transfer constant to agent ($C_{tr,X}$).[24] The value of these constants will determine the values of dispersity and degree of polymerization obtained at a given conversion. The dispersity of a polymer sample (Đ) can be estimated at full monomer conversion by the following equation:

$$Đ \approx 1 + \frac{1}{C_{tr,PnX}}$$

A high value of $C_{tr,PnX}$ that characterizes a fast exchange will result in a sample having a low dispersity (see Scheme.II.5.a)). A dispersity of 2 is achieved when $C_{tr,PnX}$ equals 1. Additionally, the evolution of molecular weights upon increasing conversion depends on the value of $C_{tr,X}$. The profile of experimental M_n will tend to get closer to the theoretical linear one at higher values of $C_{tr,X}$. When this value exceeds 50, the

experimental molecular weights will match the theoretical ones at low conversions. If this value equals one, the experimental M_n will be the same throughout the whole range of conversion and match the predicted ones at final conversion (see Scheme.II.5.b).

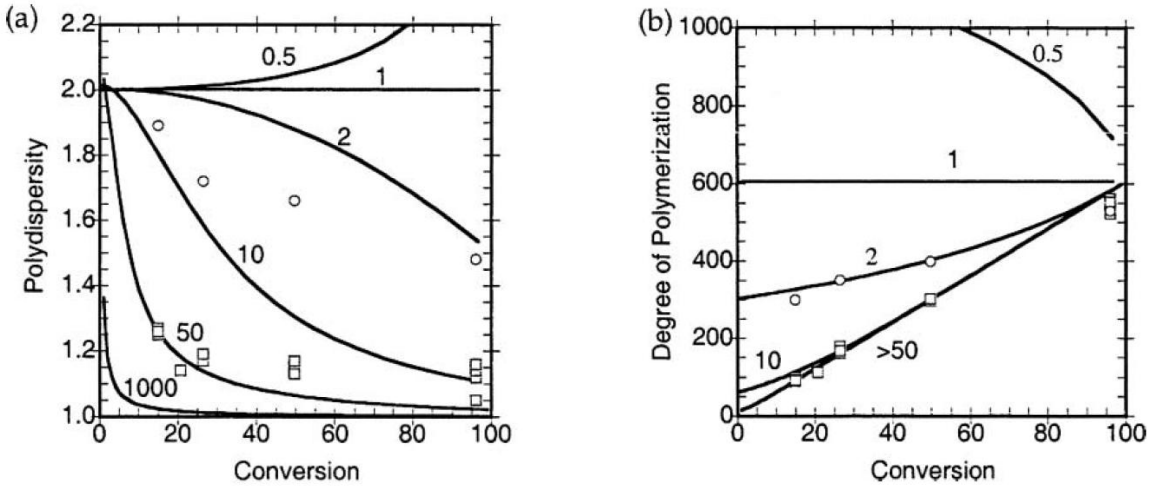

Scheme II.5. Evolution of a) dispersity as a function of conversion and $C_{tr,PnX}$ and b) degree of polymerization as a function of conversion and $C_{tr,X}$. Reproduced from reference [25].

In the next sections, the discussion will focus on modern degenerative transfer-based techniques involving radicals, therefore excluding group transfer polymerization. Roughly speaking, such techniques can be seen as a free radical polymerization process driven by a dynamic exchange induced by an appropriate reversible chain transfer agent. The main RDRP techniques and their corresponding CTAs that have been developed so far will be then introduced.

(2) Organometallic-mediated radical polymerization

Contrary to the ATRP mechanism, organometallic-mediated radical polymerization (OMRP) involves the formation of a cleavable carbon-metal bond.[26] Examples of metals used in OMRP mostly include cobalt,[27] iron,[28] chromium[29] and vanadium.[30]

In the field of OMRP, cobalt has been the most studied transition metal thus far and is specifically coined cobalt-mediated radical polymerization (CMRP).[27] Interestingly, the associated mechanism strongly depends on the nature of the ligands. Thus, the Co(II)/porphyrin complex (see Scheme.II.6.a))) is a persistent

radical and has been successfully used in the CMRP of acrylates through a reversible deactivation mechanism. When the polymerization of styrenics and methacrylates is performed, the predominant mechanism involves an H-abstraction and is then called catalytic chain transfer polymerization (CCTP). Concerning the polymerization of vinyl acetate with this same Co(II) complex, the control could only be achieved at conversions lower than 10 %.[31] The substitution of porphyrin for acetylacetonate ligands (see Figure II.12.b)) allowed controlling the polymerization of VAc under thermal initiation at 30 °C.[32] Even at high conversions, the agreement between theoretical and experimental M_n was observed in conjunction with dispersities ranging between 1.2 and 1.33. The polymerization then follows a degenerative chain transfer mechanism where dormant species are Co(III)-PVAc chains.[33] Interestingly, this can be turned into a reversible termination mechanism when adding Lewis bases such as water and pyridine.[34]

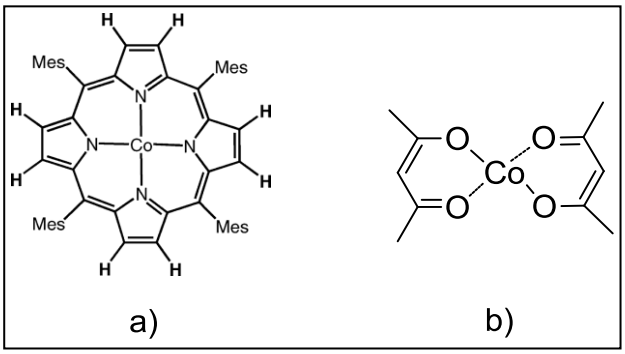

Scheme.II.6. Molecular structures of a) tetramesitylporphyrinato and b) acetylacetonate cobalt complexes.

(3) Organoheteroatom-mediated radical polymerization

Organoheteroatom-mediated radical polymerization[35] (OHMRP) involves organic compounds based on tellurium, antimony, bismuth in a predominant degenerative transfer mechanism. Iodine-transfer polymerization can also be classified as an OHMRP technique but exclusively follows a DT mechanism.

(a) Iodine-transfer polymerization

Iodine-transfer polymerization (ITP)[36] was discovered in the 70s at Daikin and constitutes the first discovered RDRP technique. In an ITP process, the chain transfer agent is an alkyl iodide. The CTA can be also generated in situ from molecular iodine in a so-called reverse iodine transfer polymerization (RITP).[37] These two techniques allow controlling the free radical polymerization of styrenics, (meth)acrylates, vinyl acetate, chlorinated and fluorinated olefins in a successful manner. However, a major drawback of this technique is the weak and light-sensitive C-I bond and the disproportionation of iodine in aqueous medium. Thus, the ITP of hydrophilic monomers is rather limited and usually requires the polymerization of derivatized monomers in non-aqueous media.

The ITP polymerization of VAc has been first reported by Iovu and Matyjaszewski.[38] Using either 1-iodoethyl acetate or methyl 2-iodoproprionate as CTA in 1,4-dimethoxybenzene at 50 °C (see Scheme II.4), they observed good matching between experimental and theoretical molecular weights up to 20000 $g.mol^{-1}$ as well as dispersities inferior to 1.5. Similarly to ATRP and brominated chain ends, a decomposition of the iodide terminal group into aldehyde moieties was observed by ^1H NMR.

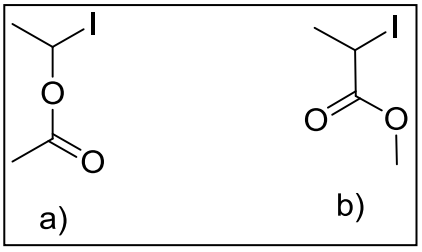

Scheme II.4. Molecular structure of a) 1-iodoethyl acetate and b) methyl 2-iodopropanoate.

(b) Tellure-mediated radical polymerization

Tellure-mediated radical polymerization (TERP) has been successfully implemented to styrenics, (meth)acrylates, N-vinyl pyrrolidone and vinyl acetate by Yamago and coworkers. The control of the polymerization of monomers with different reactivities from a single CTA constitutes a strong advantage of this technique. However, the control of molecular weight during the TERP of VAc with a methyltellanyl transfer agent (see Scheme.II.5.a)) was efficient for only M_n up to

5000 g.mol^{-1}.[35] The experimental values of Đ were reported to increase with conversion. This was attributed to the accumulation of VAc head-to-head adducts leading to invert VAc-TeMe chain ends having a lower reactivity (see SchemeII.5.b)). Using the peak resolution method, the $C_{tr,PnX}$ of a VAc-TeMe normal adduct was estimated to 110 –theoretically leading to a low Đ–the $C_{tr,PnX}$ of an inverted VAc-TeMe adduct was estimated at 1.2.[39] Note that the stibine-mediated radical polymerization (SBRP) of VAc was also reported by Yamago and coworkers.[40]

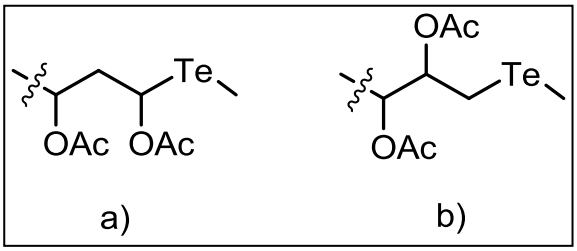

Scheme II.5. Molecular structure of a) head-to-tail VAc-TeMe adducts and b) head-to-head PVAc-TeMe adducts. Reproduced from reference 39.

(4) Reversible addition-fragmentation transfer polymerization[41]

The reversible addition-fragmentation transfer polymerization (RAFT) was first developed in 1998 simultaneously by the CSIRO and the CNRS in collaboration with Rhodia. The discovery of RAFT polymerization is rooted in seminal works on the degenerative transfer with methacrylate macromonomers and the chemistry of xanthates.[42,43] The RAFT mechanism involves thiocarbonylthio compounds (R-S(C=S)Z) as chain transfer agents (see Scheme.II.7) but is specifically coined MAcromolecular Design via the Interchange of Xanthates (MADIX) when Z is an *O*-alkyl group.[44]

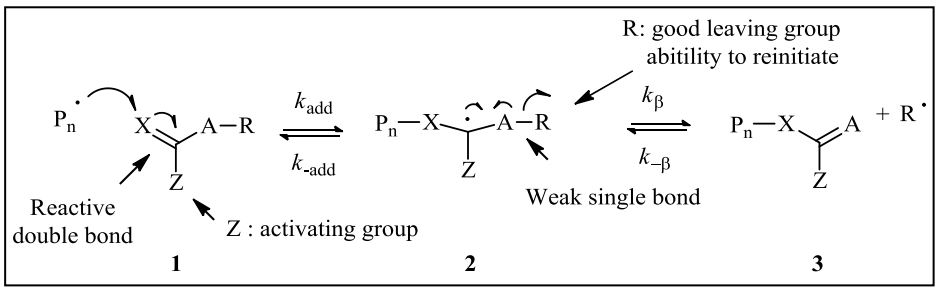

Scheme.II.7. Scheme of a reversible addition-fragmentation mechanism. In the RAFT mechanism, X=A=S whereas X=A=C for methacrylate macromonomers.

In a RAFT/MADIX process, the propagating chain adds to the C=S bond of the CTA, with a high value of the addition rate coefficient (k_{add}) as a prerequisite. An intermediate species with a carbon-centered radical is then formed (Species 2 in Figure II.13). The RAFT mechanism thus differs from other DT techniques such as OHMRP which only imply transition states. Furthermore, the existence of this reaction intermediate may induce retardation, which has been subject to intense debates in the RAFT community on the underlining kinetic reasons.[45-47] The role of the Z group is to destabilize the species 2 towards its fragmentation into the species 3 and a new radical (R°). In kinetic terms, the value of k_{β} should be higher than that of k_{-add}. in order to further favor the fragmentation over the invert addition. Additionally, the R group should also be designed to be a good leaving group to increase k_{β} versus k_{-add}. Moreover, the R group should be able to initiate a monomer species thereafter. After this initial equilibrium, a subsequent dynamic exchange between growing polymer chains and dormant chains is established (see Scheme.II.8). When synthesizing diblock copolymers, this R group criterion prompts to first polymerize the monomer having a higher radical stability.

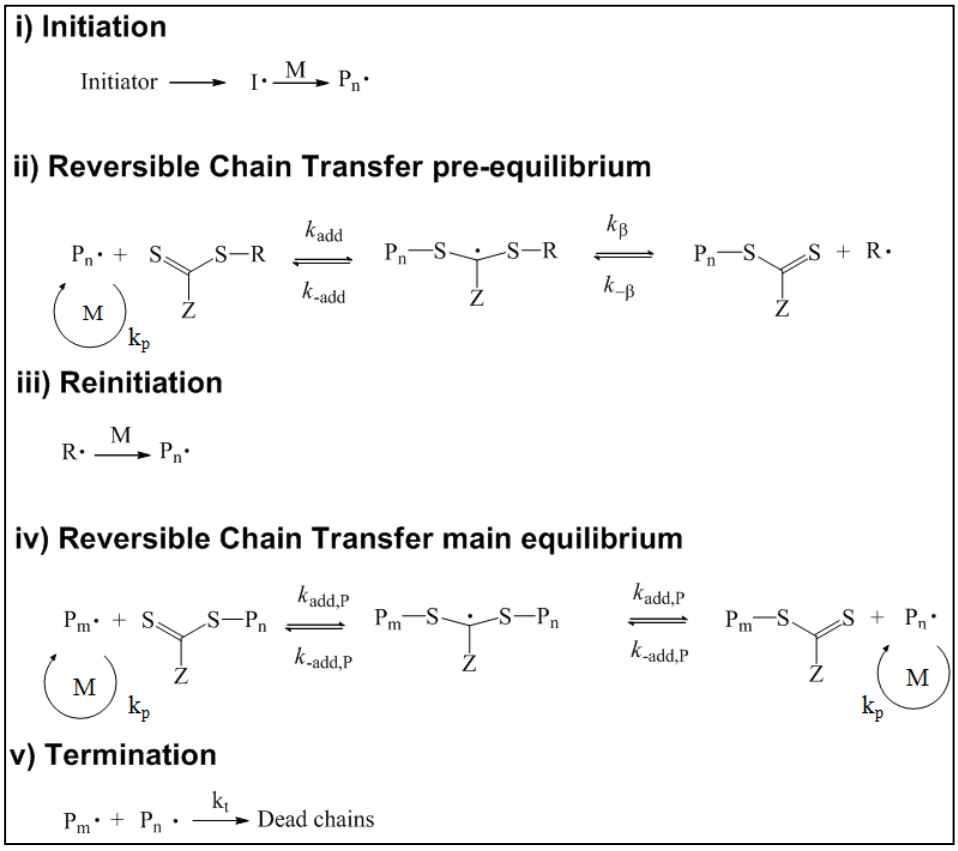

Scheme.II.8. General scheme of the RAFT polymerization showing the usual steps of free radical polymerization and the concomitant RAFT equilibria.

As mentioned above, the nature of the Z group greatly influences the reactivity of the C=S bond. In a broad outline, this group must be selected depending on the nature of the monomer (*i.e.* either MAM or LAM). The higher stability of MAM radicals requires a Z group that stabilizes the species 2 and concomitantly increases the value of k_{add} for the considered MAM. This can be achieved when the Z substituent is electrodonor (Z = phenyl, methyl) or exhibits weak electrowithdrawing properties (Z = SCH_3, pyrrolidone) (see Scheme.II.9). However, this kind of RAFT agents tends to give a bad control or even inhibit the polymerization of LAMs as a result of their poor leaving ability. An efficient control on the polymerization of LAMs actually requires a Z substituent that destabilizes the reaction intermediate 2 and promotes the fragmentation towards the species 3 (*i.e.* a high k_β). When Z is a xanthate (Z = OEt) and, to a lesser extent, a dithiocarbamate (Z = NEt_2) (see Scheme II.9), the resulting mesomeric effect affects the stability of the intermediate in such a manner. Inversely, xanthates have no effect on the polymerization of methyl methacrylate. As a matter of fact, a major challenge in RAFT polymerization is the identification of universal RAFT agents that are able to polymerize both LAMs and MAMs in a controlled manner. Fluorodithioformates (Z = F) were computed to promote both high values of k_{add} and k_β although their design with a suitable R group is yet to be achieved.[48] More recently, a pH-switchable dithiocarbamate was proven to successfully mediate the polymerization of LAMs and, in its protonated version, that of MAMs. [49,50]

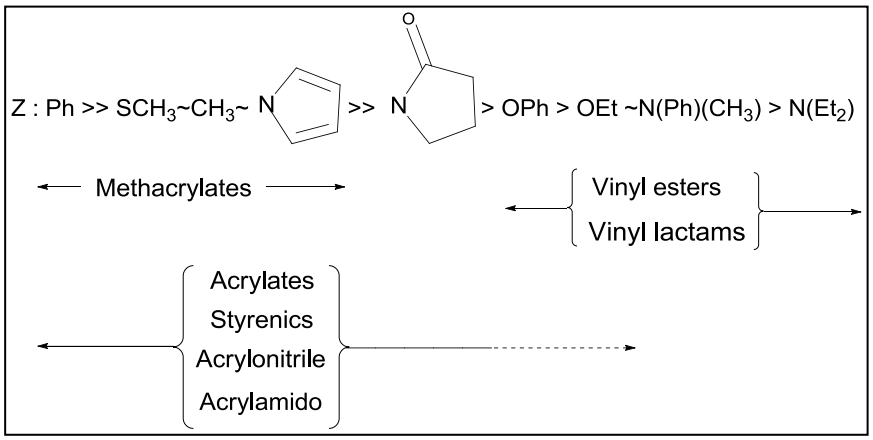

Scheme.II.9. Influence of the Z substituent on the control on the polymerization of usual vinyl monomers through RAFT/MADIX techniques.

Throughout the next chapters, the polymerization studies will be based on the use of *O*-ethyl xanthates to control the polymerization of various LAMs. This class of xanthates is particularly advantageous as no secondary fragmentation is observed contrary to *O*-isopropyl xanthates.[51] Additionally, they usually have little effect on the polymerization rates. A prominent example of such *O*-ethyl xanthates is methyl 2-((ethoxycarbonothioyl)thio)propanoate, registered under the Rhodixan A1 name. It can be readily synthesized in quantitative yields through the nucleophilic substitution of a bromoester by a xanthic salt in a protic solvent (see Scheme II.10).

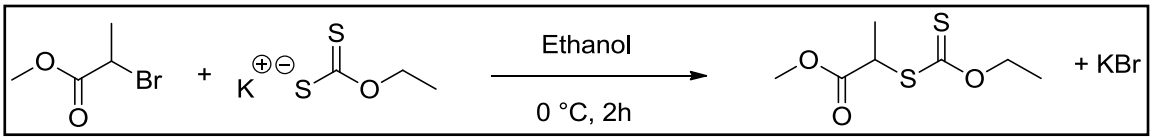

Scheme II.10. Reaction scheme for the synthesis of Rhodixan A1.

The scope and kinetic effects of this chain transfer agent on the RAFT/MADIX polymerization of various monomers have been evaluated through their respective values of $C_{tr,X}$ and $C_{tr,PnX}$ (see Scheme.II.11).[52] A specificity of Rhodixan A1 is its high activity for the RAFT/MADIX polymerization of LAMs with $C_{tr,X}$ and $C_{tr,PnX}$ exceeding 15 for vinyl acetate, vinyl phosphonates or vinyl N-pyrrolidone.

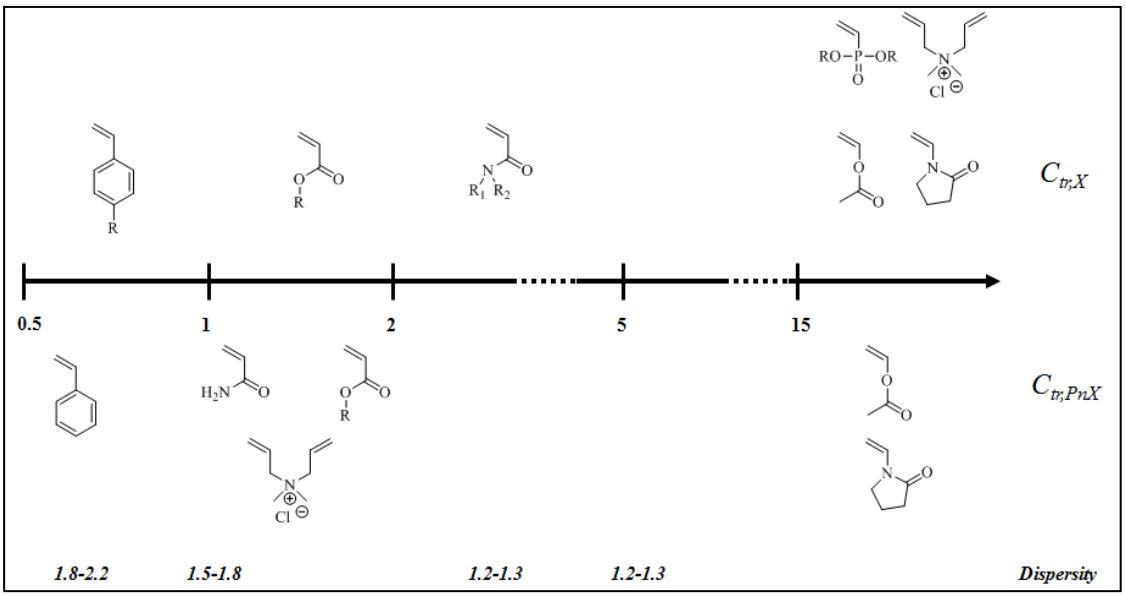

Scheme.II.11. Kinetics transfer constants of Rhodixan A1 for various monomers, determined at 60 °C.

Advantageously, it also allows the control of the polymerization of acrylates and acrylamido monomers. Following the values of $C_{tr,x}$ and $C_{tr,PnX}$ reported for these monomers, the molecular weights will be efficiently controlled whereas the dispersities can be anticipated to be higher than those obtained during the polymerizations of LAMs with a xanthate. Therefore, diblock copolymers comprising both a LAM block and a MAM one can be achieved with this CTA. As a result, Rhodixan A1 circumvents the use of universal RAFT agents.

In concluding on RDRP techniques, RAFT/MADIX polymerization is undoubtedly the technology of choice to achieve the synthesis of well-defined polymers of vinyl acetate and PVAc-based amphiphilic block copolymers. CMRP may also present interesting features to do so but the scope of hydrophilic monomers polymerizable by this technique is still restricted. Therefore, the next sections will describe the RAFT/MADIX polymerization of VAc with Rhodixan A1.

II. Poly(vinyl acetate)-based (co)polymers: from design to solubility in sc-CO_2.

A. PVAc homopolymers

1. Chain length effects

a) Synthesis of PVAc of variable chain lengths

Following the principles of RAFT/MADIX polymerization, we synthesized PVAc samples with M_n ranging from 2 k (standing for 2000 g.mol^{-1}) to 6 k (Table II.3) to probe the effect of chain length on the solubility in sc-CO_2. This aimed at constituting reference materials for the following solubility studies of block copolymers.

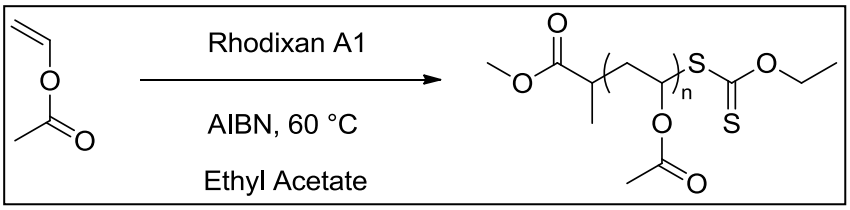

Scheme.II.12. Experimental conditions for the RAFT/MADIX polymerization of vinyl acetate.

The polymerization of VAc was carried out at 60 °C in ethyl acetate with Rhodixan A1 (see Scheme.II.12). Polymerization conditions were set up to provide a repeatable and straightforward modus operandi leading to high conversions of vinyl acetate. Ethyl acetate was selected as the solvent of polymerization as it advantageously exhibited a low transfer constant to solvent ($C_{tr,s}$ comprised between 1.7 and 3.4*10^{-4} at 60 °C, see in Table II.1) and, to a lesser extent, a low toxicological profile.

The experimental results confirmed the good control provided by Rhodixan A1 on the polymerization of VAc. Experimental values of M_n–determined by SEC–were in very good agreement with the theoretically predicted ones up to high conversion. However, dispersities were found to increase with targeted M_n (see Table II.2). As suggested by the matching between the theoretical and experimental M_n, the transfer to solvent was negligible over the course of the polymerization. This was in accordance with the low transfer constant of VAc radicals to ethyl acetate.[53]

Therefore, the noticeable increase in dispersity may be due to combined effects of chain transfer to polymer[13], monomer and head-to-head defects[39] during the course of the polymerization. It is worth mentioning that their occurrences are expected not to impact the values of M_n but only those of Đ. Chain transfer to polymer is actually known to be responsible for the formation of a substantial amount of chain branches during the free radical polymerization of VAc.[13] The values reported for the transfer constant to polymer ($C_{tr,pol}$) ranges from 1 to 8.10^{-4} depending on the polymerization conditions.[53] A similar remark applies to the chain transfer to monomer which is of same order of magnitude (*i.e.* between 1.75 and $2.75*10^{-4}$ at 60 °C). In parallel to this, the polymerization of VAc also suffers from a non-negligible proportion of regioirregularities.[53] Head-to-head additions lead to the formation of primary radicals which, once in the dormant state, presumably have a much lower interchain transfer constant ($C_{tr,PnX}$) than secondary radicals generated by head-to-tail additions.[39] In the case of organotellurium-mediated polymerization of VAc, this resulted in a significant increase in Đ upon increasing the targeted chain lengths.[39] This behaviour was also reported with the iodine-transfer polymerization of vinylidene fluoride for which the rate of inverted adducts increased with higher DP_n.[54]

Sample	Conv. (%)[a]	$M_{n\ theo}$ ($g.mol^{-1}$) [b]	$M_{n\ SEC}$ ($g.mol^{-1}$) (Đ) [c]	T_g (°C)
$PVAc_{1.8k}$-Xa	95	2000	2000 (1.20)	13.5
$PVAc_{3.8k}$-Xa	92	4050	4000 (1.30)	21.2
$PVAc_{5.8k}$-Xa	97	6000	6050 (1.61)	29.7

[a] Determined by ^1H NMR in $CDCl_3$. [b] Theoretical M_n = $[VAc]_0$/ [Rhodixan A1]$_0$×MW(VAc)×conv./100+MW(Rhodixan A1). [c] Determined by SEC in THF with PMMA standards.

Table II.2. Experimental results for the RAFT/MADIX polymerization of vinyl acetate.

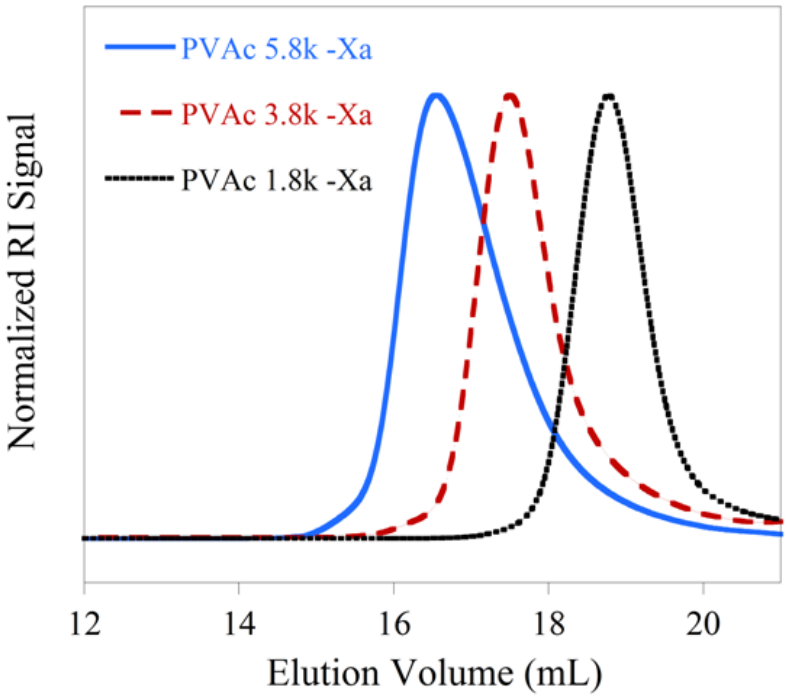

Figure II.1. Overlay of normalized SEC-RI chromatograms of PVAc samples with increasing molecular weights.

The PVAc samples synthesized with increasing chain lengths were characterized via MALDI-TOF MS measurements to assess their ω-functionalization by a xanthate moiety. A MALDI-TOF mass spectrum of a $PVAc_{1.8k}$-Xa is given in Figure II.2. All peaks are 86.1 m/z apart from each other corresponding to the molar mass of a vinyl acetate monomer unit. The unique population could be attributed to PVAc polymers initiated by a methyl propionyl radical and capped with an *O*-ethyl xanthate chain end (see Table II.3). Interestingly, no fragmentation of the chain end was induced by the MALDI-TOF MS analysis, contrary to previous reports on the MALDI-TOF analysis of xanthate-terminated polystyrenes.[55] In the low molecular weight range, the relatively high intensities may be related to the formation of the PVAc chains terminated with an inverted VAc unit (head-to-head addition) and a xanthate.[39] However, this could not be confirmed with the samples of higher M_n ($PVAc_{3.8k}$-Xa and $PVAc_{5.8k}$-Xa) where significant mass discriminations were observed. Their larger dispersities actually resulted in the higher discrimination against polymer chains of higher molecular weight. This is particularly evidenced when dispersities exceed 1.3.[56]

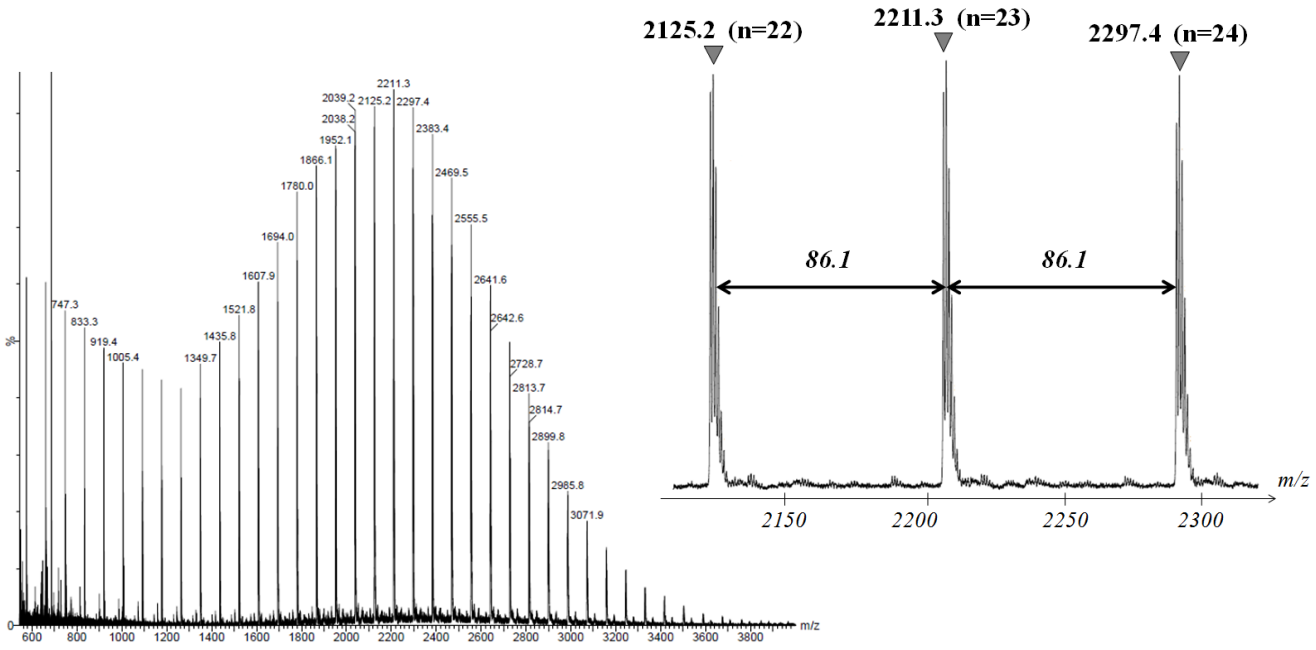

Figure.II.2. MALDI-TOF mass spectrum of a $PVAc_{1.8k}$-XA sample.

α end	ω end	DP_n	Cation	$M_{n,theo}$	$M_{n,exp}$
CH_3-O-C(=O)-CH-CH_3	-SC(=S)-OCH_2CH_3	22	Na^+	2125.3	2125.2
CH_3-O-C(=O)-CH-CH_3	-SC(=S)-OCH_2CH_3	23	Na^+	2211.4	2211.3
CH_3-O-C(=O)-CH-CH_3	-SC(=S)-OCH_2CH_3	24	Na^+	2297.5	2297.4

Table II.3. Peak assignments in the MALDI-TOF mass spectrum of $PVAc_{1.8k}$-Xa (Scheme II.2).

The PVAc samples were eventually characterized by differential scanning calorimetry (DSC). At the solid state, the T_g values of PVAc polymers exhibited a slight dependence of T_g on M_n (see in Table II.2). Hence, the experimental T_g value of 29.7 °C for a $PVAc_{5.8k}$–Xa was close to the infinite T_g value of PVAc which was reported to be 36.5 °C.[57]

b) Determination of polymer solubility through infrared spectroscopy

The solubility of these PVAc with varying chain lengths was then assessed. The measurement of polymer solubility usually relies on repeated visual observations of (de)mixing transitions in a variable-volume view cell. This allows the determination of cloud point coordinates for a sample at a single polymer /CO_2 ratio over a large range of temperatures. Based on the work of Martinez *et al.*, our approach used an

isochoric cell to measure the solubility of samples *versus* CO_2 density in a more straightforward manner.[25] It has been shown by a number of authors that the logarithm of the solubility of solid solutes in sc-CO_2 is linearly proportional to the density or to the logarithm of density.[64] Hence, solubility data in sc-CO_2 are usually presented as a function of CO_2 density. High pressure infrared spectroscopy actually offered an alternative way of determining the solubility of polymers in sc-CO_2 by measuring the growth of a characteristic vibrational band with increasing pressures (see Figure.II.3). Using the CO_2 state equation, the solubility of the polymer can thus be plotted as a function of CO_2 density. Building on that, Martinez *et al.* reported the solubility of various hyperbranched polymers in sc-CO_2 along with two isotherms at 40 °C and 100 °C.[25]

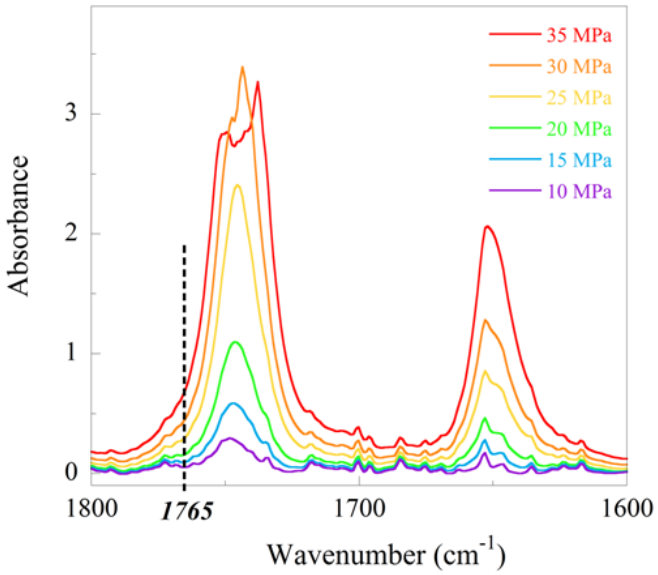

Figure II.3. Overla PVAc$_{2.7k}$–Xa block copolymer with in

Following these principles, the vibrational band of esters at 1745 cm^{-1} was selected to measure the solubility of the (co)polymers synthesized in this study (see Figure II.3). Since the absorbance of the characteristic band at 1745 cm^{-1} reached values out of the linear range of the Beer–Lambert law, absorbance values for all samples were measured at 1765 cm^{-1}. Interestingly, a red shift of around 10 cm^{-1} was observed at low pressures, which is characteristic of an electron donor–acceptor complex, *i.e.* a Lewis acid–base interaction between CO_2 (acid) and the acetate group (base). Similar findings were thus observed during the formation of an acetone–CO_2 complex and its preferred conformation.[65]

Yet, ε was assumed to be independent of pressure and temperature at higher pressures. The molar extinction coefficient (ε) of the C=O vibrational band was consequently determined at 1765 cm^{-1} from a fully solubilized sample of $PVAc_{2k}$–Xa at 40 °C and 25 MPa. This coefficient was evaluated to 39.9 L mol^{-1} cm^{-1}. The same experiment was repeated both in carbon tetrachloride and with other samples in sc-CO_2 to confirm this experimental value.

c) Solubility of PVAc in sc-CO_2

Then, we determined the solubility of PVAc polymers in CO_2 as a function of their number-average molecular masses to constitute a comparison platform for the entire study (see Figure II.4). At a CO_2 density of 0.88 g cm^{-3} (*i.e.* 220 bar and 40 °C), 1 % wt of $PVAc_{1.8k}$–Xa was fully soluble. The longer PVAc polymers were far less soluble: 0.81 % wt of $PVAc_{3.8k}$–Xa was solubilized at 0.94 g cm^{-3} whereas only 0.38 % wt of $PVAc_{5.8k}$–Xa was detected at the same density (see Figure II.4). In comparison, Lee *et al.* reported slightly lower cloud point coordinates for 0.2 % wt of a PVAc (M_n = 2300 $g.mol^{-1}$) at 186 bar and 40 °C.[15] Kilic *et al.* measured a solubility of 1 % wt for a PVAc polymer (M_n = 3090 g mol^{-1}) at 25 °C and 310 bar.[66]

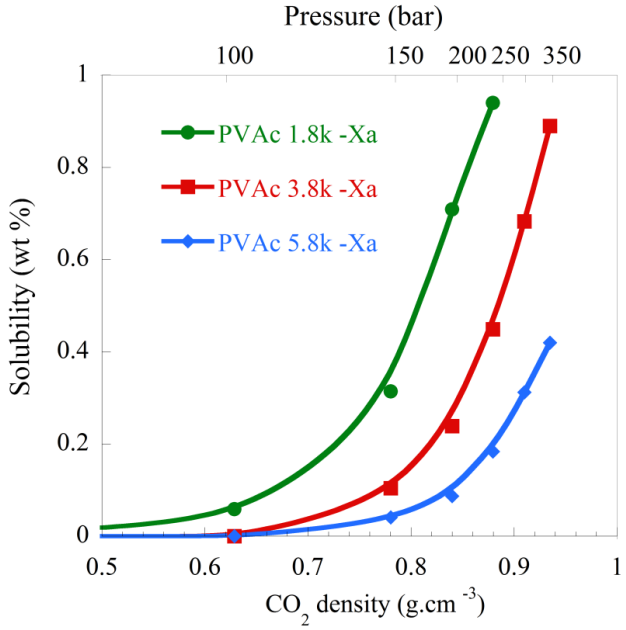

Figure II.4. Solubility (% wt) of PVAc–Xa samples with increasing chain lengths in sc-CO_2.

2. Chain end group effects

Adding to the chain length effects, chain end groups also play an important role in the solubility of low M_n polymers in sc-CO_2.[7,58] A series of PVAc samples exhibiting a M_n close to 4 k but different chain end groups were consequently synthesized and, then, evaluated as CO_2-philic materials through infrared spectroscopy.

a) Removal of the xanthate end group

In particular, the xanthate group was suggested to strongly lower the solubility of poly(vinyl acetate)-*alt*-poly(dibutyl maleate) copolymers as concluded from a comparison between samples synthesized by telomerization and by RAFT/MADIX polymerization.[58] To probe this effect, the xanthate end-capping group was initially removed from a $PVAc_{4k}$ -Xa. The reduction of the xanthate moiety to a thiol end group was first considered by means of aminolysis with a primary amine such as *n*-butylamine. However, the formation of disulfide bonds during purification steps and the subsequent doubling of the molecular weight of the whole polymer sample were observed.

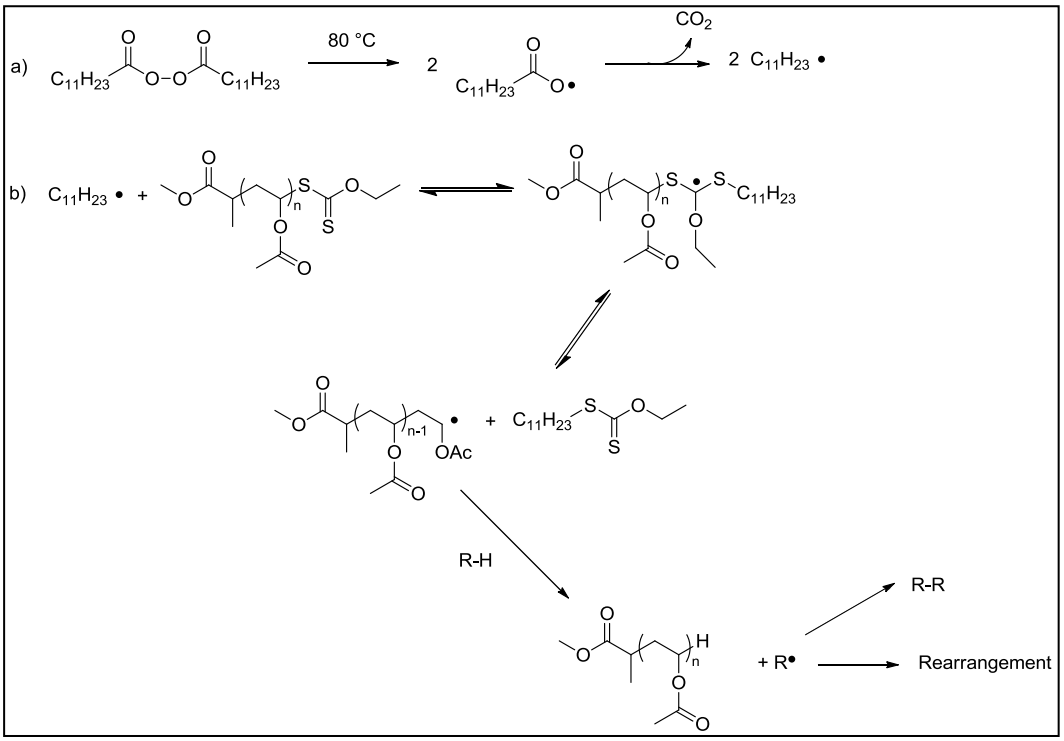

Scheme.II.13. Reaction mechanism for the removal of the xanthate using dilauroyl peroxide in 2-propanol at 80 °C.

The radical reduction of xanthates was carried out and helped solving this problem. This reduction is usually achieved through a free radical pathway using dilauroyl peroxide in a H-donor solvent (see Scheme.II.13).[59] In our case, a mixture of THF and 2-propanol was used to ensure the complete solubilization of the PVAc starting materials, following the methodology published by Tong *et al.*[60]

The removal was confirmed by SEC-UV at a wavelength of 290 nm (see Figure II.5.a)) which is the maximum absorbance wavelength at which the C=S bond absorbs in the UV domain. No high-molecular weight shoulder appeared on the SEC-RI traces, suggesting the absence of coupling reactions between PVAc macroradicals (see Figure II.5.b)).

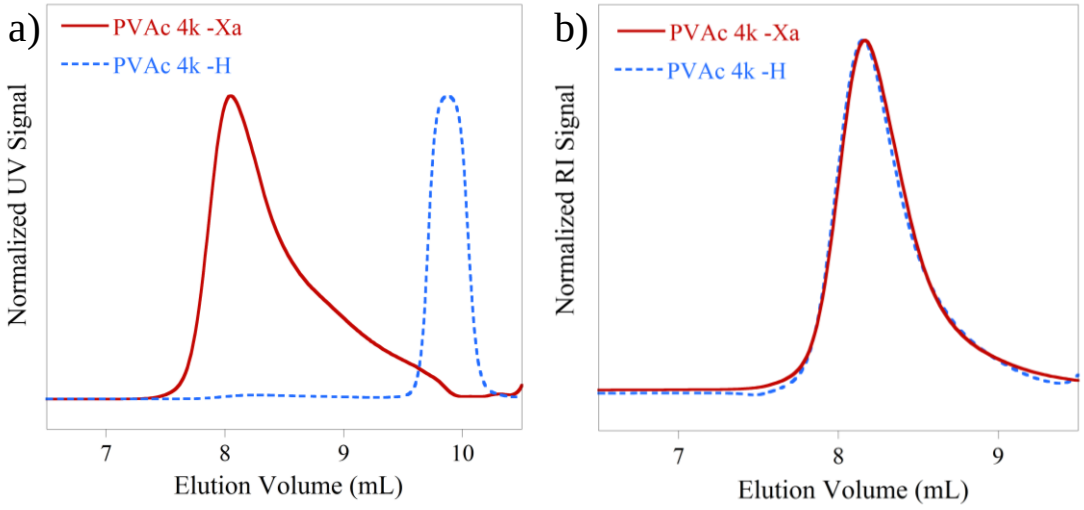

FigureII.5. Overlay of SEC chromatograms for $PVAc_{4k}$-Xa (blue dotted line) and a $PVAc_{4k}$-H (red full line) in a) UV detection at 290 nm and b) RI detection.

Additional experimental evidence of the disappearance of the xanthate moiety was given by MALDI-TOF MS analysis (see Figure.II.6.a) and b)). Again, significant mass discriminations appeared due to a dispersity of 1.4. However, the detailed views evidenced the shift of the peaks of the main population (▼) from 3244.7 m/z (see Figure II.6.a)) to 3124.9 m/z (see Figure II.6.b)). This difference of 119.8 m/z could be attributed to the loss of $-SC(=S)-OCH_2CH_3$ and the creation of a $PVAc_{4k}$-H chain via a hydrogen atom transfer to propan-2-ol. Two secondary populations were also observed after the radical reduction of the xanthate chain end but could not be attributed.

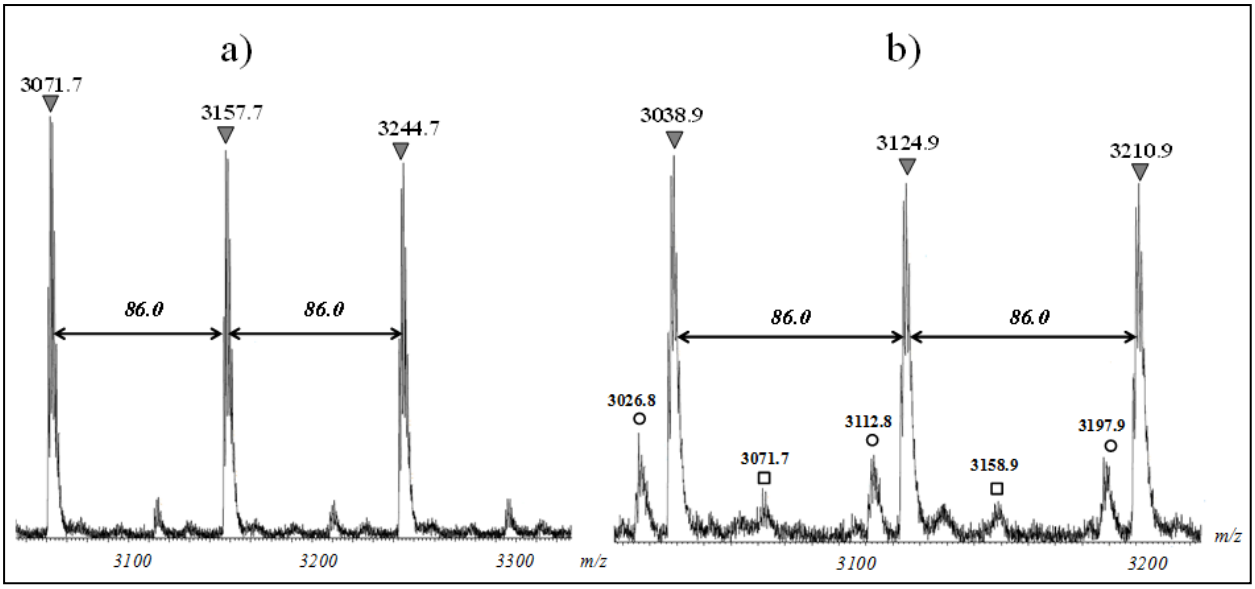

Figure.II.6. Detailed views of MALDI-TOF mass spectra corresponding to a $PVAc_{4k}$-Xa a) before and b) after reduction of the xanthate group ($PVAc_{4k}$-H).

b) Incorporation of a fluorinated end group

Along with this post-polymerization modification, the xanthate chemistry was used to introduce a CO_2-philic fluorinated moiety in the Z-group. Such fluorinated xanthates have been scarcely reported in litterature.[61-64] Recently, the copolymerization of vinylidene fluoride and 3,3,3-trifluoropropene was mediated by a xanthate with a fluorinated R-group to probe the polymerization by ^{19}F NMR.[61] Xanthates bearing an *O*-trifluoromethyl Z group were also designed to investigate the polymerization of styrene in bulk and dispersed media.[62-64] In these latter studies, the fluorinated moiety was aimed at increasing the reactivity of the transfer agent towards the propagating styryl radicals. In our case, the fluorinated moiety was incorporated with an ethylene spacer between the perfluorinated group and the dithiocarbonate group in order to preserve a reactivity similar to that of Rhodixan A1.

This fluorinated xanthate could be obtained through a one-pot synthesis with 1*H*,1*H*,2*H*,2*H*-perfluoro-1-octanol as the starting reactant. Upon deprotonation with a strong base, the alcoolate formed in situ adds to CS_2 to form a xanthate salt. The final fluorinated xanthate (namely methyl 2-((3,3,4,4,5,5,6,6,7,7,8,8,8-tridecafluorooctyloxy) carbonothioylthio)propanoate, F-xanthate, Scheme.II.14)) is then formed by a nucleophilic substitution of the xanthate salt on methyl 2-bromopropanoate in a yield of 64 % after purification on column chromatography. A

similar yield was previously reported for methyl 2-((2,2,2,-trifluoroethyloxy) carbonothioylthio) propanoate.[62]

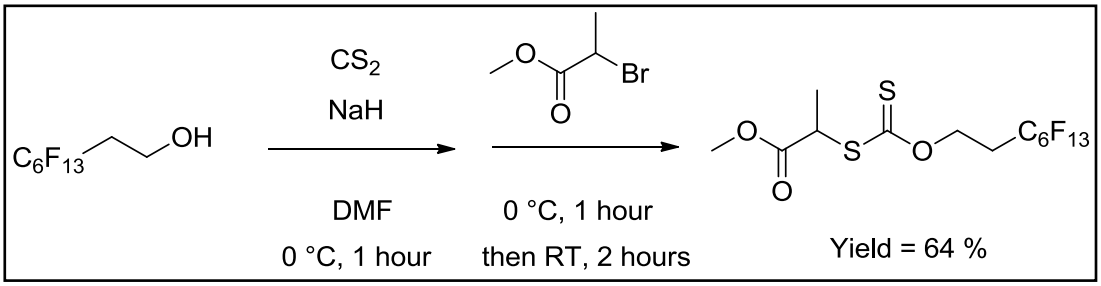

Scheme.II.14. Reaction scheme for the synthesis of F-Xanthate.

F-Xanthate was then used to mediate the polymerization of VAc. As expected, $PVAc_{3.8k}$-FXa (see Table.II.4) exhivited macromolecular characteristics (M_n, Đ, VAc conversion) similar those of a PVAc obtained by RAFT/MADIX polymerization with Rhodixan A1.

Sample	Conv. (%)[a]	$M_{n\ theo}$ (g.mol^{-1}) [b]	$M_{n\ SEC}$ (g.mol^{-1}) (Đ) [c]	T_g (°C)
$PVAc_{3.8k}$-Xa	92	4050	4000 (1.30)	21.2
$PVAc_{4.2k}$-H	-	4200	4200 (1.30)	-
$PVAc_{3.8k}$-FXa	87	4300	3850 (1.26)	15.6

[a] Determined by ^{1}H NMR in $CDCl_3$. [b] Theoretical M_n = $[VAc]_0$/ $[Rhodixan\ A1]_0$×MW(VAc)×conv./100+MW(Xanthate). [c] Determined by SEC in THF with PMMA standards.

Table II.4. Experimental results for the synthesis of PVAc samples with different chain end groups.

c) Solubility of PVAc with different end groups in sc-CO_2

The solubility of PVAc with equivalent molecular weights (M_n = 4000 g.mol^{-1}) but different chain end groups was ultimately assessed. Comparing the influence of hydrogen and xanthate termini, no substantial differences of solubility in sc-CO_2 were found (see Figure.II.6) since they were respectively soluble in proportions of 0.89 % wt and 0.87 % wt at 35 MPa. Therefore, the influence of the xanthate group was negligible in our case for this range of M_n. Differences in microstructures for poly(vinyl acetate-*alt*-dibutyl maleate) copolymers due to dissimilar types of compositional drifts between conventional and controlled radical polymerizations might explain the differences of solubilities observed by Lee *et al.*[58]

Moreover, the xanthate was effectively turned into a solubility enhancer via the introduction of the fluorinated Z-group. As expected, the incorporation of this latter moiety significantly increased the solubility of PVAc$_{3.8k}$-FXa. Indeed, 1 % wt of this sample was soluble at conditions down to 300 bar and 40 °C (see Figure II.6). Although this sample was less CO_2-philic than PVAc$_{1.8k}$-Xa, this clearly demonstrates that the limited intrinsic solubilities of PVAc polymers in sc-CO_2 can be counterbalanced and improved via an appropriate RAFT/MADIX synthesis strategy.

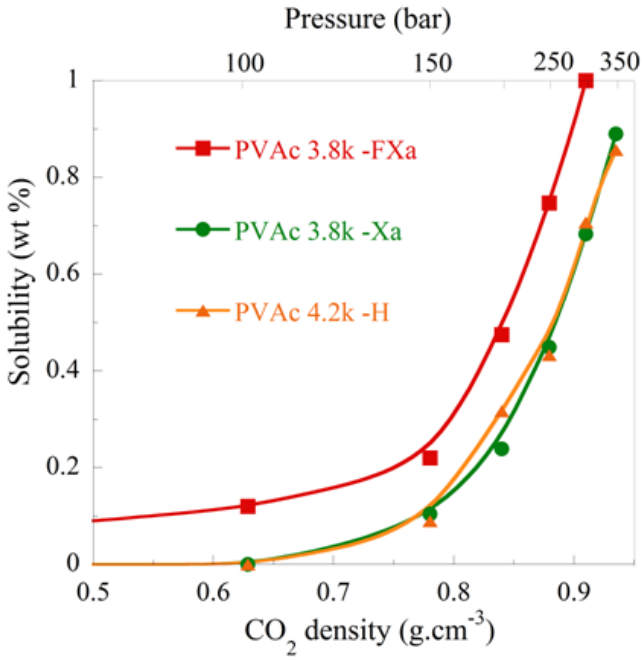

Figure II.6. Solubility (% wt) of PVAc polymers (M_n = 4 kg.mol^{-1}) with different chain end groups.

B. Poly(vinyl acetate)-based amphiphilic copolymers

1. Selection criteria of the hydrophilic monomer

The scope of RAFT/MADIX polymerization is broad considering the range of hydrophilic monomers whose polymerization can be controlled using a xanthate chain transfer agent. This includes vinyl lactams[65-67] like vinyl pyrrolidone, acrylic acid,[68] diallyl dimethyl ammonium chloride,[69] vinyl phosphonic acid[70] as well as hydrophilic acrylate and acrylamido[68] monomers, thus offering large possibilities to conceive amphiphilic copolymers for the stabilization of W/C emulsions. Advantageously, none of these polymers exhibited significant solubilities in sc-CO_2 due to their high self-interactions. However, the low pH of the W/C emulsions – ranging between 2 and 3–[71] constitutes an additional criterion to the selection of the hydrophilic monomer. In this regard, vinyl lactams and acrylamido monomers are preferable over acrylates due to their higher resistance to strong acidic conditions. As part of this initial study, the scope was also restricted to pH and temperature insensitive hydrophilic monomers. For these reasons, N,N-dimethylacrylamide was selected as it fulfilled such criteria and also a high reactivity in radical polymerization. In addition, its polymerization is efficiently controlled up to full conversion compared to the other hydrophilic monomers (*e.g.* vinyl lactams) polymerizable by RAFT/MADIX. This allowed avoiding purification steps which are problematic considering the partial solubilities of oligomers in non-solvents used for precipitation.

2. RAFT/MADIX polymerization of N,N-dimethylacrylamide

A large variety of RAFT/MADIX agents including trithiocarbonates and dithioesters successfully mediates the polymerization of DMA.[72] However, as these agents tend to inhibit the RAFT/MADIX polymerization of VAc, PDMA-PVAc diblock copolymers are not attainable following this synthetic route. The recent developments of universal RAFT agents could address this limitation. Indeed, an elegant alternative using switchable N-(4-pyridinyl)-N-methyldithiocarbamate RAFT agents was published by Benaglia *et al.*[49] who synthesized well-defined PVAc-based diblock copolymers from polystyrene or poly(methyl methacrylate) macromolecular

RAFT agents.[50] Ultimately, *O*-ethyl xanthates like Rhodixan A1 offer a much simpler access to PDMA-PVAc diblock copolymers given that they were shown to control the polymerization of acrylamido monomers.[68]

The polymerization of DMA was conducted at 60 °C in ethyl acetate under dilute conditions of 1.66 mol.L^{-1} in order to minimize exotherm (see Scheme.II.15). As evidenced by SEC, the experimental molecular weights increased upon increasing the targeted M_n (see Figure.II.7). As shown in Table II.5, number-average molar masses determined by SEC were also in agreement with the theoretical ones at the end of the polymerization. This meant that Rhodixan A1 had fully reacted, which was expected from previous kinetic results within the team.[52] Indeed, a chain transfer constant to Rhodixan A1 equal to 2.3 had previously been measured at 60 °C in another solvent (ethanol:water = 4.5:1).[52] Dispersity was in the range of 1.4-1.6 at the end of the polymerization, suggesting a relatively slow exchange of the xanthate group between dormant and active chains.[24]

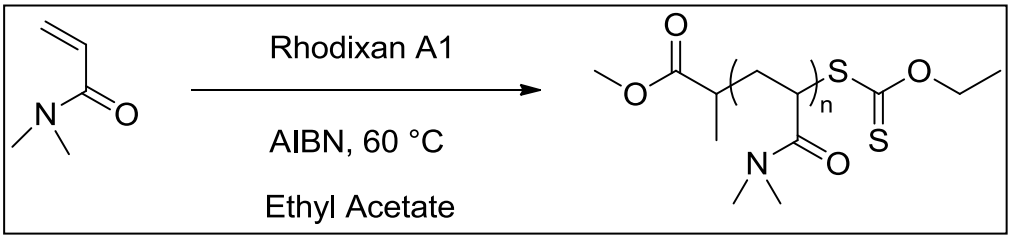

Scheme.II.15. Experimental conditions for the RAFT/MADIX polymerization of N,N-dimethylacrylamide.

A further confirmation was brought by a characteristic ^{1}H NMR signal located at 4.6-4.8 ppm corresponding to a proton located at the alpha position of a xanthate group. From this, the experimental molecular weights could be calculated and were slightly higher than the theoretical ones. (see Table II.5)

Sample	$M_{n\ theo}$ ($g.mol^{-1}$) [a]	$M_{n\ NMR}$ ($g.mol^{-1}$) [b]	$M_{n\ SEC}$ ($g.mol^{-1}$) (Đ) [c]	T_g (°C)
$PDMA_{0.4k}$- Xa	600	500	-	-6.0
$PDMA_{0.8k}$-Xa	1000	1200	750 (1.56)	13.3
$PDMA_{1.0k}$-Xa	1200	1450	1050 (1.48)	42.4
$PDMA_{1.2k}$-Xa	1400	1450	1250 (1.46)	57.6
$PDMA_{2k}$- Xa	2200	2400	2050 (1.46)	79.5
$PDMA_{10k}$-Xa	10200	-	12800 (1.55)	85.5

[a] Theoretical M_n = $[DMA]_0/[xanthate]_0 \times MW(DMA) \times Conv./100 + MW(xanthate)$. [b] Determined by integration of the signals of the proton located at the alpha position of the xanthate moieties. [c] Determined by SEC in DMF + LiBr with PMMA standards. [d] Determined by ^1H NMR in $CDCl_3$. [e] Theoretical M_n = $[VAc]_0/[PDMA\text{-}MADIX\ Agent]_0 \times MW(VAc) \times Conv./100 + M_n(PDMA\ MADIX\ Agent)$. [f] Based on theoretical masses.

Table.II.5. Experimental results for the synthesis and characterization of PDMA homopolymers.

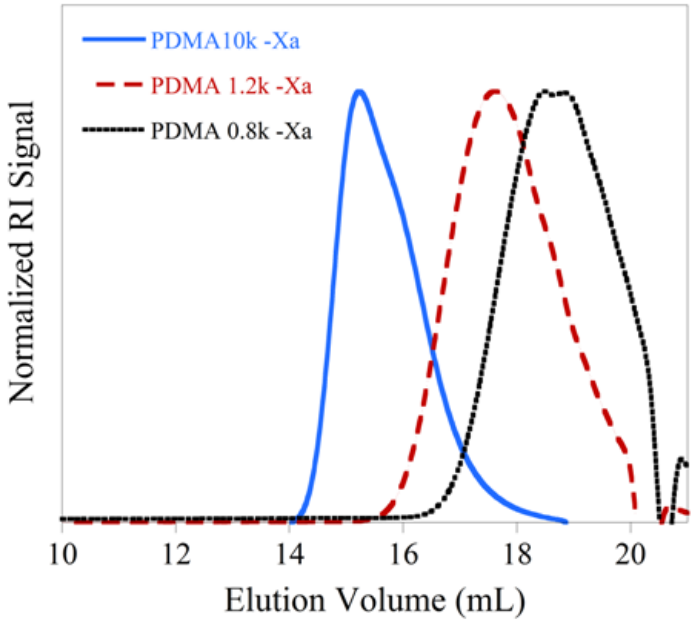

Figure.II.7. Overlay of normalized SEC-RI chromatograms of PDMA samples with increasing molecular weights.

Finally, the functionalization of PDMA chains by the xanthate fragments at both ends was confirmed by MALDI-TOF mass spectrometry (see Figure II.8). The peaks were 99.1 m/z apart from each other, which corresponds to the molar mass of a N,N-dimethylacrylamide monomer unit. The main population was attributed to PDMA chains initiated by a methyl propionyl radical and capped with a xanthate chain end (see Table II.6).

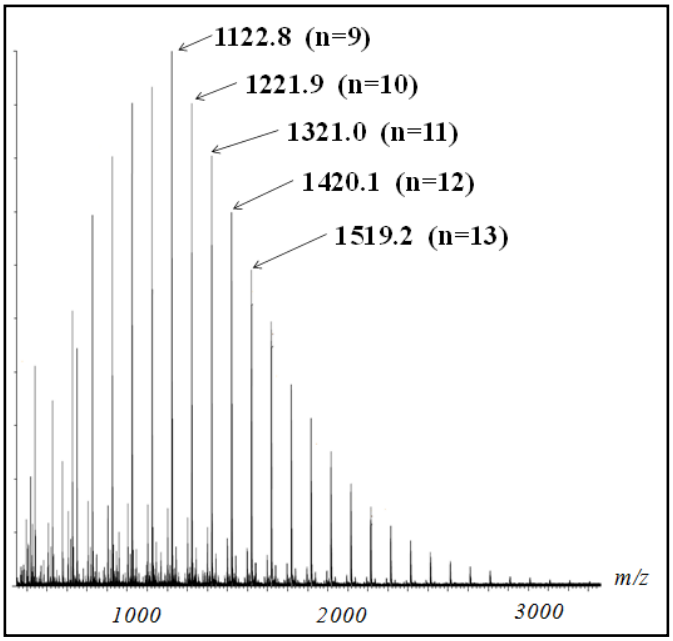

Figure.II.8. MALDI TOF mass spectrum of a PDMA RAFT/MADIX Agent ($M_{n,theo}$ = 1200 g.mol^{-1}).

α end	ω end	DP_n	Cation	$M_{n,theo}$	$M_{n,exp}$	Δ (%)
CH_3-O-C(=O)-CH-CH_3	-SC(=S)-OCH_2CH_3	9	Na^+	1122.6	1122.8	0.02
CH_3-O-C(=O)-CH-CH_3	-SC(=S)-OCH_2CH_3	10	Na^+	1221.7	1221.9	0.02
CH_3-O-C(=O)-CH-CH_3	-SC(=S)-OCH_2CH_3	11	Na^+	1320.8	1321.0	0.02

Table.II.6. Assignments of the peaks in the MALDI-TOF mass spectrum of a PDMA MADIX agent ($M_{n,theo}$ = 1200 g.mol^{-1}).

In the solid state, PDMA oligomers showed a strong dependency of T_g on molecular weight (see in Table II.5). This actually confirmed the results of Fuchise *et al.*[61] who found a mass dependency up to 20 000 g mol^{-1}. The T_g of $PDMA_{10k}$-Xa was only 85.5 °C while the infinite T_g of PDMA ranges around 122 °C. This may be due to the contribution of end groups on the free volume of the polymers, which is expected to be particularly significant for the PDMAs of lowest M_n.

3. Synthesis of PDMA-*b*-PVAc amphiphilic block copolymers

a) Synthesis

The PDMA RAFT/MADIX macromolecular agents were then used to mediate the polymerization of VAc. By using PDMA oligomers with various M_n, we targeted PDMA-*b*-PVAc polymers with various chain lengths for both blocks (see Table.II.7) and compositions (see Table.II.8). The polymerizations were conducted in ethyl acetate at 60 °C with VAc in the presence of AIBN. Chain extensions were proved successful by the displacement of the peaks on the SEC chromatograms (see Figure.II.9) and the absence of residual traces of the initial PDMA RAFT/MADIX agent. Furthermore, an increase in the chemical shift of the ^{1}H NMR signals corresponding to the proton located at the α position of the xanthate moieties from 4.6–4.8 (for PDMA) to 6.4–6.6 ppm (for PVAc) confirmed the SEC results (see Appendix). The synthesized PDMA-*b*-PVAc copolymers showed good agreements between theoretical and experimental M_n too (see in Table II.7 and 8). The slight discrepancies of these values were attributed to differences in hydrodynamic volumes with the PMMA standards. Dispersities were low ($1.11 < Đ < 1.41$) and matched the values previously reported for PVAc oligomers in this range of M_n. Hence, the PDMA radicals generated during the chain extension process proved their ability to be a good leaving group and efficiently reinitiate the RAFT/MADIX polymerization of VAc.

Sample	Conv. (%) [d]	$M_{n\ theo}$ (g.mol^{-1}) [a]	$M_{n\ SEC}$ (g.mol^{-1}) (Đ)[c]	DMA/VAc mass % [f]	T_g (°C)
$PDMA_{0.4k}$-$PVAc_{1.4k}$-Xa	81.0	2050	2700 (1.11)	21	26.2
$PDMA_{0.8k}$-$PVAc_{3k}$-Xa	85.6	4050	4600 (1.24)	21	35.0
$PDMA_{1.2k}$-$PVAc_{5k}$-Xa	91.9	6450	6900 (1.41)	19	38.0

[a] Theoretical $M_n=[DMA]_0/[xanthate]_0\times MW(DMA)\times Conv./100+MW(xanthate)$. [b] Determined by integration of the signals of the proton located at the alpha position of the xanthate moieties. [c] Determined by SEC in DMF + LiBr with PMMA standards. [d] Determined by ^{1}H NMR in $CDCl_3$. [e] Theoretical $M_n=[VAc]_0/[PDMA\text{-}MADIX\ Agent]_0\times MW(VAc)\times Conv./100+M_n(PDMA\ MADIX\ Agent)$. [f] Based on theoretical masses.

Table.II.7. Experimental results for the synthesis of PDMA-b-PVAc amphiphilic block copolymers with increasing chain lengths at a constant composition.

Sample	Conv. (%) [d]	$M_{n\ theo}$ (g.mol^{-1}) [a]	$M_{n\ SEC}$ (g.mol^{-1}) (Đ)[c]	DMA/VAc mass % [f]	T_g (°C)
$PDMA_{0.4k}$-$PVAc_{3.5k}$-Xa	86.1	4050	4300 (1.21)	10	29.2
$PDMA_{0.8k}$-$PVAc_{3k}$-Xa	85.6	4050	4600 (1.24)	21	35.0
$PDMA_{1k}$-$PVAc_{2.7k}$-Xa	86.4	3900	5100 (1.24)	27	37.5
$PDMA_{2k}$-$PVAc_{1.9k}$-Xa	83.9	4100	5500 (1.20)	52	50.1

[a] Theoretical M_n = $[DMA]_0/[xanthate]_0 \times MW(DMA) \times Conv./100 + MW(xanthate)$. [b] Determined by integration of the signals of the proton located at the alpha position of the xanthate moieties. [c] Determined by SEC in DMF + LiBr with PMMA standards. [d] Determined by ^1H NMR in $CDCl_3$. [e] Theoretical M_n = $[VAc]_0/[PDMA\text{-}MADIX\ Agent]_0 \times MW(VAc) \times Conv./100 + M_n(PDMA\ MADIX\ Agent)$. [f] Based on theoretical masses.

Table.II.8. Experimental results for the synthesis of PDMA-*b*-PVAc amphiphilic block copolymers with varying composition at a constant molecular weight.

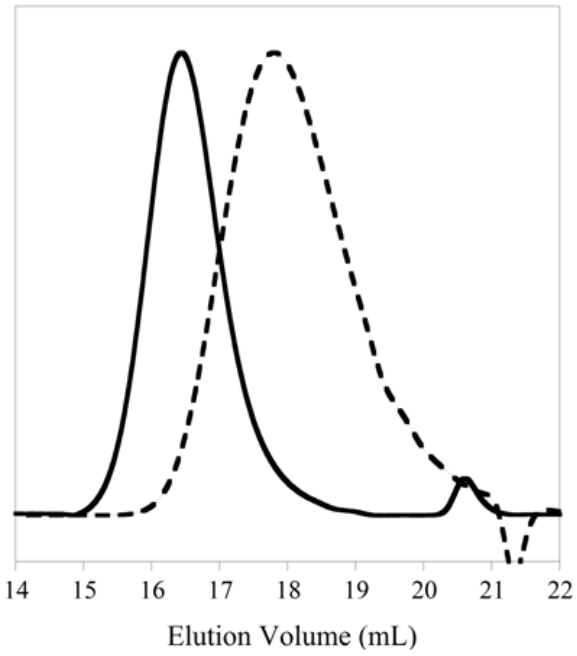

Figure.II.9. Overlays of SEC-RI chromatograms in DMF (including 10 mM LiBr) with a $PDMA_{2\ k}$ (dashed line) and a $PDMA_{2\ k}$-$PVAc_{1.9k}$-Xa block copolymer (full line).

The PDMA-*b*-PVAc copolymers exhibited a single T_g value (see in Tables II.7 and 8). T_g values ranged between 28 °C and 55 °C, *i.e.* between the T_g of each block taken separately. This excluded the possibility of having not observed the T_g of one particular block due to low molar mass effects. As indicated by the presence of a single T_g, these copolymers were miscible regardless of both their chain lengths and compositions. This located our copolymers under the order-disorder transition (ODT), indicating a low $N.\chi_{AB}$ product (*i.e.* a low degree of polymerization (N) and/or a low interaction parameter (χ_{AB})). In order to explain our observations, a PDMA-*b*-PVAc block copolymer with a theoretical M_n of 20000 g.mol^{-1} and a 50 % wt PDMA was synthesized. This copolymer exhibited a single intermediate T_g too and this clearly suggested a low interaction parameter as a result. Ultimately, a blend of PDMA-Xa ($M_{n,theo}$ = 40800 g.mol^{-1}) and PVAc-Xa ($M_{n,theo}$ = 38100 g.mol^{-1}) polymers revealed two distinct T_g. This confirmed the results published by Parada et al who observed two T_g for a blend of PDMA (M_v = 53000 g.mol^{-1}) and PVAc (M_v = 39000 g.mol^{-1}).[73]

The plot of T_g versus the theoretical DMA weight fraction appeared to be linear with an excellent correlation coefficient of 0.98 in the case of PDMA-*b*-PVAc copolymers whose M_n was close to 4000 g.mol^{-1} (see Figure II.10). According the Gordon-Taylor equation,[74] this linearity suggests an ideal volume additivity of the repeating monomer units in PDMA-*b*-PVAc copolymers.

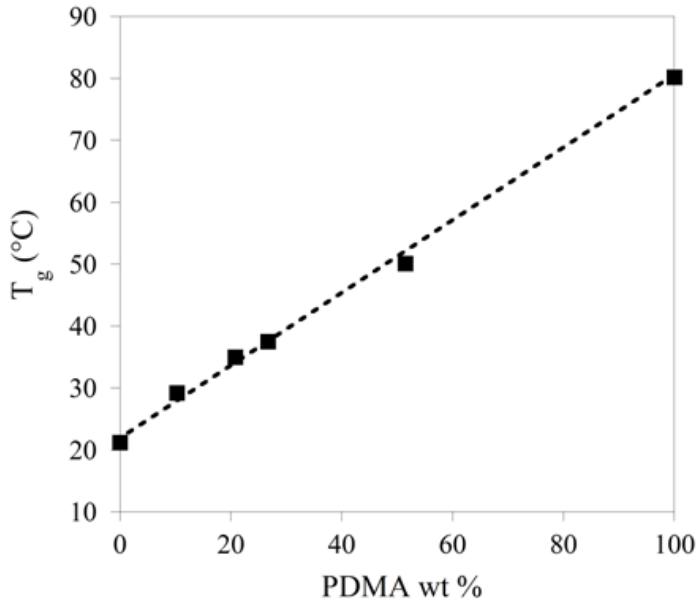

Figure.II.10. Dependency of T_g on PDMA weight fractions for the PDMA-*b*-PVAc-Xa copolymers (M_n = 4000 g.mol^{-1}).

b) Chain length effects on the solubility of PDMA-b-PVAc copolymers in sc-CO_2

The influence of a CO_2-phobic polymer block on the solubility of amphiphilic copolymers has never been examined. To clarify this point, the solubility of PDMA-*b*-PVAc-Xa samples comprising approximately 20 % wt of PDMA in sc-CO_2 was first investigated. As in the case of PVAc-Xa polymers, three different chain lengths were investigated from 2 k to 6 k (see Table II.7). While 1 % wt of the shortest copolymer (M_n = 2 k) was solubilized at 350 bar, the solubility dropped to 0.47 % wt for an equivalent copolymer with a M_n of 4 k (see Figure.II.11). The diblock of highest molar mass (M_n = 6.4 k) was poorly soluble (0.17 % wt at 350 bar). Considering the samples with similar DMA/VAc mass percentages, both the chain length and the presence of the PDMA block appeared to have a dramatic influence on the solubility in sc-CO_2. This can be simply explained by a dual increase of "CO_2-phobicity" due to both an increase of the length of the PDMA block and the decrease of the CO_2-philicity for the longest PVAc blocks.

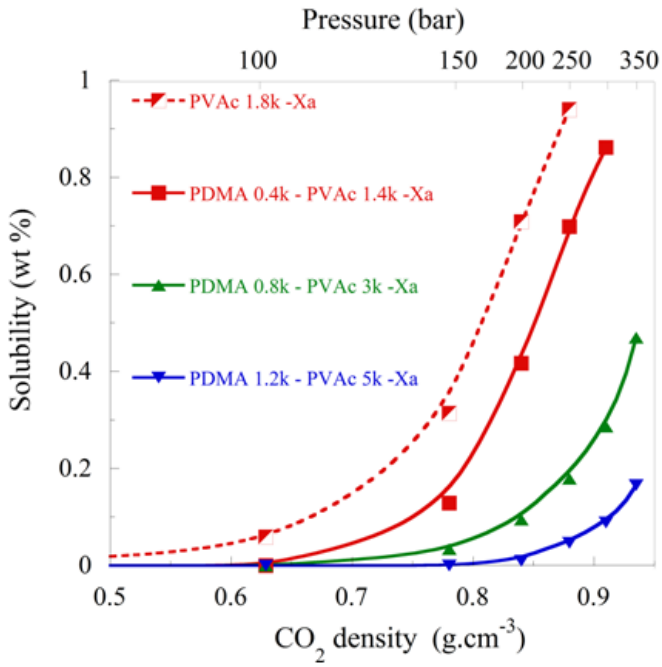

Figure.II.11. Solubility (% wt) of PVAc-Xa polymers and PDMA-*b*-PVAc-Xa copolymers in sc-CO_2 with increasing chain lengths.

A comparison with their PVAc homopolymer equivalents allows measuring the effect of the replacement of VAc units by DMA units (see Figure II.11). The values of

solubility were almost divided by a factor of 2 for both PDMA-*b*-PVAc-Xa copolymers exhibiting the longest chain lengths. These results appeared logical considering the immiscibility of PDMA in sc-CO_2. Indeed, Kilic *et al.* synthesized PDMA with a M_n of 1.3 k via nitroxide-mediated polymerization and 0.7 % wt of this polymer was found to be insoluble even at 25 °C and a high pressure of 450 bar. This was attributed to the high cohesive energy density and the high T_g of the polymer.[75]

As expected, short chain lengths must be targeted when synthesizing amphiphilic CO_2 copolymers based on such CO_2-philic PVAc blocks.

c) Composition effects on the solubility of PDMA-b-PVAc amphiphilic block copolymers in sc-CO_2

Then, the effect of incorporating a CO_2-phobic block through a variation in the PDMA weight fraction of PDMA-PVAc block copolymers was investigated. The impact of PDMA/PVAc mass ratio on the solubility in CO_2 was consequently studied at an approximate number-average molar mass of 4 k. Four different ratios from 10:90 to 50:50 were targeted to evaluate their impact on the copolymer solubility in sc-CO_2 (see Table II.8). The solubility in sc-CO_2 decreased with increasing weight

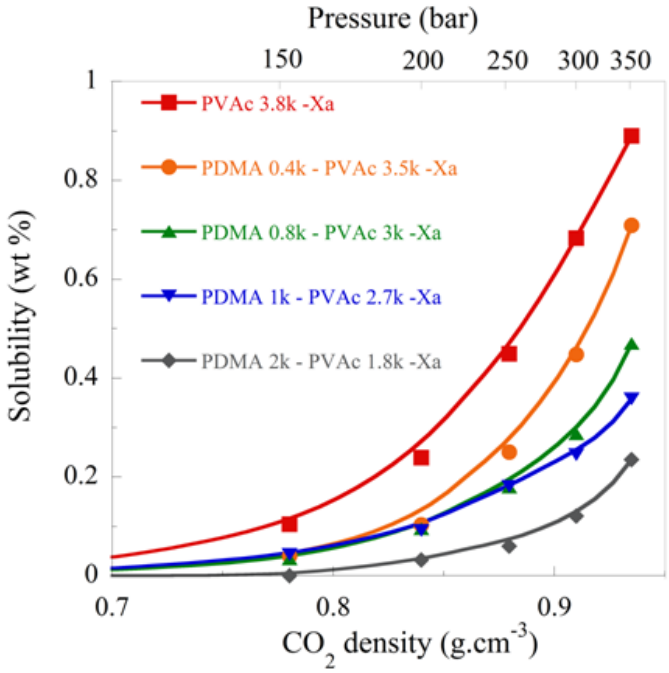

Figure.II.12. Solubility (% wt) of PVAc–Xa polymers and PDMA-PVAc-Xa block copolymers in sc-CO_2 with varying compositions at a constant chain length.

fractions of PDMA: the copolymers exhibited solubilities of 0.71, 0.47, 0.36 and 0.24 % wt for corresponding PDMA weight fractions of 0.10, 0.210, 0.27 and 0.52, respectively (see Figure II.12). This particularly emphasizes the necessity for selecting polymer surfactants with low CO_2-phobic/CO_2-philic balance to gain sufficient solubility in CO_2.

4. Incorporation of a fluorinated chain end

In spite of low molecular weights, the solubility of PVAc-based amphiphilic copolymers in sc-CO_2 is rather limited. A first approach to improve this was developed with the use of the fluorinated xanthate presented above.

a) Synthesis

A $PDMA_{0.8k}$-*b*-$PVAc_{3.2k}$-FXa diblock copolymer was then synthesized with F-Xanthate (see Table II.9). Surprisingly, the experimental molecular weights determined by SEC were relatively far from the theoretical ones, presumably due to the differences of hydrodynamic volumes with PMMA standards in SEC. The fluorinated PDMA macromolecular chain transfer agent was used to mediate the polymerization of VAc in the same conditions as previously reported. The reactivity was equivalent to that of Rhodixan A1, leading to a copolymer with macromolecular characteristics close to the theoretical expectations and similar to its non-fluorinated counterpart.

	PDMA MADIX Agent			PDMA-*b*-PVAc-FXa copolymer			
Sample	$M_{n\ theo}$ ($g.mol^{-1}$) [a]	$M_{n\ NMR}$ ($g.mol^{-1}$)[b]	$M_{n\ SEC}$ ($g.mol^{-1}$) (Đ) [c]	Conv. (%) [d]	$M_{n\ theo}$ ($g.mol^{-1}$) [a]	$M_{n\ SEC}$ ($g.mol^{-1}$) (Đ)[c]	DMA /VAc mass % [f]
$PDMA_{0.8k}$-$PVAc_{3.2k}$-FXa	1300	950	1800 (1.11)	87.0	4500	4600 (1.21)	20

[a] Theoretical M_n = $[DMA]_0$/$[F\text{-}Xanthate]_0$×MW(DMA)×Conv./100+MW(F-Xanthate). [b] Determined by integration of the signals of the proton located at the alpha position of the xanthate moieties. [c] Determined by SEC in DMF + LiBr with PMMA standards. [d] Determined by ^1H NMR in $CDCl_3$. [e] Theoretical M_n = $[VAc]_0$/$[PDMA\text{-}MADIX\ Agent]_0$× MW(VAc)×Conv./100+$M_n$(PDMA MADIX Agent). [f] Based on theoretical masses.

Table.II.9. Experimental results for the synthesis of a PDMA-*b*-PVAc amphiphilic block copolymer using a fluorinated xanthate.

b) Solubility of the block copolymer in sc-CO_2

This copolymer exhibited a solubility of 0.81 % wt in sc-CO_2 at 350 bar, whereas the soluble weight fraction of its non fluorinated counterpart was only 0.47 % wt (see Figure.II.13). Its solubility was then comparable to that of a $PVAc_{3.8k}$-Xa polymer. This result confirmed the interest of such an approach in the design of amphiphilic polymer surfactants with both improved CO_2-philicity and amphiphilicity.

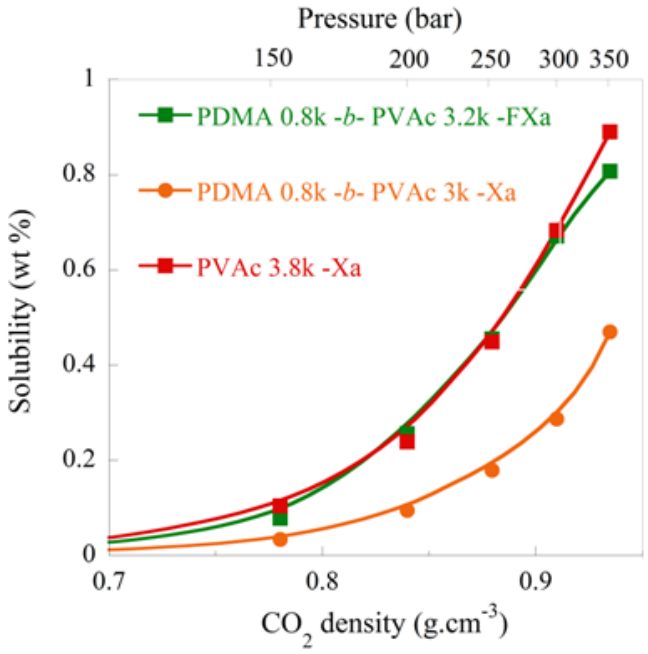

Figure.II.13. Solubility (% wt) of $PVAc_{3.8k}$–Xa and $PDMA_{0.8k}$-$PVAc_{3k}$-Xa block copolymers with/without a C_6F_{13} terminal group in sc-CO_2 at a constant chain length.

III. Conclusion

Building on RAFT/MADIX polymerization, a novel family of poly(N,N-dimethylacrylamide)-poly(vinyl acetate) diblock copolymers was described throughout this chapter. The excellent control over number-average molar masses and dispersities emphasized the advantages of using xanthate chain transfer agents to combine amphiphilic blocks derived from monomers of different reactivities (*i.e.* LAM_S and MAM_S). This constitutes a straightforward strategy, particularly compared to the use of switchable RAFT agents or conjugation strategies such as the copper-catalyzed alkyne-azide Huisgen cycloaddition.

High pressure infrared spectroscopy measurements allowed to determine the key macromolecular parameters controlling their solubility in sc-CO_2 such as chain end group, chain length and hydrophilic/CO_2-philic balance. Although this method is more complex to carry out than cloud point measurements, it provided a handful of valuable data on the solubility of PVAc-based copolymers at the thermodynamic equilibrium. Both chain length and PDMA weight fraction were proved to be limiting parameters for the solubility in sc-CO_2. A molecular weight of 4000 $g.mol^{-1}$ and a DMA/VAc ratio of 1:3 appeared to be the critical parameters to gain sufficient solubility in sc-CO_2 (*i.e.* higher than 0.5 % wt).

Referring to literature, the stabilization of W/C emulsions with these copolymers can be expected to be limited to highly-diluted emulsions. Further studies are necessary to evaluate this possibility. If not, these PVAc-based copolymers could represent a valuable addition to the field of C/W surfactants. Surface tension is actually the key parameter to stabilize concentrated W/C emulsions. Regardless of their CO_2-philicity, a strong limitation associated with PVAc is its high surface tension. The approach based on an innovative fluorinated xanthate could provide interesting results in this perspective, given that fluorinated moieties are known to lower the surface tension of polymers. Not only the solubility in sc-CO_2 could significantly be improved, but the introduction of fluorinated moieties can be also expected to improve the interfacial activity of the amphiphilic block copolymer. This will be further developed in the next chapter.

IV. References

(1) S.G. Kazarian, M.F. Vincent, F.V. Bright, C.L. Liotta and C.A. Eckert, *J. Am. Chem. Soc.*, 1996, **118,** 1729.
(2) P. Raveendran and S.L. Wallen, *J. Am. Chem. Soc.*, 2002, **124,** 12590.
(3) S. Kilic, S. Michalik, Y. Wang, J.K. Johnson, R.M. Enick and E.J. Beckman, *Ind. Eng. Chem. Res.*, 2003, **42,** 6415.
(4) P. Raveendran and S.L. Wallen, *J. Am. Chem. Soc.*, 2002, **124,** 7274.
(5) Z. Shen, M.A. McHugh, J. Xu, J. Belardi, S. Kilic, A. Mesiano, S. Bane, C. Karnikas, E.J. Beckman and R. Enick, *Polymer*, 2003, **44,** 1491.
(6) B. Tan and A.I. Cooper, *J. Am. Chem. Soc.*, 2005, **127,** 8938.
(7) B. Tan, C.L. Bray and A.I. Cooper, *Macromolecules*, 2009, **42,** 7945.
(8) B. Tan, J.Y. Lee and A.I. Cooper, *Macromolecules*, 2007, **40,** 1945.
(9) J.Y. Lee, B. Tan and A.I. Cooper, *Macromolecules*, 2007, **40,** 1955.
(10) K. Chen, N. Grant, L. Liang, H. Zhang and B. Tan, *Macromolecules*, 2010, **43,** 9355.
(11) T. Kochi, A. Nakamura, H. Ida and K. Nozaki, *J. Am. Chem. Soc.*, 2007, **129,** 7770.
(12) T. Junkers, D. Voll and C. Barner-Kowollik, *e-Polymers*, 2009, 1.
(13) D. Britton, F. Heatley and P.A. Lovell, *Macromolecules*, 1998, **31,** 2828.
(14) *Polymer Handbook*, ed. Bandrup, J., Immergut, E.H., and Grulke, E.A., Wiley-Intersciences, 1999**.**
(15) M. Kamachi, D.J. Liaw and S.I. Nozakura, *Polym. J*, 1979, **11,** 921.
(16) *The Chemistry of Free Radical Polymerization*, ed. Moad, G. and Solomon, D.H., Pergamon Press, 1995**.**
(17) A.D. Jenkins, R.G. Jones and G. Moad, *Pure Appl. Chem.*, 2010, **82,** 483.
(18) H. Fischer, *J. Polym. Sci. A Polym. Chem.*, 1999, **37,** 1885.
(19) J. Nicolas, Y. Guillaneuf, C. Lefay, D. Bertin, D. Gigmes and B. Charleux, *Prog. Polym. Sci.*, in press.
(20) W.A. Braunecker and K. Matyjaszewski, *Prog. Polym. Sci.*, 2007, **2007,** 93.
(21) K. Matyjaszewski, *Macromolecules*, 2012, **45,** 4015.
(22) H. Tang, M. Radosz and Y. Shen, *AIChE J.*, 2009, **55,** 737.
(23) M. Wakioka, K.Y. Baek, T. Ando, M. Kamigaito and M. Sawamoto, *Macromolecules*, 2001, **35,** 330.
(24) A.H.E. Muller, R.G. Zhuang, D.Y. Yan and G. Litvinenko, *Macromolecules*, 1995, **28,** 4326.
(25) M. Destarac, *Polym. Rev.*, 2011, **51,** 163.
(26) R. Poli, *Angew. Chem. Ed. Int.*, 2006, **45,** 5058.
(27) A. Debuigne, R. Poli, C. Jérôme, R. Jérôme and C. Detrembleur, *Prog. Polym. Sci.*, 2009, **34,** 211.
(28) Z. Xue and R. Poli, in *Progress in Controlled Radical Polymerization: Mechanisms and Techniques*, ed. K. Matyjaszewski, B. S. Sumerlin, and N. V. Tsarevski, American Chemical Society, 2012, Chap. 15.
(29) Y. Champouret, K.C. MacLeod, K.M. Smith, B.O. Patrick and R. Poli, *Organometallics*, 2010, **29,** 3125.
(30) M.P. Shaver, M.E. Hanhan and M.R. Jones, *Chem. Commun.*, 2010, **46,** 2127.
(31) C.H. Peng, J. Scricco, S. Li, M. Fryd and B.B. Wayland, *Macromolecules*, 2008, **41,** 2368.
(32) A. Debuigne, J.R. Caille and R. Jérôme, *Angew. Chem. Ed. Int.*, 2005, **117,** 1125.
(33) B.B. Wayland, C.H. Peng, X. Fu, Z. Lu and M. Fryd, *Macromolecules*, 2006, **39,** 8219.

(34) S. Maria, H. Kaneyoshi, K. Matyjaszewski and R. Poli, *Chem. Eur. J.*, 2007, **13,** 2480.
(35) S. Yamago, *Chem. Rev.*, 2009, **109,** 5051.
(36) G. David, C. Boyer, J. Tonnar, B. Ameduri, P. Lacroix-Desmazes and B. Boutevin, *Chem. Rev.*, 2006, **106,** 3936.
(37) P. Lacroix-Desmazes, R. Severac and B. Boutevin, *Macromolecules*, 2005, **38,** 6299.
(38) M.C. Iovu and K. Matyjaszewski, *Macromolecules*, 2003, **36,** 9346.
(39) Y. Kwak, A. Goto, T. Fukuda, Y. Kobayashi and S. Yamago, *Macromolecules*, 2006, **39,** 4671.
(40) S. Yamago, B. Ray, K. Iida, J.i. Yoshida, T. Tada, K. Yoshizawa, Y. Kwak, A. Goto and T. Fukuda, *J. Am. Chem. Soc.*, 2004, **126,** 13908.
(41) *Handbook of RAFT Polymerization*, ed. Barner-Kowollik, C., Wiley-VCH, 2008**.**
(42) J. Chiefari, Y.K. Chong, F. Ercole, J. Krstina, J. Jeffery, T.P.T. Le, R.T.A. Mayadunne, G.F. Meijs, C.L. Moad, G. Moad, E. Rizzardo and S.H. Thang, *Macromolecules*, 1998, **31,** 5559.
(43) D. Charmot, P. Corpart, H. Adam, S.Z. Zard, T. Biadatti and G. Bouhadir, *Macromol Symp.*, 2000, **150,** 23.
(44) D. Taton, M. Destarac and S.Z. Zard, in *Handbook of RAFT Polymerization*, ed. C. Barner-Kowollik, Wiley-VCH, 2008, Chap. 10.
(45) S. Perrier, C. Barner-Kowollik, J.F. Quinn, P. Vana and T.P. Davis, *Macromolecules*, 2002, **35,**
(46) M.J. Monteiro and H. de Brouwer, *Macromolecules*, 2001, **34,** 349.
(47) D. Konkolewicz, B.S. Hawkett, A. Gray-Weale and S.Ã. Perrier, *J. Polym. Sci. A Polym. Chem.*, 2009, **47,** 3455.
(48) M.L. Coote, E.I. Izgorodina, G.E. Cavigliasso, M. Roth, M. Busch and C. Barner-Kowollik, *Macromolecules*, 2006, **39,** 4585.
(49) M. Benaglia, J. Chiefari, Y.K. Chong, G. Moad, E. Rizzardo and S.H. Thang, *J. Am. Chem. Soc.*, 2009, **131,** 6914.
(50) M. Benaglia, M. Chen, Y.K. Chong, G. Moad, E. Rizzardo and S.H. Thang, *Macromolecules*, 2009, **42,** 9384.
(51) A. Favier, C. Barner-Kowollik, T.P. Davis and M.H. Stenzel, *Macromol. Chem. Phys.*, 2004, **205,** 925.
(52) A. Guinaudeau, *PhD Thesis*, University of Toulouse, **2010**.
(53) G. Moad and D.H. Solomon, in *The Chemistry of Free Radical Polymerization*, ed. G. Moad and D. H. Solomon, Pergamon Press, 1995, Chap. 5.
(54) C. Boyer, D. Valade, L. Sauguet, B. Ameduri and B. Boutevin, *Macromolecules*, 2005, **38,** 10353.
(55) M. Destarac, C. Brochon, J.M. Catala, A. Wilczewska and S.Z. Zard, *Macromol. Chem. Phys.*, 2002, **203,** 2281.
(56) K. Martin, J. Spickermann, H.J. Rader and K. Mullen, *Rap. Comm. Mass. Spec.*, 1996, **10,** 1471.
(57) A. Nojiri, K. Hattori and S. Okamoto, *Japan. J. Appl. Phys.*, 1971, **10,** 803.
(58) H. Lee, J.W. Pack, W. Wang, K.J. Thurecht and S.M. Howdle, *Macromolecules*, 2010, **43,** 2276.
(59) M. Destarac, C. Kalai, A. Wilczewska, L. Petit, E. Van Gramberen and S.Z. Zard, in *Controlled/Living Radical Polymerization: From Synthesis to Materials*, ed. K. Matyjaszewski, American Chemical Society, 2006, Chap. 38.
(60) Y.Y. Tong, R. Wang, N. Xu, F.S. Du and Z.C. Li, *J. Polym. Sci. A Polym. Chem.*, 2009, **47,** 4494.

(61) G. Kostov, F. Boschet, J. Buller, L. Badache, S. Brandsadter and B. Ameduri, *Macromolecules*, 2011, **44,** 1841.
(62) M.J. Monteiro, M.M. Adamy, B.J. Leeuwen, A.M. van Herk and M. Destarac, *Macromolecules*, 2005, **38,** 1538.
(63) M.P.F. Pepels, C.I. Holdsworth, S. Pascual and M.J. Monteiro, *Macromolecules*, 2010, **43,** 7565.
(64) M. Destarac, W. Bzducha, D. Taton, I. Gauthier-Gillaizeau and S.Z. Zard, *Macromol. Rapid Commun.*, 2002, **23,** 1049.
(65) T.L.U. Nguyen, K. Eagles, T.P. Davis, C. Barner-Kowollik and M.H. Stenzel, *J. Polym. Sci. A Polym. Chem.*, 2006, **44,** 4372.
(66) N.S. Ieong, M. Redhead, C. Bosquillon, C. Alexander, M. Kelland and R.K. O'Reilly, *Macromolecules*, 2011, **44,** 886.
(67) M. Beija, J.D. Marty and M. Destarac, *Chem. Commun.*, 2011, **47,** 2826.
(68) D. Taton, A.Z. Wilczewska and M. Destarac, *Macromol. Rapid Commun.*, 2001, **22,** 1497.
(69) M. Destarac, A. Guinaudeau, R. Geagea, S. Mazieres, E. Van Gramberen, C. Boutin, S. Chadel and J. Wilson, *J. Polym. Sci. A Polym. Chem.*, 2010, **48,** 5163.
(70) I. Blidi, R. Geagea, O. Coutelier, S. Mazieres, F. Violleau and M. Destarac, *Polym. Chem.*, 2012, **3,** 609.
(71) J.D. Holmes, K.J. Ziegler, M. Audriani, C. Ted, P.A. Bhargava, D.C. Steytler and K.P. Johnston, *J. Phys. Chem. B.*, 1999, **103,** 5703.
(72) A.J. Convertine, B.S. Lokitz, A.B. Lowe, C.W. Scales, L.J. Myrick and C.L. McCormick, *Macromol. Rapid Commun.*, 2005, **26,** 791.
(73) L.G. Parada, L.C. Cesteros, E. Meaurio and I. Katime, *Polymer*, 1998, **39,** 1019.
(74) M. Gordon and J.S. Taylor, *J. Appl. Chem.*, 1952, **2,** 493.
(75) S. Kilic, Y. Wang, J.K. Johnson, E.J. Beckman and R.M. Enick, *Polymer*, 2009, **50,** 2436.

Chapter 3

- Enhancement of solubility of poly(vinyl esters) in sc-CO_2 by means of vinyl trifluoroacetate : the key role of polymer-polymer interactions
- Distinctive features of solubility of vinyl acetate/1-(trifluoromethyl) vinyl acetate copolymers in sc-CO_2

Contents

In the previous chapter, the chain end functionalization of VAc-based polymers by a perfluorinated chain was proven an efficient strategy to improve the solubility of PVAc in sc-CO_2. Another strategy comes with a statistical approach where VAc should be copolymerized with a comonomer. This comonomer should ideally provide a decrease in the polymer-polymer interactions, and/or higher entropic contributions deriving from enhanced entropy of mixing or free volume. This entropic approach has been recently studied through the introduction of a bulky comonomer. Vinyl acetate was thus copolymerized with vinyl butyrate,[1,2] dibutyl maleate[3], vinyl pivalate[4] and vinyl octanoate[2] to promote the «CO_2-philicity» of these polymers in binary or ternary mixtures. The enhanced solubilities were attributed to a higher free volume. However, the first strategy concerning the decrease of polymer-polymer interactions has never been studied in the case of all-(vinyl ester)-based copolymers thus far.

Within this work, two different fluorinated vinyl esters were considered to do so (see Scheme III.1). The first part of this chapter will be devoted to vinyl trifluoroacetate (VTFAc), the fluorinated analogous of vinyl acetate. This actually constitutes an ideal system to study polymer-polymer interactions as the steric hindrance of VAc and VTFAc can be expected to be very close. Building on the unprecedented RAFT/MADIX polymerization of VTFAc and its copolymerization with VAc, a library of well-defined VTFAc-based statistical copolymers will be synthesized. Their solubility will be investigated through cloud-point measurements. It will be then taken advantage of their statistical nature to identify the factors governing their solubility.

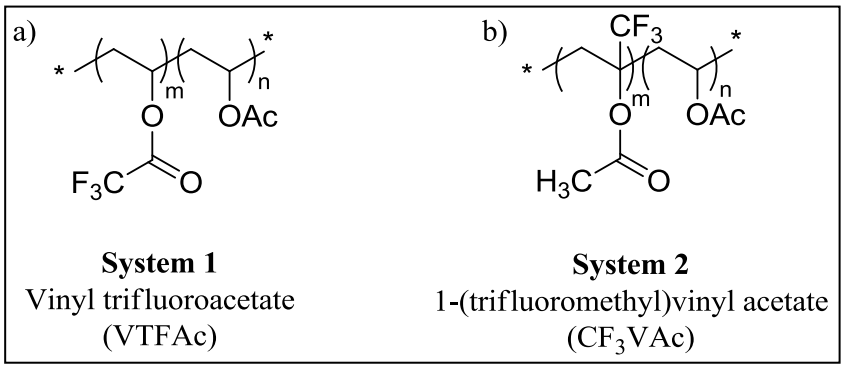

Scheme III.1. Schematic representation of the copolymers studied in this chapter.

In a second phase, this work will focus on the positioning of trifluoromethyl groups on the main chain of a PVAc-based copolymer. This can be achieved through the copolymerization of VAc with 1-(trifluoromethyl) vinyl acetate. Following the previous approach, the RAFT/MADIX copolymerization of these monomers and the solubility of the resulting copolymers in sc-CO_2 will be explored. Due to the dissimilarities between PVTFAc-based copolymers and this second system, some distinctive features of solubility will be highlighted.

Throughout this chapter, the use of these two systems to design amphiphilic block copolymers will be also questioned.

I. Enhancement of solubility of poly(vinyl esters) in sc-CO_2 by means of vinyl trifluoroacetate

Fluorinated vinyl esters have not been much studied in terms of polymerization, characterization and physical properties. Indeed, they are usually synthesized by addition of the corresponding fluorinated carboxylic acids to acetylene[5,6], which limits their availability. In this family, vinyl trifluoroacetate is one of the few commercially available monomers to date. Its polymerization is exclusively achieved by radical means, either under thermal or photochemical conditions[5,6] with azo initiators similarly to non-fluorous vinyl esters such as vinyl acetate. Significantly, the polymerization of vinyl fluorinated esters, and vinyl trifluoroacetate among others, has never been studied by RDRP techniques. In our efforts to develop the macromolecular engineering of vinyl trifluoroacetate, the RAFT/MADIX polymerization of VTFAc under thermal initiation was consequently investigated with the use of 2-mercaptopropionic acid methyl ester *O*-ethyl dithiocarbonate, a chain transfer agent which has been proven efficient for the RAFT/MADIX polymerization of vinyl acetate.[7]

A. RAFT/MADIX polymerization of VTFAc

1. Synthesis of PVTFAc of variable chain lengths

All polymerizations were conducted at 60 °C in 2-butanone with 0.3 % wt of initiator to monomer to ensure the solubility of the polymer in the reaction medium and high conversions (see Scheme III.2).

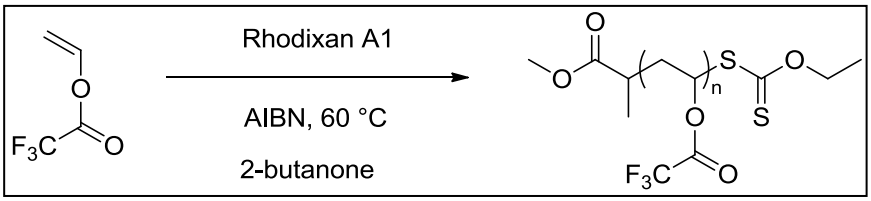

Scheme III.2. RAFT/MADIX polymerization of VTFAc.

A blank conventional polymerization experiment was first carried out in these conditions to give a PVTFAc sample with a moderate molecular weight around 14000

g.mol^{-1} and a dispersity of 1.61 (run 1 of Table III.1). Decreasing amounts of Rhodixan A1 were then introduced to give samples with increasing molecular weights and higher dispersities (runs 2 to 6 of Table III.1). A shift towards higher molecular weights as evidenced by SEC in DMF further supported the control on M_n (see Figure III.1). Dispersities were comprised between 1.07 and 1.23 (runs 2 to 5 of Table III.1), which indicates a high interchain transfer constant. The dispersity values increased with higher molecular weights which may be related to the formation of head-to-head adducts or chain transfer to polymer as in the case of vinyl acetate.[8,9]

Run	$M_{n,\ targeted}$ (g.mol^{-1})	Conversion (%) [a]	$M_{n,theo}$ (g.mol^{-1}) [b]	$M_{n\ NMR}$ (g.mol^{-1}) [a]	$M_{n\ SEC,THF}$ (g.mol^{-1}) (Đ) [c]	$M_{n\ SEC,DMF}$ (g.mol^{-1}) (Đ) [d]	T_g (°C)	T_m (°C)
1	-	73	-	-	5200 (1.15)	14300 (1.61)	55	148
2	3600	65	2200	2500	2700 (1.11)	4100 (1.07)	43	132
3	5500	71	4000	5100	4000 (1.12)	5900 (1.11)	43	137
4	8200	72	6000	6500	5000 (1.12)	7900 (1.15)	48	143
5	20200	72	14600	-	n.d. [d]	13900 (1.23)	51	146
6	40200	72	29000	-	5500 (1.17)	13700 (1.43)	56	148

[a] Determined by ^{1}H NMR in acetone-d_6 [b] Theoretical M_n = ([VTFAc]$_0$×MW(VTFAc)×conv.(VTFAc)/([Rhodixan A1]$_0$/100)+MW(Rhodixan A1). [c] Determined by SEC in THF with PS standards. [d] n.d.: Not determined. [e] Determined by SEC in DMF + 10 mM LiBr with PMMA standards.

Table III.1. Experimental results for the RAFT/MADIX polymerization of vinyl trifluoroacetate.

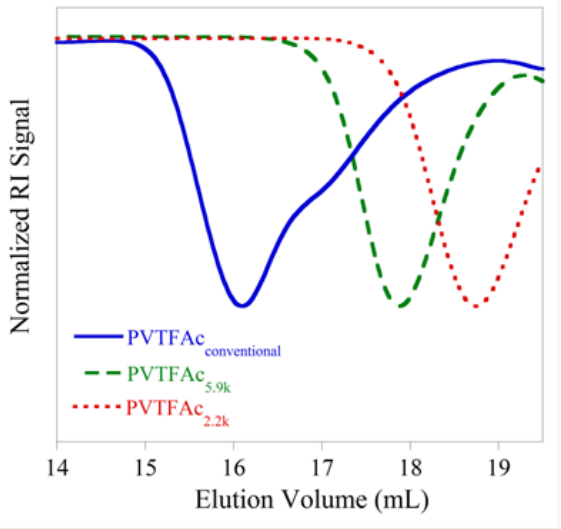

Figure III.1. Overlay of SEC chromatograms (RI detection, in DMF) for the conventional radical polymerization of VTFAc (run 1 of Table III.1) and its RAFT/MADIX polymerization (runs 2 and 3 of Table III.1).

A general remark concerns the determination of experimental molecular weights of PVTFAc by SEC, which has never been reported in the literature. While samples possessing theoretical molecular weights lower than 5000 g.mol^{-1} were well eluted by SEC in THF (see runs 2 and 3 of Table III.1), higher molecular weights could not be well separated (runs 4 to 6 of Table III.1). This was attributed to the low solubility of PVTFAc in THF. To overcome this, DMF with 10 mM of lithium bromide appeared a better solvent for the SEC of PVTFAc samples. A conventional calibration performed with poly(methyl methacrylate) standards gave realistic but slightly higher molecular weights compared to the theoretical ones. Molecular weights of 14000 g.mol^{-1} were thus determined for runs 1, 5 and 6 (see Table III.1). This similarity was attributed to a limited kinetic chain length during the polymerization of VTFAc.

To confirm this hypothesis, the PVTFAc samples (runs 1, 5 and 6 of Table III.1) were converted into PVAc in order to be unambiguously characterized by SEC in THF. Subsequent basic methanolysis/acetylation steps were performed to produce the corresponding PVAc samples. The PVAc sample corresponding to the free radical radical polymerization experiment (run 1 of Table III.1) exhibited a molecular weight of 8800 g.mol^{-1} and a dispersity of 1.86. In contrast to this, the M_n of PVAc polymers synthesized through the RAFT/MADIX polymerization of VTFAc (runs 5 and 6 of Table III.1) were respectively 6500 and 7200 g.mol^{-1} while dispersities were 1.42, and 1.47. Considering the differences in molecular weight between VAc and VTFAc monomer units -respectively 86.1 and 140.1 g.mol^{-1}-, this confirmed the limitations brought by kinetic chain length effects. Furthermore, ^{1}H NMR spectra of PVTFAc supported this. A characteristic triplet at 4.41 ppm which was attributed to a –CH_2-CH_2-O-(C=O)-CF_3 chain end was observed in the conventional free radical polymerization experiment (run 1 of Table III.1). The free radical polymerization of VTFAc was thus thought to be strongly influenced by irreversible chain transfer events.

2. ^{1}H NMR analysis

In case of an efficient RAFT/MADIX polymerization, the attachment of the xanthate group to the last VTFAc repeating unit should provide an unambiguous signature in ^{1}H NMR experiments. A characteristic ^{1}H NMR signal located around 6.90 ppm in RAFT/MADIX experiments was thus attributed to the protons placed in the alpha position of the xanthate moiety (see Figure A.III.1 of Appendix). The chemical shift was higher than the corresponding signal described in the RAFT/MADIX polymerization of vinyl acetate which is located around 6.40 ppm.[10] Building on this signal, the experimental $M_{n,NMR}$ were determined (see Table III.1 and Appendix for details on the calculation of $M_{n,NMR}$). The matching between theoretical and experimental M_n determined by ^{1}H NMR brought an additional strong evidence of the efficient control of the polymerization of VTFAc (see runs 2 to 4 of Table III.1).

3. Kinetics of the RAFT/MADIX polymerization of VTFAc

The kinetics of the RAFT/MADIX polymerization of VTFAc is an important experiment to gain knowledge on the evolution of M_n and Đ with conversion. Contrary to the previous experiments carried out under argon atmosphere in Schlenk flasks, the kinetic studies were performed in glass tubes sealed under vacuum. Three different molecular weights were targeted with increasing amounts of Rhodixan A1 of respectively $5.9*10^{-2}$, $1.2*10^{-1}$ and $2.4*10^{-1}$ mol. They were then compared to a control experience without chain transfer agent. The samples were characterized by ^{1}H NMR and SEC in DMF.

First of all, a strong retardation that was amplified with increasing amounts of chain transfer agent was noted (see Figure III.2.a)). This contrasts with the case of the RAFT/MADIX polymerization of VAc where *O*-ethyl xanthates gave a moderate rate retardation.[7] This retardation may be caused by a low fragmentation rate due to the low stability of the VTFAc radicals. Concerning both the molecular weights and dispersities obtained during the kinetics experiments, PVTFAc samples synthesized by conventional free radical polymerization exhibited molecular weights close to 20000 g.mol^{-1} and dispersities in the range of 1.50 - 1.60 regardless of conversion

(see Figures III.2a) and b)). The differences observed with a previous experiment (see run 1 of Table III.1) may be due to a difference of pressure inside the reaction vessel. In contrast with the conventional free radical polymerizations, SEC in DMF revealed the increase of M_n with conversion for the higher targeted molecular weights by RAFT/MADIX polymerization (8200 and 4200 g.mol^{-1}), and thereby the living character of the polymerization (see Figure III.2.b)). As previously stated, dispersities increased with both conversion and molecular weights (see Figure III.2.c)). Finally, NMR measurements were also a resourceful tool to confirm the efficient influence of Rhodixan A1 on the radical polymerization of VTFAc. Indeed, it revealed the linear increase of $M_{n,NMR}$ with conversion for the three targeted molecular weights (see Figure III.2.d)). Interestingly, early kinetic studies additionally showed that the chain transfer agent was fully consumed after conversions close to 10 %, suggesting a high transfer constant ($C_{tr,X}$) to Rhodixan A1.[11]

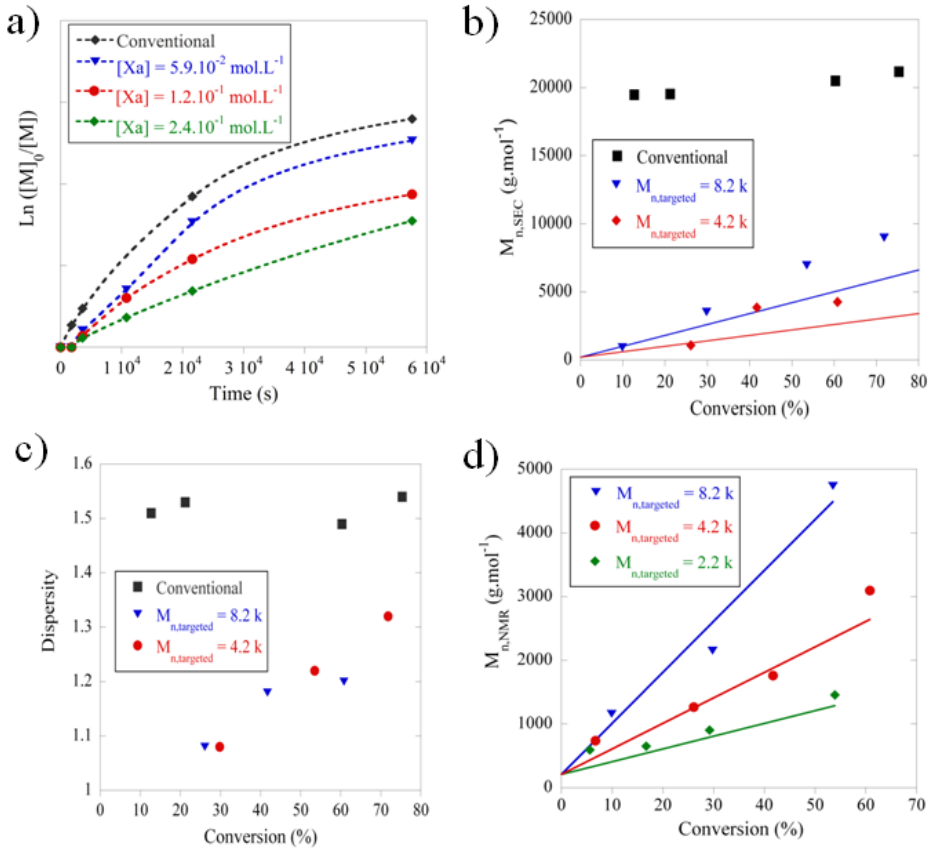

Figure III.2. Experimental results (a) First-order kinetics, b) $M_{n,SEC}$, c) Dispersity and d) $M_{n,NMR}$ versus conversion plots for the kinetics of the RAFT/MADIX polymerization of VTFAc performed at 60 °C in Carius tubes. Straight lines indicate theoretical molecular weights.

4. Synthesis of amphiphilic block copolymers with a PVTFAc block

The direct synthesis of amphiphilic diblock copolymers based on VTFAc was then investigated. To make a parallel with the previous chapter, the first attempts were performed using a poly(N,N-dimethyl acrylamide) macromolecular CTA with a molecular weight of 800 g.mol^{-1}. However, this synthesis pathway appeared unsuccessful as either no or low conversions of VTFAc were observed. The amide groups might act as inhibitors of the polymerization of VTFAc. On the other hand, the use of a poly(poly(ethylene glycol)) acrylate (PPEGA) macromolecular CTA that exhibited a reactivity towards VTFAc similar to Rhodixan A1 was considered (see Scheme III.3).

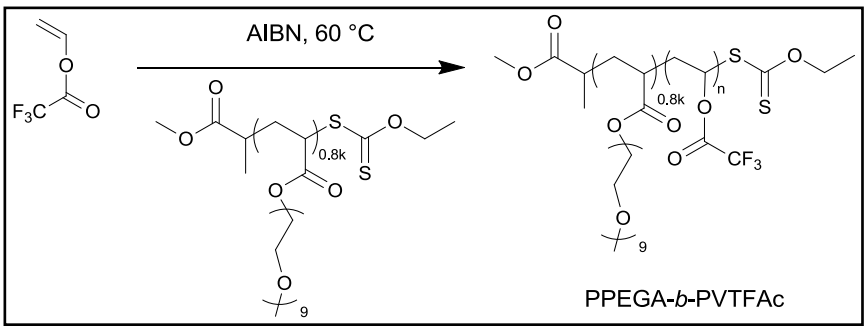

Scheme III.3. RAFT/MADIX polymerization of VTFAc using a poly(poly(ethylene glycol) acrylate) macromolecular chain transfer agent.

A PPEGA oligomer ($M_{n,theo}$= 1000 g mol^{-1}, $M_{n,SEC}$= 1400 g mol^{-1}, Đ= 1.61) was first synthesized by RAFT/MADIX polymerization. It was then used as a RAFT/MADIX CTA for the polymerization of VTFAc. The final conversion was 73 %, similarly to the RAFT/MADIX polymerization of VTFAc starting from Rhodixan A1. Even though the RI detection was biased by the opposite refractive index of the two blocks[12], an experimental M_n of 4100 g.mol^{-1} in agreement with the theoretical one as well as a dispersity of 1.58 were determined via SEC in THF. The chain extension was quantitative as demonstrated by SEC coupled with a viscosimetric detection (see Figure III.3). As a result, this strategy allowed to synthesize the PPEGA-*b*-PVTFAc copolymer.

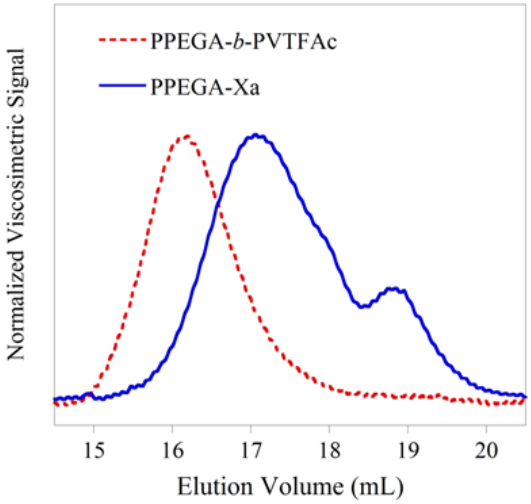

Figure III.3. Overlays of SEC (THF, viscosimetric detection) of a poly((polyethylene glycol)acrylate) xanthate macromolecular chain transfer agent (PPEGA-Xa) and the resulting PPEGA-*b*-PVTFAc amphiphilic block copolymer.

5. Thermal properties

Thermal studies by DSC revealed the semi-crystalline character of PVTFAc. A melting point temperature (T_m) of 148 °C was evidenced for the highest molecular weights while T_m gradually decreased from 148 to 118 with shorter chain lengths (see Table III.1). Similarly, glass transition temperatures (T_g) of PVTFAc ranged from 56 to 41 °C and were chain-length dependent on the considered range of molecular weights. By comparison to poly(vinyl acetate) whose infinite T_g is close to 40 °C, the presence of fluorinated moieties consequently appeared to harden the polymer.

In the case of the PPEGA-*b*-PVTFAc amphiphilic block copolymer, a value of melting temperature of 105 °C was determined. Interestingly, this value was lower than that of the PVTFAc homopolymer of equivalent molecular weight (121 °C, see run 2 of Table III.1). It was also hypothesized that the PPEGA block may induce a liquid crystal behaviour in the amphiphilic copolymers. An observation with a polarizing optical microscope was attempted but the amphiphilic copolymer appeared to degrade in a range of temperature close to its observed T_m.

B. Statistical copolymers of VAc and VTFAc

1. RAFT/MADIX synthesis of P(VAc-*stat*-VTFAc) copolymers

Once the RAFT/MADIX polymerization of VTFAc could be successfully evidenced, the focus was paid on the controlled copolymerization of VAc and VTFAc. As stated earlier, this aimed at creating a library of statistical copolymers with well-defined macromolecular characteristics. For these two monomers, the reactivity ratios were respectively evaluated to r_{VTFAc} = 0.32 and r_{VAc} = 0.60 for the bulk free radical copolymerization at 60 °C, which indicates a tendency to cross-propagation between monomers.[5] From this, the decreasing and disappearance of crystalline domains could be also expected upon richer compositions in vinyl acetate units.

The RAFT/MADIX copolymerization of VAc and VTFAc was performed in experimental conditions similar to the polymerization of VTFAc at the difference of 2-butanone being replaced by ethyl acetate (see Scheme III.4). This solvent actually presents a lower transfer constant to solvent for the polymerization of VAc at 60 °C – $C_{tr,ethyl\ acetate} \approx 3.10^{-4}$ and $C_{tr,2\text{-butanone}} \approx 74.10^{-4}$-,[13,14] which appeared a critical point to synthesize well-defined P(VAc-*stat*-VTFAc) copolymers.

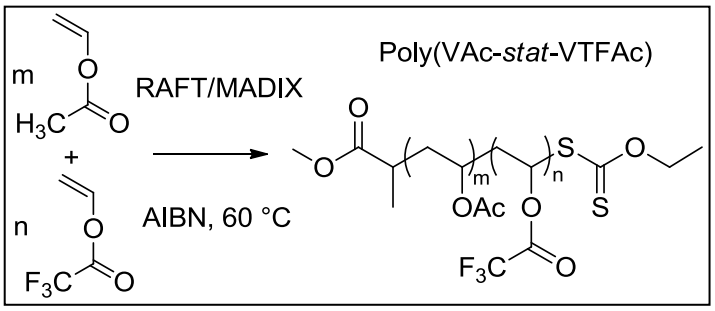

Scheme III.4. RAFT/MADIX copolymerization of VAc and VTFAc.

A range of P(VAc-*stat*-VTFAc) copolymers having varying compositions and molecular weights around 4000 g.mol^{-1} were synthesized (see runs 7 to 11 of Table III.2). Conversions of VTFAc were significantly higher in the presence of vinyl acetate. The control of copolymerization was excellent as experimental M_n were only

slightly higher than theoretical ones. Dispersities ranged from 1.32 to 1.51 while increasing with higher compositions in VAc. This can be related to the higher probability of chain transfer to polymer and monomer upon increasing ratios of VAc.

Run	Sample	$M_{n,\ targeted}$ (g.mol^{-1})	Feed ratio (mol %)		Conversion [a] (%)		Copolymer Composition (mol %) [a]		$M_{n,theo}$ (g.mol^{-1}) [b]	$M_{n,SEC}$ (g.mol^{-1}) (Đ) [c]
			VAc	VTFAc	VAc	VTFAc	VAc	VTFAc		
7	P(VAc_{26}-*stat*-$VTFAc_{74}$)	4200	25	75	97	95	26	74	4200	4600 (1.07)
8	P(VAc_{34}-*stat*-$VTFAc_{66}$)	4200	34	66	94	97	34	66	4200	3800 (1.04)[e]
9	P(VAc_{50}-*stat*-$VTFAc_{50}$)	4200	50	50	94	95	50	50	4200	4400 (1.12)
10	P(VAc_{73}-*stat*-$VTFAc_{27}$)	4100	75	25	94	98	73	27	4100	4400 (1.16)
11	P(VAc_{89}-*stat*-$VTFAc_{11}$)	4300	90	10	94	100	89	11	4300	4500 (1.24)
12	PVAc	4300	100	0	94	-	100	-	4300	4200 (1.31)[d]

[a] Determined by ^{1}H NMR in acetone-d_6 on crude samples [b] Theoretical M_n = ([VTFAc]$_0$×MW(VTFAc)×conv.(VTFAc)+[VAc]$_0$×MW(VAc)×conv.(VAc))/([RhodixanA1]$_0$*100)+MW(RhodixanA1). [c] Determined by SEC in DMF + 10 mM LiBr with PMMA standards. [d] Performed at 50 % wt in ethyl acetate.

Table III.2. Experimental results for the synthesis of P(VAc-*stat*-VTFAc) copolymers through RAFT/MADIX polymerization.

2. Synthesis of P(VAc-*stat*-VTFAc)-based amphiphilic block copolymers

A series of amphiphilic copolymers incorporating increasing amounts of VAc were then synthesized using a PPEGA macromolecular CTA with a M_n of 1000 g.mol^{-1} (see Scheme III.5). As expected, the experimental M_n matched the theoretical ones and the copolymer composition was close to the initial feed ratio (see Table III.3). Low dispersities were also determined by SEC in THF (1.13 < Đ < 1.58) and lower values of dispersity were observed for a copolymer with an equimolar ratio of VAc and VTFAc (see run 15 of Table III.3).

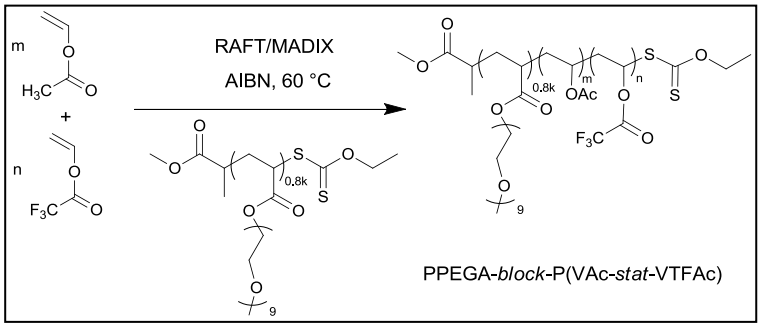

Scheme III.5. RAFT/MADIX copolymerization of VAc and VTFAc using a PPEGA-Xa macromolecular chain transfer agent.

Run	Sample	$M_{n,targeted}$ (g.mol^{-1})	Feed ratio (mol %)		Conversion (%) [a]		Copolymer Composition (mol %) [a]		$M_{n,theo}$ (g.mol^{-1}) [b]	$M_{n\ SEC,THF}$ (g.mol^{-1}) (Đ) [c]
			VAc	VTFAc	VAc	VTFAc	VAc	VTFAc		
13	PPEGA-*b*-PVTFAc	5400	-	100	-	73	-	100	4200	4100 (1.58)
14	PPEGA-*b*-P(VAc_{26}-*stat*-$VTFAc_{74}$)	5000	25	75	94	90	26	74	4200	4200 (1.24)
15	PPEGA-*b*-P(VAc_{50}-*stat*-$VTFAc_{50}$)	5000	50	50	89	90	50	50	4100	4500 (1.13)
16	PPEGA-*b*-P(VAc_{73}-*stat*-$VTFAc_{27}$)	4400	75	25	89	96	74	26	4200	4300 (1.21)
17	PPEGA-*b*-P(VAc_{89}-*stat*-$VTFAc_{11}$)	4400	90	10	94	100	89	11	4200	4200 (1.29)
18	PPEGA-*b*-PVAc	4500	100	-	86	-	100	-	4000	4100 (1.22)-

[a] Determined by ^{1}H NMR [b] Theoretical M_n = ([VTFAc]$_0$×MW(VTFAc)×conv.(VTFAc) +[VAc]$_0$×MW(VAc)×conv.(VAc))/([Chain Transfer Agent]$_0$*100)+MW(Chain Transfer Agent). [c] Determined by SEC in THF with PS standards.

Table III.3. Experimental results for the synthesis of PPEGA-*b*-P(VAc-*stat*-VTFAc) amphiphilic block copolymers.

3. Thermal properties of P(VAc-*stat*-VTFAc) copolymers

In the solid state, the dependency of T_g on copolymer composition was rather slight as the range of T_g was comprised between 20 °C and 44 °C (see runs 7 to 12 of Table III.4). As expected, the value of T_g increased with higher ratios of VTFAc repeating units. In comparison, the variations in the melting point temperatures were much greater as they varied from 137 °C to 104 and 82 for VAc molar percentages of, respectively, 0, 26 and 34 % (see runs 2, 7 and 8 of Table III.4). The copolymers were then amorphous with higher ratios of VAc.

Run	Sample	$M_{n,theo}$ (g.mol^{-1})	$M_{n,SEC,THF}$ (g.mol^{-1}) (Đ)	T_g (°C)	T_m (°C)
2	PVTFAc	4000	4000 (1.11)	43	137
7	P(VAc_{26}-*stat*-$VTFAc_{74}$)	4200	4600 (1.07)	43	104
8	P(VAc_{34}-*stat*-$VTFAc_{66}$)	4200	3800 (1.04)	44	82
9	P(VAc_{50}-*stat*-$VTFAc_{50}$)	4200	4400 (1.12)	35	-
10	P(VAc_{73}-*stat*-$VTFAc_{27}$)	4100	4400 (1.16)	30	-
11	P(VAc_{89}-*stat*-$VTFAc_{11}$)	4300	4500 (1.24)	30	-
12	PVAc	4300	4200 (1.31)	21	-

Table III.4. Thermal properties of P(VAc-*stat*-VTFAc) copolymers.

The amphiphilic block copolymers exhibited an opposite behaviour. The values of T_g increased upon increasing amounts of VAc in the statistical block even though PVTFAc has a higher T_g than PVAc (see Table III.5). This surprising behaviour may be due to the lowering of interactions between the PPEGA block and PVTFAc. However, a second transition glass transition temperature could not be observed even at higher heating rates. The presence of cristalline domains was only noted for the PPEGA-*b*-PVTFAc (run 13) and PPEGA-*b*-P(VAc-*stat*-VTFAc) (run 14). In contrast to the values of T_m reported for their PVTFAc and P(VAc_{25}-*stat*-$VTFAc_{75}$) equivalents –respectively close to 137 and 104 °C-, the lower values of T_m for the amphiphilic block copolymers may indicate a plasticizing effect originating from the PPEGA block.

Run	Sample	$M_{n\ SEC,THF}$ (g.mol^{-1}) (Đ) [c]	T_g (°C)	T_m (°C)
13	PPEGA-*b*-PVTFAc	4100 (1.58)	-27	105
14	PPEGA-*b*-P(VAc_{26}-*stat*-$VTFAc_{74}$)	4200 (1.24)	-21	83
15	PPEGA-*b*-P(VAc_{50}-*stat*-$VTFAc_{50}$)	4500 (1.13)	-15	-
16	PPEGA-*b*-P(VAc_{73}-*stat*-$VTFAc_{27}$)	4300 (1.21)	-7	-
17	PPEGA-*b*-P(VAc_{89}-*stat*-$VTFAc_{11}$)	4200 (1.29)	-5	-
18	PPEGA-*b*-PVAc	4100 (1.22)	-4	-

Table III.5. Thermal properties of PPEGA-*b*-P(VAc-*stat*-VTFAc) copolymers.

4. Solubility of P(VAc-*stat*-VTFAc) copolymers in sc-CO_2

The sc-CO_2 solubility of P(VAc-*stat*-VTFAc) polymers having a molecular weight around 4000 g.mol^{-1} was then studied by cloud point measurements. Briefly, a small amount (0.2 % wt) of polymer was introduced in a variable-volume cell filled with sc-CO_2. The pressure-induced isothermal (40 °C) monophasic-to-biphasic transition was then visually observed. Hence the cloud point of a reference sample of PVAc was thus located at 281 bar (see Figure III.4). With gradual incorporation of 11, 27 and 50 mole percent of VTFAc units into the polymer chains, the cloud point pressures dramatically dropped to 245, 212, and 177 bar. Thereafter, samples incorporating higher fractions of VTFAc (runs 8 to 7 in Table III.4) exhibited a peculiar solubility behavior: a cloud-point-type transition could actually be observed at 203 and 271 bar in coexistence with a precipitated solid. Note that these pressures are anticipated to increase with either higher polymer molecular weights or polymer content.[15]

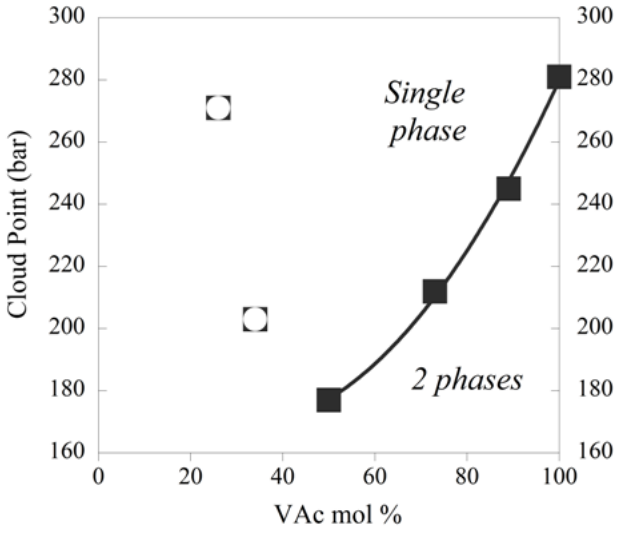

Figure III.4. Cloud point pressures of poly(VAc-*stat*-VTFAc) (0.2 % wt of polymer at 40 °C) as a function of vinyl acetate molar percentage. Closed symbols denote a single cloud point whereas open ones indicate the coexistence of a precipitate.

By means of comparison, two samples of PVAc-based polymer of equivalent M_n incorporating either vinyl pivalate or dibutyl maleate comonomers were synthesized and evaluated as CO_2-philic materials. Details about their synthesis can be found in the experimental section. Their cloud point pressures were respectively

220 bar and 269 bar, highlighting the unprecedented pressure transition induced by the presence of VTFAc monomer units in a poly(vinyl ester) polymer chain.

5. Physicals parameters governing the solubility

In order to gain understanding of the solubility behaviour, the respective contributions of polymer-solvent and polymer-polymer interactions were evaluated.

a) Polymer-CO_2 interactions

The following DFT calculations have been performed by Dr. Thierry Tassaing (Institut des Sciences Moléculaires, University of Bordeaux 1).

Polymer-solvent interactions were calculated by using model structures, namely ethyl acetate (EtAc) and ethyl trifluoroacetate (EtTFAc), that are representative of the main functional groups of the backbone of PVAc and PVTFAc. The equilibrium geometries of these model structures and their complexes with CO_2 have been optimized using Density Functional Theory calculations at the CAM-B3LYP level using Dunning's aug-cc-pVDZ basis set (see Figure III.5). This new functional has been used in order to better account for dispersion forces than standard DFT methods usually do.[16] The methyl-side and trifluoromethyl side of the

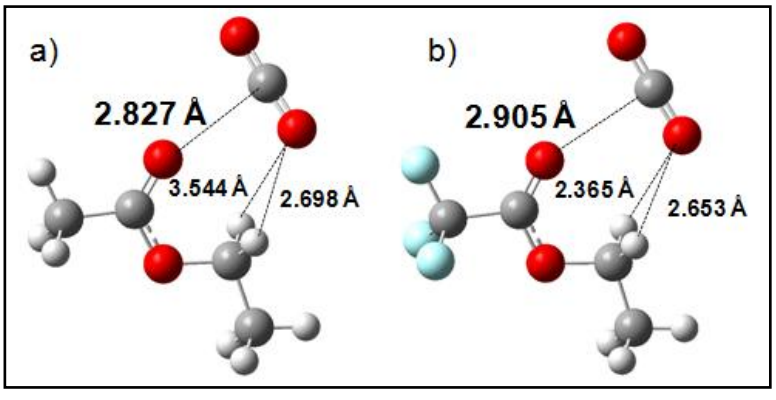

Figure III.5. Optimized structures (CAM-B3LYP/aug-cc-pVDZ) for the ethyl side of the configuration of a) the ethyl acetate - CO_2 complex and b) the ethyl trifluoroacetate - CO_2 complex.

model compounds-CO_2 complexes were not compared. Indeed, the fluorine atoms in EtTFAc were calculated to carry negative partial charges close to -0.52 e, which render unfavorable any fluorine-CO_2 interactions.[17] The resultant equilibrium geometries on the ethyl side (see Figure III.5) were equivalent for both complexes as CO_2 was found to be above the acetate group where the oxygen atom interacts with CO_2 through a LA-LB interaction. A weak hydrogen bond appeared in both complexes between a hydrogen atom of the ethyl group and an oxygen atom of CO_2 as evidenced by the shortening of the C-H bonds (see Figure III.5). Such structure is consistent with previous results obtained for methyl acetate complexes.[18] Intermolecular distances between the carbon atom of CO_2 and the oxygen atom of the acetate group (d(C•••O)) were estimated at 2.827 Å for EtAc and 2.905 Å for EtTFAc. By the same token, the stabilization energy was significantly lower (0.5 kcal.mol^{-1}) for the EtTFAc-CO_2 complex in comparison with the EtAc-CO_2 complex. The interactions between CO_2 and the fluorinated moiety were consequently weaker. Additionally, steric effects could not account for this energy difference given the geometry of the complexes. This was also supported by the charge distributions on both model compounds (see Table III.6). The absolute partial charge on the oxygen atom of the carbonyl group was higher for EtAc than for EtTFAc. This might be related to the inductive effect differences imposed by the CH_3 and CF_3 groups, respectively. As a result, replacing the CH_3 group by a CF_3 substituent in the acetate functionality leads to a decrease of the partial negative charge on the carbonyl group that in turn leads to a decrease of the interaction between CO_2 and the acetate group. The solubility behavior of the P(VAc-*stat*-VTFAc) copolymers was not consequently governed by polymer-solvent interactions.

Molecular Species	ΔE_{cor} BSSE+ZPE (kcal.mol^{-1})	d(C•••O) (Å)	q_O (e)
EtAc-CO_2	-1.92	2.827	-0.75
EtTFAc-CO_2	-1.44	2.905	-0.67

Table III.6. Basis Set Superposition Errors and Zero Point Energy Corrected Interaction Energies (ΔE_{cor}) - Intermolecular d(C•••O) and d(O•••H) distances for the acetate-CO_2 complexes calculated at the CAM-B3LYP level using the aug-cc-pVDZ basis sets - Charge on the oxygen atom of the isolated acetate molecule (q_O).

b) Polymer-polymer interactions

Polymer-polymer interactions were qualitatively estimated from surface tension values which are commonly measured with sessile drop experiments. A solution of polymer at 10 % wt in 2-butanone was placed on a glass substrate and then spin-coated to create a thin film of polymer. A drop of water was deposited on the surface and water contact angles were measured by the drop-shaped analysis-profile technique. The values of surface tension at the air/polymer interface could be then extrapolated from the empirical equation of state proposed by Li and Neumann for a hydrophobic solid surface:[19]

$$\cos(\theta) = -1 + 2\sqrt{\frac{\gamma^{air/polymer}}{\gamma^{air/water}}}e^{-0.0001247(\gamma^{air/water}-\gamma^{air/polymer})^2}$$

where θ, $\gamma^{air/polymer}$ and $\gamma^{air/water}$ stand for, respectively, the water contact angle, the surface tension at the air/polymer interface and the surface tension at the air/water interface.

Water contact angles increased from 58° for a pure PVAc sample to 75, 76, 86 and 88° for P(VAc-*stat*-VTFAc) copolymers with respective 11, 27, 50 and 66 % mol of VTFAc units (see runs 11 to 7 of Table III.7). The surface tension of PVAc was calculated to be 49 mN.m^{-1} while those of P(VAc-*stat*-VTFAc) gradually decreased until reaching a surface tension of 30 mN.m^{-1} at 66 % mol of VTFAc repeating units. This also corresponded to the surface tension of a 4k PVTFAc homopolymer. Interestingly, these surface tension values followed the same tendency as the solubility measurements (see Figure III.6). This clearly indicated the prominent role of polymer/polymer interactions in the solubility of amorphous P(VAc-*stat*-VTFAc) polymers in sc-CO_2. This also confirmed previous works where polymer-polymer interactions were postulated to be the key driving force in the solubility of polymers in sc-CO_2.[20,21]

Run	Sample	$M_{n,theo}$ (g.mol^{-1})[a]	T_g (°C)	T_m (°C)	P_{cloud} (bar) [b]	θ (°) [d]	γ (mN.m^{-1})[e]
7	P(VAc_{26}-*stat*-$VTFAc_{74}$)	4200	43	104	271 [c]	89	30
8	P(VAc_{34}-*stat*-$VTFAc_{66}$)	4200	44	82	203 [c]	88	30
9	P(VAc_{50}-*stat*-$VTFAc_{50}$)	4200	35	-	177	85	33
10	P(VAc_{73}-*stat*-$VTFAc_{27}$)	4100	30	-	212	76	38
11	P(VAc_{89}-*stat*-$VTFAc_{11}$)	4300	30	-	245	75	39
12	PVAc	4300	21	-	281	58	49
19	P(VAc_{51}-*alt*-DBM_{49})	4400	-12	-	269	80	36
20	P(VAc_{10}-*stat*-$VPiv_{90}$)	4300	33	-	220	89	30

[a] Determined by ^{1}H NMR. [b] Onset of turbidity with 0.2 % wt of polymer in sc-CO_2 at 40 °C (standard deviation: +/- 3 bar, repeatability +/- 5 bar) . [c] Determined from a biphasic mixture. [d] Contact angles, reported as average values of four measurements. [e] Surface tension.

Table III.7. Experimental results for the solubility and surface tension of P(VAc-*stat*-VTFAc) copolymers.

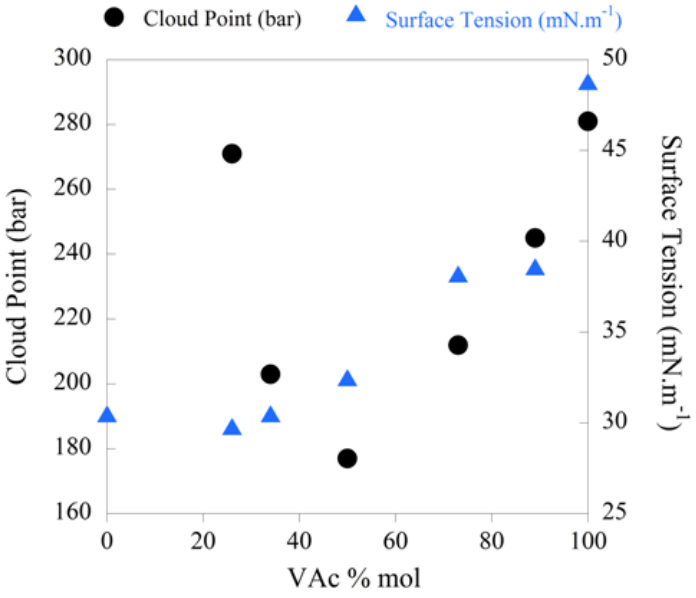

Figure III.6. Cloud point pressures and surface tension values of poly(VAc-*stat*-VTFAc) as a function of VAc molar percentage.

Therefore, the observed hybrid behavior with both a cloud point and an insoluble fraction (see Figure III.4) may be explained by higher polymer–polymer self-interactions resulting from the appearance of crystalline domains. To confirm this, additional measurements on the P(VAc_{34}-*stat*-$VTFAc_{66}$) sample (run 8 of Table III.7) were consequently performed at a higher temperature to melt the crystalline zones. Benefiting from the plasticizing effect of CO_2, a single cloud point could be observed at 240 bar and 60 °C. As expected, this increase in solubility pressures corresponded to the sc-CO_2 density decreasing with higher temperatures.

In the light of this, stronger polymer-polymer interactions could explain the lower solubility observed for the P(VAc_{51}-*alt*-DBM_{49}) sample (run 19 of Table III.7) although its lower T_g should favor its mixing entropy. On the other hand, the P(VAc_{10}-*stat*-$VPiv_{90}$) sample (run 20 of Table III.7) exhibited a surface tension equivalent to a P(VAc_{34}-*stat*-$VTFAc_{66}$) sample even though the cloud point was nearly 50 bar higher. This may suggest that interactions between VAc and vinyl pivalate units are more enthalpically favorable than those between VAc and VTFAc ones, thus decreasing CO_2-solubility.[22]

6. Solubility of P(VAc-*stat*-VTFAc)-based amphiphilic block copolymers in sc-CO_2

Finally, the solubility of amphiphilic block copolymers was evaluated starting from a non-fluorous PPEGA-*b*-PVAc copolymer. This copolymer exhibited a cloud point at 337 bar (see Figure III.7). Decreasing the % mol VAc to 89, 74, 50 and 26 gave lower cloud points of respectively 303, 296, 285 and 277 bar (see runs 13 to 17 of Table III.7). However, the decreasing trend in cloud points was much lower than this observed with their non-amphiphilic P(VAc-*stat*-VTFAc) copolymer equivalents possessing a similar molecular weight of 4000 $g.mol^{-1}$ (see Figure III.7). The presence of a PPEGA CO_2-phobic group thus induced a significant difference in the solubility of these copolymers in terms of both values and evolutions of cloud points. Concerning the purely fluorinated amphiphilic block copolymer (run 13), a cloud point value of 261 bar was determined whereas a precipitate was observed meanwhile. This phenomenon was due to the presence of a crystalline domain with a high melting point temperature. On the opposite, a single cloud point could be

observed for the PPEGA-*b*-P(VAc$_{26}$-*stat*-VTFAc$_{74}$) copolymer where the melting point temperature was low enough to induce its full plasticization by CO_2. Finally, increasing the concentration of this copolymer from 0.2 to 0.5 % wt resulted in a cloud point pressure observed at 354 bar.

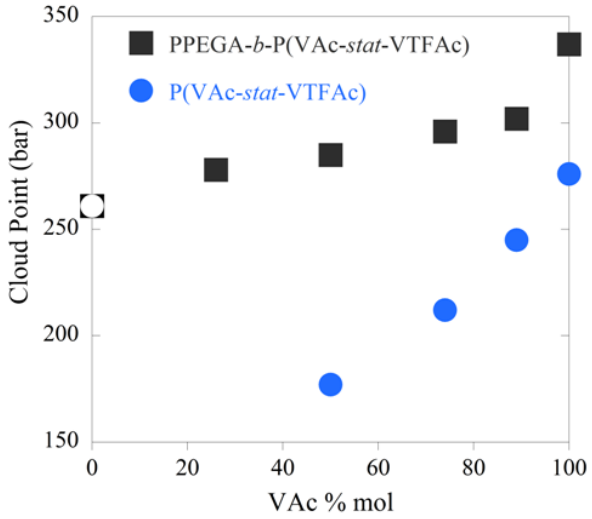

Figure III.7. Cloud point pressures of poly(vinyl trifluoroacetate)-based copolymers of equivalent molecular weight in sc-CO_2. Open symbols mark the coexistence with a solid precipitate.

II. Distinctive features of solubility of vinyl acetate/1-(trifluoromethyl) vinyl acetate copolymers in sc-CO_2

Following the previous results, the incorporation of VTFAc repeating units led to the lowering of polymer-polymer interactions but concomitantly decreased polymer-CO_2 interactions. It would be consequently of great interest to consider a comonomer capable of decreasing polymer-polymer interactions while preserving an equivalent level of polymer-solvent interactions. In this regard, a promising strategy to combine these features would be the positioning of trifluoromethyl groups on the main chain of a poly(vinyl acetate)-based copolymer. Indeed, the presence of this trifluoromethyl group on the alpha position of the acetate group may lower the surface tension of the polymer chains without hindering the formation of acetate-CO_2 complexes and weakening the chemical stability. It appeared that the commercially available 1-(trifluoromethyl) vinyl acetate monomer (CF_3VAc) should fulfill these criteria.

A. RAFT/MADIX copolymerization of vinyl acetate and 1-(trifluoromethyl) vinyl acetate

In spite of a large interest towards fluorinated polymers and their applications, 1-(trifluoromethyl) vinyl acetate has attracted little attention so far. Even though poly(CF_3VAc) oligomers can be obtained under anionic conditions, this monomer actually does not homopolymerize under free-radical conditions.[23] The presence of the trifluoromethyl group makes the C=C double bond less polarizable, which lowers the reactivity of the monomer in homopolymerization and copolymerization systems. However, free-radical copolymerization with monomers of different reactivities such as styrene and VAc can still be achieved.[24,25] A P(VAc-*stat*-CF_3VAc) copolymer (M_n = 19500 g.mol^{-1}, Đ = 1.95) could be thus obtained from the bulk copolymerization of VAc and CF_3VAc at 80 °C with 2 % mol of AIBN.[24] The reactivity ratios of VAc and CF_3VAc were respectively evaluated to r_{VAc} = 0.25 and r_{CF_3VAc} = 0.20 in bulk at 70 °C.[25] Therefore, due to a stronger tendency to alternation, the molar fraction of CF_3VAc in the copolymer cannot exceed 0.5.

As a matter of fact, the control of the copolymerization of VAc and CF_3VAc can only be achieved through an efficient control on the polymerization of VAc. The applicability and scope of various RDRP techniques on such control have been extensively discussed in Chapter 2. Based on this knowledge, *O*-ethyl xanthates are consequently natural candidates to mediate the copolymerization of VAc and CF_3VAc.

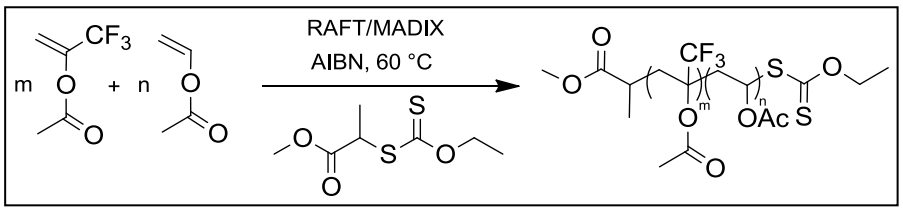

Scheme III.6. RAFT/MADIX copolymerization of VAc and CF_3VAc.

1. Synthesis of P(VAc-*stat*-CF_3VAc) copolymers of variable chain lengths

By means of comparison, a free radical bulk copolymerization of VAc and CF_3VAc with a 50:50 molar feed ratio was first performed with a AIBN molar percentage of 0.3 %. Compared to the results of Ober *et al.*,[24] a copolymer having a higher M_n of 28000 g.mol^{-1} and an equivalent dispersity of 1.90 was obtained (see run 21 of Table III.8). The difference in experimental M_n was attributed to the lower amount of AIBN introduced in our polymerizations. RAFT/MADIX copolymerization experiments were then run at this same feed ratio (see runs 22 and 23 of Table III.8). The successful mediation of the copolymerization by Rhodixan A1 was evidenced by SEC in THF (see Figure III.8) as lower molecular weights were obtained upon the increase of concentration of the xanthate. In spite of partial monomer conversions (< 29 %), experimental molecular weights were very close to the theoretical ones in the range between 2000 and 4000 g.mol^{-1}. Compared to a xanthate-free experiment, the dispersities obtained in RAFT/MADIX polymerizations were systematically lower ($1.51 < Đ < 1.67$) and tended to decrease with increasing theoretical M_n (see runs 22 and 23 of Table III.8).

Run	Sample	$M_{n,targeted}$ (g.mol^{-1})[b]	Feed ratio (mol %)		Conversion (%)		Composition (mol %)		$M_{n,theo}$ (g.mol^{-1}) [e]	$M_{n,SEC}$ (g.mol^{-1}) [f] (Đ)
			VAc	CF_3 VAc	VAc[c]	CF_3 VAc[d]	VAc	CF_3 VAc		
21	P(VAc-*stat*-CF_3VAc)	-	50	50	36	36	50	50	-	28000 (1.90)
22	P(VAc_{50}-*stat*-CF_3VAc_{50})[a]	7200	50	50	29	29	50	50	2100	2200 (1.67)
23	P(VAc_{50}-*stat*-CF_3VAc_{50})	15000	50	50	27	27	50	50	4100	3700 (1.51)

[a] Samples are named from the molar fractions in each monomer. [b] $M_{n,targeted}$ = (([CF_3VAc]$_0$×MW(CF_3VAc)+[VAc]$_0$×MW(VAc))/[RhodixanA1]$_0$+MW(RhodixanA1). [c] Determined by ^{1}H NMR in acetone-d_6 [d] Determined by ^{19}F NMR in acetone-d_6. [e] $M_{n,theoretical}$ = ([CF_3VAc]$_0$×MW(CF_3VAc)×conv.(CF_3VAc) +[VAc]$_0$×MW(VAc)×conv.(VAc))/([RhodixanA1]$_0$*100)+MW(RhodixanA1). [f] Determined by SEC in THF with PS standards.

Table III.8. Experimental results for the synthesis of poly(VAc-*stat*-CF_3VAc) copolymers of variable chain lengths.

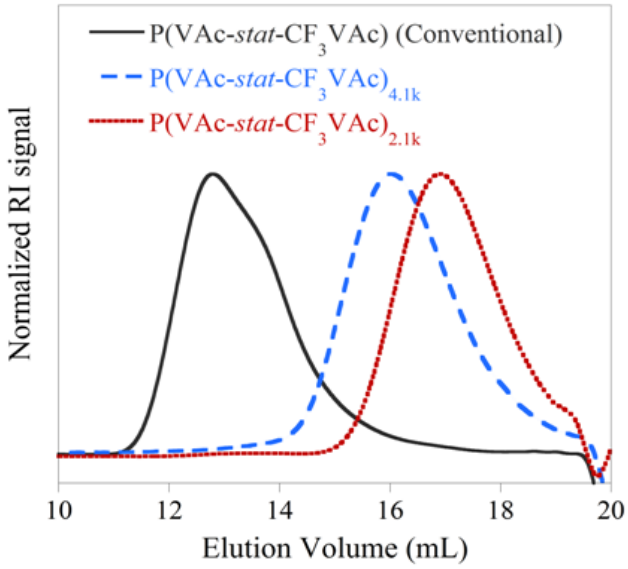

Figure III.8. Overlays of SEC chromatograms (RI detection, in THF) for the free-radical bulk copolymerization of VAc and CF_3VAc at 60 °C (run 21 of Table III.9) and the corresponding RAFT/MADIX copolymerizations (runs 22 and 23 of Table III.9).

2. MALDI-TOF mass spectrometry

The controlled character of the copolymerization could be further confirmed by MALDI-TOF mass spectrometry and ^{1}H NMR experiments. Indeed, the populations revealed on the MALDI-TOF mass spectrum of the run 3 were all capped by both groups of the xanthate, $C_4H_7O_2$ and $C_3H_5OS_2$ (see Figure III.9 and Table III.9). In accordance with the reactivity ratios and the inability of CF_3VAc to homopolymerize under free-radical conditions, the main populations were either predominantly composed of VAc repeating units or comprised an equivalent number of VAc and CF_3VAc monomers. Some minor populations comprising more CF_3VAc repeating units were also revealed at 1585.3, 1739.3, 1825.3 and 1893.3 m/z. Even though MALDI-TOF is not a quantitative technique, this qualitatively agreed with previous findings of Schmaljohann and Ober who identified a small molar percentage of 3 % of CF_3VAc-CF_3VAc diads through ^{1}H-^{1}H-DQCOSY NMR.[24] This could be due to the occurrence of invert adducts during the course of the polymerization.

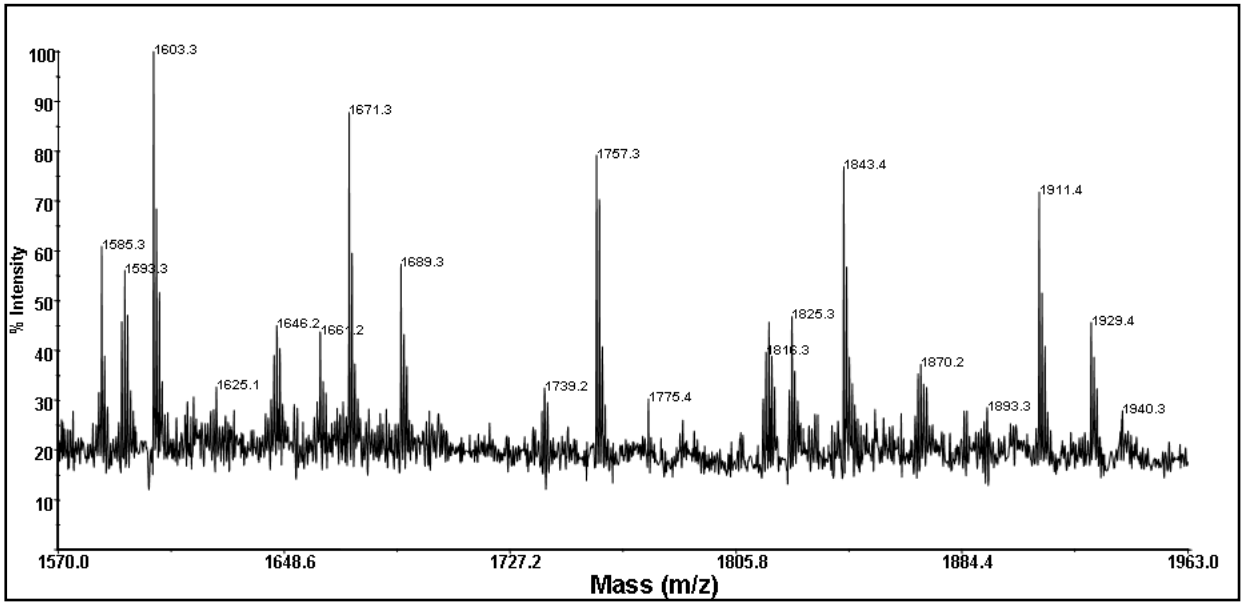

Figure III.9. Enlargement of the MALDI-TOF mass spectrum of a P(VAc-*stat*-CF_3VAc) (run 3 of Table III.8, reflectron mode, NaI cationization). Note that peaks at 1646.2, 1661.2, 1816.3 and 1870.2 m/z could not be assigned but might be due to matrix aggregates.

Experimental monoisotopic mass (m/z)	($DP_{m,VAc}$, DP_{n,CF_3VAc})	Theoretical monoisotopic mass (m/z)	Δ (%)
1585.3	(5,6)	1585.3	0.000
1603.3	(7,5)	1603.4	0.006
1671.3	(6,6)	1671.4	0.006
1689.3	(8,5)	1689.4	0.006
1739.2	(5,7)	1739.3	0.006
1757.3	(7,6)	1757.4	0.006
1775.4	(9,5)	1775.5	0.006
1825.3	(6,7)	1825.4	0.005
1843.4	(8,6)	1843.4	0.000
1893.3	(5,8)	1893.4	0.005
1911.4	(7,7)	1911.4	0.000
1929.4	(9,6)	1929.5	0.005

Table III.9. Assignments of the peaks (displayed in the MALDI-TOF mass spectrum on Figure II.9) for a P(VAc-*stat*-CF_3VAc) copolymer (run 23 of Table III.8).

3. Synthesis of P(VAc-*stat*-CF_3VAc) copolymers of variable compositions

Molecular weights of 4000 g.mol^{-1} with molar contents in CF_3VAc lower than 50 % were then targeted to create a library of copolymers with varying compositions. VAc conversions gradually decreased with increasing amounts of CF_3VAc in the feed ratio (see runs 3 to 6 of Table III.10). In agreement with the reactivity ratios, the final compositions of the copolymers were close to the initial feed ratios. The experimental M_n determined by SEC were relatively close to the theoretical ones. Upon varying the CF_3VAc content from 13 up to 50 % mol, dispersity increased from 1.19 to 1.51 (see runs 3 to 6 of Table III.10). This was attributed to the low xanthate reactivity towards CF_3VAc macroradicals, in a similar fashion to other 1,1-disubstituted monomers like ethyl alpha-acetoxyacrylate and methacrylates.[26,27] In other terms, the increase of dispersities with higher CF_3VAc contents can be related to a decrease of the RAFT/MADIX interchain transfer constant ($C_{tr,PnX}$).[28] Interestingly, P(VAc-*stat*-CF_3VAc) exhibited a enhanced thermal stability at temperatures up to 280 °C (run 23

of Table III.8) whilst its P(VAc_{50}-*stat*-$VTFAc_{50}$) equivalent readily degraded at around 130 °C.

Run	Sample	$M_{n,targeted}$ (g.mol^{-1})[b]	Feed ratio		Conversion		Composition		$M_{n,theo}$ (g.mol^{-1})[e]	$M_{n,SEC}$ (g.mol^{-1}) (Đ)[f]
			VAc	CF_3 VAc	VAc[c]	CF_3 VAc[d]	VAc	CF_3 VAc		
23	P(VAc_{50}-*stat*-CF_3VAc_{50})	15000	50	50	27	27	50	50	4100	3700 (1.51)
24	P(VAc_{57}-*stat*-CF_3VAc_{43})	7100	66	33	48	74	57	43	4300	3600 (1.37)
25	P(VAc_{67}-*stat*-CF_3VAc_{33})	6300	75	25	60	89	67	33	4500	3800 (1.26)
26	P(VAc_{87}-*stat*-CF_3VAc_{13})	5300	90	10	74	100	87	13	4300	4300 (1.19)
27	PVAc	4400	100	-	93	-	100	-	4200	4200 (1.31)[g]

[a] Samples are named from the molar fractions in each monomer. [b] $M_{n,targeted}$ = (([CF_3VAc]$_0$×MW(CF_3VAc)+[VAc]$_0$×MW(VAc))/[RhodixanA1]$_0$+MW(RhodixanA1). [c] Determined by ^{1}H NMR in acetone-d_6 [d] Determined by ^{19}F NMR in acetone-d_6. [e] $M_{n,theoretical}$ = ([CF_3VAc]$_0$×MW(CF_3VAc)×conv.(CF_3VAc) +[VAc]$_0$×MW(VAc)×conv.(VAc))/([RhodixanA1]$_0$*100)+MW(RhodixanA1). [f] Determined by SEC in THF with PS standards. [g] Synthesized at 50 % wt in ethyl acetate.

Table III.10. Experimental results for the RAFT/MADIX synthesis of poly(VAc-*stat*-CF_3VAc) copolymers of variable compositions.

4. Synthesis of amphiphilic block copolymers

The possibilities of synthesizing block copolymers with a P(VAc-*stat*-CF_3VAc) block were then evaluated. In parallel to Chapter 1, a PDMA oligomer having a molecular weight of 1000 g.mol^{-1} -synthesized by RAFT/MADIX polymerization- was used as a macromolecular CTA for the RAFT/MADIX bulk copolymerization of VAc and CF_3VAc (see Scheme III.7). In all cases, a final molecular weight around 4200 g.mol^{-1} was targeted taking into account the conversions observed with different compositions.

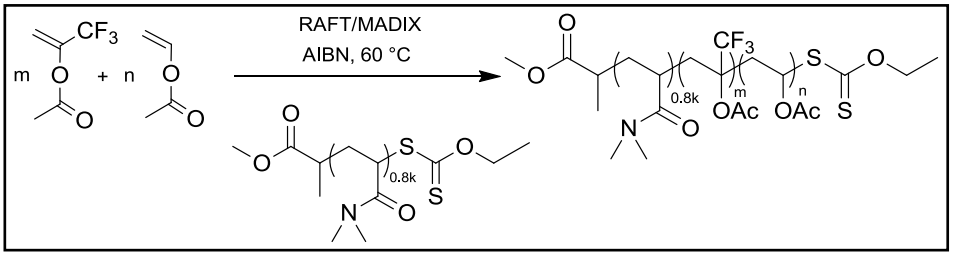

Scheme III.7. RAFT/MADIX copolymerization of VAc and CF_3VAc using a $PDMA_{o.8k}$-Xa oligomer as a xanthate chain transfer agent.

As expected, the conversions were similar to those reported for the RAFT/MADIX copolymerization with Rhodixan A1 (see Table III.11). The final compositions were also relatively close to the initial feed ratios. The experimental molecular weights determined by SEC-THF matched the theoretical ones whereas dispersity was lower than 1.5 (see runs 28 to 30 of Table III.11). However, the SEC molecular weights decreased with increasing amounts of CF_3VAc in the feed ratio. This resulted from the partial conversion of the PDMA macromolecular CTA as clearly evidenced by SEC-THF equipped with a UV detector at 290 nm (see Figure III.10). The presence of unreacted CTA -particularly obvious at high % mol of CF_3VAc (see runs 30 and 31 of Table III.11)- actually biased the determination of M_n by SEC. The CTA appeared to be fully consumed at the end of the reaction if only the % mol of CF_3VAc did not exceed 25 % in the feed ratio. Note that this experimental fact was not observed when Rhodixan A1 was used as CTA. This suggests that the value of $C_{tr,X}$ for Rhodixan A1 is higher than that of the PDMA macromolecular CTA.

			Feed ratio (mol %)		Conversion (%)		Copolymer Composition (mol %) [b]				
Run	CTA	$M_{n,\ targeted}$ (g.mol^{-1})	VAc	CF_3 VAc	VAc[a]	CF_3 VAc [b]	VAc	CF_3 VAc	$M_{n,theo}$ (g.mol^{-1})	$M_{n,SEC}$[d] (g.mol^{-1}) (Đ)	T_g (°C)
28	$PDMA_{0.8k}$-Xa	5100	90	10	74	100	87	13	4200	5100 (1.31)	46
29	$PDMA_{0.8k}$-Xa	5700	75	25	59	93	66	34	4300	4600 (1.29)	49
30	$PDMA_{0.8k}$-Xa	6300	66	33	44	66	57	43	3900	3400 (1.46)	50
31	$PDMA_{0.8k}$-Xa	13300	50	50	25	25	50	50	4100	n.d. [d]	n.d. [d]

[a] Determined by ^{1}H NMR. [b] Determined by ^{19}F NMR. [c] Determined by SEC in THF with PS standards. [d] n.d.: not determined due to a bimodal distribution.

Table III.11. Experimental results for the RAFT/MADIX copolymerization of VAc and CF_3VAc using a $PDMA_{0.8k}$-Xa oligomer as a xanthate chain transfer agent.

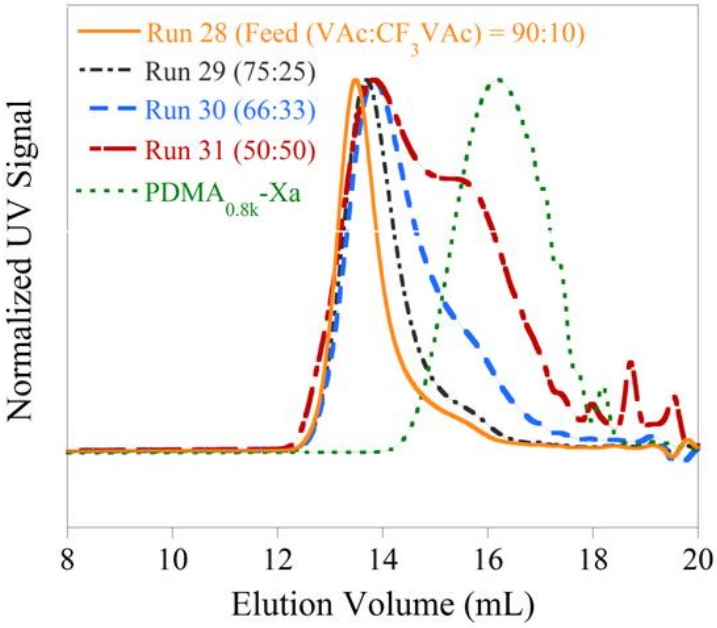

Figure III.10. Overlay of SEC-UV chromatograms for the RAFT/MADIX copolymerization of VAc and CF_3VAc starting from a $PDMA_{0.8k}$-Xa oligomer CTA.

B. Solubility of P(VAc-*stat*-CF_3VAc)-based copolymers in sc-CO_2

1. Solubility of P(VAc-*stat*-CF_3VAc) statistical copolymers

The solubility of the resulting copolymers in sc-CO_2 was then studied by cloud point measurements. Studies were performed with 0.2 % wt of polymer content to allow a comparison with literature results.[17,21] Note that these values are expected to increase upon increasing molecular weights and polymer content.[15] While a PVAc sample of 4000 g.mol^{-1} exhibited a cloud point at 281 bar, those of statistical copolymers containing 13 and 33 % mol of CF_3VAc decreased respectively down to 245 and 222 bar (see runs 27 down to 25 in Table III.12 and Figure III). Then, the cloud point pressures increased again to 228 and 245 bar for higher CF_3VAc molar contents of 43 and 50 %, respectively (see runs 24 to 23 in Table III.12). The existence of a composition-solubility optimum for such copolymers could thus be evidenced at a VAc-CF_3VAc ratio of 2:1 with a maximum $\Delta P_{cloud,max}$ of 59 bar (with $\Delta P_{cloud} = P_{cloud}(Sample) - P_{cloud}(PVAc)$). This maximum value compared favorably with previously reported results for copolymers of different structures. This optimum value is lower than the one obtained with poly(vinyl acetate-*stat*-vinyl

trifluoroacetate), P(VAc_{50}-*stat*-$VTFAc_{50}$) ($\Delta P_{cloud,max}$ = 104 bar, see run 9 in Table III.12),[21] slightly higher than the one observed for poly(vinyl acetate-*alt*-dibutyl maleate), P(VAc_{49}-*alt*-DBM_{51}) ($\Delta P_{cloud,max}$ = 12 bar, see run 21 in Table III.12) and comparable with the one found in the case of poly(vinyl acetate-*stat*-vinyl pivalate) (P(VAc_{10}-*stat*-$VPiv_{90}$), see run 20 of Table III.12).[4]

Run	Sample	$M_{n,theoretical}$ (g.mol^{-1})	T_g (°C)	P_{cloud} (bar) [a]	ΔP_{cloud} (bar) [b]	Θ (°) [c]	γ (mN.m^{-1})[d]
23	P(VAc_{50}-*stat*-CF_3VAc_{50})	4100	44	245	36	83	34
24	P(VAc_{57}-*stat*-CF_3VAc_{43})	4300	42	228	53	80	35
25	P(VAc_{67}-*stat*-CF_3VAc_{33})	4500	37	222	59	80	35
26	P(VAc_{87}-*stat*-CF_3VAc_{13})	4300	34	245	36	72	40
27	PVAc	4200	21	281	0	58	49
9	P(VAc_{50}-*stat*-$VTFAc_{50}$)	4200	35	177	104	85	33
19	P(VAc_{49}-*alt*-DBM_{51})	4400	-12	269	12	80	36
20	P(VAc_{10}-*stat*-$VPiv_{90}$)	4300	33	220	61	89	30

[a] Onset of turbidity with 0.2 % wt of polymer at 40 °C (standard deviation: +/- 3 bar, repeatability +/- 5 bar). [b] $\Delta P_{cloud} = P_{cloud}$(Sample) – P_{cloud}(PVAc, run 27). [c] Contact angles, reported as average values of four measurements. [d] Surface tension.

Table III.12. Experimental results for the solubility and physical properties of the poly(VAc-*stat*-CF_3VAc) copolymers.

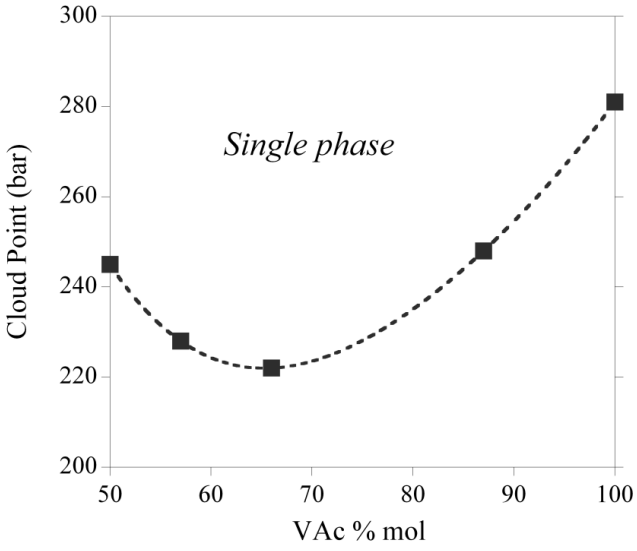

Figure III.11. Cloud point pressures of poly(VAc-*stat*-CF_3VAc) copolymers (0.2 % wt of polymer at 40 °C) as a function of VAc molar percentage.

2. Physical parameters governing the solubility behaviour

a) Polymer-polymer interactions

The solubility behaviour could be first rationalized by polymer-polymer interactions through the surface tension of the polymer samples. This was evaluated from water contact angles.[19] From a PVAc sample exhibiting a surface tension of 49 $mN.m^{-1}$ (run 27 of Table III.13), increasing the CF_3VAc ratio from 13 to 33 % mol in the PVAc-based polymer chains resulted in a drop from 40 and 35 $mN.m^{-1}$ (see runs 26 and 27 of Table III.13) Then, a plateau of surface tension appeared at around 34-35 $mN.m^{-1}$ for higher ratios (see runs 14 and 25 of Table III.13). Singularly, the position of this plateau in terms of VAc-CF_3VAc ratios corresponded to the previously described optimal composition and lower observed cloud points. A drop in polymer-polymer interactions was thus clearly correlated to the initial decrease of cloud point pressures.

b) Polymer-CO_2 interactions

The following DFT calculations have been performed by Dr. Thierry Tassaing (Institut des Sciences Moléculaires, University of Bordeaux 1).

Lower polymer-CO_2 interactions were then postulated to induce the following increase in P_{cloud}. The contribution of polymer-solvent interactions was evaluated with Density Functional Theory calculations at the CAM-B3LYP level using Dunning's aug-cc-pVDZ basis set.[16] Equilibrium geometries of representative model structures, namely isopropyl acetate (iPrAc) and 1,1,1-trifluoropropan-2-yl acetate (TFiPrAc), were optimized along with their complexes with the CO_2 molecule. The methyl and ester sides of the model compound-CO_2 complexes were both compared (see Figure III.12 and Figure A.III.4 in Appendix). No significant differences between interactions energies and $d_{(C\cdots O)}$ intermolecular distances were found for the ester side-CO_2 complexes (see Table A.III.3 in Appendix). In the case of the methyl-side-CO_2 complexes, CO_2 was found to be above the acetate group where the oxygen atom interacts with CO_2 through a LA-LB interaction. As expected, the aforementioned hydrogen bond between an hydrogen of the acetate group and the lone pair of oxygen

in CO_2 was also evidenced in these structures. These distances were closed to 2.61 Å in both complexes. Intermolecular distances between the carbon atom of CO_2 and the oxygen atom of the acetate group ($d_{(C\cdots O)}$) were also equivalent and estimated at 2.799 Å for iPrAc and 2.817 Å for TFiPrAc. The stabilization energy was only slightly higher of 0.15 kcal.mol^{-1} for the iPrAc-CO_2 complex (see Table III.13). This consequently differs from the case of ethyl trifluoroacetate –a model compound for poly(vinyl trifluoroacetate), as previously reported in the first part of this chapter- where the stabilization energy was lower of 0.5 kcal.mol^{-1} compared to ethyl acetate. Finally, absolute partial charges on the oxygen atom of the carbonyl group were equivalent for both model structures. It consequently appeared from DFT calculations that polymer-solvent interactions were of the same order for the iPrAc and TFiPrAc complexes and could not explain the variations in the P_{cloud} observed for high ratios of CF_3VAc.

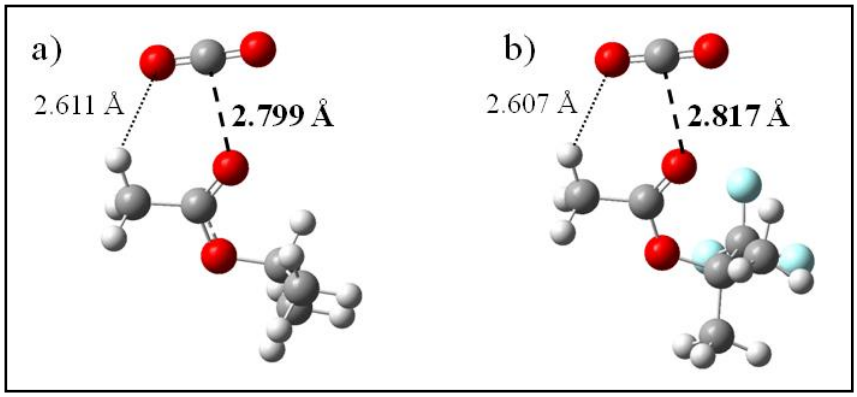

Figure III.12. Optimized structures (CAM-B3LYP/aug-cc-pVDZ) for the methyl side of the configuration of a) the isopropyl acetate–CO_2 complex and b) the 1,1,1-trifluoropropan-2-yl acetate–CO_2 complex.

	$\Delta E_{cor,BSSE+ZPE}$ (kcal.mol^{-1})	$d_{(C\cdots O)}$ (Å)	$d_{(O\cdots H)}$ (Å)	q_O (e)
iPrAc - CO_2	-2.18	2.799	2.611	-0.78
TFiPrVAc - CO_2	-2.03	2.817	2.607	-0.76

Table III.13. Basis Set Superposition Errors and Zero Point Energy Corrected Interaction Energies (ΔE_{cor}) - Intermolecular d(C•••O) and d(O•••H) distances for the acetate-CO_2 complexes calculated at the CAM-B3LYP level using the aug-cc-pVDZ basis sets - Charge on the oxygen atom of the isolated acetate molecule (q_O).

c) Entropy of mixing

From this, the solubility behaviour observed for VAc-CF_3VAc ratios higher than 67:33 was postulated to originate from a lower chain flexibility and consequently a decrease in the entropy of mixing. This was reflected by increasing T_g of 37, 42, and 44 °C for molar percentages in CF_3VAc of 33, 43 and 50, respectively (see Table III.12). In other polymer/CO_2 case studies, the importance of entropy of mixing was also put forward to explain the solubility of poly(methyl acrylate) in sc-CO_2 while poly(methyl methacrylate) is insoluble.[29] Thus, entropy of mixing dominated over enthalpic polymer-polymer interactions beyond this specific 66:33 ratio. Furthermore, this effect is expected to amplify upon increasing molecular weights and polymer content.[15]

3. Solubility of a P(VAc-*stat*-CF_3VAc)-based amphiphilic block copolymer

In order to provide a direct comparison with the results presented in Chapter 1, the solubility of the $PDMA_{0.8k}$-*b*-$P(VAc_{34}$-*stat*-$CF_3VAc_{66})_{3.3k}$ copolymer (run 29 of Table III.11) was evaluated through infrared spectroscopy. The solubility of this copolymer in sc-CO_2 approached 0.65 % wt at 350 bar and 40 °C while only 0.47 % wt of its non-fluorinated equivalent was soluble in the same conditions (see Figure III.13). However, the $PDMA_{0.8k}$-*b*-$P(VAc_{34}$-*stat*-$CF_3VAc_{66})_{3.3k}$ sample appeared less soluble than the $PDMA_{0.8k}$-*b*-$PVAc_{3.3k}$-FXa copolymer described in Chapter 1. The strategy based on the chain end functionalization thus appeared a better strategy to improve the solubility of PVAc-based amphiphilic block copolymers.

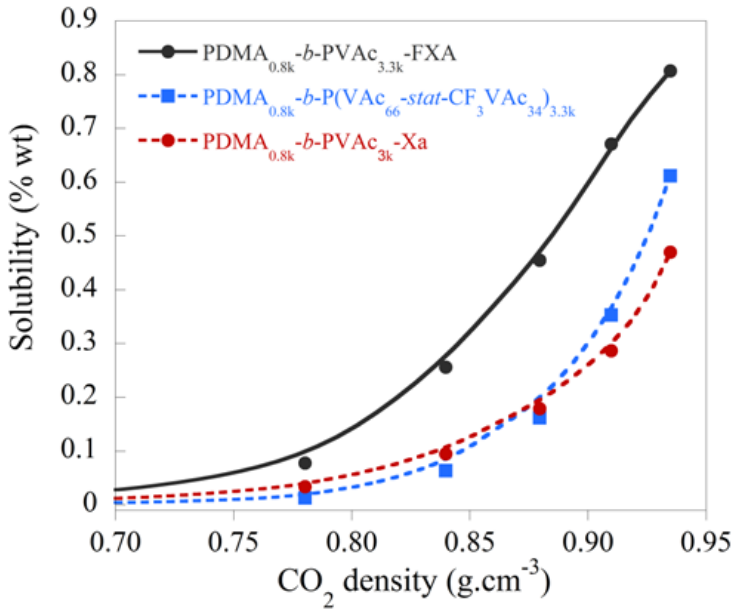

Figure III.13. Solubility (% wt) of amphiphilic block copolymers in sc-CO_2 at 40 °C as measured by infrared spectroscopy.

III. Conclusion

Throughout this third chapter, the different roles of polymer-polymer interactions, polymer-CO_2 ones and entropy of mixing in the solubility of PVAc-based copolymers have been explored. To do so, two monomers incorporating trifluoromethyl groups positioned either on the pendent ester group –VTFAc- or on the polymer backbone –CF_3VAc- were copolymerized with VAc. In both cases, the successful RAFT/MADIX copolymerization could be reported, which further expands the range of monomers polymerizable through this RDRP technique. Libraries of copolymers with a constant molecular weight around 4000 g.mol^{-1} and various compositions in the fluorinated monomers could thus be synthesized.

The solubility of these copolymers was studied through cloud point measurements. As expected, the presence of trifluoromethyl groups in the pendent group strongly decreased the cloud point pressure. The depletion could even fall of approximately 100 bar for a P(VAc$_{50}$-*stat*-VTFAc$_{50}$) copolymer compared to a reference PVAc polymer. The whole solubility behaviour could be rationalized through DFT calculations and sessile drop measurements. While polymer-CO_2 interactions were lowered due to the presence of the fluorinated group, the parallel profiles of surface tension and solubility suggested the prominent role of polymer-polymer interactions over polymer-CO_2 ones. Even though this key role has earlier been hypothesized for CO_2-philic polymers, these results constitute the first experimental confirmations of such a role. The beneficial use of VTFAc to design amphiphilic block copolymers with enhanced solubilities could be also evidenced.

The set of P(VAc-*stat*-CF_3VAc) copolymers gave a different angle of perspective. Two regimes of solubility were observed in conjunction with an optimum of composition-solubility. The initial decrease in cloud point pressures could be explained by the lowering of polymer-polymer interactions until a plateau of surface tension was reached. Since the strength of polymer-CO_2 interactions were barely affected by the positioning of the trifluoromethyl moiety, entropy of mixing was then considered the driving force for the following increase of cloud point pressures.

Ultimately, the phase behaviors of both P(VAc-*stat*-CF_3VAc) and P(VAc-*stat*-VTFAc) could be compared to fluorine-free PVAc-based materials. These polymers were selected from previous works performed within S. Howdle's group.[3,4] Interestingly, the cloud point pressure of a vinyl pivalate-based copolymer (P(VAc_{10}-*stat*-$VPiv_{90}$)) was of the same order than the P(VAc_{67}-*stat*-CF_3VAc_{33}) copolymer. When placed in the pendent ester group such as in (P(VAc_{10}-*stat*-$VPiv_{90}$), the tert-butyl group consequently provided equivalent levels of CO_2-philicity to the polymeric materials. This is of interest in itself as the presence of fluorinated groups is usually thought to induce higher solubility than hydrocarbon functionalities. However, the solubility of the (P(VAc_{10}-*stat*-$VPiv_{90}$) copolymer was still significantly lower than that of P(VAc_{50}-*stat*-$VTFAc_{50}$) in contrast to higher values of surface tension and T_g for the P(VAc_{50}-*stat*-$VTFAc_{50}$) sample. This might be related to the enthalpic factors between VAc and the other comonomer which seem more unfavorable in the case of VTFAc and consequently enhances the solubility of P(VAc_{50}-*stat*-$VTFAc_{50}$).[30] The determination of the reduced Flory-Huggins interaction parameters between VAc and each one of the monomers (*i.e.* vinyl pivalate and VTFAc) could help bring further understanding to this pending question.

Another perspective for this work would be the synthesis and use of new fluorinated monomers that present higher resistance and concomitantly preserve low polymer-polymer interactions and high levels of polymer-CO_2 interactions. The replacement of VAc by another vinyl ester (*e.g.* vinyl pivalate) in the copolymerization systems should be also questioned to further pursue the lowering of CO_2 pressures necessary to dissolve such materials.

IV. References

(1) H. Lee, E. Terry, M. Zong, N. Arrowsmith, S. Perrier, K.J. Thurecht and S.M. Howdle, *J. Am. Chem. Soc.*, 2008, **130,** 12242.
(2) E.J. Park, A.P. Richez, N.A. Birkin, H. Lee, N. Arrowsmith, K.J. Thurecht and S.M. Howdle, *Polymer*, 2011, **52,** 5403.
(3) H. Lee, J.W. Pack, W. Wang, K.J. Thurecht and S.M. Howdle, *Macromolecules*, 2010, **43,** 2276.
(4) N.A. Birkin, N.J. Arrowsmith, E.J. Park, A.P. Richez and S.M. Howdle, *Polym. Chem.*, 2011, **2,** 1293.
(5) H.C. Haas, E.S. Emerson and N.W. Schuler, *J. Polym. Sci.*, 1956, **22,** 291.
(6) K. Yamada, T. Nakano and Y. Okamoto, *Polym. J.*, 1998, **30,** 641.
(7) M.H. Stenzel, L. Cummins, G.E. Roberts, T.P. Davis, P. Vana and C. Barner-Kowollik, *Macromol. Chem. Phys.*, 2003, **204,** 1160.
(8) Y. Kwak, A. Goto, T. Fukuda, Y. Kobayashi and S. Yamago, *Macromolecules*, 2006, **39,** 4671.
(9) D. Britton, F. Heatley and P.A. Lovell, *Macromolecules*, 1998, **31,** 2828.
(10) E. Girard, T. Tassaing, J.D. Marty and M. Destarac, *Polym. Chem.*, 2011, **2,** 2222.
(11) A.H.E. Muller, R.G. Zhuang, D.Y. Yan and G. Litvinenko, *Macromolecules*, 1995, **28,** 4326.
(12) M.H. Repollet-Pedrosa, R.L. Weber, A.L. Schmitt and M.K. Mahanthappa, *Macromolecules*, 2010, **43,** 7900.
(13) *The Chemistry of Free Radical Polymerization*, ed. G. Moad and D.H. Solomon, Pergamon Press, 1995**.**
(14) *Polymer Handbook*, ed. J. Bandrup, E.H. Immergut, and E.A. Grulke, Wiley-Intersciences, 1999**.**
(15) C.F. Kirby and M.A. McHugh, *Chem. Rev.*, 1999, **99,** 565.
(16) X. Wu, M.C. Vargas, S. Nayak, V. Lotrich and G. Scoles, *J. Chem. Phys.*, 2001, **115,** 8748.
(17) P. Raveendran and S.L. Wallen, *J. Phys. Chem. B*, 2003, **107,** 1473.
(18) P. Raveendran and S.L. Wallen, *J. Am. Chem. Soc.*, 2002, **124,** 12590.
(19) D. Li and A.W. Neumann, *J. Coll. Int. Sci.*, 1992, **148,** 190.
(20) M.L. O'Neill, Q. Cao, M. Fang, K.P. Johnston, S.P. Wilkinson, C.D. Smith, J.L. Kerschner and S.H. Jureller, *Ind. Eng. Chem. Res.*, 1998, **37,** 3067.
(21) M.E. Wright, K.M. Lott, M.A. McHugh and Z. Shen, *Macromolecules*, 2003, **36,** 2242.
(22) T. Sarbu, T.J. Styranec and E.J. Beckman, *Ind. Eng. Chem. Res.*, 2000, **39,** 4678.
(23) T. Narita, T. Hagiwara, H. Hamana, H. Ogawa and S. Endo, *Polym. J.*, 1990, **22,** 162.
(24) D. Schmaljohann and C.K. Ober, *PMSE Preprints*, 2000, **83,** 384.
(25) H.C. Haas, R.L. McDonald and C.K. Chiklis, *J. Polym. Sci. ; Part A*, 1969, **7,** 633.
(26) D. Batt-Coutrot, J.J. Robin, W. Bzducha and M. Destarac, *Macromol. Chem. Phys.*, 2005, **206,** 1709.
(27) D. Charmot, P. Corpart, H. Adam, S.Z. Zard, T. Biadatti and G. Bouhadir, *Macromol Symp.*, 2000, **150,** 23.
(28) G. Moad and C. Barner-Kowollik, in *Handbook of RAFT Polymerization*, ed. C. Barner-Kowollik, Wiley-VCH, 2008, Chap. 3.
(29) F. Rindfleisch, T.P. DiNoia and M.A. McHugh, *J. Phys. Chem.*, 1996, **100,** 15581.
(30) T. Sarbu, T. Styranec and E.J. Beckman, *Nature*, 2000, **405,** 165.

Chapter 4

- Macromolecular engineering of vinylidene fluoride
- Macromolecular engineering of vinylidene fluoride through RAFT/MADIX polymerization
- Poly(vinylidene fluoride)-based CO_2-philic macromolecular surfactants

Contents

Following the paradigm that fluorination of polymer constitutes throughout this thesis, the use of an original fluorinated monomer -vinylidene fluoride (VDF)- as the CO_2-philic building block for the design of sc-CO_2 macromolecular surfactants was eventually considered. Although the solubility of PVDF homopolymers and PVDF-based copolymers in sc-CO_2 has been widely studied (see Chapter 1), amphiphilic copolymers comprising a PVDF-based block are surprisingly absent from the CO_2 literature. Most solubility studies actually implied commercial samples of PVDF due to the obstacle that the synthesis of PVDF represents. This will be detailed in the initial sections of this chapter.

The experimental works presented herein will focus on the macromolecular engineering of VDF-based copolymers through RAFT/MADIX polymerization. The possibilities of mediating the radical polymerization of VDF through RAFT/MADIX polymerization will be first investigated. In a second part, the synthesis of amorphous PVDF-based copolymers will be described through the copolymerization with an innovative comonomer, perfluoromethyl vinyl ether (PMVE). The synthesis of amphiphilic block copolymers will subsequently be attempted in an effort of developing new sc-CO_2 macromolecular surfactants. Finally, the solubility of these copolymers will be presented.

I. Macromolecular engineering of poly(vinylidene fluoride)

A. Polymerization of VDF

1. Synthesis of PVDF

Vinylidene fluoride ($CH_2=CF_2$) is a flammable, non-explosive and gaseous monomer with a boiling point at -82 °C. Interestingly, it also exhibits a low toxicological profile in contrast to other fluoroalkenes such as tetrafluoroethylene.

Poly(vinylidene fluoride) is exclusively synthesized through the radical polymerization of VDF, similarly to poly(vinyl acetate). The VDF radicals are extremely instable leading to some distinctive features of PVDF:

- PVDF exhibits a high proportion of inverted adducts resulting from head-to-head additions during the course of polymerization. The molar percentages of defects usually range between 3 and 7 mol % depending on the reaction conditions.[1]
- PVDF may possess significant amounts of branches as a result of chain transfer to polymer. $C_{tr,pol}$ values have never been determined though.

It also exclusively terminates by recombination.[2]

A major limitation in the polymerization of VDF is the insolubility of PVDF in most common organic solvents. Dimethylsulfoxide (DMSO) and amide solvents including N,N-dimethylformamide (DMF), N,N-dimethylacetamide (DMAc) and N-methylpyrrolidone constitute the only examples of solvents in which high molecular weight PVDF are soluble. They are usual elution solvents for the SEC of PVDF. However, their use as synthesis solvents lead to the inhibition of the radical polymerization of VDF.[3]

As a consequence, the homogeneous polymerization is usually restricted to the synthesis of PVDF oligomers, especially through telomerization reactions. For this purpose, the range of solvents is much larger including acetone, butan-2-one, acetonitrile and 1,1,1,3,3-pentafluorobutane as usual synthesis solvents.

Though requiring extremely high pressures (P > 1500 bar), sc-CO_2 can advantageously combine the possibility of performing the polymerization in a homogenous process and obtaining PVDF of higher molecular weight as a result of its inertness towards radicals. Beuermann and coworkers thus recovered PVDF samples with molecular weights up to 9200 g.mol^{-1}.[4] However, a phase separation was observed for higher molecular weights, leading to a heterogeneous process.

The synthesis of high molecular weight PVDF is performed via heterogeneous processes such as emulsion, dispersion or precipitation polymerizations. A large range of properties can be reached through the variations in the polymerization procedures and parameters. On an industrial scale, water is the preferred continuous phase to produce latexes of PVDF. Recently, an increasing number of academic studies focused on the use of low pressure sc-CO_2 in dispersion[5] or precipitation[6,7] polymerizations of PVDF. The direct recovery of dry PVDF powders without additional purification or precipitation steps represents the main benefit of using CO_2.

2. Physical properties of PVDF

PVDF exhibits unique properties of resistance to thermal ageing or weather aggressions and excellent inertness to a wide range of chemical environments.[8] For these reasons, PVDF is a speciality fluoropolymer with one of the largest production tonnage. Interestingly, PVDF-based oligomers have been claimed to be biodegradable due their weaker -CH_2- linkage.[9]

Regarding its thermal properties, PVDF is a semi-crystalline polymer with different allotropic phases depending on macromolecular parameters and synthesis conditions. The melting temperatures of PVDF are usually in the range of 155-192 °C while its T_g lies between -40 and -30 °C.[1] The whole properties of PVDF and its applications have been covered in a review by Bruno Ameduri.[1]

B. Reversible activation deactivation (co)polymerization of VDF

Radicals generated by initiation of a VDF monomer are extremely unstable due to the presence of two strong electrowithdrawing fluorine atoms next to the radical center. Even though some basic knowledge on the kinetic parameters of the polymerization of VDF are missing in literature, the VDF monomer is presumably more reactive compared to other common monomers such as styrene and methyl methacrylate. As a matter of fact, VDF can be considered a less-activated monomer (LAM), along with vinyl esters. The successful polymerizations of VDF mediated by either ATRP complexes or stable nitroxides have never been reported so far, presumably due to the same factors encountered for the RDRP of VAc.

1. Reversible deactivation techniques by recombination

A peculiar example of a RDRP technique based on an oxygen-activated triethyl borane initiator was developed by Chung and coworkers.[10] This was applied to the terpolymerization of VDF, tetrafluoroethylene and chlorotrifluoroethylene. At room temperature, the triethyl borane was oxidized upon exposure to oxygen to form a peroxiborane. Following the hypothesized mechanism (see Scheme IV.1), this peroxy compounds underwent a homolytic cleavage to an alkoxy radical able to initiate fluorinated olefins and a borinate radical. This radical was then thought to exhibit enhanced stability due to a back-donation to the empty p orbitals. Similarly to stable nitroxide radicals, a weak and reversible bond was formed with the radical active center. This may explain the increase in molecular weights with higher conversion that were observed by SEC. Dispersities close to 2.5 were obtained in the meantime.

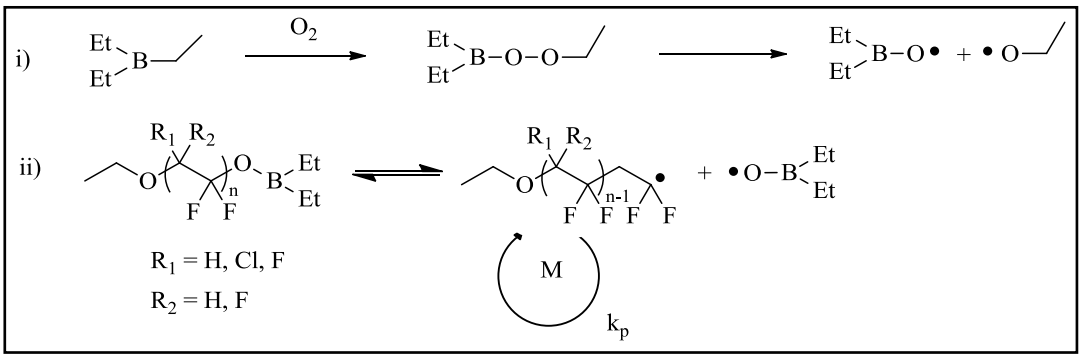

Scheme IV.1. Hypothesized mechanism for the triethylborane-mediated polymerization of fluorinated olefins in the presence of oxygen.

2. Degenerative transfer techniques

a) Iodine transfer polymerization of VDF

The first reports on the RDRP of VDF appeared in the patent literature in the late 1970s with ITP, some years before ATRP and RAFT were reported. A deeper understanding on the kinetics of the ITP of VDF in solution came with further reports published by Ameduri and coworkers. In a first study, the nature of the chain transfer agent was found to have an important effect on the ITP of VDF initiated by tert-butyl peroxypivalate (tBPPi) in 1,1,1,3,3-pentafluorobutane at 74 °C.[11] Using $C_6F_{13}I$ as CTA, the polymerization could be well controlled with experimental molecular weights in fair agreement with the targeted ones. The control was evidenced for molecular weights up to 25 repeating units (*i.e.* 1600 g.mol^{-1}). Similarly, an increase in molecular weights with conversion was demonstrated by SEC with a $C_6F_{13}CH_2CF_2I$ CTA mimicking the PVDF-I chain end.[12] However, the proportion of inverted chain ends (*i.e.* -CF_2-CH_2-I) was showed to increase for higher targeted molecular weights.[11] When $HCF_2CF_2CH_2I$ was used to mediate the polymerization of ITP, the poor control was evidenced with experimental M_n significantly higher than those predicted. These distinctive behaviours could be rationalized in terms of the underlying kinetic parameters.[12] Thus, the transfer constants to agent ($C_{tr,X}$) in the same experimental conditions were evaluated at 7.5, 7.4 and 0.3 for, respectively, $C_6F_{13}I$, $C_6F_{13}CH_2CF_2I$ and $HCF_2CF_2CH_2I$, which confirmed the previous observations. Additionally, the values of the interchain transfer constant ($C_{tr,PnX}$) for a PVDF-CH_2CF_2I and a PVDF-CF_2CH_2I were evaluated at 7.4 and 0.3. The CF_2CH_2-I bond is therefore much less reactive due to a stronger bond energy compared to the CF_2CH_2-I.

This problem inherent to ITP could be circumvented by Asandei and coworkers using $Mn(CO)_5$ in the ITP of VDF performed at mild temperatures under exposure to visible light.[13] In this work, radical initiators were generated through the abstraction of halides from fluorinated iodides with $Mn(CO)_5$. Even though irreversible $Mn(CO)_5I$ complexes were formed, the weak C-I bond energy in fluorinated halides allowed to use small amounts of Mn complexes. A strong advantage of this process over usual thermal ones was the quantitative activation of both CH_2CF_2-I and CF_2CH_2-I chain ends. Building on this enhanced control, PVDF

with molecular weights up to 23000 g.mol^{-1} and low dispersities could be produced through a heterogeneous process in dimethyl carbonate.

A large range of PVDF-based copolymers could be synthesized with the ITP process. A global overview on such copolymers and their applications can be found in a review written by Ameduri.[1]

b) RAFT/MADIX copolymerization of VDF

The RAFT/MADIX polymerization of VDF has never been reported so far. However, recent works have highlighted the relevance of RAFT/MADIX technology in the radical copolymerization of fluoroolefins. Kostov *et al.*[14] synthesized copolymers of VDF and 3,3,3-trifluoropropene in presence of a fluorinated xanthate (see Scheme IV.2.a)), whose livingness could be demonstrated via a chain extension with VAc. Inversely, the chain extension with a feed ratio of VDF and 3,3,3-trifluoropropene from a PVAc-Xa macromolecular RAFT/MADIX chain transfer agent did not result in a shift to higher molecular weights in SEC. This suggested that the VDF radicals were less stable than the VAc ones. This made up the only example so far of a successful RAFT/MADIX process applied to VDF.

It is also worth noting that Liu *et al.*[15] successfully demonstrated the living/controlled character of statistical copolymers of chlorotrifluoroethylene and butyl vinyl ether synthesized at room temperature under ^{60}Co γ-ray irradiation in the presence of *S*-benzyl *O*-ethyl dithiocarbonate (see Figure IV.2.b))

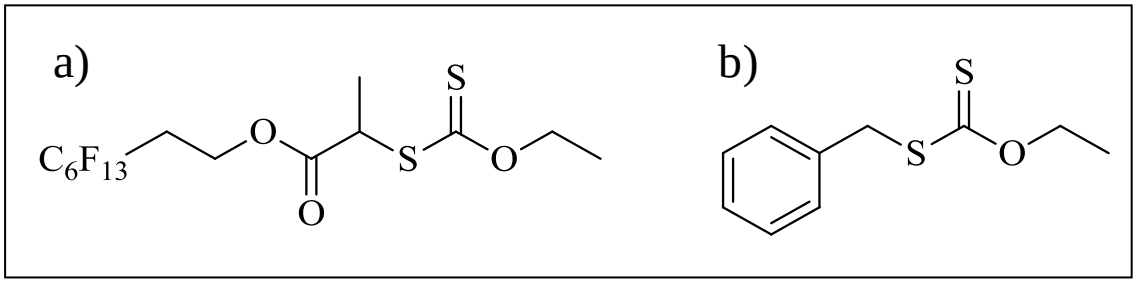

Scheme IV.2. Molecular structures of chain transfer agents used for the RAFT/MADIX copolymerization of fluorinated olefins.

3. Synthesis of PVDF-based amphiphilic block copolymers via RDRP techniques

a) Via ATRP

Examples of fluorinated amphiphilic copolymers that incorporate polyfluoroolefin blocks are scarce in literature. The first examples came from derivative strategies using VDF telomers synthesized with chloroform as the telogen agent.[16] PVDF-CCl_3 could then be used as a macromolecular halide initiator to polymerize styrene, methyl methacrylate, butyl acrylate and methyl acrylate. Recently, the same strategy was applied for the polymerization of sodium styrene sulfonate.[17] In all cases, the consumption of the PVDF macromolecular chain transfer agent was quantitative, thus leading to well-defined amphiphilic block copolymers.

The fluorine atoms of PVDF can also be potential ATRP initiators to synthesize graft copolymers.[18] Following this strategy, pH-sensitive PVDF-*graft*-poly(2-(N,N-dimethylamino)ethyl methacrylate) copolymers were synthesized using a Cu(I)/N,N,N′,N′,N′′-pentamethyl diethylenetriamine complex. The copolymerization of VDF with 8-bromo-1H,1H,2H-perfluorooct-1-ene is an alternative strategy to produce PVDF-*graft*-polystyrene copolymers with the bromine atoms as ATRP initiation sites.[19]

b) Via ITP

For its part, ITP allowed the direct synthesis of PVDF-*b*-polystyrene block copolymers from iodoperfluoralkane chain transfer agents.[20] However, the scope of ITP –and reverse ITP too– for the direct synthesis of amphiphilic block copolymers polymerization is rather limited. It has been successfully applied only to hydrophobic monomers including styrenics, (meth)acrylates, vinyl acetate (VAc) so far.[21] The use of protected hydrophilic monomers is required to obtain amphiphilic block copolymers. PVDF-*b*-poly(styrene sulfonate) block copolymers could be obtained starting from a protected styrenic monomer.[17] However, a major problem encountered with this approach is the presence of residual PVDF homopolymers resulting from the low reactive CH_2-I chain ends.

So far, two strategies were considered to overcome this drawback of ITP. The $Mn(CO)_5$-based ITP was demonstrated an efficient technique to do so.[13] Well-defined PVDF-based block copolymers comprising a block of either polystyrene, poly(methyl acrylate), polybutadiene, poly(vinyl chloride), poly(acrylonitrile) or poly(vinyl acetate) could be obtained. Conjugation strategies such as copper-catalyzed Huisgen cycloaddition are another solution to obtain pure diblock copolymers. The iodine chain end was transformed into an azide moiety to operate a click reaction with an alkyne-terminated polystyrene.[22]

c) Via RAFT/MADIX polymerization

Considering these limitations, the RAFT[23-25]/MADIX[26] process offers greater perspectives for the generation of fluorinated amphiphilic copolymers due to its well-established applicability to a broad range of hydrophilic monomers.[26,27] Yet, the only example of PVDF-based copolymers synthesized by RAFT/MADIX polymerization are poly(vinyl acetate)-*block*-(VDF-*co*-3,3,3-trifluorpropene) copolymers. This chapter thus aims at demonstrating the applicability of the RAFT process to the direct synthesis of PVDF-based amphiphilic block copolymers comprising a hydrophilic block.

II. Macromolecular engineering of vinylidene fluoride through RAFT/MADIX polymerization

A prerequisite to achieve such a challenge is to demonstrate the efficiency of the RAFT/MADIX process to control the polymerization of VDF. This will be the focus of the upcoming experimental paragraphs.

A. RAFT/MADIX polymerization of VDF with Rhodixan A1

1. Initiation conditions

In this work, only the RAFT/MADIX polymerization of VDF under thermal conditions was considered. In contrast to the RAFT/MADIX polymerization of usual monomers where AIBN is predominantly used, peroxides, peroxyesters and peroxydicarbonates constitute the most frequent initiators for the radical polymerization of VDF in solution.[1] Following some previous works on the ITP of VDF, tert-butyl peroxypivalate (tBPPi) was selected as the initiator for the RAFT/MADIX polymerization of VDF. Its decomposition mechanism at different temperatures has been investigated by Guiot *et al.* during the course of the free radical polymerization of VDF (see Scheme IV.3).[28] Tert-butyl and methyl radicals are the radical species resulting from the decomposition of TBPPi. These radicals were shown to give predominantly head additions on VDF.

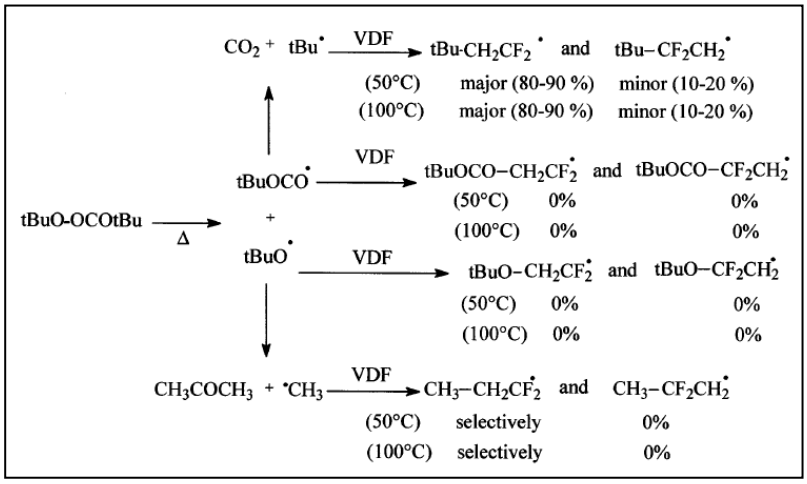

Scheme IV.3. Decomposition mechanism of tert-butyl peroxypivalate (tBPPi) under thermal conditions and initiation of the free radical polymerization of VDF. Reproduced from reference 28.

The frame of the ITP of VDF was a starting point for this work. The conditions set up by Boyer *et al.* were reproduced with Rhodixan A1 replacing the ITP chain transfer agent (see Scheme IV.4).[29] A first polymerization was performed at 74 °C in 1,1,1,3,3-pentafluorobutane with a targeted DP_n of 60 and tert-butyl peroxypivalate (tBPPi) as the initiator. This temperature of 74 °C corresponded to a half-life time of 1 hour for this initiator. Note also that this fluorinated solvent is particularly suitable for radical polymerization as it does induce no transfer to solvent. More importantly, the initial RAFT agent-to-initiator ratio was equal to 10, which should ensure a minimal amount of dead chains at the end of the RAFT/MADIX polymerization.

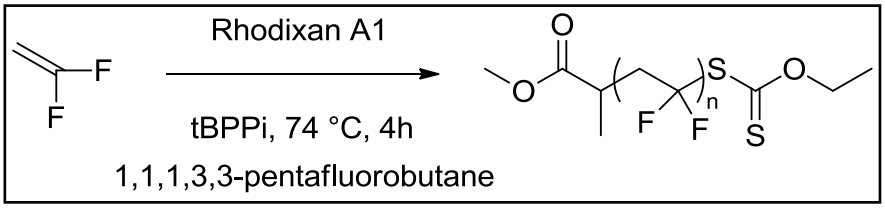

Scheme IV.4. Reaction scheme for the RAFT/MADIX polymerization of VDF.

Contrary to the results of Boyer *et al.,* the yield of the reaction was extremely low (see Table IV.1). Then, the molar ratio of chain transfer agent (CTA) to tBPPi was gradually decreased from 10 to 1 until high conversions of VDF were obtained (see runs 1 to 3 of Table IV.1). In contrast to the high [CTA]/[tBPPi] ratio experiments where PVDF was recovered as a precipitate (runs 1 and 2 of Table IV.1), a milky and stable dispersion of PVDF was observed with an equimolar ratio and a higher conversions in VDF (run 3 of Table IV.3).

The first results were promising with low dispersities that increased with higher conversions (see Table IV.1). Experimental M_n were higher than the theoretical ones. This may be attributed to a difference of hydrodynamic volumes between PVDF samples and poly(methyl methacrylate) standards in the SEC eluent. The use of viscosimetric detection should be useful to outweigh the limitations of conventional calibration. The Mark-Houwink-Sakurada parameters of, respectively, PVDF ($K = 31.8.10^{-4}$ mL.g^{-1} and $a = 0.603$)[30] and PMMA ($K = 10.0.10^{-4}$ mL.g^{-1} and $a = 0.6961$)[31]- in DMF + 10 mM LiBr at 40 °C could be also used

Run	$[CTA]_0$ / $[tBPPi]_0$	$M_{n,\ targeted}$ ($g.mol^{-1}$)	Yield (%) [a]	$M_{n,theo}$ ($g.mol^{-1}$)	$M_{n,SEC}$ [b] ($g.mol^{-1}$) (Đ)	Head-to-head adducts (%) [d]	T_g (°C)	T_m (°C)
1	10	4200	<5	-	3200 (1.15)	1.6 (0.1)[e]	n.o.[f]	83-132
2	2.5	4200	20	1000	5200 (1.15)	5.3 (7.5)[e]	n.o.	96-140
3	1	4200	82	3400	8700 (1.60)	8.3 (9.8)[e]	n.o.	144-171

[a] Measured by gravimetry. [b] Determined by SEC in DMF + 10 mM LiBr with PMMA standards. [c] n.d.: Not determined due to nearly isorefractive response. [d] Determined by ^{19}F NMR. [e] Tail-to-tail adducts determined by ^{1}H NMR. [f] Not observed.

Table IV.1. Experimental results for the RAFT/MADIX polymerization of VDF with increasing concentrations of tBPPi.

2. Synthesis of PVDF with variable chain lengths

A lower M_n of PVDF was then targeted to assess the mediation of the polymerization with Rhodixan A1 (see Table IV.2). Interestingly, a lower dispersity of 1.33 was determined by SEC with RI detection. Overall, the values of dispersity increased with higher M_n. This may be related to the formation of an increasing amount of head-to-head VDF adducts upon increasing chain length (see Table IV.2), This was also noticed during the ITP of VDF.[11,2] The results on both the head-to-head and tail-to-tail additions partially supported this hypothesis. A difference of only, respectively, 0.6 and 3.6 % was found in the two samples. As a matter of fact, chain transfer events and, particularly, to polymer cannot be ruled out to explain the increase in dispersity.

A shift to higher molecular weights with increasing times of reactions was evidenced through SEC-RI (see Figure IV.1.a)). SEC-UV analysis with a wavelength set at the maximum absorption of the dithiocarbonate group (290 nm) provided further convincing evidence that M_n increased with time due to a reversible transfer of the *O*-ethyl xanthate group between dormant and growing PVDF chains (see Figure IV.1.b)). However, the absence of data on conversion prevents from drawing a

definitive conclusion. To do so, the use of an internal standard with characteristic ^{19}F NMR signals should be helpful.

Run	$[CTA]_0$ / $[tBPPi]_0$	$M_{n,\ targeted}$ (g.mol^{-1})	Yield (%)[a]	$M_{n,theo}$ (g.mol^{-1})	$M_{n,SEC}$ [b] (g.mol^{-1}) (Đ)	Head-to-head adducts (%) [c]	T_g (°C)	T_m (°C)
4	1	2100	80	1750	6200 (1.33)	7.7 (6.2)[d]	n.o.[e]	127-172
5	1	4200	82	3400	8700 (1.60)	8.3 (9.8)[d]	n.o.[e]	144-171

[a] Measured by gravimetry. [b] Determined by SEC in DMF + 10 mM LiBr with PMMA standards [c] Determined by ^{19}F NMR. [d] Tail-to-tail adducts determined by ^{1}H NMR. [e] Not observed

Table IV.2. Experimental results for the RAFT/MADIX polymerization of VDF with increasing molecular weights.

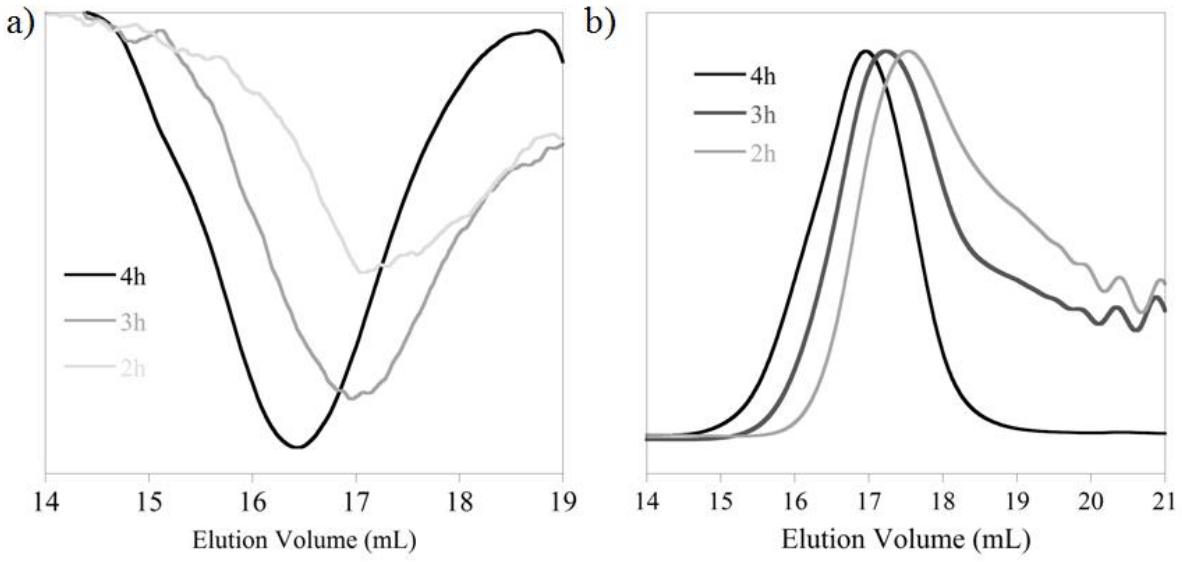

Figure IV.1. Overlays of a) SEC-RI and b) SEC-UV chromatograms at different sampling times for the RAFT/MADIX polymerization of VDF (run 4 of Table IV.2).

A specific feature that appears from these experiments is the modulation of thermal properties resulting from the control of chain length. The values of T_m were lower than those reported for commercial samples of PVDF. The melting temperatures of PVDF are usually in the range of 155-192 °C.[1] The T_m of the two

samples synthesized by RAFT/MADIX polymerization were in the range of, respectively, 127-172 and 144-171 °C (see runs 4 and 5 of Table IV.2). However, no glass transitions could be observed for the same samples. This may be related either to the high cristallinity of PVDF –typically reported between 50 and 70 %–[1] or the limitations of the DSC apparatus.

3. Kinetics of the RAFT/MADIX polymerization of VDF

The kinetics of the RAFT/MADIX polymerization of VDF was then investigated in Carius tubes. The experimental conditions –temperature, CTA-to-initiator ratios– were the same as the one described for the polymerizations performed in autoclaves. A blank experiment was first performed in the absence of CTA. The experiments proceeded up to high conversion (≈ 65 %) as determined by gravimetry (see Figure IV.2). Regardless of conversion, molecular weights decreased from 14000 to 12000 $g.mol^{-1}$ upon increasing conversions. The values of dispersity were comprised between 1.7 and 1.8.

Then, different DP_n were targeted using the fluorinated xanthate described in Chapter 1 at two different concentrations. This chain transfer agent was particularly interesting as its distinctive signals in ^{19}F NMR provided a practical way to determine the conversion of VDF. This is of special importance at low conversions where gravimetric methods lack precision. For the two experiments, the polymerization of VDF in the presence of F-Xa followed a first order kinetics (see Figure IV.2). However, conversions were systemically lower than 20 %. The differences in conversions observed with the experiments performed in autoclaves might be related to the difference of inside pressure in the vessels. Regardless of this, the presence of the xanthate induced a strong retardation. The higher the concentration of the xanthate, the stronger the retardation was. Even though the reasons for such retardation remain unclear, several hypotheses can be made by analogy with the RAFT/MADIX polymerization of VAc:

- A low addition rate coefficient (k_{add}) of the VDF radicals to the C=S bond. Such a physical reason was evidenced for the RAFT/MADIX polymerization of ethylene with fluorodithioformates through

computational methods.[32] In the case of VAc, the value of k_{add} is actually enhanced due to favorable H-bondings in the transition state, in contrast to the ethylene radicals.

- A low fragmentation rate coefficient (k_{β}) of the RAFT intermediate due to the low stability of VDF radicals.
- A slow reinitiation of VDF by methyl propionyl radicals resulting from the fragmentation of the RAFT intermediate.

When targeting a DP_n of 60 with F-Xa, the evolution of molecular weights was linear at low conversions even though the values of M_n were higher than the theoretical ones (see Figure IV.2.b). The reasons for such discrepancies have been discussed earlier. In spite of the restricted range of conversions, the values of dispersity quickly increased up to 1.4. However, the low initial values of Đ suggested a high interchain transfer constant ($C_{tr,PnX}$).

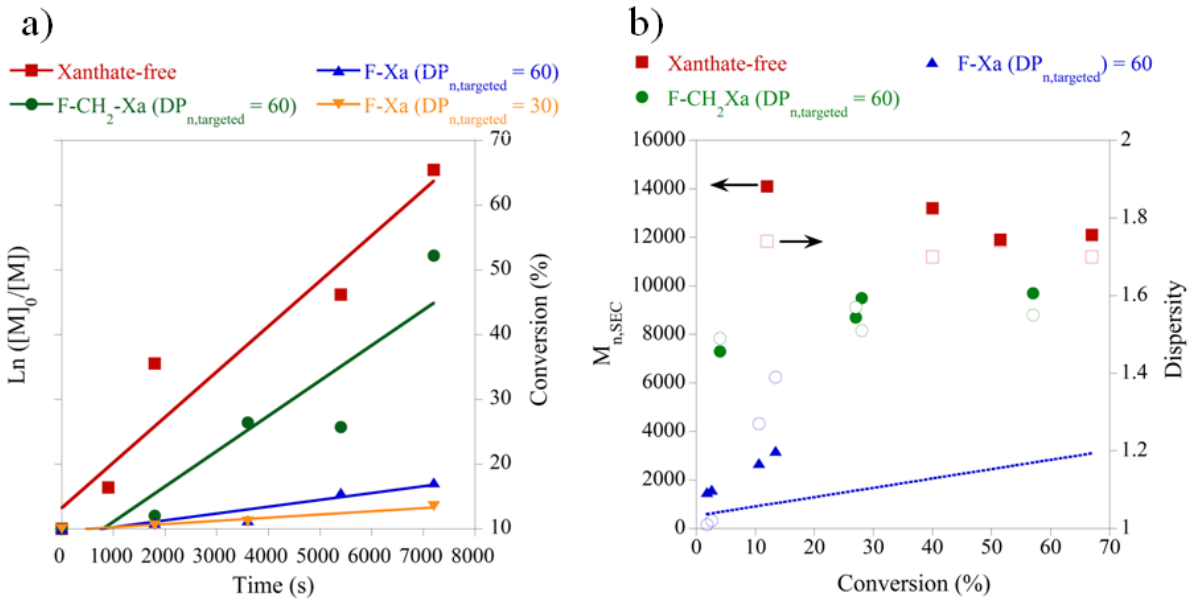

Figure IV.2. a) Kinetics plots and b) evolution of M_n and Dispersity versus Conversion for the RAFT/MADIX polymerization of VDF in Carius tubes.

Ultimately, the RAFT/MADIX polymerization of VDF was performed with a fluorinated primary xanthate mimicking an inverted VDF adduct, namely 1,1,2,2-tetrafluoro-3-(*O*-ethyl dithiocarbonate) propane (F-CH_2-Xa). To do so, the fluorinated xanthate had to be synthesized. The pathway to this compound

proceeded via a nucleophilic substitution of the commercially available 1,1,2,2-tetrafluoro-3-iodopropane using a xanthate salt (see Scheme IV.5). A yield of 73 % was obtained. This xanthate was then used for the polymerization experiments and a DP_n of 60 was targeted. The kinetics was also of first order but a moderate retardation was observed in contrast to F-Xa. The molecular weights determined by SEC were comprised between 7000 and 10000 $g.mol^{-1}$ even at low conversions, which indicated a slow consumption of the RAFT/MADIX agent (*i.e.* a low $C_{tr,X}$). Dispersities were intermediate between those of xanthate-free experiments and RAFT/MADIX polymerization with F-Xa ($1.4 < Đ < 1.6$).

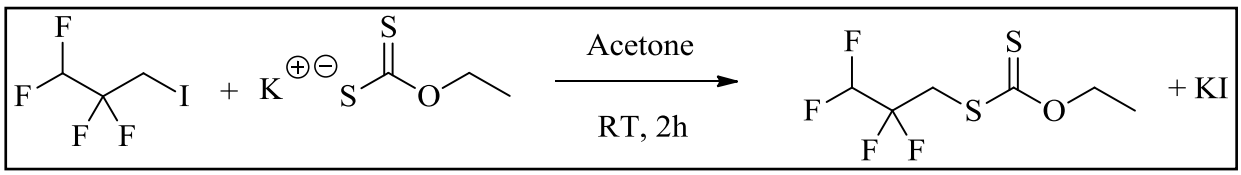

Scheme IV.5. Synthetic pathway to 1,1,2,2-tetrafluoro-3-(O-ethyl dithiocarbonate) propane.

As a conclusion, the design of the RAFT/MADIX agent was evidenced to be of particular importance for an efficient RAFT/MADIX polymerization of VDF. As result of the observed retardation and differences in control, a deeper insight into the role of both Z and R-group seems necessary to gain a better understanding of the reaction. These same experiments should also be repeated in autoclaves with an appropriate internal standard.

4. MALDI-TOF mass spectrometry

Other convincing experimental evidence of the controlled character of the RAFT/MADIX polymerization could be obtained through MALDI-TOF mass spectrometry measurements. Due to the difficulty to characterize fluorinated polymers in MALDI-TOF mass spectrometry, this technique was scarcely used for the characterization of PVDF.[11,33] Nevertheless, this could be achieved for a low molecular weight PDVF (run 1 of Table IV.1, see also Figure IV.3). The results confirmed the formation of xanthate-capped PVDF as the main population of polymer chains (▽). The main population was centered at m/z = 1063.4,

corresponding to a PVDF chain of 13 monomer units bearing the two xanthate fragments at both ends. It also revealed another population corresponding to PVDF chains terminated by a $-CH=CF_2$ group (○). This could not result from termination by disproportionation as PVDF only terminates by combination. As a result, this population was attributed to the degradation products possibly arising from the laser beam.[34]

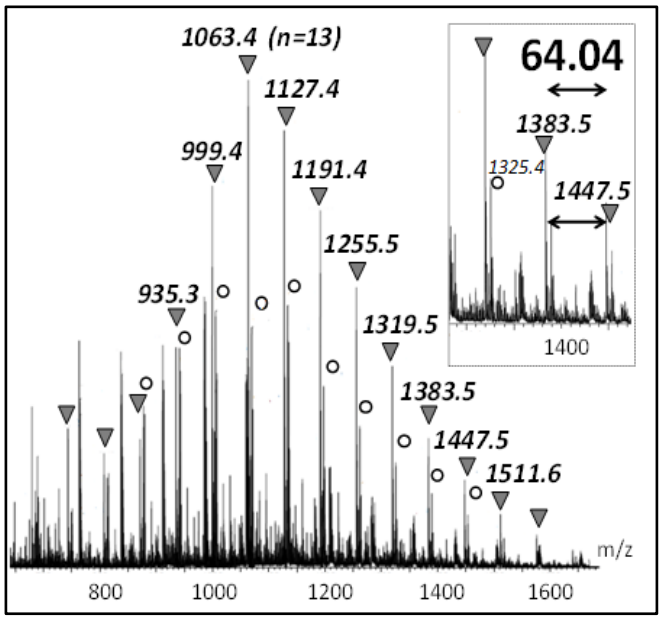

Figure IV.3. MALDI-TOF mass spectrum of a PVDF polymer synthesized in the presence of the Rhodixan A1 RAFT/MADIX agent (NaI cationization, Run 1 of Table IV.1).

Experimental m/z	Theoretical m/z	Assignment	Δ (%)
935.3	935.12	DP_n = 11	0.019
999.4	999.13	12	0.027
1063.4	1063.14	13	0.024
1127.4	1127.15	14	0.022
1191.4	1191.16	15	0.020
1255.5	1255.17	16	0.026
1319.5	1319.18	17	0.024
1383.5	1383.19	18	0.022
1447.5	1447.20	19	0.021
1511.6	1511.21	20	0.026

Table IV.3. Assignments of the peaks of the population noted (▽in Figure IV.3.

5. NMR analysis

a) Normal VDF-xanthate adducts

An additional evidence of the efficiency of the RAFT/MADIX process came with ^{19}F NMR analysis. All ^{19}F NMR spectra of low conversion samples exhibited two complex signals around -72 ppm (see Figure IV.4).

A doublet of doublet of doublets (ddd) centered at -72.5 ppm was first observed (see Figure IV.4). The roof effect was characteristic of an AB system. A proton-decoupled ^{19}F NMR experiment performed on this same sample showed the existence of a doublet of doublet with a scalar coupling constant J_{AB} of 240 Hz (see Figure IV.5). This value is in agreement with the usual coupling constants reported for fluorine atoms in a geminal position which range between 150 and 300 Hz.[35] This evidences the non-equivalency of two fluorine atoms. The ddd signal was related to the dissimilarity of hydrogen atoms located at the alpha position of a stereogenic center and the two fluorine atoms. The coupling constant for this system

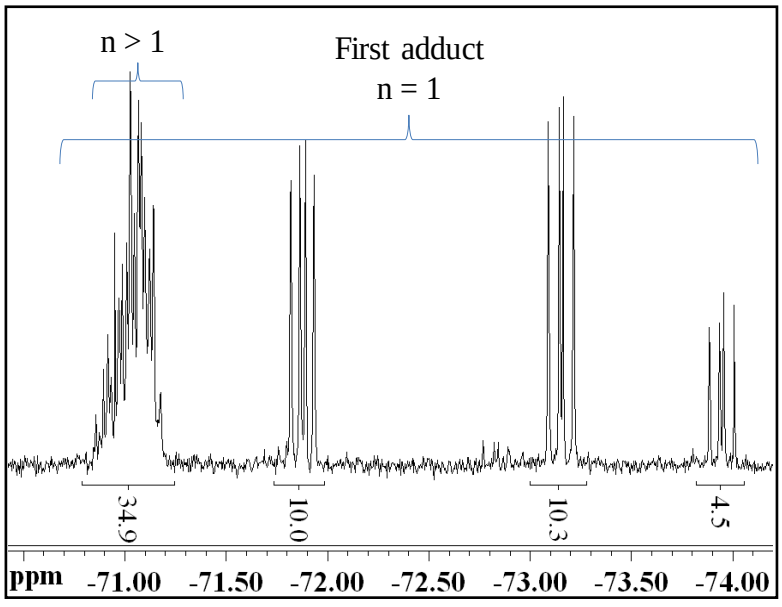

Figure IV.4. Expansion of the -70 to -74 ppm region in the ^{19}F NMR spectrum of a PVDF obtained during the course of a RAFT/MADIX polymerization (1 h, run 2 of Table IV.1).

was calculated at 12.9 Hz. Again, this agreed with usual coupling constants reported for a hydrogen atom and a fluorine one placed in a vicinal position.[35] The usual values for this coupling lie between 9 and 13 Hz. As a consequence, the molecular structure was postulated, which corresponded to a single insertion of a VDF monomer between the two fragments of the xanthate (see Scheme IV.6).

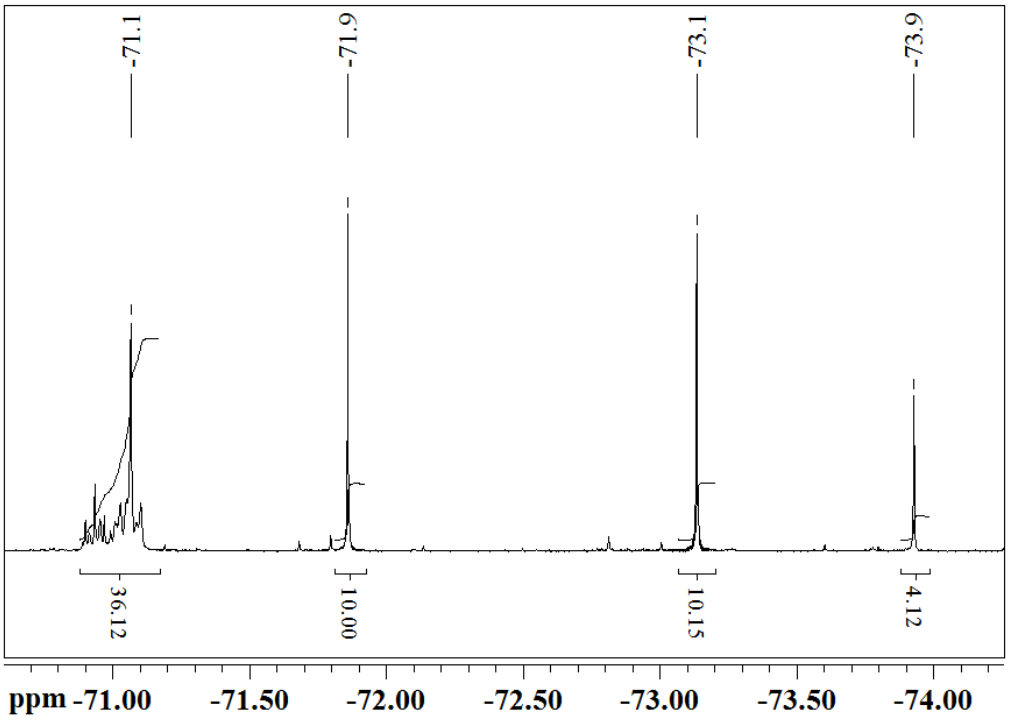

Figure IV.5. Expansion of the -70 to -74 ppm region in the ^{19}F NMR spectrum of a PVDF obtained during the course of a RAFT/MADIX polymerization (run 2 of Table IV.1).

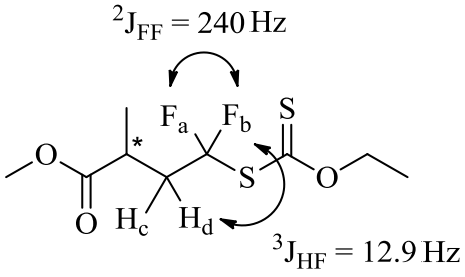

Scheme IV.6. Representation of the single VDF-xanthate adduct deduced from the ^{19}F and $^{19}F\{^{1}H\}$ NMR signals.

A second signal slightly upshielded at -71 ppm was observed. $^{19}F\{^{1}H\}$ NMR experiments revealed that this signal was actually an overlay of triplets (see Figure IV.6). The scalar F-F coupling constants were calculated at 10.5 Hz. This corresponded to the coupling constant of two fluorine atoms in a gamma position reported in literature ($^{4}J_{FF} \approx$ 7-10 Hz).[35] As a consequence, this signal was attributed to VDF oligomers end-capped with a xanthate group. Note that Boyer *et al.* reported a $^{4}J_{FF}$ coupling constant of 9.8 Hz for a $-CF_2-CH_2-CF_2-I$ chain end.[11] In contrast to the $-CH_2-CF_2-I$ chain end, the xanthate-PVDF chain ends appeared to be more upshielded (-38 ppm versus -71 ppm). The presence of the xanthate group also specifically induced the non-equivalency of the two fluorine atoms. However, the corresponding signal could not be isolated in ^{1}H NMR.

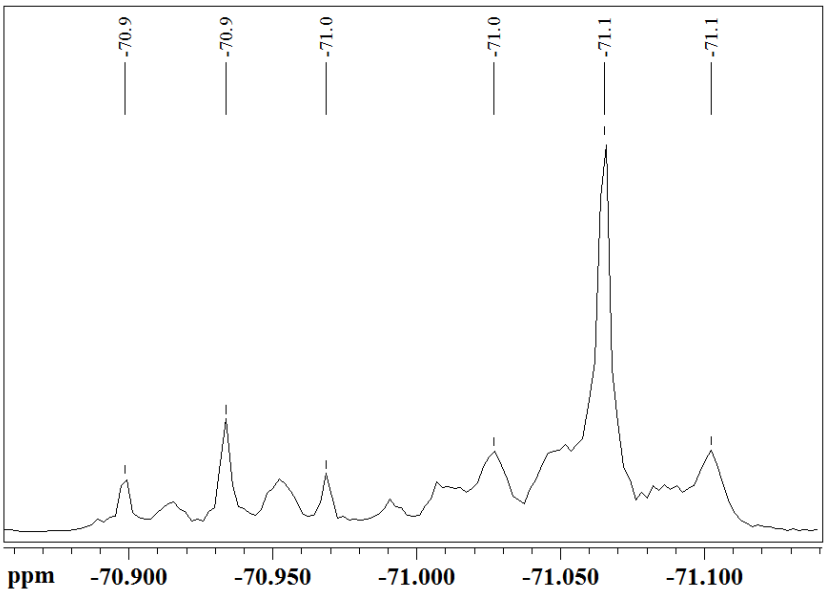

Figure IV.6. Expansion of the -70 to -71 ppm zone in the ^{19}F NMR spectrum of a PVDF obtained during the course of a RAFT/MADIX polymerization (run 2 of Table IV.1).

b) Inverted PVDF-xanthate adducts

The inverse addition of VDF monomers during the course of the polymerization of VDF is a well-established fact. As a consequence, the formation of inverted CF_2-CH_2-I chain ends was reported during the course of the ITP of VDF.[29] As evidenced during the kinetic experiments, the difference in $C_{tr,X}$ for normal and

inverted chain ends have a great impact on the evolution of molecular weights with conversion.

The identification of CF_2-CH_2-Xa inverted chain ends in ^{19}F NMR spectra was made possible with the help of the F-CH_2-Xa fluorinated primary xanthate**.** In ^{19}F NMR, the signal corresponding to the fluorine atoms in the beta position relatively to the xanthate group was a triplet of quadruplets located at -116.7 ppm. The ^{1}H NMR signal of protons located in the alpha position of both the xanthate group and -CF_2- was a triplet at 4.03 ppm ($^{3}J_{HF}$ = 17.4 Hz). From this, the transposition of this signal to the polymer counterpart could be identified in the ^{19}F NMR of PVDF synthesized by RAFT/MADIX polymerization (*vide infra*).

c) ^{19}F NMR analysis of PVDF synthesized by RAFT/MADIX polymerization

An important part of work was devoted to the identification of ^{19}NMR signals of PVDF. A characteristic ^{19}F NMR spectrum for low molecular weight samples is presented below (see Figure IV.7 and Table IV.4). The peaks could be attributed through previous works performed by Ameduri and coworkers.[28,29] Interestingly, the peaks corresponding to the initiation by tert-butyl and methyl propionyl radicals could be identified at -91.9 and -93.5 ppm (see Table IV.4). The absence of a signal corresponding to a initiation by methyl radicals at -95.7 ppm was also noted.[28] A tiny triplet located at -115.4 ppm was attributed to a CF_2-CH_2-Xa chain end on the basis of the model compound presented above.

Building on the existence of the specific chain end signals, the molecular weights of the oligomers could be determined by ^{19}F NMR. The following formula was used:

$$\mathrm{DPn\ (19F\ NMR)} = \frac{\int_{-74}^{-71} \mathrm{CF2} + \int_{-96}^{-90} \mathrm{CF2} + \int_{-116}^{-112} \mathrm{CF2}}{\int_{-74}^{-71} \mathrm{CF2} + \int_{-115.4} \mathrm{CF2}}$$

The DP_n calculated by ^{19}F NMR was equal to 12.3 (run 1 of Table IV.1). This was in agreement with the corresponding MALDI-TOF spectrum, the highest peak of which corresponded to a DP_n of 13 (see Figure IV.3).

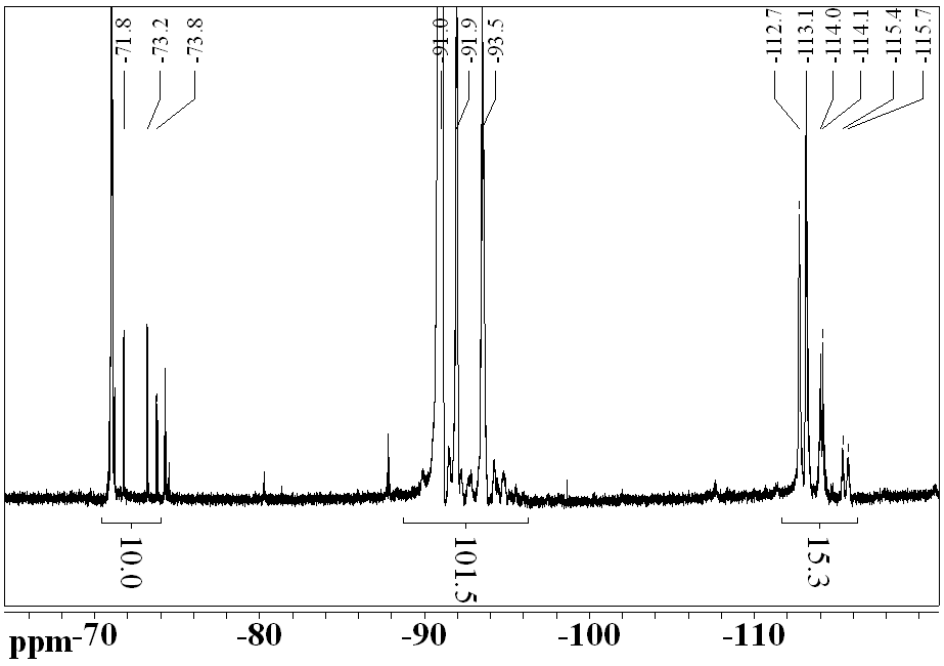

Figure IV.7. ^{19}F NMR of PVDF synthesized by RAFT/MADIX polymerization (run 1 of Table IV.1).

Chemical shift (ppm)	Signal	Assignments
-71.0	multiplet	$-CH_2-CF_2-S-C(=S)-OEt$
-73.0	dd	$CH_3-O-C(=O)-C(-CH_3)-CH_2CF_2-S-C(=S)-OEt$
-91.0	multiplet	$-CH_2CF_2-CH_2CF_2-CH_2CF_2-$
-91.9	multiplet	$(CH_3)_3-CH_2CF_2-$
-93.5	multiplet	$CH_3-O-C(=O)-C(-CH_3)-CH_2CF_2-$
-107.6	multiplet	$CH_3CF_2-CF_2CH_2-CF_2$
-112.7	multiplet	$(CH_3)_3-CF_2CH_2-$
-113.1	multiplet	$CH_3-O-C(=O)-C(-CH_3)-CF_2CH_2-$
-114.1	d ($^2J_{FH}$= 43.8 Hz)	$HCF_2-CH_2-CH_2-CF_2-$
-115.4	t ($^3J_{FH}$= 14.4 Hz)	$-CH_2-CF_2-CF_2-CH_2-S-C(=S)-OEt$
-115.7	multiplet	$-CH_2-CF_2-CF_2-CH_2-CH_2-$

Table IV.4. Assignments of the ^{19}F NMR peaks in Figure IV.7.

B. RAFT/MADIX polymerization of VDF using a hydrophilic macromolecular chain transfer agent

1. Direct synthesis of amphiphilic diblock copolymers

Once the RAFT/MADIX polymerization of VDF with Rhodixan A1 was successfully evidenced, the direct synthesis of amphiphilic block copolymers with a PVDF block was investigated. For this purpose, two poly(N,N-dimethylacrylamide) macromolecular chain transfer agents (M_n = 600 and 1000 g.mol^{-1}) were synthesized following the procedure described in Chapter 1. They were subsequently used for chain extension experiments with the RAFT/MADIX polymerization of VDF.

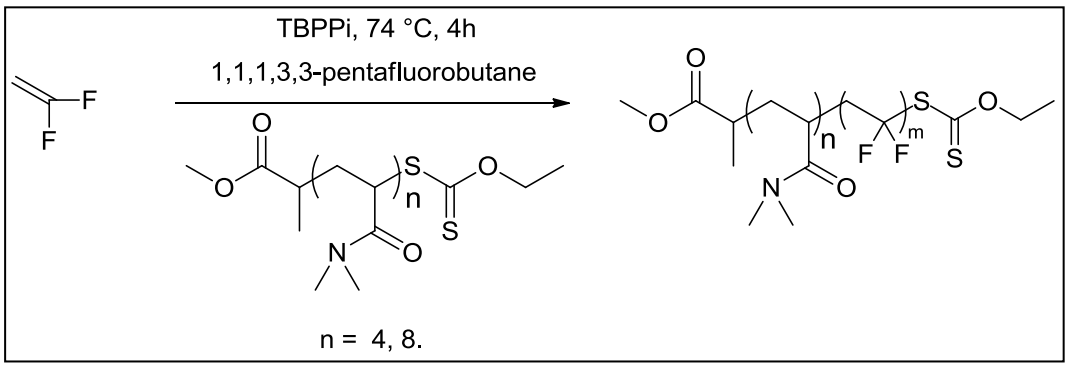

Scheme IV.7. RAFT/MADIX polymerization of VDF using PDMA macromolecular chain transfer agents.

The application of the same initiation conditions only resulted in a low yield of VDF when a PDMA macromolecular CTA (M_n = 600 g.mol-1) was used (see run 6 of Table IV.4). In spite of this, the full consumption of this agent could be observed by SEC through UV detection (see Figure IV.8.a)). A decrease in the $[CTA]_0/[tBPPi]_0$ ratio from 1 to 0.5 resulted in an increase in conversion to 80 % (see run 7 of Table IV.4). The experimental M_n were close to the theoretical ones while a low dispersity of 1.40 was determined. However, the UV detection revealed that the distribution was multimodal, which might be related to a heterogeneous process. A PDMA macromolecular CTA with a higher molecular weight of 1000 g.mol^{-1} was then used for the polymerization of VDF with a $[CTA]_0/[tBPPi]_0$ ratio of 0.5 (see run 8 of Table IV.4). The final conversion was even lower -30 %- but a well-defined diblock copolymer could be obtained (see Figure IV.8.b)).

Run	CTA	$[CTA]_0$ / $[TBPPi]_0$	$M_{n,\ targeted}$ (g.mol^{-1})	Yield [a] (%)	$M_{n,theo}$ (g.mol^{-1})	$M_{n,SEC}$ [b] (g.mol^{-1}) (Đ)	T_g (°C)	T_m (°C)
6	$PDMA_{0.4k}$-Xa	1	3800	45	1650	n.d.[c]	6.8	106-162
7	$PDMA_{0.4k}$-Xa	0.5	3800	80	2750	3500 (1.40)	12.0	77-135
8	$PDMA_{0.8k}$-Xa	0.5	3700	30	1800	n.d.[c]	13.5	114-161

[a] Measured by gravimetry. [b] Determined by SEC in DMF + 10 mM LiBr with PMMA standards. [c] n.d: Not determined due to nearly isorefractive response.

Table IV.5. Experimental results for the synthesis of PDMA-*b*-PVDF copolymers.

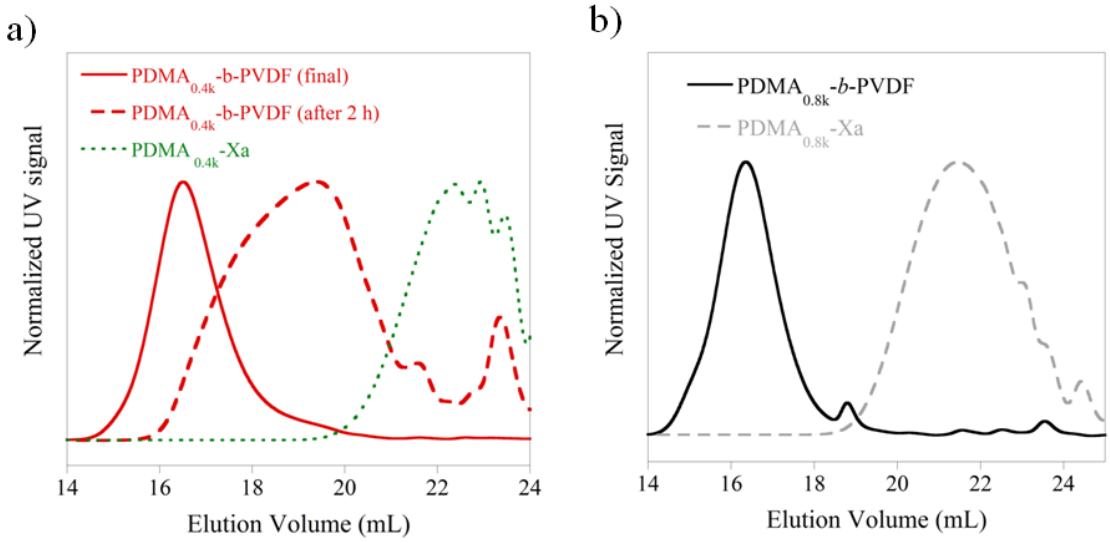

Figure IV.8. Overlays of SEC-UV chromatograms for the RAFT/MADIX polymerization of VDF from a) a $PDMA_{0.4k}$ macromolecular agent (run 6 of Table IV.4) and b) a $PDMA_{0.8k}$ macromolecular agent (run 8 of Table IV.4).

2. Thermal properties

The thermal properties were in fair agreement with the predicted PVDF chain lengths (see runs 6 and 8 of Table IV.5). The observed T_m was slightly higher for run 6 where the theoretical PVDF molecular weight should be higher of 200 g.mol^{-1} compared to run 8. In all cases, a single T_g which was close to those of the starting PDMA macromolecular CTA was observed.

III. PVDF-based CO_2-philic macromolecular surfactants

As specified in Chapter 1, only PVDF oligomers exhibit significant solubilities in sc-CO_2 under mild conditions due to the high melting temperature of PVDF. To overcome this, VDF can be copolymerized with appropriate comonomers to yield amorphous copolymers. The comonomers that were studied so far include hexafluoropropylene and vinyl acetate.[36,37] Thereafter, the use of a new comonomer –perfluoromethyl vinyl ether (PMVE)– will be presented (see Scheme IV.8).

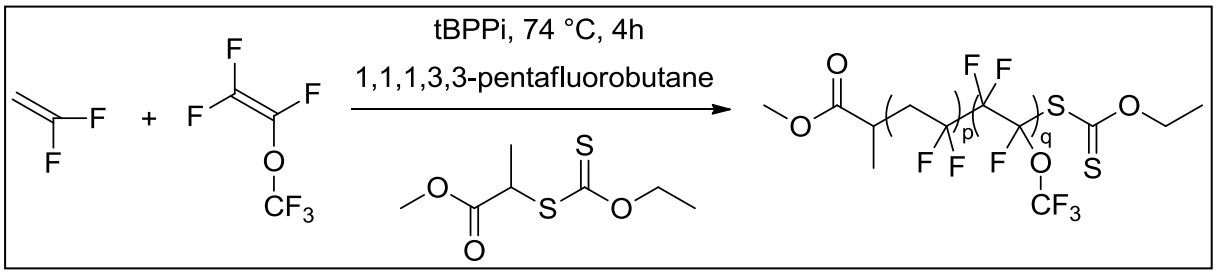

Scheme IV.8. RAFT/MADIX copolymerization of VDF and PMVE.

A. Synthesis of PVDF-based amorphous copolymers

The free radical copolymerization of VDF and PMVE was first investigated by Otaghazine *et al.*[38] Using 1 % mol of tBBPi as the initiator, the reactivity ratios of VDF and PMVE at 74 °C were evaluated at r_{VDF} = 3.40 and r_{PMVE} = 0. The iodine-transfer copolymerization of VDF and PMVE could successfully be implemented in an emulsion process.[39] The CTA used in this study were mono- and difunctional fluorinated alkyl iodides. Well-defined copolymers exhibiting molecular weights up to 21000 g.mol^{-1} and low dispersities (1.3 < Đ < 1.8) through this process were obtained. The iodide chain ends of these telechelic copolymers could then be transformed into various terminal groups to produce photochemically cross-linked films.[40]

B. RAFT/MADIX copolymerization of VDF with PMVE

1. Synthesis of P(VDF-*co*-PMVE) of variable chain lengths

The experimental conditions set up for the RAFT/MADIX polymerization of VDF were applied for its copolymerization with PMVE (see Scheme IV.8). Three different molecular weights of 2400, 4200 and 6000 g.mol^{-1} were targeted introducing 5.5, 2.6 and 1.8 moles of Rhodixan A1, respectively (see Table IV.6). A VDF:PMVE feed ratio around 70:30 was targeted to ensure the total disappearance of crystalline zones in the final samples. The yields were comprised between 71 and 85 %, as observed during the RAFT/MADIX polymerization of VDF. The values of molecular weights determined by SEC in DMF were higher than the theoretical ones, likely due to the differences of hydrodynamic volumes between polymer samples and PMMA standards. However, the efficiency of the RAFT/MADIX polymerization could be demonstrated by the displacement of polymer peaks towards higher molecular weights in SEC upon decreasing the initial concentration of CTA (see Figure IV.9).

			Feed ratio (mol %)		Copolymer Composition (mol %) [b]					
Run	CTA	$M_{n,\ targeted}$ (g.mol^{-1})	VDF	PMVE	VDF	PMVE	Yield [c] (%)	$M_{n,theo}$ (g.mol^{-1})	$M_{n,SEC}$[d] (g.mol^{-1}) (Đ)	T_g (°C)
9	Rhodixan A1	2400	65	35	63	37	85	1850	3700 (1.26)[g]	-36.6
10	Rhodixan A1	4200	70	30	74	26	71	3000	6000 (1.58)[g]	-41.4
11	Rhodixan A1	6000	70	30	71	29	81	4850	8900 (1.63)[g]	-39.5

[a] See Table S1 in Supporting Information for values of concentration. [b] Determined by ^{19}F NMR. [c] Measured by gravimetry. [d] Determined by SEC in DMF + 10 mM LiBr with PMMA standards. [e] n.d: Not determined due to nearly isorefractive response. [f] Not observed [g] Determined by SEC in THF with PS standards.

Table IV.6. Experimental results for the synthesis of P(VDF-*co*-PMVE) statistical copolymers by RAFT/MADIX polymerization.

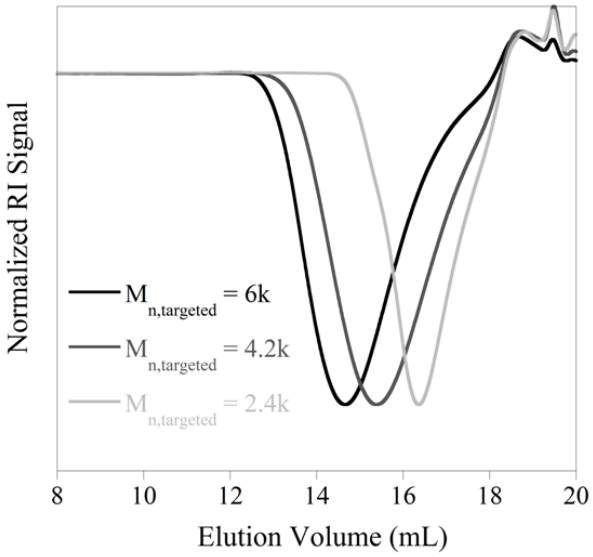

Figure IV.9. Overlays of SEC-RI chromatograms for the RAFT/MADIX polymerization of VDF and PMVE (runs 9-11 of Table IV.6, with 5.5, 2.6, and 1.8 mmol of CTA, respectively).

2. NMR analysis of P(VDF-*co*-PMVE) copolymers

The microstructure of the copolymers was then studied through NMR. ^{19}F NMR and ^{1}H NMR spectra of run 9 are given in Appendix. In contrast to the RAFT/MADIX polymerization of VDF, the lowering of triplet signals at 2.5 ppm corresponding to tail-to-tail VDF additions was noted, which was also previously reported by Boyer *et al.*[39] This was confirmed by weak signals corresponding of head-to-head additions in ^{19}F NMR (see Appendix). Furthermore, a ^{19}F NMR signal observed at 144 ppm (see Appendix) corresponding to the addition of an inverted VDF adduct to PMVE may indicate the existence of a competition between this addition and inverted VDF-VDF ones.

The copolymer compositions were calculated following the NMR peak assignments and the methodology of Otaghazine *et al.*[38] In the case of runs 10 and 11, the copolymer compositions were in agreement with the reactivity ratios and some previous results. Concerning run 9, the discrepancy might be due to some errors in the feed ratio due to inaccurate weighting.

3. MALDI-TOF mass spectrometry

A MALDI-TOF mass spectrometry analysis was then performed on the shortest P(VDF-*co*-PMVE) copolymer (run 9 of Table IV.6, see Figure IV.10). The peak assignments confirmed the successful mediation of the copolymerization of VDF and PMVE by the xanthate chain transfer agent (see Table IV.7). The different peak populations were separated by either 64.0 m/z or 166.0 m/z, *i.e.* a VDF repeating unit or a PMVE one. All populations included both fragments of the xanthate while no secondary initiation was revealed. The absence of chains comprising a majority of PMVE repeating units was also noted as expected from the inability of the PMVE radicals to homopolymerize. Interestingly, a minor population corresponding to a loss of 20 m/z was revealed. This was attributed to a loss of fluoride hydrogen (HF), presumably during the course of the MALDI-TOF analysis. This observation is supported by similar findings in the MALDI-TOF mass spectrometry analysis of PVDF and a perfluoropolyether.[33,41]

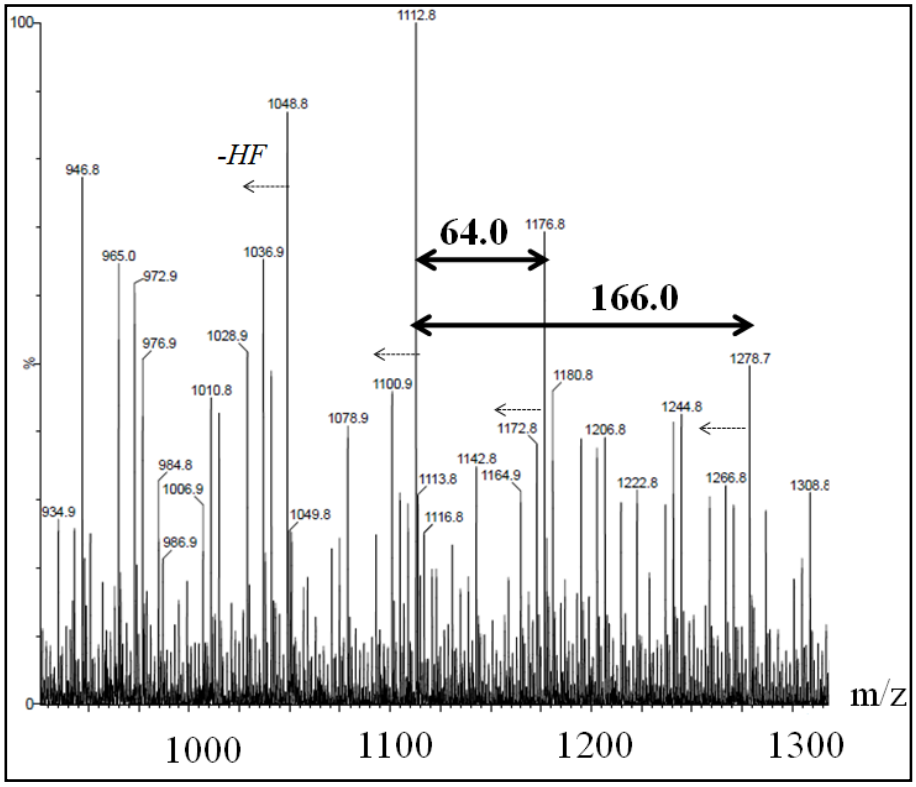

Figure IV.10. MALDI-TOF mass spectrum of a P(VDF-*co*-PMVE) copolymer synthesized in the presence of the RAFT/MADIX agent (NaI cationization, linear mode, run 6 of Table IV.1).

Experimental m/z	Theoretical m/z	Assignment ($DP_{n,VDF}$, $DP_{n,PMVE}$)	Δ (%)
1036.9	1037.10	(10,1)	0.019
1100.9	1101.11	(11,1)	0.019
1164.9	1165.12	(12,1)	0.019
1228.9	1229.13	(13,1)	0.019
1010.8	1011.06	(7,2)	0.026
1074.8	1075.07	(8,2)	0.025
1048.8	1049.03	(5,3)	0.022
1112.8	1113.04	(6,3)	0.022
1176.8	1177.05	(7,3)	0.021
1240.8	1241.06	(8,3)	0.021
1304.8	1305.07	(9,3)	0.021
1278.7	1279.03	(6,4)	0.026

Table IV.7. Peak assignments for the MALDI-TOF spectrum of a P(VDF-*co*-PMVE) copolymer (run 9 of Table 10 and Figure IV.10).

4. Thermal properties

The thermal properties of the resulting copolymers were also studied (see Table IV.6). For all samples, no melting temperatures could be observed. Regardless of chain length and composition, the values of T_g were all comprised between -41 and -36 °C. These values are slightly higher than those reported of Boyer *et al.* which were comprised between -50 and -43 °C.[39] The differences may originate from the nature of the chain end group which was a C_6F_{13} perfluorinated chain in their study.

In spite of its lower molecular weight, the P(VDF-*co*-PMVE) copolymer (run 9 of Table IV.6) exhibited the highest value of T_g. This may be explained by its composition richer in PMVE repeating units.[39]

5. Synthesis of amphiphilic block copolymers

a) RAFT/MADIX polymerization of VDF and PMVE from PDMA macromolecular chain transfer agents

The copolymerization of VDF and PVME was then mediated with PDMA macromolecular RAFT/MADIX agents having different chain lengths (see Scheme IV.9). A $[CTA]_0/[tBBPi]_0$ molar ratio of 1 and a VDF:PMVE feed ratio of 70:30 were selected for all polymerizations (see Table IV.8).

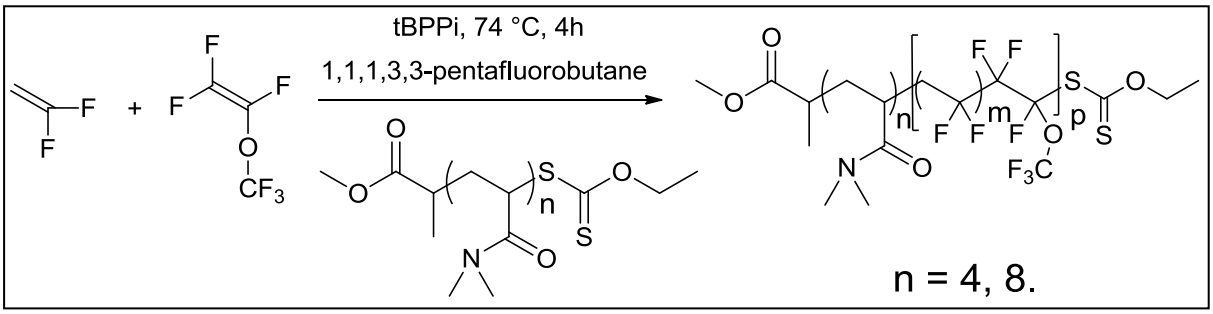

Scheme IV.9. RAFT/MADIX copolymerization of VDF and PMVE using PDMA macromolecular chain transfer agents.

In contrast to the synthesis of PDMA-*b*-PVDF copolymers, the polymerizations homogenously proceeded due to the enhanced solubility of the copolymers in 1,1,1,3,3-pentafluorobutane. High yields comprised between 75 and 90 % were obtained (see runs 12 to 15 of Table IV.8). The copolymer compositions were close to the feed ratios. The formation of block copolymers could be confirmed by the complete consumption of the PDMA RAFT/MADIX agent and a shift to higher molecular weights in SEC (see Figure IV.11). However, the experimental M_n were systemically higher than the predicted ones whether they were determined through SEC either in DMF or in THF. The help of a multiple detection SEC equipped with a light-scattering detector seems necessary to provide a deeper understanding of this discrepancy between theoretical and experimental ones. Concerning the values of dispersities, these determined in THF were comprised between 1.38 and 1.55. Their values were higher compared to PMMA standards in DMF ($1.53 < Đ < 1.75$). In both cases, the longer the chain length, the lower the dispersities.

			Feed ratio (mol %)		Copolymer Composition (mol %) [b]						
Run	CTA	$M_{n,\ targeted}$ ($g.mol^{-1}$)	VDF	PMVE	VDF	PMVE	Yield [c] (%)	$M_{n,theo}$ ($g.mol^{-1}$)	$M_{n,SEC}$[d] ($g.mol^{-1}$) (Đ)	$M_{n,SEC}$[f] ($g.mol^{-1}$) (Đ)	T_g (°C)
12	$PDMA_{0.4k}$-Xa	3000	70	30	69	31	85	2600	4800 (1.75)	4800 (1.55)	-13.6
13	$PDMA_{0.4k}$-Xa	4600	70	30	69	31	75	3500	5900 (1.74)	6200 (1.54)	-21.6
14	$PDMA_{0.8k}$-Xa	2600	70	30	73	27	90	2400	n.o.[e]	3200 (1.62)	13.7
15	$PDMA_{0.8k}$-Xa	5500	70	30	68	32	75	4200	7400 (1.53)	7500 (1.38)	-4.1

[a] See Table S1 in Supporting Information for values of concentration. [b] Determined by ^{19}F NMR. [c] Measured by gravimetry. [d] Determined by SEC in DMF + 10 mM LiBr with PMMA standards. [e] n.d: Not determined due to nearly isorefractive response. [f] Determined by SEC in THF with PS standards.

Table IV.8. Experimental results for the synthesis of P(VDF-*co*-PMVE)-based amphiphilic copolymers by RAFT/MADIX polymerization.

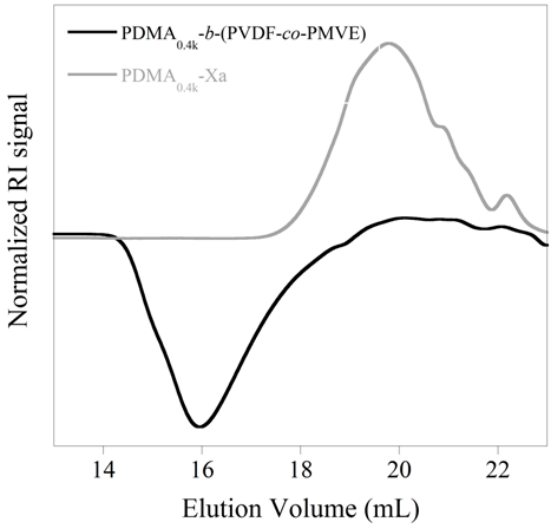

Figure IV.11. Overlays of SEC-RI chromatograms for the RAFT/MADIX copolymerization of VDF and PMVE from a $PDMA_{0.4k}$ macromolecular CTA (run 13 of Table IV.8).

b) Thermal properties

Similarly to the statistical P(VDF-*co*-PVME) copolymers, the amphiphilic block copolymers were amorphous. As expected, the values of T_g were comprised between those of the two blocks taken separately. However, the $PDMA_{0.8k}$-*b*-P(VDF-*co*-PMVE)$_{1.3k}$ copolymer was an exception as its T_g matched that of a $PDMA_{0.8k}$ (as reported in Chapter 2). This might be related to a composition in the fluorinated block that is low. As a general trend, the longer the fluorinated block, the lower the values of T_g for a given PDMA block.

C. Solubility of PVDF-based statistical copolymers in sc-CO_2

The solubility of the whole set of P(VDF-*co*-PMVE) copolymers in sc-CO_2 was eventually determined through cloud point measurements.

1. Solubility of P(VDF-*co*-PMVE) statistical copolymers in sc-CO_2

The solubility of the shortest P(VDF-*co*-PMVE)$_{1.8K}$ sample was first investigated. At 0.5 % wt, a cloud point was observed at 118 bar and 40 °C (see Table IV.9). An increase in concentration to 1 % wt had virtually no effect on its solubility. In such conditions, a CO_2 density around 0.71 g.cm^{-3} was consequently sufficient to solubilize these materials. By means of comparison, a Krytox polymer (M_w = 2500 g.mol^{-1}) exhibited a cloud point around 100 bar at 40 °C for a polymer content of 0.5 % wt.[42] Upon a higher polymer content of 1 % wt, a cloud point close to 105 bar was observed.

An increase in the chain length of P(VDF-*co*-PMVE) copolymers resulted in a large increase in cloud point pressures (see Table IV.9). The P(VDF-*co*-PMVE)$_{3k}$ copolymer thus exhibited a cloud point pressure at 189 bar for a polymer content of 0.2 % wt. Upon increasing the polymer fraction in the binary mixture to 1 % wt, a moderate increase of 23 bar was noted. A similar behaviour was observed for the P(VDF-*co*-PMVE)$_{4.8k}$ copolymer. For this last copolymer, the jump of cloud point pressures was much less pronounced in spite of a larger increase in chain length. These observations on P(VDF-*co*-PMVE) copolymers differ from the case of Krytox

Run	Samples	$M_{n,theo}$ (g.mol^{-1})	$M_{n,SEC}$ (g.mol^{-1}) [a]	Đ [a]	T_g (°C)	Cloud Point (bar) [b]	
						0.2 % wt	1 % wt
9	P(VDF-*co*-PMVE)$_{1.8K}$	1850	3700	1.26	-37	118 [c]	115
10	P(VDF-*co*-PMVE)$_{3k}$	3000	6000	1.58	-41	189	212
11	P(VDF-*co*-PMVE)$_{4.8K}$	4850	8900	1.63	-40	198	219

[a] Determined by SEC in THF. [b] Onset of turbidity at 40 °C. [c] Performed with 0.5 % wt.

Table IV.9. Experimental results for the solubility of P(VDF-*co*-PMVE) copolymers in sc-CO_2.

polymers where the cloud point pressures of samples with a M_w of 2500 and 7500 g.mol^{-1} were lower than that of a Krytox having a M_w of 5000 g.mol^{-1}.[43]

2. Solubility of PDMA-*b*-P(VDF-*co*-PMVE) amphiphilic copolymers

a) Influence of the chain length of the P(VDF-co-PMVE) block

The solubility of amphiphilic block copolymers was then explored through cloud point measurements and infrared spectroscopy. The cloud point measurements were first performed at 40 °C for a polymer content of 1 % wt (see Table.IV.10). For a CO_2-phobic block with a M_n of 400 g.mol^{-1}, the sample with the shortest P(VDF-*co*-PMVE) chain length (M_n = 1850 g.mol^{-1}) exhibited the lowest phase transition pressure at 235 bar (see run 12 of Table IV.10). By means of comparison, the difference of cloud point pressures with the P(VDF-*co*-PMVE)$_{1.8k}$ copolymers was 120 bar (see run 9 of Table IV.9). When the M_n of the CO_2-philic block was increased from 1900 to 2900 g.mol^{-1} -with a similar CO_2-phobic PDMA block of 400 g.mol^{-1}-, a cloud point pressure was observed at 257 bar (see run 13 of Table IV.10).

Run	Samples	$M_{n,theo}$ (g.mol^{-1})	$M_{n,SEC}$ (g.mol^{-1}) [a]	Đ [a]	T_g (°C)	PDMA /P(VDF-*co*-PVME) % wt	Cloud Point (bar) [b]
12	PDMA$_{0.4k}$-*b*-P(VDF-*co*-PMVE)$_{1.9k}$	2550	4800	1.55	-14	17	235
13	PDMA$_{0.4k}$-*b*-P(VDF-*co*-PMVE)$_{2.9k}$	3500	5900	1.74	-22	12	257
14	PDMA$_{0.8k}$-*b*-P(VDF-*co*-PMVE)$_{1.3k}$	2350	3200	1.62	14	37	347
15	PDMA$_{0.8k}$-*b*-P(VDF-*co*-PMVE)$_{3.3k}$	4300	7500	1.53	-4	19	295

[a] Determined by SEC in THF. [b] Onset of turbidity at 40 °C with 1 % wt of polymer.

Table IV.10. Experimental results for the solubility of P(VDF-*co*-PMVE) copolymers in sc-CO_2.

Infrared spectroscopy was then performed following the procedure presented in Chapter 1. The characteristic band at 1650 cm^{-1} –corresponding to the carbonyl group of N,N-dimethylacrylamide– was used to probe the solubility of these copolymers. In agreement with the cloud point results, the solubility of the block copolymer with a longer P(VDF-*co*-PMVE) chain length was found to be lower. However, a discrepancy between both techniques appeared. Thus, 1 % wt of $PDMA_{0.4k}$-*b*-$P(VDF\text{-}co\text{-}PMVE)_{2.9k}$ should be fully soluble around 150 bar at 40 °C while its cloud point pressure was observed at 257 bar. A possible bias coming from the infrared measurement was hypothesized as the determination of solubilities implies the theoretical molecular weight of the copolymer as a calculation parameter. The differences between experimental and theoretical molecular weights –as pointed out during the part about the synthesis of the copolymers –may explain the differences in solubility. Consequently, a determination of the absolute molecular weight of the copolymers through light scattering techniques seems necessary to further compare the results.

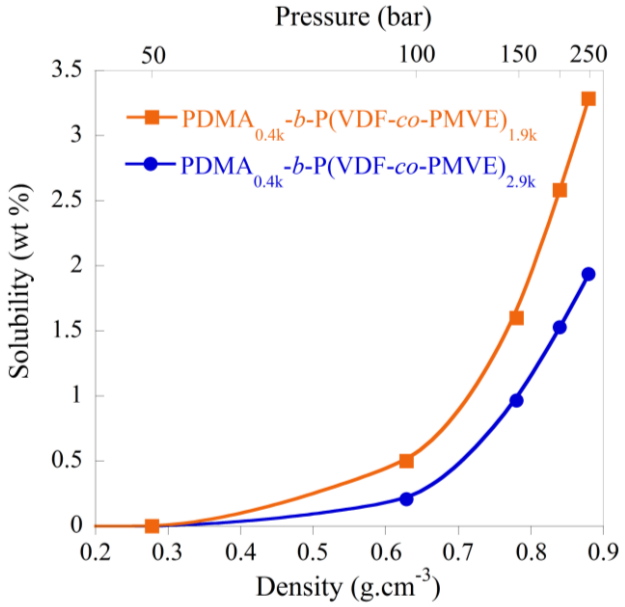

Figure II.12. Solubility (% wt) of $PDMA_{0.4k}$-*b*-P(VDF-*co*-PMVE) polymers with different P(VDF-*co*-PMVE) chain lengths.

In contrast to the first set of amphiphilic copolymers, an opposite trend was observed for the samples with a PDMA block of 800 $g.mol^{-1}$. The $PDMA_{0.8k}$-*b*-$P(VDF\text{-}co\text{-}PMVE)_{3.3k}$ copolymer exhibited a cloud point pressure at 295 bar while the phase transition was observed at 347 bar for the $PDMA_{0.8k}$-*b*-$P(VDF\text{-}co\text{-}PMVE)_{1.3k}$ (see runs

14 and 15 of Table IV.10). The low CO_2-philic/CO_2-phobic balance of the $PDMA_{0.8k}$-*b*-$P(VDF\text{-}co\text{-}PMVE)_{1.3k}$ presumably limits its solubility. The opposite behaviour observed with the $PDMA_{0.4k}$-based copolymers (runs 12 and 13 of Table IV.10) may result from the higher PDMA/P(VDF-*co*-PMVE) % wt calculated for the set of $PDMA_{0.8k}$-based copolymers (see Table IV.10).

These opposite tendencies were confirmed by infrared spectroscopy where the solubility of $PDMA_{0.8k}$-*b*-$P(VDF\text{-}co\text{-}PMVE)_{3.3k}$ was higher (see Figure IV.13). Around 4 % wt of this copolymer was fully soluble at 300 bar and 40 °C whereas the solubility of $PDMA_{0.8k}$-*b*-$P(VDF\text{-}co\text{-}PMVE)_{1.3k}$ was limited to 2 % wt in the same conditions.

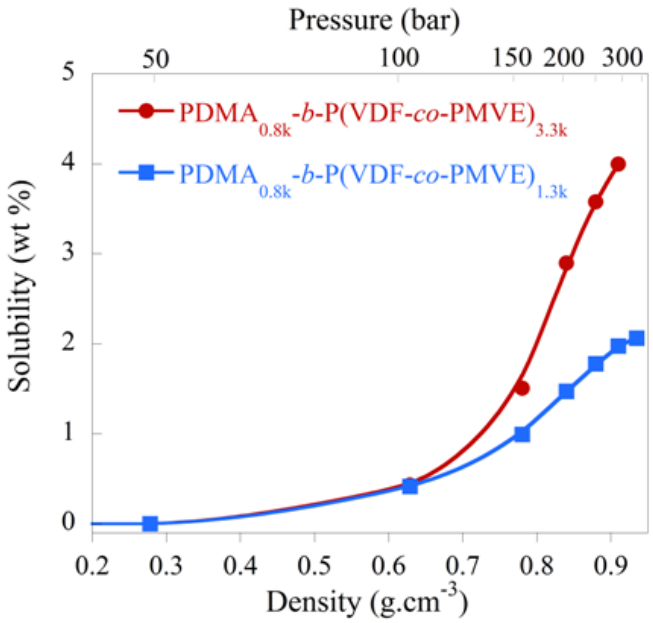

Figure II.13. Solubility (% wt) of $PDMA_{0.8k}$-*b*-P(VDF-*co*-PMVE) polymers with different P(VDF-*co*-PMVE) chain lengths.

By means of comparison, the solubility of a $PPEGA_{0.8k}$-*b*-$P(VAc_{25}\text{-}stat\text{-}VTFAc_{75})_{3.2k}$ copolymer was lower compared to the $PDMA_{0.8k}$-*b*-$P(VDF\text{-}co\text{-}PMVE)_{3.3k}$ copolymer. The PVTFAc-based copolymer exhibited a cloud point pressure around 350 bar at 40 °C for a polymer content of 0.5 % wt. This confirmed P(VDF-*co*-PMVE)-based amphiphilic block copolymers as materials with high solubilities in sc-CO_2.

b) Influence of composition at a constant chain length

Considering that PDMA$_{0.4k}$-*b*-P(VDF-*co*-PMVE)$_{1.9k}$ and PDMA$_{0.8k}$-*b*-P(VDF-*co*-PMVE)$_{1.3k}$ have the same theoretical chain lengths, the copolymers can be compared in terms of composition. The latter has a mass fraction of CO_2-phobic block in the copolymer of 17 % while the former incorporates 38 % of PDMA repeating units. As expected, the copolymer with the lowest mass fraction of PDMA exhibited a cloud point pressure that was lower of 120 bar. Note that the experimental molecular weight of PDMA$_{0.8k}$-*b*-P(VDF-*co*-PMVE)$_{1.3k}$ is also smaller, so chain length effects can be ruled out to explain such a difference in cloud point pressures. This behaviour was again confirmed by infrared spectroscopy where the solubility of PDMA$_{0.4k}$-*b*-P(VDF-*co*-PMVE)$_{1.9k}$ was lower in comparison with the PDMA$_{0.8k}$-*b*-P(VDF-*co*-PMVE)$_{1.3k}$ copolymer (see Figure IV.14).

Considering this large difference in cloud point pressures, the composition effects seem to prevail over chain length effects for this class of copolymers. However, this conclusion should be confirmed by a larger set of samples to provide a more general overview on their solubility.

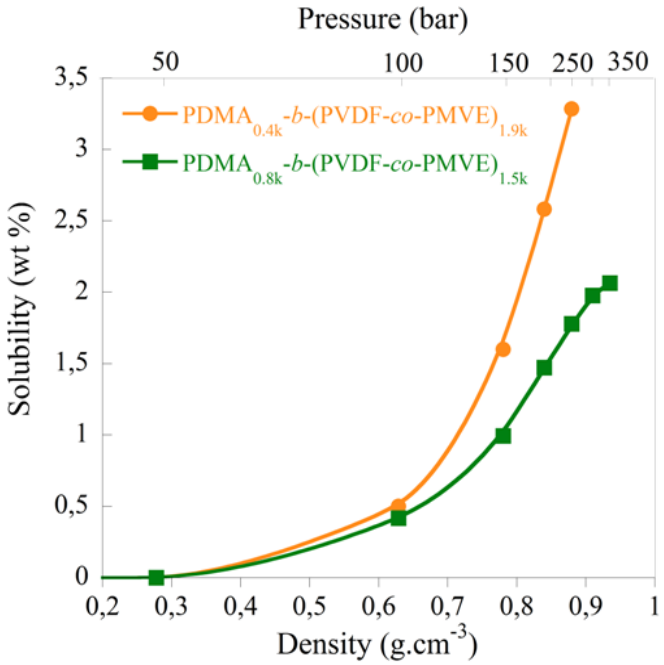

Figure II.14. Solubility (% wt) of PDMA-*b*-P(VDF-*co*-PMVE) copolymers with different compositions and equivalent chain lengths.

c) Influence of temperature

Ultimately, temperature effects were investigated through cloud point measurements performed with temperature ranging between 27 and 60 °C. As seen on Figure IV.15, variations in this range of temperature resulted in the linear increase in cloud point pressures. This could be simply explained by the simultaneous decrease in CO_2-density upon increasing temperature (see Figure IV.15). This linear dependency indicated that the tested copolymer exhibited neither LCST nor UCST behaviours in temperatures from 27 to 60 °C.

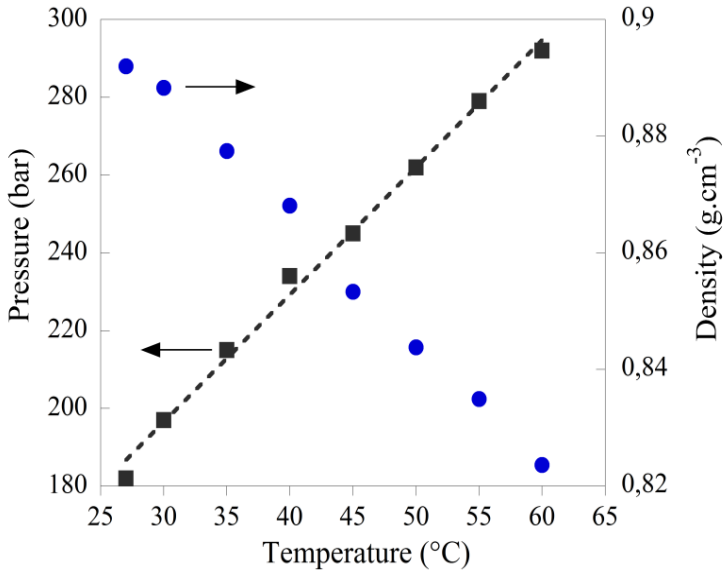

Figure IV.15. Influence of temperature on the solubility of $PDMA_{0.4k}$-*b*-P(VDF-*co*-PMVE)$_{1.3k}$ (run 12 of Table IV.12).

IV. Conclusions

In this last chapter, a new generation of fluorinated amphiphilic block copolymers for supercritical carbon dioxide has been presented. The CO_2-philic block was based on VDF as the repeating unit. The unprecedented RAFT/MADIX homopolymerization of VDF could be demonstrated as a prerequisite. Straightforward experimental proofs, including SEC, MALDI-TOF mass spectrometry and ^{19}F NMR analyses, supported the controlled character of the polymerization of VDF. This represents a new addition to the short list of monomers whose RAFT polymerization is mediated by an *O*-ethyl xanthate chain transfer agent. However, a deeper and complete understanding of this process is yet to be provided. In particular, the nature of the initiator, the design of the CTA and the role of inverted adducts during the polymerization reaction should be questioned in further studies. The identification of a suitable internal standard should also be investigated to pursue the kinetic experiments in autoclaves. Using an appropriate SEC with multiple detectors should shed further light on the control on molecular weight provided by the RAFT/MADIX agent. Ultimately, the strong advantages of polymerizing VDF by RAFT/MADIX polymerization could be evidenced by the direct synthesis of amphiphilic block copolymers incorporating a hydrophilic block. Considering the scope of monomers that can be polymerized through the RAFT/MADIX technology and the very large applications of PVDF, this certainly paves the way to PVDF-based block copolymers with innovative applications.

The knowledge gained on the RAFT/MADIX polymerization of VDF could then be used to study the RAFT/MADIX copolymerization of VDF with perfluoromethyl vinyl ether. Well-defined amorphous PVDF-based copolymers of various chain lengths were obtained. These materials exhibited a high solubility which was close to that of perfluoropolyethers. This represents a new strategy to decrease the solubility of PVDF-based copolymers as well as a new addition to the field of (co)polymers having a high solubility in sc-CO_2. Compared to the copolymers presented in Chapter 3, their solubility appeared comparable to that of the most soluble P(VAc-stat-VTFAc) copolymer.

Similarly, the P(VDF-*co*-PMVE)-based amphiphilic block copolymers exhibited cloud points under mild conditions of pressures ($P < 350$ bar). Their

solubility was superior to those of P(VAc-*stat*-VTFAc)-based amphiphilic copolymers presented in Chapter 3. By tuning the chain length of the CO_2-philic block and the composition of the block copolymer, opposite trends in solubility could be deduced which depended on the chain length of either the fluorinated block or the hydrophilic one. Though, more samples should be studied to clarify this. The influence of macromolecular characteristics on the self-assembly of these copolymers and their adsorption at the water/CO_2 interface these copolymers should be further studied to confirm their potential as new macromolecular surfactants for supercritical carbon dioxide.

V. References

(1) B. Ameduri, *Chem. Rev.*, 2009, **109,** 6632.
(2) R. Timmerman and W. Greyson, *J. Appl. Polym. Sci.*, 1962, **6,** 456.
(3) M. Duc, B. Ameduri, B. Boutevin, M. Kharroubi and J.M. Sage, *Macromol. Chem. Phys.*, 1998, **199,** 1271.
(4) S. Beuermann and M. Imran-ul-haq, *J. Polym. Sci. A Polym. Chem.*, 2007, **45,** 5626.
(5) P.A. Mueller, G. Storti, M. Morbidelli, I. Costa, A. Galia, O. Scialdone and G. Filardo, *Macromolecules*, 2006, **39,** 6483.
(6) J. Liu, H. Tai and S.M. Howdle, *Polymer*, 2005, **46,** 1467.
(7) H. Tai, W. Wang, R. Martin, J. Liu, E. Lester, P. Licence, H.M. Woods and S.M. Howdle, *Macromolecules*, 2005, **38,** 355.
(8) *Well-Architectured Fluoropolymers: Synthesis, Properties and Applications*, ed. B. Ameduri and B. Boutevin, Elsevier, 2004**.**
(9) G. Kostov, F. Boschet and B. Ameduri, *J. Fluor. Chem.*, 2009, **130,** 1192.
(10) T.C. Chung and A. Petchsuk, *Macromolecules*, 2002, **35,** 7678.
(11) C. Boyer, D. Valade, L. Sauguet, B. Ameduri and B. Boutevin, *Macromolecules*, 2005, **38,** 10353.
(12) C. Boyer, D. Valade, P. Lacroix-Desmazes, B. Ameduri and B. Boutevin, *J. Polym. Sci. A Polym. Chem.*, 2006, **44,** 5763.
(13) A.D. Asandei, O.I. Adebolu and C.P. Simpson, *J. Am. Chem. Soc.*, 2012, **134,** 6080.
(14) G. Kostov, F. Boschet, J. Buller, L. Badache, S. Brandsadter and B. Ameduri, *Macromolecules*, 2011, **44,** 1841.
(15) L. Liu, D. Lu, H. Wang, Q. Dong, P. Wang and R. Bai, *Chem. Commun.*, 2011, **47,** 7839.
(16) M. Destarac, K. Matyjaszewski, E. Silverman, B. Ameduri and B. Boutevin, *Macromolecules*, 2000, **33,** 4613.
(17) G. Laruelle, E. Nicol, B. Ameduri, J.F. Tassin and N. Ajellal, *J. Polym. Sci. A Polym. Chem.*, 2011, **49,** 3960.
(18) J. Xue, L. Chen, H.L. Wang, Z.B. Zhang, X.L. Zhu, E.T. Kang and K.G. Neoh, *Langmuir*, 2008, **24,** 14151.
(19) L. Sauguet, C. Boyer, B. Ameduri and B. Boutevin, *Macromolecules*, 2006, **39,** 9087.
(20) D. Valade, C. Boyer, B. Ameduri and B. Boutevin, *Macromolecules*, 2006, **39,** 8639.
(21) M.C. Iovu and K. Matyjaszewski, *Macromolecules*, 2003, **36,** 9346.
(22) R. Vukicevic, U. Schwadtke, S. Schmucker, P. Schafer, D. Kuckling and S. Beuermann, *Polym. Chem.*, 2012, **3,** 409.
(23) *Handbook of RAFT Polymerization*, ed. C. Barner-Kowollik, Wiley-VCH, 2008**.**
(24) G. Moad, E. Rizzardo and S.H. Thang, *Aust. J. Chem.*, 2005, **58,** 379.
(25) C. Boyer, M.H. Stenzel and T.P. Davis, *J. Polym. Sci. A Polym. Chem.*, 2011, **49,** 551.
(26) D. Taton, M. Destarac and S.Z. Zard, in *Handbook of RAFT Polymerization*, ed. C. Barner-Kowollik, Wiley-VCH, 2008, Chap. 10.
(27) A.B. Lowe and C.L. McCormick, *Prog. Polym. Sci.*, 2007, **32,** 283.
(28) J. Guiot, B. Ameduri and B. Boutevin, *Macromolecules*, 2002, **35,** 8694.
(29) C. Boyer, D. Valade, L. Sauguet, B. Ameduri and B. Boutevin, *Macromolecules*, 2005, **38,** 10353.
(30) R. Severac, *PhD Thesis*, University of Montpellier 2, **2005**.
(31) G. Delaittre, M. Save, M. Gaborieau, P. Castignolles, J. Rieger and B. Charleux, *Polym. Chem.*, 2012, **3,** 1526.

(32) M.L. Coote, E.I. Izgorodina, G.E. Cavigliasso, M. Roth, M. Busch and C. Barner-Kowollik, *Macromolecules*, 2006, **39,** 4585.
(33) B. Ameduri, C. Ladaviere, F. Delolme and B. Boutevin, *Macromolecules*, 2004, **37,** 7602.
(34) M. Destarac, C. Brochon, J.M. Catala, A. Wilczewska and S.Z. Zard, *Macromol. Chem. Phys.*, 2002, **203,** 2281.
(35) *Nuclear Magnetic Resonance for Organic Chemists*, ed. D. W. Matheson, Academic Press, 1967**.**
(36) E. Möller and S. Beuermann, *Macromol. React. Eng.*, 2011, **5,** 8.
(37) B. Baradie, M.S. Shoichet, Z. Shen, M.A. McHugh, L. Hong, Y. Wang, J.K. Johnson, E.J. Beckman and R.M. Enick, *Macromolecules*, 2004, **37,** 7799.
(38) B. Otazaghine, L. Sauguet, M. Boucher and B. Ameduri, *Eur. Pol. J.*, 2005, **41,** 1747.
(39) C. Boyer, B. Ameduri and M.H. Hung, *Macromolecules*, 2010, **43,** 3652.
(40) G. Kostov, M. Holan, B. Ameduri and M.H. Hung, *Macromolecules*, 2012, **45,** 7375.
(41) A. Marie, S. Alves, F. Fournier and J.C. Tabet, *Anal. Chem.*, 2003, **75,** 1294.
(42) T.A. Hoefling, R.M. Enick and E.J. Beckman, *J. Phys. Chem.*, 1991, **95,** 7127.
(43) D.A. Newman, T.A. Hoefling, R.R. Beitle, E.J. Beckman and R.M. Enick, *J. Supercrit. Fluids*, 1993, **5,** 205.

Conclusion

As described in the introduction, the constant objective of this thesis was to develop the macromolecular engineering of surfactants for supercritical carbon dioxide. Looking at the bibliography, it first appeared that the potential of vinyl monomers including vinyl esters and fluorinated olefins had not totally been fulfilled yet. Systematic studies regarding the influence of polymer macromolecular characteristics on their solubility in sc-CO_2 and their activity at the water/carbon dioxide interface were still scarce.

In order to improve the understanding of the structure-property relationships of polymers with CO_2, RAFT/MADIX polymerization was proven an efficient and precise tool to create libraries of original (co)polymers with various compositions, chain lengths and end groups. The first case study concerned the use of vinyl acetate as a building block for the design of amphiphilic block copolymers. Building on infrared spectroscopy, the solubility of these copolymers could be mapped in function of their chain length and composition. In spite of the solubility of PVAc restricted to low molecular-weight polymers, amphiphilic block copolymers comprising a block CO_2-phobic poly(N,N-dimethylacrylamide) were demonstrated to exhibit significant mass fractions soluble in sc-CO_2. A molecular weight of 4000 g.mol^{-1} and a composition of 20 % w/w in the CO_2-phobic block were identified as the key macromolecular parameters to obtain solubilities higher than 0.5 % wt at 40 °C. In the pursuit of enhanced solubility, the design of a fluorinated xanthate and its use in RAFT/MADIX polymerization were revealed to significantly improve the solubility of PVAc-based (co)polymers.

This brought to investigate the physical parameters governing the solubility of poly(vinyl acetate) in sc-CO_2. While the solubilities of fluorinated poly(acrylates) and poly(siloxanes) were related to their weak polymer-polymer interactions, PVAc has usually been regarded as a CO_2-philic polymer, mainly focusing on its specific Lewis-type and hydrogen-bond-type polymer–CO_2 interactions. In contrast to previous studies focusing on entropy of mixing, the role of polymer-polymer interactions in the solubility of PVAc-based copolymers was explored. To do so, original poly(vinyl esters) bearing a trifluoromethyl group either on the ester group or on the main chain were synthesized. At a constant molecular weight of 4000 g.mol^{-1} and a polymer content of 0.2 % wt, decreases of approximately 60 and 100 bars were observed for, respectively the former and the latter strategies. In both cases, a

simultaneous decrease in polymer-polymer interactions was evidenced, highlighting their role in such solubility behaviours. The different positionings of the fluorinated moiety also allowed identifying distinctive features of solubility with entropy of mixing as a secondary lever.

Ultimately, the beneficial use of vinylidene fluoride as the building block for the design of CO_2-philic (co)polymers could be evidenced. From a strategy based on its unprecedented RAFT/MADIX copolymerization with a fluorinated vinyl ether, a new generation of highly-soluble statistical copolymers could be synthesized. These copolymers showed levels of solubility comparable to the widespread perfluoropolyethers. The direct synthesis of amphiphilic block copolymers was eventually achieved. In addition to a high solubility, different trends that should be further clarified were observed as a function of composition and chain length.

Taking a step back, this thesis is part of a larger project to develop new macromolecular surfactants for sc-CO_2. In the pursuit of identifying new CO_2-philic polymers and designing efficient amphiphiles, a large amount of work within this thesis has been devoted to further develop the chemistry toolbox. In particular, encouraging results were obtained with the VAc and VTFAc monomers, which triggers new perspectives. The identification of a fluorinated poly(vinyl ester) with both enhanced solubility and stability constitutes a short-term perspective of this work. A further understanding of the RAFT/MADIX polymerization of vinylidene fluoride should be also considered to expand the scope of this chemistry to other comonomers including fluorinated olefins and vinyl esters and new hydrophilic blocks.

Considering only the solubility of polymers, it would be of interest to synthesize macromolecules with tunable properties such as lower and/or upper critical solution ones. Provided that appropriate equipments are available, the self-assembly of amphiphilic and double-CO_2-philic copolymers should be also a large field of investigation. This topic is of special interest considering the need for CO_2-thickeners in oil field applications. Ultimately, studies dedicated to explore the interfacial activity of these amphiphilic copolymers represent a natural continuation of this work. In particular, the determination of surface tension at the water/CO_2 interface in presence of amphiphilic block copolymers is an essential step in this

direction. The identification of a low cohesive energy density solvent as a model solvent for CO_2 may be helpful to overcome the difficulties related to the in-situ measurements. A complete understanding of the polymer structure-self-assembly-stabilization of emulsions relationships should be then achieved. The stabilization of W/C emulsions with high solid contents could be then expected. The extension of these projects from water to other green solvents exhibiting different polarities and basicities should further help the generalization of (in)organic reactions performed in sc-CO_2.

****

Experimental Section

Chapter 2

Materials

Vinyl acetate (VAc, Acros Organics, 99+%), *N*,*N*-dimethylacrylamide (DMA, Aldrich, 99%) and ethyl acetate (Fischer Scientific, Laboratory reagent grade) were distilled on CaH_2. 2,2′-Azobisisobutyronitrile (AIBN, Acros Organics, 98%) was recrystallized twice from methanol and dried *in vacuo*. Carbon disulfide (Sigma-Aldrich, anhydrous, >99%) was distilled on P_2O_5. The *O*-ethyl-*S*-(1-methoxycarbonyl) ethyldithiocarbonate RAFT/MADIX agent (Rhodixan A1 (Xa)) was obtained from Rhodia and used as received. Carbon dioxide (CO_2 N45 TP, Air Liquide), *N*,*N*-dimethylformamide (DMF, Sigma-Aldrich, Chromasolv Plus for HPLC , >99.9%), tetrahydrofuran (THF for preparative HPLC , stabilized with BHT, SDS), lithium bromide (Aldrich, 99+%), 1*H*,1*H*,2*H*,2*H*-perfluoro-1-octanol (Aldrich, 97%), sodium hydride (Aldrich, 60% dispersion in mineral oil), methyl 2-bromopropionate (Aldrich, 98%) were used as received. Sodium trifluoroacetate (NaTFA, Fluka, for HPLC, >99.0%), *trans*-2-[3-(4-*tertb*utylphenyl)-2-methyl-2propenylidene] malononitrile (DCTB, Aldrich, matrix substance for MALDI-MS, > 99.0 % (HPLC)), *trans*-3-indoleacrylic acid (IAA, Fluka, matrix substance for MALDI-MS, > 99.0 % (HPLC)), dilauroyl peroxide (Acros Organics, 99 %), tetrahydrofuran (THF, Sigma-Aldrich, anhydrous, > 99.9%, inhibitor-free) and propan-2-ol (Acros Organics, 99.5+ %) were used as received.

RAFT/MADIX synthesis of PVAc

In a typical experiment, a mixture of vinyl acetate (2.8 g, 3.2×10^{-2} mol), AIBN (8 mg, 0.049 mmol) and Rhodixan A1 (97 mg, 0.47 mmol) in ethyl acetate (2.9 g) was degassed by four freeze–pump-thaw cycles, backfilled with argon, sealed and placed in an oil bath at 60 °C. After 15 h, the reaction was stopped by cooling in liquid nitrogen. Conversion was determined by ^{1}H NMR in $CDCl_3$. The polymer was dried *in vacuo*. ($M_{n,theo}$ = 6000 g.mol^{-1}, $M_{n,SEC}$ = 6050 g.mol^{-1}, $Đ$ = 1.61) The same protocol was applied to produce a $PVAc_{3.8k}$–FXa sample replacing Rhodixan A1 with *F*-xanthate.

Removal of the xanthate terminal group of PVAc

A PVAc ($PVAc_{4k}$-Xa, $M_{n\ theo}$ = 4200 $g.mol^{-1}$) was synthesized with Rhodixan A1. A sample of this polymer (0.5 g, 0.11 mmol) was mixed with dilauroyl peroxide (113.6 mg, 0.285 mmol) in THF (1.5 mL) and propan-2-ol (3 mL). The mixture was degassed via four freeze-pump-thaw cycles, backfilled with argon, sealed and placed in an oil bath at 80 °C. After 4 h, the reaction was cooled in liquid nitrogen. The polymer was dried *in vacuo*.

Synthesis of methyl 2-((3,3,4,4,5,5,6,6,7,7,8,8,8- tridecafluorooctyloxy) carbonothioylthio)propanoate (F-xanthate)

Carbon disulfide (1.217 g, 15.98 mmol) was added to a solution of 1*H*,1*H*,2*H*,2*H*-perfluoro-1-octanol (3 g, 7.99 mmol) in *N*,*N*-dimethylformamide (40 mL). The mixture was cooled down to 0 °C in an ice bath and sodium hydride (319.7 mg, 7.99 mmol) was added. The mixture was stirred at 0 °C for 1 h and methyl 2-bromopropionate (1.334 g, 7.99 mmol) was then added dropwise. The mixture was stirred at 0 °C for 1 h and then at RT for 2 h. After concentration under vacuum, the mixture was diluted with diethyl ether, washed twice with water and finally with brine. The organic phase was collected and dried overnight on $MgSO_4$. After concentration, the product was purified by chromatography on silica gel using heptane/ethyl acetate (9 : 1) to yield 2.73 g (64%) of pure *F*-xanthate as a yellow viscous oil. ^{1}H NMR (300 MHz, $CDCl_3$): δ (ppm) = 4.81 (t, 2H), 4.40 (q, 1H), 3.69 (q, 2H), 3.64 (s, 3H), 2.79 (m, 2H), 1.47 (d, 3H). ^{13}C NMR (300 MHz, $CDCl_3$): δ (ppm) = 211.2 (s, S*C*(=S)), 170.7 (s, C-*C*(=O)-O), 100–125 (m, fluorinated carbon atoms), 65.6 (s, O-*C*H_2-C), 52.3 (s, *C*H_3-O), 46.3 (s, *C*-CH_3), 29.0 (t, CH_2-*C*H_2-CF_2), 16.3 (s, *C*H_3-C). ^{19}F NMR (300 MHz, $CDCl_3$): δ (ppm) = −81.7 (t, 3F, C*F*$_3$), −113.5 (m, 2F, C*F*$_2$-CH_2), −122.4 (m, 2F, C*F*$_2$-CF_2-CH_2), −123.5 (m, 2F, C_3F_7-C*F*$_2$), −123.9 (m, 2F, C_2F_5-C*F*$_2$), −126.9 (m, 2F, CF_3-C*F*$_2$). GC-MS: accurate mass: 527.0 amu (theoretical mass of $C_{13}H_{11}S_2O_3F_{13}$ = 526.3 amu).

RAFT/MADIX synthesis of PDMA macro-chain transfer agents

In a typical experiment, a mixture of *N*,*N*-dimethylacrylamide (1.62 g, 1.63 mmol), AIBN (4 mg, 0.024 mmol) and Rhodixan A1 (166 mg, 0.8 mmol) in ethyl acetate (7.2 g) was degassed by four freeze–pump–thaw cycles, backfilled with argon, sealed and placed in an oil bath at 60 °C. After 15 h, the reaction was stopped by

cooling in liquid nitrogen. Conversion was determined by ^{1}H NMR in $CDCl_3$. The polymer was dried *in vacuo*. ($M_{n,theo}$ = 2200 g.mol^{-1}, $M_{n,SEC}$ = 2050 g.mol^{-1}, $Đ$ = 1.46).

RAFT/MADIX synthesis of PDMA-*b*-PVAc-Xa block copolymers

In a typical experiment, AIBN (7.2 mg, 0.04 mmol) and vinyl acetate (1.52 g, 17.6 mmol) were added to a solution of PDMA macro-chain transfer agent (0.5 g, 0.42 mmol) in ethyl acetate (2.5 g), then degassed by four freeze–pump–thaw cycles, backfilled with argon, sealed and placed in an oil bath at 60 °C. After 15 h, the reaction was stopped by cooling in liquid nitrogen. Conversion was determined by ^{1}H NMR in $CDCl_3$. The polymer was dried *in vacuo*. ($M_{n,theo}$ = 3900 g.mol^{-1}, $M_{n,SEC}$ = 5100 g.mol^{-1}, $Đ$ = 1.24)

Characterization techniques

NMR measurements

^{1}H NMR spectra were recorded with a Bruker AMX 300 apparatus. All spectra were referenced to the solvent residual peak ($CHCl_3$ at 7.26 ppm or DMSO at 2.5 ppm).

Size exclusion chromatography

SEC in THF was performed using a Waters e2695 Separations Module equipped with a Waters 2414 RI Detector thermostated at 35 °C, a 100 µL injection loop and a set of 3 Shodex columns (K-804L, K-802.5 and K-G) thermostated at 40 °C. A calibration was performed using poly(methyl methacrylate) standards (Polymer Standard Services, Germany) ranging from 875 to 625 000 g.mol^{-1}. Flow rate was 1 mL.min^{-1} and toluene was used as a flow marker. Prior to injections, samples were diluted at a concentration of 10 g.L^{-1} overnight and filtered through a 0.45 µm PTFE filter. Data were handled with the Wyatt Astra 5.3.4.14 software.

SEC in DMF containing 10 mM of LiBr was performed using a 100 µL injection loop, a set of three Shodex columns (KD-G, K-805L and KD-802) thermostated at 55 °C and a Waters 410 Differential Refractometer thermostated at 40 °C. A calibration was performed using the same poly(methyl methacrylate) standards that described above. Flow rate was 1 mL.min^{-1} and toluene was used as a

flow marker. Prior to injections, samples were diluted at a concentration of 10 $g.L^{-1}$, stirred overnight and filtered through a 0.45 μm PTFE filter.

MALDI-TOF mass spectrometry

MALDI-TOF MS measurements were performed on an applied Biosystems Voyager System 4243. Positive-ion spectra were acquired in the reflectron mode. The matrix was DCTB and NaTFA was used as a cationization agent for the PVAc samples. IAA and NaTFA were used for the PDMA oligomers. The polymer sample, the matrix and the salt were dissolved in THF and premixed in a 10:1.5:10 ratio.

Differential scanning calorimetry

DSC measurements were performed with a Mettler-Toledo DSC Star System apparatus under a nitrogen atmosphere at a heating rate of 10 $°C.min^{-1}$ and a cooling rate of 10 $°C.min^{-1}$. In a typical procedure, 5–8 mg of samples were weighed in a 40 μL aluminium crucible with a high-precision balance and sealed with a perforated lid. Glass transition temperature was measured as the temperature of inflexion mid-point on cooling.

Infrared spectroscopy

The infrared absorption experiments were performed using a homemade stainless optical cell withstanding high pressures up to 35 MPa (350 bar) and temperatures up to 250 °C. Optical access was given by four cylindrical windows, two silicon windows for the infrared absorption measurements with a path length of 5.05 mm and two other sapphire windows for direct observation of the solution to ensure that there was no demixing in the sample. The cell volume was 4.3 cm^3 and the homogeneity was ensured with a magnetic stirrer disposed at the bottom of the cell. The sealing was obtained using the unsupported area principle. All windows were positioned on the flat surface of the stainless plug with a 100 μm kapton foil placed between the window and the plug in order to compensate for imperfections at the two surfaces. Flat Teflon seals were used to ensure sealing between the plug and the cell body. The heating was performed with four cartridge heaters disposed in the body of the cell in which two thermocouples were put. The first one was located close to the cartridge in order to achieve a good temperature regulation and the second one was kept close to the sample area to measure the temperature with an accuracy of

about $T \approx \pm 0.5$ °C. The cell was connected *via* a stainless steel capillary to a hydraulic pressurizing system which allowed to adjust the pressure up to 35 MPa with an absolute uncertainty of ±0.1 MPa and a relative error of ±0.3 %. The infrared absorption measurements were performed with a Biorad interferometer (type FTS-60A). Single-beam spectra recorded in the spectral range 400–6000 cm^{-1} with 2 cm^{-1} resolution were obtained by Fourier transformation of 30 accumulated interferograms. The spectra were collected at a temperature of 40 °C as a function of pressure from 5 to 35 MPa. The CO_2 contribution was then removed. After identification of the specific vibrational modes associated with functional groups of the solute, the intensity of these characteristic infrared bands allows to determine the concentration of the solute in solution according to the Beer–Lambert law, $A = \varepsilon lc$ with A, sample absorbance without dimension; ε, molar extinction coefficient ($L.mol^{-1}.cm^{-1}$); l, optical path length (cm) and c, sample concentration ($mol.L^{-1}$).

Chapter 3

Materials

Vinyl trifluoroacetate (Aldrich, 98%), vinyl acetate (Aldrich, >99.9%), 1-(trifluoromethyl) vinyl acetate (Alfa Aesar, 97%), poly(ethylene glycol) methyl ether acrylate (average M_n of 480 g.mol^{-1}, Aldrich), N,N-dimethylformamide (DMF, Sigma-Aldrich, Chromasolv Plus for HPLC, >99.9%), tetrahydrofuran (THF for preparative HPLC, stabilized with BHT, SDS), lithium bromide (Aldrich, 99+%), acetic acid (Sigma-Aldrich, ACS reagent, >99.7%), acetic anhydride (Sigma-Aldrich, ACS reagent, >98.0%), pyridine (Sigma-Aldrich, anhydrous, 99.8%) dithranol (Fluka, matrix substance for MALDI-MS >98%) and carbon dioxide (CO_2 N45 TP, Air Liquide) were used as received. Ethyl acetate (Fischer Scientific, Laboratory reagent grade) and 2-butanone (Sigma-Aldrich, ACS reagent, >99.0%) were distilled on CaH_2. 2,2-Azobisisobutyronitrile (AIBN, Acros Organics, 98%) was recrystallized twice from methanol and dried under vacuum. RAFT/MADIX agent (2-mercaptopropionic acid methyl ester O-ethyl dithiocarbonate, Rhodixan A1) was obtained from Rhodia and used as received.

Procedure for the kinetics of the RAFT/MADIX polymerization of VTFAc

A stock solution containing VTFAc, Rhodixan A1, AIBN and 2-butanone was prepared. Aliquots of the stock solution were transferred to 15 mL individual glass tubes which were thoroughly deoxygenated by freeze–pump–thaw cycles. The tubes were then placed in a constant temperature oil bath at 60°C and a tube was removed at regular time intervals. The reactions were stopped by cooling the solution in liquid nitrogen. Final conversions were measured by ^{1}H NMR in acetone-d_6 and the polymer samples were characterized by size-exclusion chromatography in DMF.

RAFT/MADIX polymerization of VTFAc

In a typical experiment, a mixture of vinyl trifluoroacetate (2.1 g, 14.7 mmol), AIBN (7.3 mg, 0.04 mmol) and Rhodixan A1 (138.9 mg, 0.07 mmol) in 2-butanone (2.3 g) was transferred into a home-made 15-mL Schlenk tube equipped with a Rotaflo® stopcock. The solution was degassed by four freeze–pump–thaw cycles, backfilled with argon and placed in an oil bath at 60 °C. After 16 h, the reaction was

stopped by cooling in liquid nitrogen. Conversion was determined by ^{1}H NMR in acetone-d_6. The polymer was dried in vacuo and characterized by size-exclusion chromatography (SEC) in DMF. (Conversion = 67 %, $M_{n,theo}$= 2300 g.mol^{-1}, $M_{n,NMR}$= 2700 g.mol^{-1}, $M_{n,SEC}$= 4100 g.mol^{-1}, Đ= 1.07).

RAFT/MADIX copolymerization of VAc and VTFAc

In a typical experiment, a mixture of vinyl trifluoroacetate (2.15 g, 15.3 mmol), vinyl acetate (1.31 g, 15.2 mmol), AIBN (14.9 mg, 0.1 mmol) and Rhodixan A1 (46 mg, 0.2 mmol) in ethyl acetate (3.56 g) was transferred into a home-made 15-mL Schlenk tube equipped with a Rotaflo® stopcock. The solution was degassed by four freeze–pump–thaw cycles, backfilled with argon and placed in an oil bath at 60 °C. After 16 h, the reaction was stopped by cooling in liquid nitrogen. Conversion was determined by ^{1}H NMR in acetone-d_6. The polymer was dried in vacuo and characterized by SEC in THF. ($M_{n,theo}$= 4100 g mol^{-1}, $M_{n,SEC}$= 4400 g mol^{-1}, Đ= 1.16).

RAFT/MADIX polymerization of poly(ethylene glycol) methyl ether acrylate

In a typical experiment, a mixture of poly(ethylene glycol) methyl ether acrylate (10 g, 20.8 mmol), AIBN (34.7 mg, 0.2 mmol) and Rhodixan A1 (2.6 g, 12.5 mmol) in ethyl acetate (12.5 g) was transferred into a Schlenk, degassed by four freeze–pump–thaw cycles, backfilled with argon and placed in an oil bath at 70 °C. After 16 h, the reaction was stopped by cooling in liquid nitrogen. Conversion was determined by ^{1}H NMR in $CDCl_3$ (>99%). The polymer was dried in vacuo and characterized by SEC in THF. ($M_{n,theo}$= 1000 g.mol^{-1}, $M_{n,SEC}$= 1400 g.mol^{-1}, Đ= 1.61, $M_{n,NMR}$= 1000 g.mol^{-1}). This macromolecular CTA was then used for the RAFT/MADIX polymerization of VTFAc and the RAFT/MADIX polymerization of VAc and VTFAc (*vide supra*).

Basic methanolysis of polymers

The polymer samples (100 mg) were saponified for 2 h at 25 °C with a 2 % wt solution of sodium hydroxide in methanol (10 mL). The saponification steps were quantitative as evidenced by ^{1}H NMR in DMSO-$_{d6}$. The resulting poly(vinyl alcohol) samples were filtered off, washed with methanol, dried under vacuum and characterized by ^{1}H NMR in DMSO-d_6. Recovery was typically higher than 90%.

Acetylation of poly(vinyl alcohol) samples

A mixture of a poly(vinyl alcohol) sample (100 mg), acetic acid (2 mL), acetic anhydride (2 mL) and pyridine (0.2 mL) was transferred into a Schlenk, degassed with argon and placed in an oil bath at 100 °C. After 24 h, the solution was cooled with liquid nitrogen and dried under vacuum. Quantitative acetylation was confirmed by ^{1}H NMR in $CDCl_3$. The resulting poly(vinyl acetate) samples were characterized by SEC in THF.

RAFT/MADIX copolymerization of vinyl acetate and dibutyl maleate

A mixture of vinyl acetate (1.50 g, 17.3 mmol), AIBN (14.3 mg, 0.09 mmol), dibutyl maleate (4.11 g, 17.3 mmol) and Rhodixan A1 (215 mg, 1 mmol) was transferred into a Schlenk, degassed by four freeze–pump–thaw cycles, backfilled with argon and placed in an oil bath at 60 °C. After 48 h, the reaction was stopped by cooling in liquid nitrogen. Conversion was determined by ^{1}H NMR in $CDCl_3$. The solution was diluted with ethyl acetate and transferred into a Spectra/Por 6 regenerated cellulose dialysis tubing (Molecular Weight Cut-Off = 1 kD). The solution was then dialyzed against ethyl acetate for 3 days. The polymer was then dried under vacuum and characterized by size-exclusion chromatography in THF. ($M_{n,theo}$= 4400 g.mol^{-1}, $M_{n,SEC}$= 3600 g.mol^{-1}, Đ= 1.21).

RAFT/MADIX copolymerization of vinyl acetate and vinyl pivalate

A mixture of vinyl acetate (250 mg, 2.9 mmol), vinyl pivalate (3.38 g, 26.1 mmol), AIBN (5 mg, 0.03 mmol) and Rhodixan A1 (291 mg, 1.4 mmol) in ethyl acetate (3.9 g) was transferred into a Schlenk, degassed by four freeze–pump–thaw cycles, backfilled with argon and placed in an oil bath at 60 °C. After 16 h, the reaction was stopped by cooling in liquid nitrogen. Conversion was determined by ^{1}H NMR in $CDCl_3$. The polymer was dried under vacuum and characterized by size-exclusion chromatography in THF. ($M_{n,theo}$= 4300 g.mol^{-1}, $M_{n,SEC}$= 4800 g.mol^{-1}, Đ= 1.22).

RAFT/MADIX copolymerization of vinyl acetate and (1-trifluoromethyl) vinyl acetate

In a typical experiment, a mixture of (1-trifluoromethyl), vinyl acetate (3.70 g, 23.3 mmol), vinyl acetate (2.0 g, 23.2 mmol), AIBN (19.5 mg, 0.1 mmol) and Rhodixan A1 (80.5 mg, 0.39 mmol) was degassed by four freeze–pump–thaw cycles, backfilled with argon and placed in an oil bath at 60 °C. After 20 h, the reaction was stopped by cooling in liquid nitrogen. Conversion was determined by ^{1}H NMR (Conv(VAc) = 27 %) and ^{19}F NMR (Conv(CF_3VAc) = 27 %) in acetone-d_6. The polymer sample was dried under vacuum and characterized by size-exclusion chromatography in THF. ($M_{n,theo}$= 4100 g.mol^{-1}, $M_{n,SEC}$= 3700 g.mol^{-1}, Đ= 1.51). A similar protocol was used for the RAFT/MADIX copolymerization of VAc and CF_3VAc mediated by a $PDMA_{0.8k}$ macromolecular CTA.

Characterization techniques

MALDI-TOF mass spectrometry of P(VAc-*stat*-CF_3VAc)

The MALDI–TOF mass spectrum was obtained with a Voyager-DE PRO (Applied Biosystems, Framingham, MA) equipped with a nitrogen laser emitting at 337 nm with a 3 ns pulse duration. The instrument was operated in linear or reflectron modes. The ions were accelerated under a potential of 20 kV. The positive ions were detected in all cases. The spectra were the sum of 300 shots and an external mass calibration of mass analyzer was performed with a mixture of peptides (Sequazyme, Applied Biosystems, Framingham, MA). Samples were prepared by mixing a solution of 1,8,9-anthracenetriol (dithranol) at 10 g.L^{-1} in THF and a solution of poly(vinyl acetate-*stat*-1-(trifluoromethyl) vinyl acetate) at 10 g.L^{-1} in DMF. To enhance cationization of polymers, a solution of NaI at 10 g.L^{-1} in acetone were added to solutions. The whole mixture which corresponded to a ratio of 45:5:5 v/v/v was spotted on the MALDI sample plate and air-dried.

NMR measurements.

^{1}H NMR and ^{19}F NMR spectra were recorded with a Bruker AMX 300 apparatus. All spectra were referenced to the solvent residual peak (chloroform at 7.26 ppm, DMSO at 2.50 ppm or acetone at 2.05 ppm).

Size exclusion chromatography.

SEC-RI/Viscosimeter in THF was performed using a Waters e2695 Separations Module equipped with a Waters 2414 RI Detector thermostated at 35 °C, a 100 mL injection loop and a set of 3 Shodex columns (K-804L, K-802.5 and K-G) thermostated at 40 °C. A calibration was performed using poly(styrene) standards (Varian) ranging from 580 to 295 800 $g.mol^{-1}$. Flow rate was 1 $mL.min^{-1}$ and toluene was used as a flow marker. Prior to injections, samples were diluted at a concentration of 10 $g.L^{-1}$ overnight and filtered through a 0.45 mm PTFE filter. Data were handled with the Wyatt Astra 5.3.4.14 software.

SEC-RI/UV in THF was performed using a 100 mL injection loop, a set of two Styragel columns (HR4E, HR1 columns) and a Shodex precolumn thermostated at 55 °C. The detectors were a Waters 410 differential refractometer thermostated at 40 °C and a Waters 2489 UV/Visible detector thermostated at 40°C and set at a wavelength value of 290 nm. A calibration was performed using poly(styrene) standards (Varian) ranging from 580 to 295 800 $g\ mol^{-1}$. Flow rate was 1 $mL\ min^{-1}$ and toluene was used as a flow marker. Prior to injections, samples were diluted at a concentration of 10 $g\ L^{-1}$, stirred overnight and filtered through a 0.45 mm PTFE filter.

SEC in DMF containing 10 mM of LiBr was performed using a 100 mL injection loop, a set of three Shodex columns (K-805L, KD-802 and KD-G columns) thermostated at 55 °C, a Waters 410 differential refractometer thermostated at 40 °C and Waters 2489 UV/Visible detector thermostated at 40°C and set at a wavelength value of 290 nm. A calibration was performed using poly(methyl methacrylate) standards (Varian) ranging from 875 to 298 900 $g.mol^{-1}$. Flow rate was 1 $mL\ min^{-1}$ and toluene was used as a flow marker. Prior to injections, samples were diluted at a concentration of 10 $g.L^{-1}$, stirred overnight and filtered through a 0.45 mm PTFE filter.

Differential scanning calorimetry.

DSC measurements were performed with a Mettler-Toledo DSC Star System apparatus under a nitrogen atmosphere at a heating rate of 10 $°C.min^{-1}$ and a cooling rate of 10 $°C.min^{-1}$. In a typical procedure, 5–8 mg of samples were weighed in a 40 mL aluminium crucible with a high precision balance and sealed with a perforated lid. Glass transition temperature was measured as the temperature of inflexion mid-

point on heating.

Cloud points measurements in supercritical carbon dioxide.

The cloud points were obtained using a high pressure phase equilibrium apparatus (Top Industrie, France). This high-pressure unit is composed of a variable volume view cell (from 9.6 cm^3 to 31.3 cm^3) equipped with 3 sapphire windows and a magnetic stirrer. The temperature of the cell was maintained at 40 °C by a thermostated bath. Temperature was measured by a thermocouple (J type, precision of ± 0.1 K) placed in the centre of the cell. Pressure was measured using a pressure transducer (Keller) equipped with a pressure numerical display. Phase transitions were filmed with a camera and observed on a video screen. In a typical experiment, 40 mg of the studied sample was weighed with a high precision balance and transferred into the main chamber of the cell. The cell was sealed and heated to 40 °C. CO_2 (20.0 g) was injected into the cell by an automatic syringe pump (260D, Teledyne ISCO, USA) thermostated at 2 °C. The polymer-CO_2 solution was pressurized at 350 bar and equilibrated under stirring for 30 min. The cloud points were observed by slowly lowering the pressure inside the cell. The cloud point pressure was defined as the point at which it was no longer possible to see the back of the cell through the CO_2/polymer mixture. At least three repeated measurements were performed to determine the cloud point pressure. Standards deviations were typically within +/- 3 bar. Repeatability was within +/- 5 bar.

Infrared spectroscopy in supercritical carbon dioxide.

The materials and methods used to determine the solubility of copolymers in sc-CO_2 by infrared spectroscopy were described in Chapter 2.

Computational Methods

The computational calculations were performed at the “Pôle Modélisation” of the “Institut des Sciences Moléculaires” and the MCIA (Mésocentre de Calcul Intensif Aquitain, DRIMM, Université de Bordeaux 1).

Preliminary geometry optimizations were carried out using a semi empirical model (AM1)[2] to determine the most stable conformations for the model compounds and their complexes with CO_2. These semi-empirical calculations were carried out using the AMPAC software.[3] The lowest energy conformers obtained at the AM1 level

were further investigated using the density functional theory (DFT) implemented in the Gaussian 2009 package.[4] DFT calculations of geometry, energies, and vibrational frequencies reported in this paper were carried out with the CAM-B3LYP[5] functional using the augmented correlation-consistent polarized Valence Double basis sets (aug-cc-pVDZ) proposed by Dunning and co-workers.[6-9] Geometry computations were not subjected to a particular symmetry constraint, except for isolated CO_2 ($D_{\infty h}$ symmetry). Stabilization energies of the model compounds $-CO_2$ complexes investigated in this paper were calculated using the "supermolecule" method as the difference in energy between each complex and the sum of the isolated model compounds. The calculated stabilization energies were corrected for the basis set superposition errors (BSSE) using the full counter-poise method[10] and the Zero Point Energy contribution. Finally, the atomic charge distribution was calculated in the model NBO/NPA (Natural Bond Orbital, Natural Population Analysis)[11] which is recognized to better account for the charge distribution than standard methods like that initially proposed by Mulliken.

Sessile Drop Experiments

A 10 % wt solution of polymer in 2-butanone was prepared and filtered through a 0.2 mm PTFE filter. A drop of this solution was deposited onto a round glass substrate. The substrate was then spin-coated at a constant spinning rate of 2000 rpm for 60 s. Water contact angle measurements were performed with a sessile drop tensiometer (KRUSS GmbH, model DSA 10-MK2, Germany) at room temperature. The size and shape of an ultra-pure water drop (resistivity = 18.2 $M\Omega.cm^{-1}$) deposited at the surface of the coated substrate was analyzed by the Drop Shape Analysis software. Measurements for each compound were performed the same day and repeated six times.

Chapter 4

Materials

VDF (or 1,1-difluoroethylene) and 1,1,1,3,3-pentafluorobutane were kindly offered by Solvay S.A. (Tavaux, France, and Brussels, Belgium). Perfluoro(methyl vinyl ether) (PMVE) was kindly offered by Dupont Performance Elastomer. Tert-butyl peroxypivalate (tBPPi, 75% in isododecane) were gifts from Akzo Nobel (Chalons sur Marne, France). They were used as supplied. N,N-dimethylacrylamide (DMA, Aldrich, 99%) and ethyl acetate (Fischer Scientific, Laboratory reagent grade) were distilled on CaH_2. 2,2-Azobisisobutyronitrile (AIBN, Acros Organics, 98%) was recrystallized twice from methanol and dried under vacuum. RAFT/MADIX agent (2-mercaptopropionic acid methyl ester O-ethyl dithiocarbonate, Rhodixan A1) was obtained from Rhodia and used as received. N,N-dimethylformamide (DMF, Sigma-Aldrich, Chromasolv Plus for HPLC, >99.9%), tetrahydrofuran (THF for preparative HPLC, stabilized with BHT, SDS), 2-butanone (Sigma-Aldrich, ACS reagent, >99.0%), pentane (Sigma-Aldrich, reagent grade, 98.0%), lithium bromide (Aldrich, 99+%), sodium iodide (NaI, Aldrich, >99.99 % trace metal basis), 2,5-dihydroxybenzoic acid (DHB, Fluka, matrix substance for MALDI-MS, >99.5 % (HPLC), Ultra Pure), 1,1,2,2-tetrafluoro-3-iodopropane (Aldrich, 98 %) and potassium ethyl xanthogenate (Aldrich, 97 %) were used as received.

RAFT/MADIX polymerization of vinylidene fluoride

A 100-mL Hastelloy autoclave equipped with inlet and outlet valves, a manometer and a rupture disc was degassed and pressurized with 30 bar of nitrogen to check the absence of potential leaks. Then, a 20 mm Hg vacuum was operated for 30 min. A pre-degassed solution of tert-butyl peroxypivalate (1.21 g, $5.2.10^{-3}$ mol), Rhodixan A1 (1.085 g, $5.2.10^{-3}$ mol) in 1,1,1,3,3-pentafluorobutane (65 mL) was degassed with N_2 for 20 minutes and transferred under vacuum into the autoclave. The autoclave was cooled down to -65 °C with acetone ice. VDF (10 g, 0.156 mol) was then introduced and the introduced amount was estimated by double weighing. Then, the autoclave was progressively heated to 74 °C while the pressure increased to 15 bar in the meantime. After 4 hours of reaction, the autoclave was placed in an ice bath for 60 minutes and 1.20 g of unreacted VDF were progressively released. After

opening the autoclave, a milky mixture was obtained. After evaporation of 1,1,1,3,3-pentafluorobutane, the sample was dissolved in DMF and precipitated by adding water into the DMF solution. A white powder was obtained and dried under vacuum. A gravimetric yield of 80 % was obtained. The sample was characterized by ^{19}F and ^{1}H NMR spectroscopy in DMF-d_7 and by SEC in DMF. ($M_{n,theo}$=1750 g.mol^{-1}, $M_{n,SEC=}$ 6200 g.mol^{-1}, Đ = 1.30).

RAFT/MADIX copolymerization of vinylidene fluoride and perfluoromethyl vinyl ether

A 100-mL Hastelloy autoclave that was equipped with inlet and outlet valves, a manometer and a rupture disc was degassed and pressurized with 30 bar of nitrogen to check the absence of potential leaks. Then, a 20 mm Hg vacuum was operated for 30 min. A solution of tert-butyl peroxypivalate (1.27 g, 5.5.10^{-3} mol), Rhodixan A1 (1.145 g, 5.5.10^{-3} mol) in 1,1,1,3,3-pentafluorobutane (65 mL) was degassed with N_2 for 20 minutes and transferred under vacuum into the autoclave. The autoclave was cooled down to -65 °C with acetone ice. PMVE (7 g, 4.2.10^{-2} mol) and then VDF (5 g, 7.8.10^{-2} mol) were introduced. The total introduced amount of monomers was estimated by double weighing. Then, the autoclave was progressively heated to 74 °C while the pressure increased to 7 bar in the meantime. After 4 hours of reaction, the autoclave was placed in an ice bath for 60 minutes and 0.8 g of unreacted monomers was progressively released. After opening the autoclave, a clear solution was obtained. A viscous oil was then obtained after evaporation of 1,1,1,3,3-pentafluorobutane and dried under vacuum. A gravimetric yield of 85 % was obtained. The sample was characterized by ^{19}F and ^{1}H NMR spectroscopy in acetone-d_6 and by SEC in DMF and THF. ($M_{n,theo}$=1850 g.mol^{-1}, $M_{n,SEC=}$ 3700 g.mol^{-1}, Đ = 1.26).

RAFT/MADIX synthesis of PDMA macro-chain transfer agents

In a typical experiment, a mixture of N,N-dimethylacrylamide(1.62 g, 1.63 mmol), AIBN (4 mg, 0.024 mmol) and Rhodixan A1(166 mg, 0.8 mmol) in ethyl acetate (7.2 g) was degassed by four freeze–pump–thaw cycles, backfilled with argon, sealed and placed in an oil bath at 60 °C. After 15h, the reaction was stopped by cooling in liquid nitrogen. Conversion was determined by ^{1}H NMR in $CDCl_3$. The polymer was dried in vacuo. The sample was characterized by ^{1}H NMR spectroscopy

in $CDCl_3$ and by SEC in DMF. ($M_{n,theo}$=1000 g.mol^{-1}, $M_{n,SEC=}$ 750 g.mol^{-1}, Đ = 1.56). This

Synthesis of 1,1,2,2-tetrafluoro-3-(O-ethyl dithiocarbonate)propane

Potassium ethyl xanthogenate (3.20 g, 19.4 mmol, 1.1 eq.) was slowly added under stirring at room temperature to a solution of 1,1,2,2-tetrafluoro-3-iodopropane (4.5 g, 17.6 mmol, 1 eq.) in acetone (60 mL). The reaction mixture was stirred overnight. After acetone was removed with a rotary evaporator and the product was diluted with diethyl ether (100 mL) and washed three times with water (30 mL). The organic phase was collected and dried overnight on $MgSO_4$. Diethyl ether was removed with a rotary evaporator to give 1,1,2,2-tetrafluoro-3-(O-ethyl dithiocarbonate)propane (3.05 g, 73 %) as a red liquid. ^{1}H NMR (300 MHz, acetone-d_6): δ (ppm) = 6.38 (tt, 1H, $^2J_{HF}$ = 52.8 Hz), 4.72 (q, 2H, $^3J_{HH}$ = 7.2 Hz), 4.03 (t, 2H, $^3J_{HF}$ = 17.4 Hz), 1.44 (t, 3H, $^3J_{HH}$ = 7.2 Hz). ^{13}C NMR (300 MHz, acetone-d_6): δ (ppm) = 216.8 (s, S*C*(=S)), 107–115 (m, fluorinated carbon atoms), 67.1 (s, O-*C*H$_2$-C), 29.0 (t, S-CH$_2$-CF$_2$), 16.6 (s,*C*H$_3$-C). ^{19}F NMR (300 MHz, acetone-d_6): δ (ppm) = -116.7 (tq, 2F, HCF$_2$-C*F*$_2$-CH$_2$, $^3J_{HF}$ = 18.0 Hz, $^3J_{FF}$ = 54.0 Hz), -137.6 (d, 2F, HC*F*$_2$-CF$_2$, $^2J_{HF}$ = 54.0 Hz). GC-MS: accurate mass: 237.0 amu (theoretical mass of $C_6H_8S_2OF_4$ = 236.2 amu).

Characterization techniques

NMR measurements

^{1}H NMR and ^{19}F NMR spectra were recorded with a Bruker AMX 300 apparatus. All spectra were referenced to the solvent residual peak (chloroform at 7.26 ppm, acetone at 2.05 ppm or DMF at 8.01 ppm).

Size exclusion chromatography

SEC in THF was performed using a Waters e2695 Separations Module equipped with a Waters 2414 RI Detector thermostated at 35 °C, a 100 mL injection loop and a set of 3 Shodex columns (K-804L, K-802.5 and K-G) thermostated at 40 °C. A calibration was performed using poly(styrene) standards (Varian) ranging from 580 to 295 800 g mol^{-1}. Flow rate was 1 mL.min^{-1} and toluene was used as a flow marker. Prior to injections, samples were diluted at a concentration of 10 g.L^{-1}

overnight and filtered through a 0.45 mm PTFE filter. Data were handled with the Wyatt Astra 5.3.4.14 software.

SEC in DMF containing 10 mM of LiBr was performed using a 100 mL injection loop and a set of three Shodex columns (K-805L and KD-802 and KD-G columns) thermostated at 55 °C. The detectors were a Waters 410 differential refractometer thermostated at 40 °C and a Waters 2489 UV/Visible detector thermostated at 40°C and set at a wavelength value of 290 nm. A calibration was performed using poly(methyl methacrylate) standards (Varian) ranging from 875 to 298 900 g mol^{-1}. Flow rate was 1 mL min^{-1} and toluene was used as a flow marker. Prior to injections, samples were diluted at a concentration of 10 g L^{-1}, stirred overnight and filtered through a 0.45 mm PTFE filter.

MALDI-TOF mass spectrometry

MALDI-TOF MS measurements were performed on an applied Biosystems Voyager System 4243. Positive-ion spectra and acquired in the reflectron mode. The matrix was DHB and NaI was used as a cationization agent for the PVDF samples. Concerning the P(VDF-co-PMVE) sample, the matrix and the salt were pentaflurobenzaldehyde and NaI. In both cases, the polymer sample, the matrix and the salt were dissolved in acetone and premixed in a 1:1:3 ratio, respectively.

Differential scanning calorimetry

DSC measurements were performed with a Mettler-Toledo DSC Star System apparatus under a nitrogen atmosphere at a heating rate of 10 °C.min^{-1} and a cooling rate of 2 °C.min^{-1}. In a typical procedure, 5–8 mg of samples were weighed in a 40 mL aluminium crucible with a high precision balance and sealed with a perforated lid. Glass transition temperature was measured as the temperature of inflexion mid-point on cooling.

Solubility measurements in supercritical carbon dioxide.

The materials and methods used to determine the solubility of copolymers in sc-CO_2 by either cloud point measurements or infrared spectroscopy were respectively described in Chapter 3 and Chapter 2. A path length of 4.70 mm was used for IR experiments.

References

(1) M. J. S. Dewar, E. G. Zoebisch, E. F. Healy and J. J. P. Stewart, *J. Am. Chem. Soc.*, **1985**, *107*, 3902.
(2) AMPAC 8, r 1992–2004 Semichem, Inc. PO Box 1649, Shawnee, KS 66222.
(3) M. J. Frisch, G. W. Trucks, H. B. Schlegel, G. E. Scuseria,M. A. Robb, J. R. Cheeseman, G. Scalmani, V. Barone, B. Mennucci, G. A. Petersson, H. Nakatsuji, M. Caricato, X. Li, H. P. Hratchian, A. F. Izmaylov, J. Bloino, G. Zheng, J. L. Sonnenberg, M. Hada, M. Ehara, K. Toyota, R. Fukuda, J. Hasegawa, M. Ishida, T. Nakajima, Y. Honda, O. Kitao, H. Nakai, T. Vreven, J. A. Maaaaaa Jr, J. E. Peralta, F. Ogliaro, M. Bearpark, J. J. Heyd, E. Brothers, K. N. Kudin, V. N. Staroverov, R. Kobayashi, J. Normand, K. Raghavachari, A. Rendell, J. C. Burant, S. S. Iyengar, J. Tomasi, M. Cossi, N. Rega, J. M. Millam, M. Klene, J. E. Knox, J. B. Cross, V. Bakken, C. Adamo, J. Jaramillo, R. Gomperts, R. E. Stratmann, O. Yazyev, A. J. Austin, R. Cammi, C. Pomelli, J. W. Ochterski, R. L. Martin, K. Morokuma, V. G. Zakrzewski, G. A. Voth, P. Salvador, J. J. Dannenberg, S. Dapprich, A. D. Daniels, O. Farkas, J. B. Foresman, J. V. Ortiz, J. Cioslowski and D. J. Fox, Gaussian 09, Revision A.2, Gaussian Inc., Wallingford CT, **2009**.
(4) T. Yanai, D. P. Tew and N. C. Handy, *Chem. Phys. Lett.*, **2004**, *393*, 51.
(5) T. H. Dunning, *J. Chem. Phys.*, **1989**, *90*, 1007.
(6) A. K. Wilson, T. V. Mourik and T. H. Dunning, *J. Mol. Struct.*, **1996**, *388*, 339.
(7) H. Tatewaki and S. Huzinaga, *J. Comput. Chem.*, **1980**, *3*, 205.
(8) R. A. Kendall, T. H. Dunning and R. J. Harrison, *J. Chem. Phys.*,**1992**, *96*, 6796.
(9) S. F. Boys and F. Bernardi, *Mol. Phys.*, **1970**, *19*, 553.
(10) A. E. Reed, R. B. Weinstock and F. Weinhold, *J. Chem. Phys.*, **1985**, *83*, 735.

Appendix

Chapter 2

A. ^{1}H NMR spectrum of a PDMA polymer synthesized by RAFT/MADIX polymerization

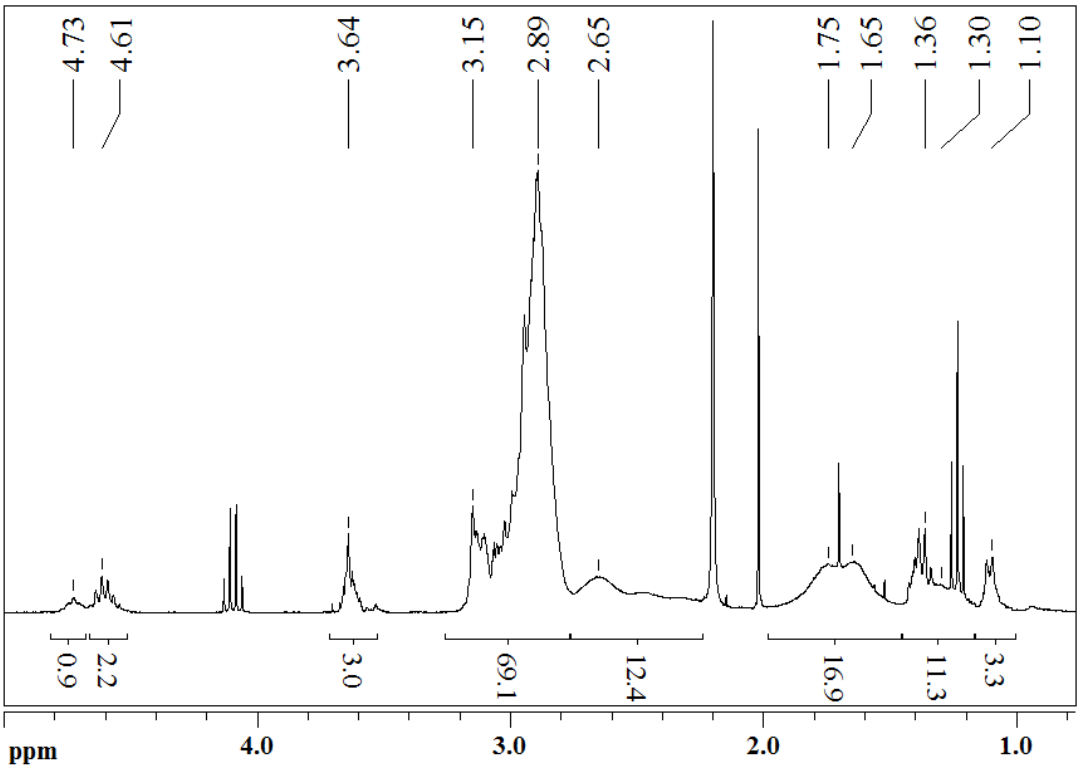

Figure A.II.1. ^{1}H NMR spectrum of a PDMA$_{0.8k}$-Xa synthesized by RAFT/MADIX polymerization.

Chemical shift (ppm)	Assignment
1.10	CH_3-O-(C=O)-CH(-C*H*$_3$)-CH_2-CH(CON(CH_3)$_2$)-
1.36	-S-(C=S)-O-CH_2-C*H*$_3$
1.20 - 2.0	-(C*H*$_2$-CH(-CON(CH_3)$_2$))-
2.2 – 2.8	-(CH_2-C*H*(-CON(CH_3)$_2$))-
2.8 – 3.15	-(CH_2-CH(-CON(C*H*$_3$)$_2$))-
3.64	C*H*$_3$-O-(C=O)-CH(-CH_3)-CH_2-CH(CON(CH_3)$_2$)-
4.61	-S-(C=S)-O-C*H*$_2$-CH_3
4.73	-CH_2-C*H*(CON(CH_3)$_2$)-S-(C=S)-O-CH_2-CH_3

Table A.II.1. Peak assignments for the ^{1}H NMR spectrum of a PDMA$_{0.8k}$-Xa synthesized by RAFT/MADIX polymerization (Figure A.II.1).

B. ^{1}H NMR spectrum of PDMA-*b*-PVAc copolymers synthesized by RAFT/MADIX polymerization

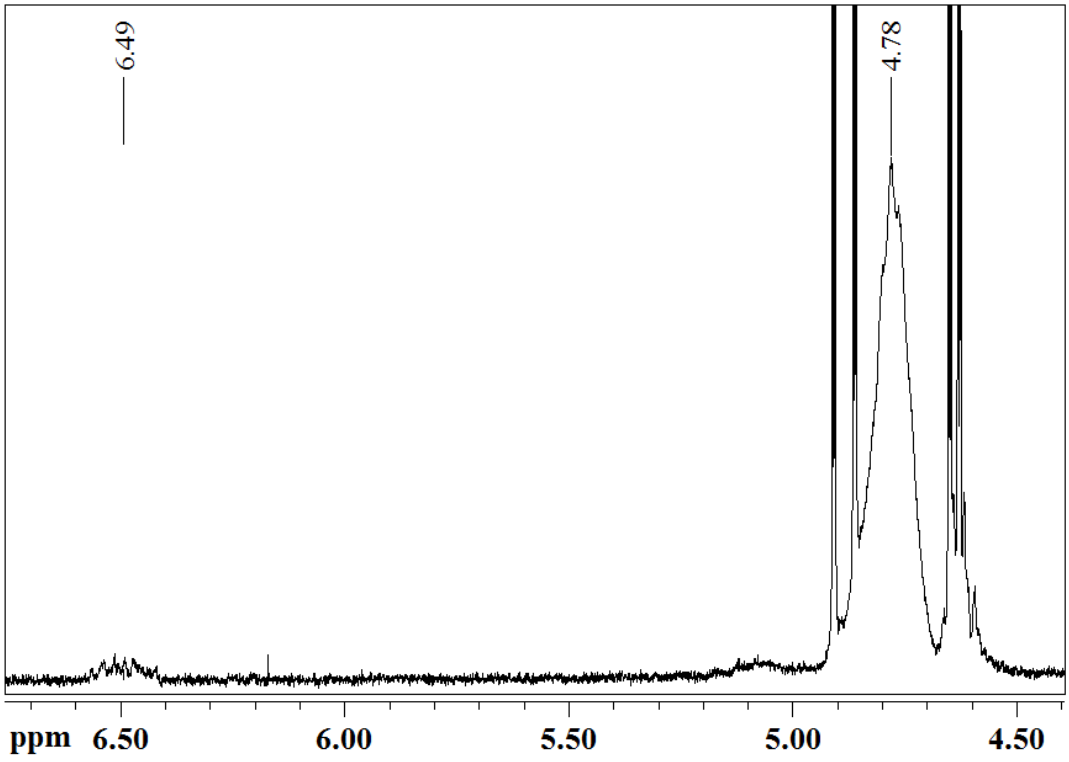

Figure A.II.2. Enlargement of the 4.50-6.50 ppm region for a ^{1}H NMR spectrum of a $PDMA_{2k}$-*b*-$PVAc_{1.9k}$ copolymer.

Chemical shift (ppm)	Assignment
4.60	-S-(C=S)-O-CH_2-CH_3
4.78	-(CH_2-CH(-O-(C=O)-CH_3)-
4.90	-(CH_2-CH(-O-(C=O)-CH_3)-
6.49	-(CH_2-CH(-O-(C=O)-CH_3)-S-(C=S)-OEt

Table A.II.1. Peak assignments for the ^{1}H NMR spectrum of a $PDMA_{2k}$-*b*-$PVAc_{1.9k}$ synthesized by RAFT/MADIX polymerization (Figure A.II.2).

Chapter 3

A. Calculation of $M_{n,theo}$ and $M_{n,NMR}$ for a poly(vinyl trifluoroacetate) sample

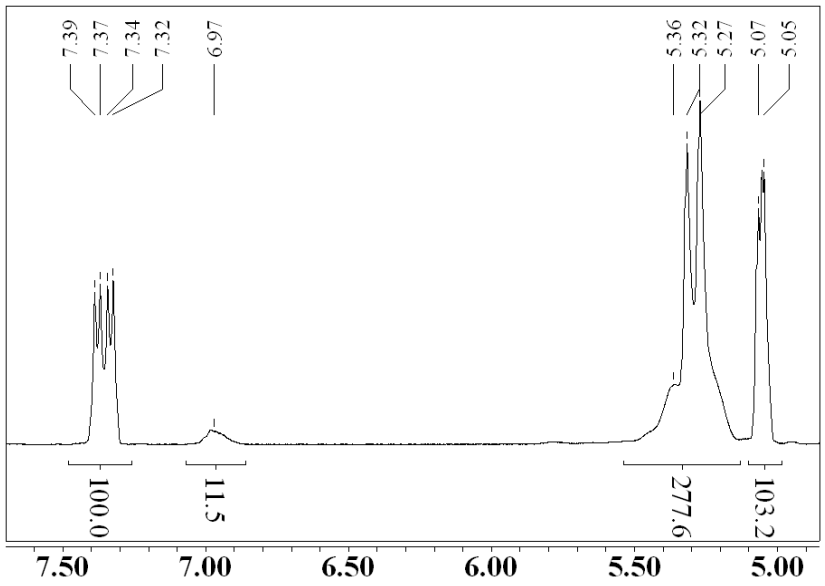

Figure A.III.1. Expansion in the 5.00-7.50 ppm region of a ^{1}H NMR spectrum of a crude poly(vinyl trifluoroacetate) sample (run 1 in Table III.1).

Chemical shift (ppm)	Assignment
5.06	C*H*$_2$=CH-C(=O)-O-CF$_3$ (monomer)
5.29	CH$_2$=C*H*-C(=O)-O-CF$_3$ (monomer)
5.36	-(CH$_2$-C*H*-C(=O)-O-CF$_3$)- (polymer)
6.97	-(CH$_2$-C*H*-C(=O)-O-CF$_3$)-S-C(=S)-O-CH$_2$-CH$_3$ (polymer chain end)
7.36	C*H*$_2$=CH-C(=O)-O-CF$_3$ (monomer)

Table A.III.1. Assignments of ^{1}H NMR signals for a poly(vinyl trifluoroacetate) synthesized by RAFT/MADIX polymerization (Run 1 of Table III.1 and Figure A.III.1).

Knowing the characteristic chemical shifts of vinyl trifluoroacetate (5.29 and 7.36 ppm) and of poly(vinyl trifluoroacetate) monomer unit (5.36 ppm), the conversion could be determined:

$$\textbf{Conversion} = \frac{\int_{5.36+5.29}^{\text{polymer+monomer}} CH - \int_{7.36}^{\text{monomer}} CH2}{\int_{5.36+5.29}^{\text{polymer+monomer}} CH} * 100 = 65\ \%$$

And then:

$$\textbf{Mn, theo} = \text{Conversion} * \frac{[\text{Vinyl trifluoroacetate}](t=0) * \text{MW(Vinyl trifluoroacetate)}}{[\text{RAFT MADIX Agent}](t=0)} + \text{MW(RAFT MADIX Agent)}$$

$$= 2300\ \text{g/mol}$$

From the characteristic signal (6.97 ppm) of a poly(vinyl trifluoroacetate) monomer unit located at the alpha position to the xanthate moiety, the number-average polymerization degree ($DP_{n,NMR}$) was assessed from the following formula:

$$\textbf{DPn, NMR} = \frac{[\int_{\mathbf{5.36+5.29}}^{\mathbf{polymer+monomer}} \boldsymbol{CH} - \int_{\mathbf{7.36}}^{\mathbf{monomer}} \boldsymbol{CH2}] + \int_{\mathbf{6.97}}^{\mathbf{polymer}} \boldsymbol{CH}}{\int_{\mathbf{6.97}}^{\mathbf{polymer}} \boldsymbol{CH}} = \mathbf{16.4}$$

and then:

$$\textbf{Mn, NMR} = \text{DPn, NMR} * \text{MW (Vinyl Trifluoroacetate)} + \text{MW(RAFT MADIX Agent)}$$

$$= 2500\ \text{g/mol}$$

B. P(VAc-*stat*-CF_3VAc) copolymers

1. ^{1}H NMR spectrum of crude poly(VAc-*stat*-CF_3VAc) copolymers

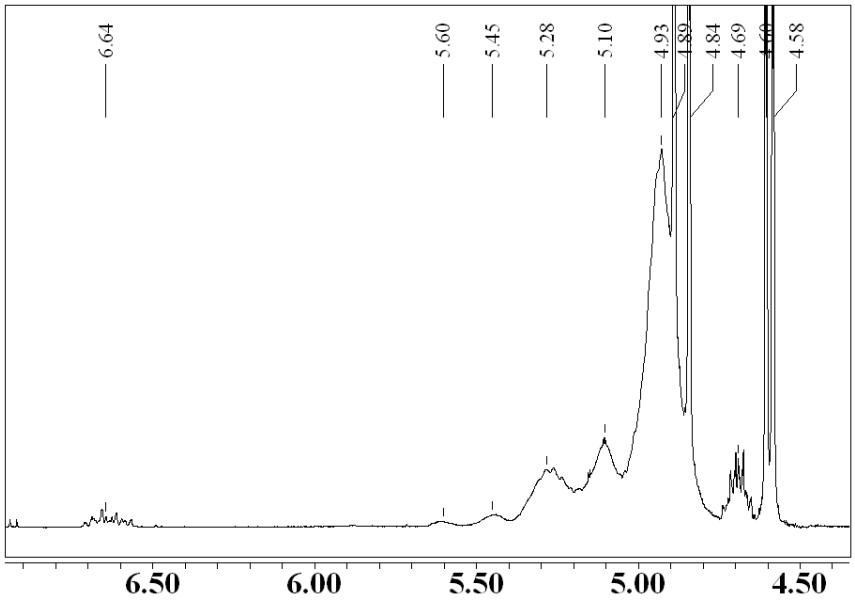

Figure A.III.2. Enlargement of the 4.50-7.00 ppm region of a ^{1}H NMR spectrum of a crude poly(VAc-*stat*-CF_3VAc) sample (run 6 of Table III.).

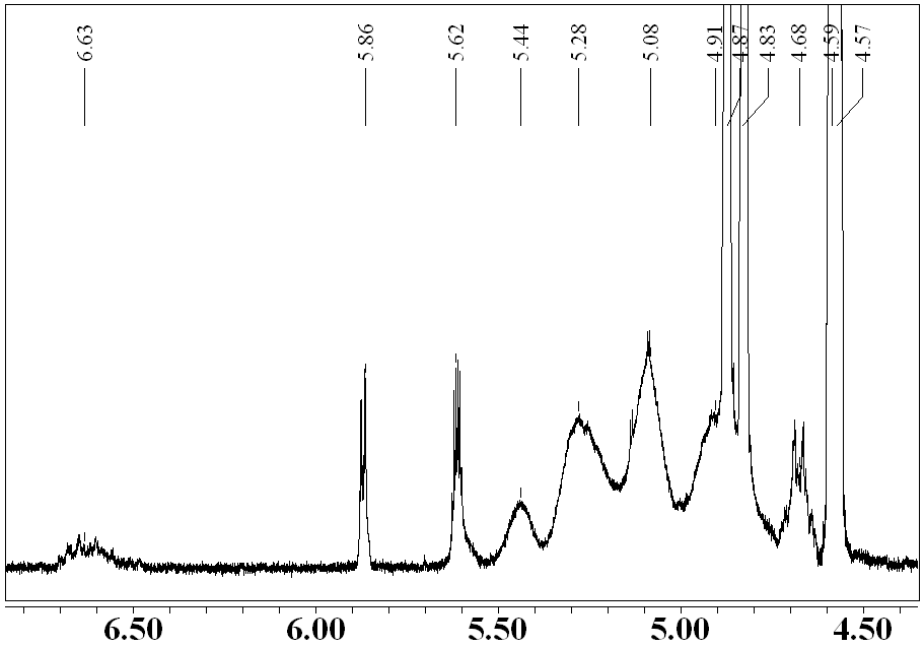

Figure A.III.3. Enlargement of the 4.50-7.00 ppm region of a ^{1}H NMR spectrum of a crude poly(VAc-*stat*-CF_3VAc) sample (run 3 of Table 1)

Chemical shift (ppm)	Assignment
4.58 - 4.60	C***H₂***=CH-C(=O)-O-CH_3 (monomer)
4.69	-S-C(=S)-O-C***H₂***-CH_3
4.84 - 4.89	CH_2=C***H***-C(=O)-O-CH_3 (monomer)
4.93 - 5.60	-(CH_2-C***H***-C(=O)-O-CH_3)-(polymer, VAc units)
5.62 – 5.86	C***H₂***=C-(CF_3)-C(=O)-O-CH_3 (monomer)
6.64	-(CH_2-C***H***-C(=O)-O-CH_3)-S-C(=S)-O-CH_2-CH_3 (polymer chain end)

Table A.III.2. Assignments of ^{1}H NMR signals for poly(VAc-*stat*-CF_3VAc) copolymers synthesized by RAFT/MADIX polymerization (Figures A.III.2 and A.III.3).

2. Additional computational results on the ester side of model structures

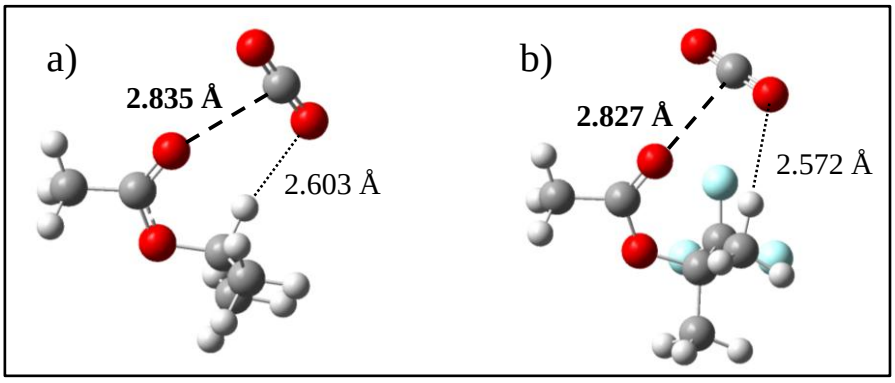

Figure A.III.4. Optimized structures (CAM-B3LYP/aug-cc-pVDZ) for the ester side of the configuration of a) the isopropyl acetate-CO_2 complex and b) the 1,1,1-trifluoropropan-2-yl acetate- CO_2 complex.

	$\Delta E_{cor\ BSSE+ZPE}$ (kcal.mol^{-1})	$d_{(C\cdots O)}$ (Å)	$d_{(O\cdots H)}$ (Å)	q_O (e)
iPrAc-CO_2	-1.92	2.835	2.603	-0.78
TFiPrVAc-CO_2	-1.89	2.827	2.572	-0.76

Table A.III.3. Basis set superposition errors and zero point energy corrected interaction energies (ΔE_{cor}) - Intermolecular $d_{(C\cdots O)}$ and $d_{(O\cdots H)}$ distance for the acetate-CO_2 complexes calculated at the CAM-B3LYP level using the aug-cc-pVDZ basis sets - Charge on the oxygen atom of the isolated acetate molecule (q_O).

Chapter IV

A. ^{19}F NMR spectrum of a PVDF synthesized by RAFT/MADIX polymerization and initiated by tBPPi

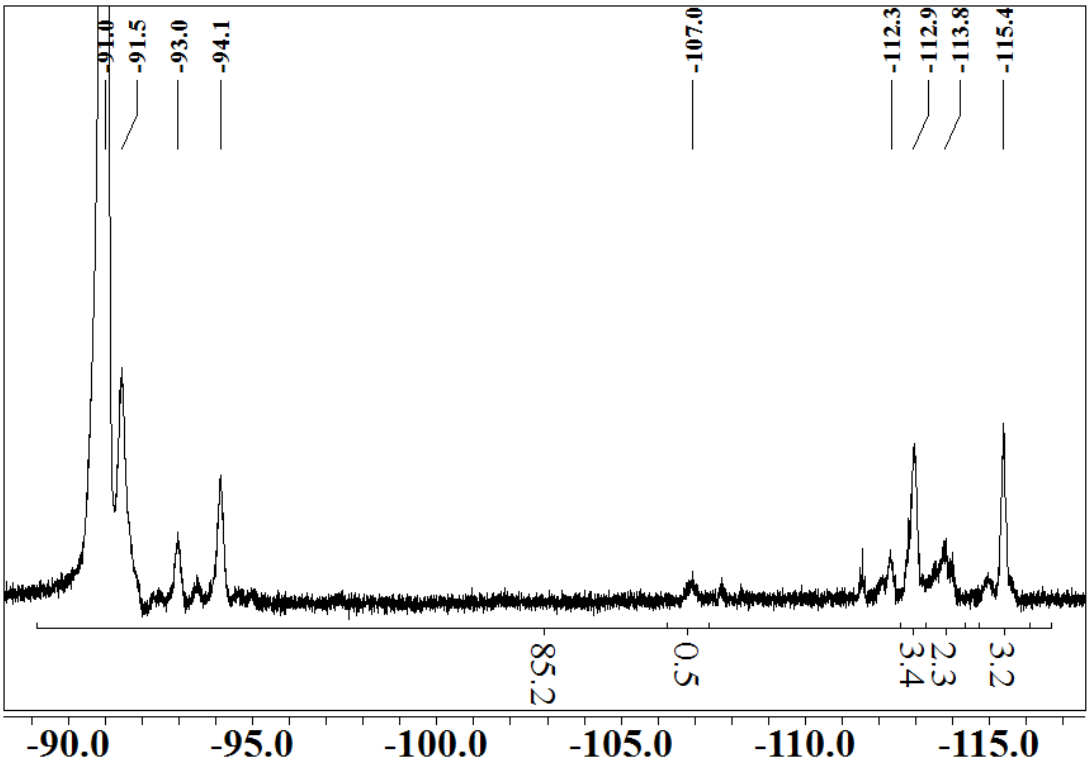

Figure A.IV.1. ^{19}F NMR spectrum of a PVDF synthesized by RAFT/MADIX polymerization (run 5 of Table IV.3).

Chemical shift (ppm)	Assignment
-91.0	$-CF_2-CH_2C\boldsymbol{F_2}-CH_2CF_2-CH_2$
-91.5	$-CH_2C\boldsymbol{F_2}-CH_2CF_2-\ CF_2CH_2-$
-93.0	$CH_3-O-C(=O)-CH(-CH_3)-CH_2C\boldsymbol{F_2}-$
-94.1	$-CF_2CH_2-CH_2C\boldsymbol{F_2}-CH_2$
-112.3	$(CH_3)_3C-C\boldsymbol{F_2}CH_2-$
-112.9	$CH_3-O-C(=O)-CH(-CH_3)-C\boldsymbol{F_2}CH_2-$
-113.8	$-CH_2C\boldsymbol{F_2}-CF_2CH_2-CH_2CF_2-$
-115.4	$-CH_2CF_2-C\boldsymbol{F_2}CH_2-CH_2-$

Table A.IV.1. Assignments of ^{19}F NMR signals for a PVDF polymer synthesized by RAFT/MADIX polymerization (Run 5 of Table IV.3).

B. Determination of the fraction of head-to-head and tail-to-tail additions for PVDF homopolymers

The rate of head-to-head inverted adducts (%HH) could be measured through ^{19}F NMR measurements. The following formula was used:

$$\%HH = \frac{\int_{-112.9} CF2 + \int_{-115.4} CF2}{\int_{-116}^{-91} CF2} \times 100$$

C. NMR analysis of P(VDF-*co*-PMVE) copolymers

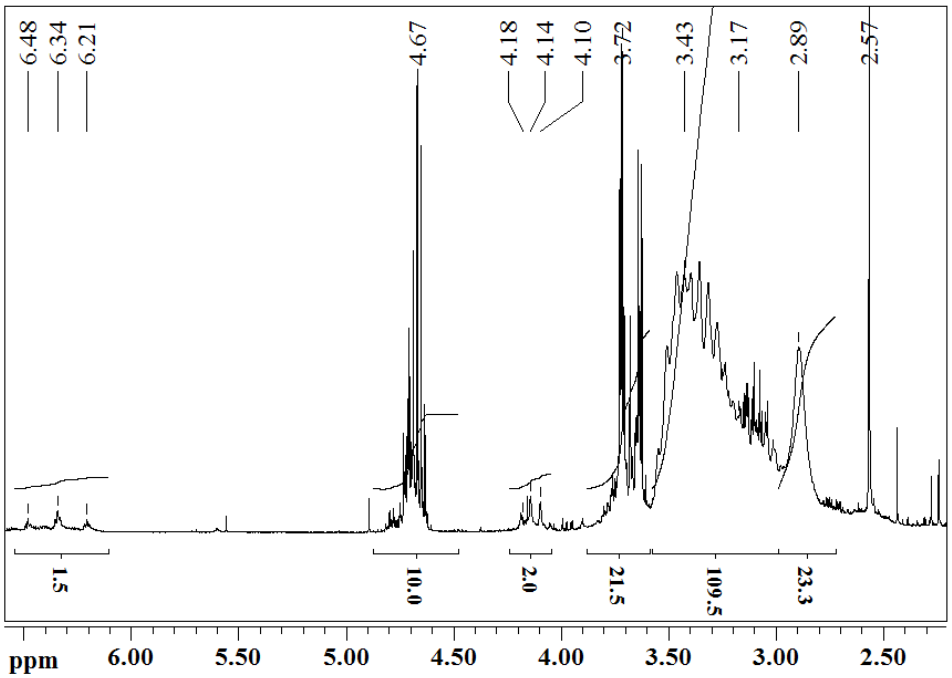

Figure A.IV.2. ^{1}H NMR spectrum of a P(VDF-*co*-PMVE) copolymer (run 9 of Table IV.6).

Chemical shift (ppm)	Assignment
3.0 – 3.6	-CH_2CF_2-C***H***$_2CF_2$-CH_2CF_2-
3.72	-S-C(=S)-O-C***H₂***-CH_3
4.14 (t, $^3J_{HF}$ = 12.4 Hz)	-CH_2CF_2-CF_2C***H₂***-S-(C=S)-OEt
4.67 (q, $^3J_{HF}$ = 5.4 Hz)	-CH_2CF_2-C***H₂***CF_2-S-(C=S)-OEt (supposed)
6.34 (t, $^2J_{HF}$ = 41.1 Hz))	-CH_2CF_2-CH_2F_2-***H***

Table A.IV.2. Assignments of ^{1}H NMR signals for a P(VDF-*co*-PMVE) copolymer synthesized by RAFT/MADIX polymerization (Run 9 of Table IV.6 and Figure A.IV.2).

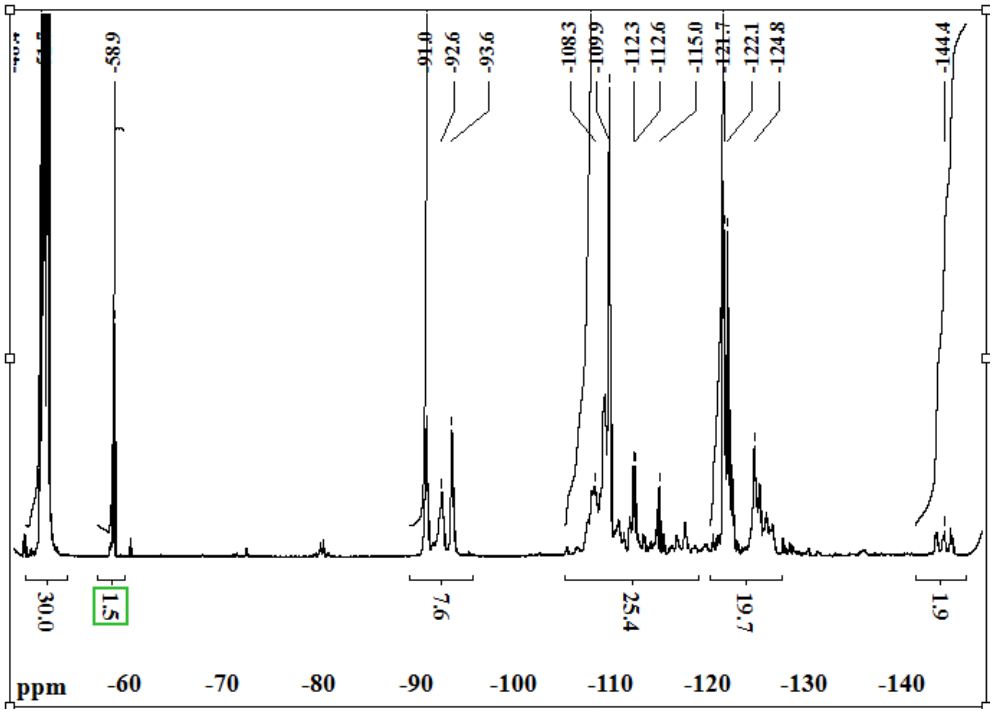

Figure A.IV.3. ^{19}F NMR spectrum of a P(VDF-*co*-PMVE) copolymer (run 9 of Table IV.6).

Chemical shift (ppm)	Assignment
-51.7	-O-C***F₃***
-58.9	Non attributed
-91.0	-CH_2-CF_2-CH_2C***F₂***-CH_2CF_2-
-92.6	$(CH_3)_3$-CH_2**CF_2**-
-93.6	CH_3-O-C(=O)-CH(-CH_3)-CH_2C***F₂***-
-109.3	-CH_2C***F₂***-CF_2CF(-OCF_3)-
-112.3	CH_3-O-C(=O)-CH(-CH_3)-C***F₂***CH_2-
-112.6	-CH_2C***F₂***-CF_2CH_2-CH_2CF_2-
-115.0	-CH_2CF_2-C***F₂***CH_2-CH_2CF_2-
-122.1	-CH_2CF_2-C***F₂***CF(-OCF_3)-
-124.8	-CH_2CF_2-C***F₂***CF(-OCF_3)-CF_2CH_2-
-144.4	-CH_2CF_2-CF_2C***F***(-OCF_3)-CF_2CH_2-

Table A.IV.3. Assignments of ^1H NMR signals for a P(VDF-*co*-PMVE) copolymer synthesized by RAFT/MADIX polymerization (Run 9 of Table IV.6 and Figure A.IV.2).

Résumé de thèse

Introduction

Dans le cadre du durcissement des réglementations quant à l'utilisation et à l'émission des produits chimiques dangereux pour la santé et l'environnement, les fluides supercritiques représentent une alternative crédible et verte pour supplanter les solvants organiques usuels et diminuer les émissions de carbone organique volatil (COV). En particulier, l'utilisation du dioxyde de carbone à l'état supercritique (sc-CO_2) est particulièrement avantageuse en raison de son abondance et de son caractère non-toxique, biocompatible et recyclable. De plus, le CO_2 est supercritique dans des conditions relativement modérées (T = 31 °C, P = 73,8 bar). Cependant, une large majorité de catalyseurs, de polymères et, plus généralement, de composés polaires et ioniques est très peu soluble dans le CO_2, du fait de son caractère apolaire et de sa faible constante diélectrique. Ceci limite donc fortement les champs d'applications du CO_2 supercritique. La formation et la stabilisation d'émulsions pourraient être considérées comme un moyen universel de disperser des composés polaires ou ioniques dans une phase continue de CO_2. La stabilisation d'émulsions, de miniémulsions ou de microémulsions de type eau/CO_2, CO_2/eau, liquide ionique/CO_2 a donc attiré une attention croissante dans la littérature scientifique. Cependant, les propriétés intrinsèques du CO_2 (viscosité faible, diffusivité élevée, densité faible) rendent la stabilisation de macroémulsions et miniémulsions particulièrement difficile en l'absence d'agitation ou de processus d'émulsification. En conséquence, les microémulsions, thermodynamiquement stables, sont du plus grand intérêt afin de réaliser des réactions organiques dans ces microréacteurs mais nécessitent des tensioactifs capables de réduire considérablement la tension interfaciale. Pour se faire, de nombreuses études ont porté sur le domaine des tensioactifs moléculaires et leur capacité à stabiliser des microémulsions eau/CO_2. Cette situation contraste avec leurs homologues polymères : dans ce domaine, la majorité des études s'est concentré sur la solubilité des homopolymères et des copolymères dans le CO_2. Ainsi, les études portant sur la stabilisation de (micro)émulsions par des copolymères amphiphiles restent rares dans la littérature. En particulier, les relations entre la structure des tensioactifs polymères, leurs propriétés de solubilité et leur activité interfaciale restent encore à explorer. Pour réaliser ce type d'études, l'émergence de puissantes techniques de polymérisation

pour générer des macromolécules bien définies a ouvert de nouvelles perspectives. Les technologies de désactivation réversible en polymérisation radicalaire et, en particulier, le processus d'addition-fragmentation réversible par transfert de chaîne (RAFT) sont, en effet, des outils très efficaces pour synthétiser des polymères présentant des caractéristiques macromoléculaires précises et établir des relations structure-propriétés. En s'appuyant sur l'utilisation de la technique RAFT, l'objectif de ce travail a été d'approfondir les connaissances sur les liens entre la structure des polymères et leurs solubilités dans le sc-CO_2, en préalable à la stabilisation d'émulsions dans le sc-CO_2.

Chapitre 1

Le chapitre 1 constitue une introduction bibliographique au sujet. Le CO_2 et les principales classes de polymères présentant une importante « CO_2-philie » sont présentés. Les facteurs qui régissent leur solubilité sont explicités pour chaque classe de polymères ainsi que les différentes stratégies qui ont été envisagées pour améliorer cette propriété. Ensuite, l'auto-assemblage de copolymères à blocs amphiphiles dans le sc-CO_2 et leurs applications en tant que stabilisants d'émulsions sont couverts.

Le diagramme de phase ci-dessous résume les principales solubilités de polymères CO_2-philes à 22 °C (voir figure I.1).

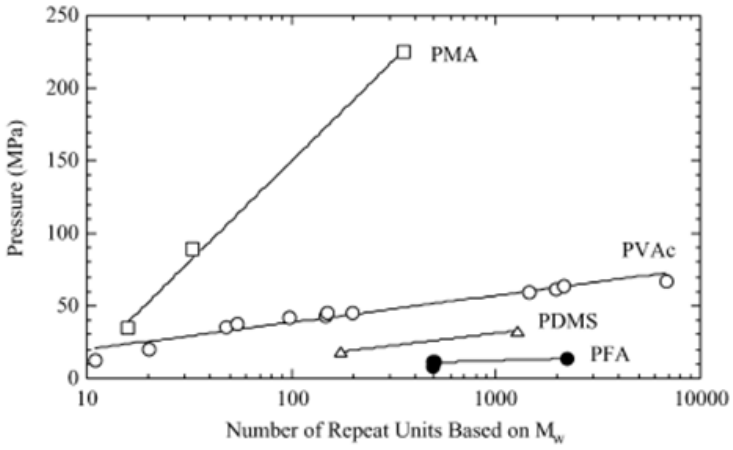

Figure I.1. Diagrammes de phase Pression-Nombre d'unités de répétition pour des fractions massiques en polymère de 5 % à 22 °C dans des mélanges binaires de CO_2 et de poly(acrylate de méthyle) (PMA), de poly(acétate de vinyle) (PVAc), de poly (diméthylsiloxane) (PDMS) ou de poly(acrylate) fluoré (PFA).

Quelques lignes directrices peuvent être tirées de la nature des polymères et de leur solubilité relative dans le sc-CO_2 : le facteur le plus important est, sans aucun doute, une faible densité d'énergie cohésive qui se matérialise par de faibles interactions polymère-polymère. Cela peut être illustré par les solubilités relatives du poly(acrylate) fluoré, du poly (diméthylsiloxane) et du poly(acétate de vinyle) et leurs valeurs de tension de surface, respectivement de l'ordre de 10-15, 16-20 et 36 $mN.m^{-1}$ (voir le tableau I.1). Bien que la tension de surface du poly(oxyde de propylène) soit inférieure à celle du poly(acétate de vinyle), la présence de sites de base de Lewis

multidentés dans le PVAc améliore considérablement la solubilité du PVAc dans le sc-CO_2. Ainsi, les interactions polymère-CO_2 peuvent être considérées comme un levier secondaire pour améliorer la CO_2-philie. D'après les valeurs respectives de T_g pour le PVAc et le PPO, ces interactions dominent l'entropie de mélange. L'entropie de mélange semble donc un paramètre mineur par rapport à ces deux facteurs enthalpiques que sont les interactions polymère-solvant et les interactions polymère-polymère. Cependant, il peut parfois jouer un rôle important, par exemple, lorsque l'on compare la solubilité du poly(acrylate de méthyle) et du poly (méthacrylate de méthyle).

Polymère	M_w ($g.mol^{-1}$)	Solubilité	Tension de surface ($mN.m^{-1}$)	T_g (°C)
Poly(acrylate) fluoré	254000	110 bar 25 °C	10-15	-
Poly(diméthylsiloxane)	273500	380 bar 62 °C	19-20	-100
Poly(acétate de vinyle)	182000	637 bar 25 °C	36	35
Poly(oxide de propylene)	2030	436 bar 30 °C	30-32	-60
Poly(acrylate de méthyle)	30700	2250 bar 25 °C	41	19
Poly(methacrylate de méthyle)	3000	Insoluble	41	105

Tableau I.1. Solubilité dans le CO_2 et principales proprieties physiques de quelques homopolymères.

Chapitre 2

Le chapitre 2 introduit les différentes techniques de polymérisation radicalaire par désactivation réversible (PRDR). Par la suite, la polymérisation RAFT/MADIX est appliquée à la synthèse de poly(acétate de vinyle) et à une étude complète et détaillée sur la solubilité de ces homopolymères et de copolymères à blocs amphiphiles incorporant un bloc hydrophile de poly(N,N-diméthylacrylamide) (PDMA) dans le CO_2 (voir Figure II.1). L'influence des caractéristiques macromoléculaires tels que la composition, la longueur de la chaîne ou le groupement terminal, est discutée à l'aide des résultats de solubilité obtenus par spectroscopie infrarouge.

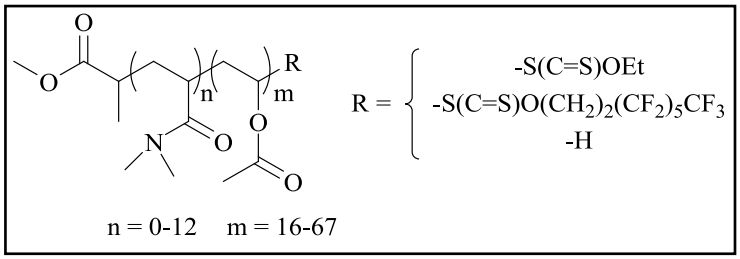

Figure II.1. Structure chimique générale des (co)polymères synthétisés pour cette étude.

La mesure de la solubilité du polymère repose généralement sur des observations visuelles répétées de transitions de mixtion/démixtion dans une cellule à volume variable. Ceci permet de déterminer les coordonnées du point de trouble pour un échantillon à une fraction massique donnée de polymère dans le CO_2, sur une large plage de températures. L'approche retenue repose sur l'utilisation d'une cellule isochore, afin de mesurer la solubilité des échantillons par rapport à la densité du CO_2. La spectroscopie infrarouge à haute pression offre ainsi une façon originale de déterminer la solubilité des polymères dans le sc-CO_2 en mesurant la croissance d'une bande de vibration caractéristique par application de pressions croissantes (voir Figure.II.2). En utilisant l'équation d'état du CO_2, la solubilité du polymère peut donc être représentée en fonction de la densité du CO_2.

Conformément à ces principes, la bande de vibration des esters à 1745 cm^{-1} a été choisie pour mesurer la solubilité des (co)polymères synthétisés dans cette étude (voir Figure II.2). Lorsque l'absorbance de la bande caractéristique à 1745 cm^{-1} a

atteint des valeurs hors du domaine linéaire de la loi de Beer-Lambert, les valeurs d'absorbance pour les échantillons ont été mesurées à 1765 cm^{-1}.

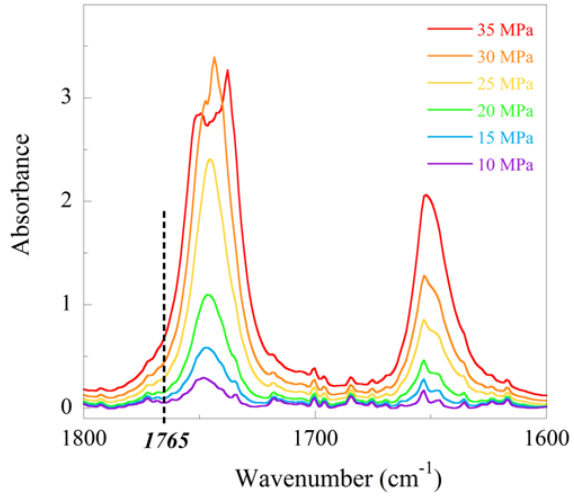

Figure II.2. Superposition de spectrogrammes infrarouges pour un copolymère à blocs PDMA$_{1k}$–*b*–PVAc$_{2.7k}$–Xa avec des pressions croissantes.

La solubilité des polymères de PVAc dans le CO_2 en fonction de leurs longueurs de chaîne a d'abord été déterminée, afin de constituer une plate-forme de comparaison pour le chapitre (voir Figure II.3). À une densité de 0,88 $g.cm^{-3}$ en CO_2 (soit 220 bar et 40 °C), une fraction massique de 1% de PVAc$_{1.8k}$-Xa a été entièrement solubilisée. Les PVAc possédant une longueur de chaîne plus importante se sont ensuite révélé beaucoup moins solubles : une fraction massique de 0,81 % de PVAc$_{3.8k}$-Xa a été solubilisée à 0,94 g cm^{-3} alors que seulement 0,38 % de PVAc$_{5.8k}$-Xa a été détectée à la même densité (voir Figure II.3).

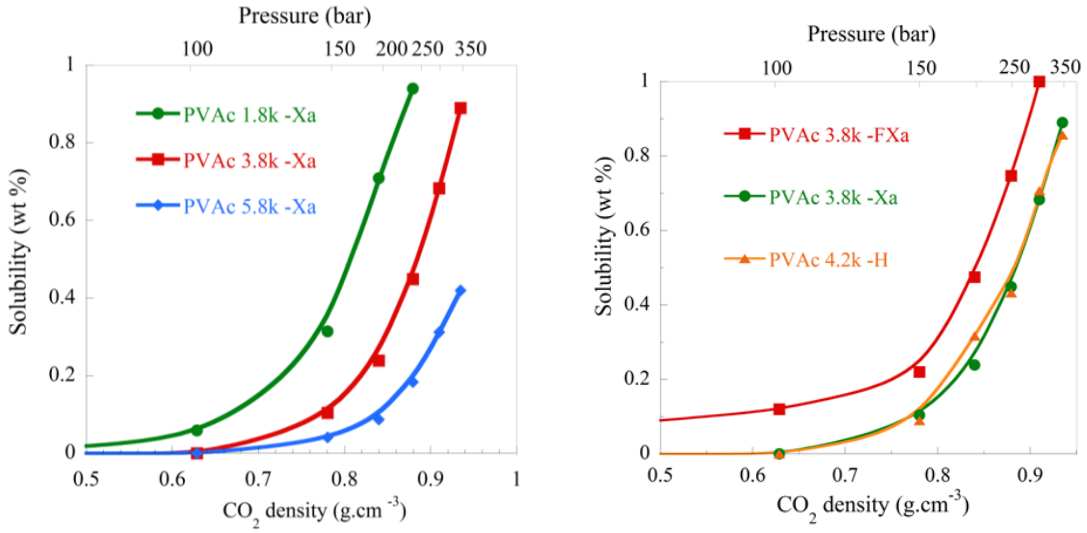

Figure II.2. Solubilités (% wt) dans le sc-CO_2 d'échantillons de PVAc de longueurs de chaîne croissantes (gauche) ou différant par la nature du groupement terminal.

La solubilité d'échantillons de poly(acétate de vinyle) possédant des masses moléculaires en nombre équivalentes (M_n = 4000 g.mol-1), mais différents groupements terminaux a été également évaluée. La comparaison de l'influence d'un groupement de type xanthate avec un polymère dont cette extrémité a été retirée n'a pas livré de différences substantielles quant à leur solubilité (voir Figure.II.2, droite). En outre, le groupement terminal de la chaîne polymère a pu être modifié en s'appuyant sur la synthèse d'un xanthate fluoré et son application dans la polymérisation RAFT/MADIX de l'acétate de vinyle. Comme attendu, l'intégration de cette dernière fonctionnalité a augmenté de manière significative la solubilité de l'échantillon $PVAc_{3.8k}$-FXa (voir Figure II.2, droite). En effet, une fraction massique de 1 % de cet échantillon s'est révélée soluble à 300 bar et 40 °C. Bien que cet échantillon soit moins CO_2-phile que $PVAc_{1.8k}$-Xa, ceci démontre clairement que les solubilités limitées des polymères PVAc dans le sc-CO_2 peuvent être contrebalancées par de telles stratégies de fonctionnalisation.

L'influence d'un bloc CO_2-phobique polymère sur la solubilité des copolymères amphiphiles n'avait jamais été examinée jusque-là dans la littérature. Pour clarifier ce point, la solubilité dans le sc-CO_2 de copolymères à blocs de PDMA-*b*-PVAc-Xa comprenant environ 20 % en poids de la PDMA a d'abord été étudiée. Comme dans le cas des homopolymères, trois longueurs de chaînes différentes ont été étudiées, de 2 à 6 kg.mol^{-1}. Alors qu'une fraction massique de 1% du copolymère

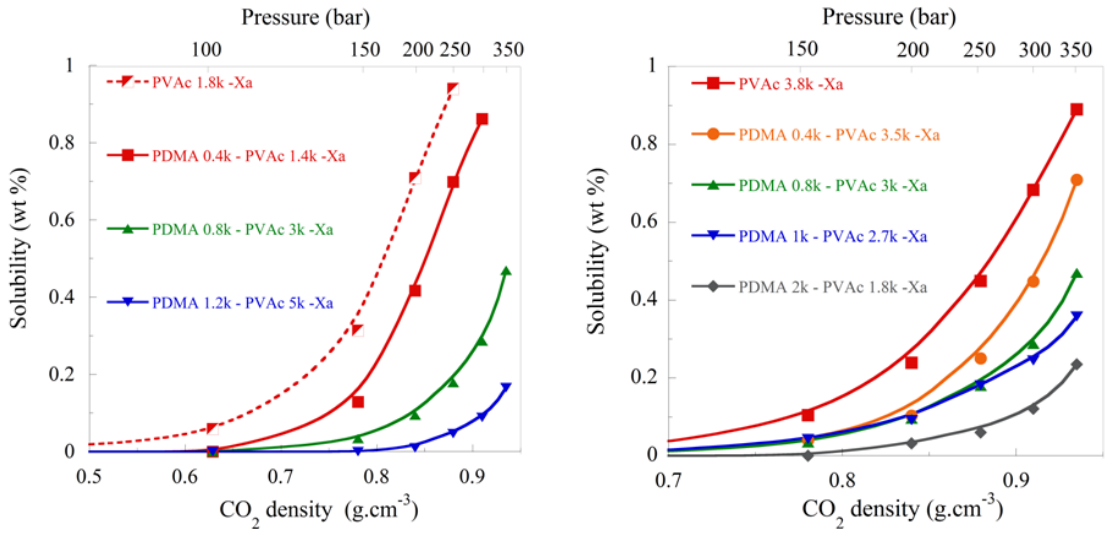

Figure.II.3. Solubilités (% wt) d'homopolymères de PVAc et de copolymères à blocs de PDMA-*b*-PVAc-Xa dans le sc-CO_2, à gauche, de compositions équivalentes et de longueurs de chaînes croissantes et, à droite, de compositions variables avec une longueur de chaîne équivalente.

de masse la plus faible (M_n = 2 k) a pu être solubilisé à 350 bar, la solubilité tombe à 0,47 % pour un copolymère de masse 4000 g.mol^{-1} (voir Figure.II.3, gauche). Le dibloc de masse molaire plus élevée (M_n = 6,4 k) ést, pour sa part, peu soluble (0,17 % à 350 bar). Considérant les échantillons avec des rapports massiques identiques en DMA/VAc, la longueur de la chaîne et la présence du bloc PDMA semblent donc avoir une influence majeure sur la solubilité dans le sc-CO_2. Ceci peut être expliqué par une simple augmentation de double "CO_2-phobie", due à la fois à l'augmentation de la longueur du bloc de PDMA et à la diminution de la CO_2-philie pour les plus longs blocs de PVAc.

Une comparaison avec leurs équivalents homopolymères de PVAc permet de mesurer l'effet du remplacement d'unités VAc par des unités DMA (voir la figure II.3). Les valeurs de solubilité ont été presque divisées par un facteur de 2 pour les deux copolymères PDMA-*b*-PVAc-Xa présentant des longueurs de chaîne plus importantes. Ces résultats sont logiques, compte tenu de la non-miscibilité du PDMA dans le sc-CO_2. De courtes longueurs des chaînes doivent donc être ciblées lors de la synthèse des copolymères amphiphiles de CO_2 basés sur des blocs de PVAc

L'effet de l'incorporation d'un bloc CO_2-phobe a été ensuite étudié sur des échantillons de masse molaire moyenne en nombre de 4 k. Quatre ratios différents de 10:90 à 50:50 ont été ciblés pour évaluer leur impact sur la solubilité des copolymères dans le sc-CO_2. La solubilité dans le sc-CO_2 a diminué avec l'augmentation du poids, ce qui a pu être quantifiée précisément (voir Figure II.3 droite).

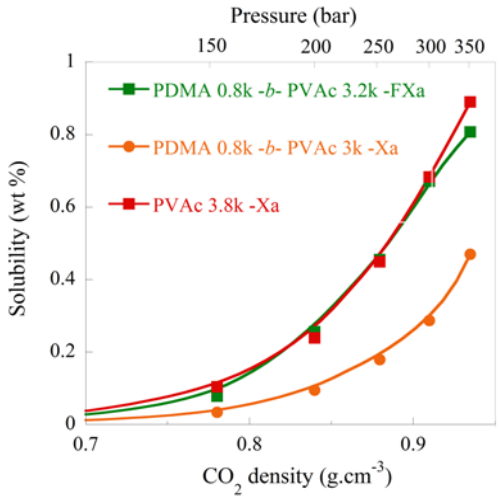

Figure.II.4. Solubilités (% wt) d'un homopolymère de $PVAc_{3.8k}$–Xa et de copolymères à blocs de $PDMA_{0.8k}$-b-$PVAc_{3k}$-Xa avec ou sans groupement terminal fluoré.

Une solubilité de 0,81% en masse a été observée dans le sc-CO_2 à 350 bar, alors que la fraction soluble de son homologue non-fluoré était seulement de 0,47% (voir la Figure.II.4). Sa solubilité est alors comparable à celle d'un homopolymère de $PVAc_{3.8k}$-Xa. Ce résultat confirme l'intérêt d'une telle approche dans la conception de tensioactifs polymères amphiphiles, afin d'améliorer simultanément leur CO_2-philie et leur caractère amphiphile.

Chapitre 3

Le chapitre 3 présente de nouvelles stratégies pour améliorer la solubilité des poly(ester de vinyle). L'approche retenue est basée sur la synthèse de copolymères statistiques de VAc et d'esters de vinyle fluorés. Une première partie du travail a été consacrée à décrire la (co)polymérisation de monomères vinyliques fluorés originaux par le procédé RAFT / MADIX (voir Schéma III.1). Leurs solubilités dans le CO_2 sont ensuite présentées et les facteurs régissant leur solubilité explicités par une méthodologie combinant calculs DFT et mesures expérimentales de tension de surface. L'utilisation de ces poly(esters de vinyle) fluorés dans la conception de polymères amphiphiles solubles constitue l'objet final de ce chapitre.

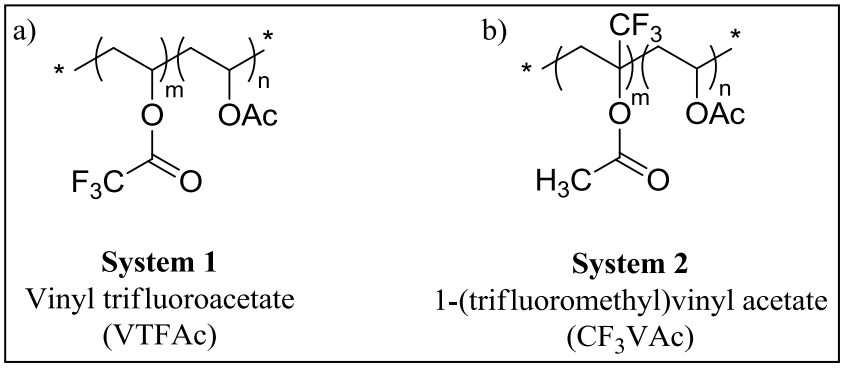

Schéma III.1. Structure chimique générale des (co)polymères statistiques synthétisés pour ce chapitre.

La solubilité de copolymères statistiques d'acétate de vinyle et de trifluoroacetate de vinyle (VTFAc) ayant une masse moléculaire en nombre d'environ 4000 $g.mol^{-1}$ a d'abord été étudiée par des mesures de points de trouble. En quelques mots, une fraction massique de 0,2% de polymère a été introduite dans une cellule à volume variable qui est alors remplie de CO_2. La transition isotherme correspondant à une séparation de phase (à 40 °C) a ensuite été observée visuellement. Le point de trouble d'un échantillon de référence de PVAc a pu être observé à 281 bar (voir Figure III.1 gauche). Avec l'incorporation progressive de 11, 27 et 50 mol % d'unités VTFAc dans les chaînes de polymères, les pressions de point de trouble ont considérablement chuté à, respectivement 245, 212, et 177 bar. Par la suite, les échantillons comportant des fractions plus élevées de VTFAc ont présenté un comportement de solubilité diffèrent: un point de trouble a pu effectivement être observé à 203 et 271 bar en coexistence avec une solide précipité.

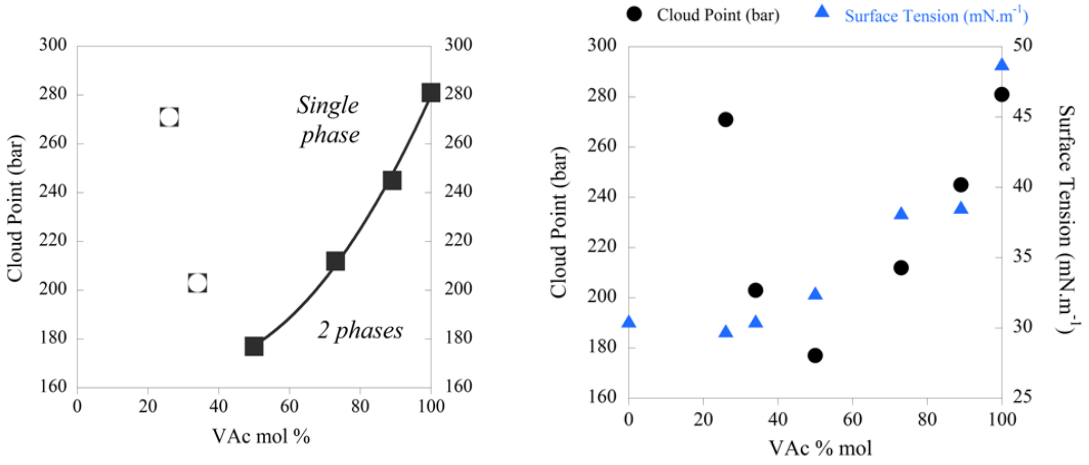

Figure III.1. Pressions de point de troubles de copolymères statistiques de poly(VAc-*stat*-VTFAc) (0,2 % en masse de polymère à 40 °C) en fonction du pourcentage d'acétate de vinyle dans le copolymère (gauche) (les symboles fermés indiquent un seul point de trouble alors ceux ouverts dénotent la coexistence d'un précipité) et tension de surface pour ces même copolymères (droite).

Afin de comprendre les tendances de solubilité observées, les contributions respectives des interactions polymère-solvant et polymère-polymère ont été évaluées. Les interactions polymère-solvant ont été calculées à l'aide de structures modèles, l'acétate d'éthyle, à savoir (EtAc) et trifluoroacétate d'éthyle (EtTFAc), qui sont représentatifs des principaux groupes fonctionnels du PVAc et du PVTFAc. Les géométries d'équilibre de ces structures de modèles et de leurs complexes avec une molécule de CO_2 ont été optimisées en utilisant des calculs basés sur la théorie de la densité fonctionnelle au niveau CAM-B3LYP en utilisant la base de Dunning aug-cc-pVDZ (voir Figure III.2).

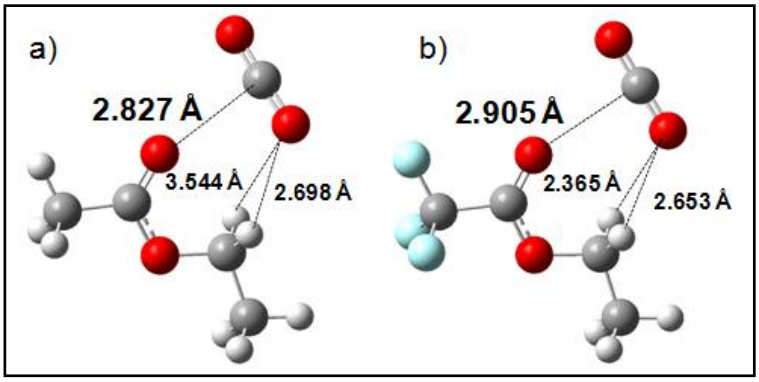

Figure III.2. Structures optimisées (CAM-B3LYP/aug-cc-pVDZ) pour le côté éthyle des complexes a) acétate d'éthyle-CO_2 et b) trifluoroacetate d'éthyle-CO_2.

Espèces moléculaires	ΔE_{cor} BSSE+ZPE (kcal.mol^{-1})	d(C•••O) (Å)	q_O (e)
EtAc-CO_2	-1.92	2.827	-0.75
EtTFAc-CO_2	-1.44	2.905	-0.67

Table III.6. Erreur de superposition des bases et énergie d'interaction corrigée au point zéro (ΔE_{cor}) – Distances intermoléculaires d(C•••O) et d(O•••H) pour les complexes acétate-CO_2 calculées au niveau CAM-B3LYP en utilisant la base aug-cc-pVDZ - Charge sur l'atome d'oxygène de la molécule d'acétate isolée (q_O).

D'après les résultats obtenus, le remplacement du groupe CH_3 par un substituant CF_3 dans la fonctionnalité acétate conduit à une diminution de la charge partielle négative sur le groupe carbonyle, ce qui, à son tour, conduit à une diminution de l'interaction entre le CO_2 et le groupe acétate. En conséquence, le comportement de solubilité des copolymères de P(VAc-*stat*-VTFAc) n'est pas régi par des interactions polymère-solvant.

Les interactions polymère-polymère ont été, ensuite, qualitativement estimées à partir des valeurs de tension de surface mesurées par des expériences de goutte sessile. Une solution de polymère à 10 % dans la 2-butanone est placée sur un substrat de verre et ensuite séchée par spin-coating pour créer un film mince de polymère. Une goutte d'eau est alors déposée sur la surface du polymère et les angles de contact sont mesurés à partir de la forme de la goutte. Les valeurs de tension superficielle à l'interface air / polymère peuvent alors être extrapolées à partir de l'équation empirique de l'état proposée par Li et Neumann pour une surface hydrophobe solide. Fait intéressant, ces valeurs de tension superficielle suivent la même tendance que les mesures de solubilité (voir Figure III.1 droite). Ceci semble donc clairement démontré le rôle prépondérant des interactions polymère-polymère dans la solubilité des copolymères de poly(VAc-*stat*-VTFAc) amorphes dans le sc-CO_2. Par conséquent, le comportement hybride observé avec un point de trouble et une fraction insoluble (voir Figure III.1 droite) peut aussi s'expliquer par la hausse des interactions polymère-polymère résultant de l'apparition de domaines cristallins.

Suite aux résultats précédents, l'incorporation d'unités VTFAc a donc conduit à l'abaissement des interactions polymère-polymère, mais, dans le même temps, à

une diminution des interactions polymère-CO_2. Il serait, par conséquent, d'un grand intérêt d'envisager un comonomère capable de diminuer les interactions polymère-polymère tout en préservant un niveau équivalent d'interactions polymère-solvant. À cet égard, une stratégie prometteuse pour combiner ces caractéristiques serait la mise en place de groupements trifluorométhyles sur la chaîne principale d'un poly(acétate de vinyle). En effet, la présence de ce groupe trifluorométhyle en position alpha du groupement acétate pourrait abaisser la tension superficielle des chaînes de polymères sans modifier de manière importante l'énergie des complexes acétate-CO_2 et à la stabilité chimique du polymère. Le monomère d'acétate de 1-(trifluorométhyle)-vinyle (CF_3VAc), qui semble réunir ces avantages, a donc été étudié suivant la méthodologie présentée pour le trifluoroacétate de vinyle.

La solubilité des copolymères statistiques d'acétate de vinyle et d'acétate de 1-(trifluorométhyl)-vinyle a d'abord été estimée par des mesures de points de troubles. Ces copolymères ont présenté deux phases de comportement distincts avec un minimum en point de trouble observé à 222 bar et correspondant à une composition 2:1 en VAc:CF_3VAc (voir Figure III.3). Les mesures de tension de surface ont révélé que cet optimum pouvait être corrélé à un minimum de tension de surface pour les différentes compositions étudiées. Au-delà de cette composition 2:1, la tension de surface est alors apparue constante et n'a pas pu expliquer l'augmentation des pressions de points de trouble.

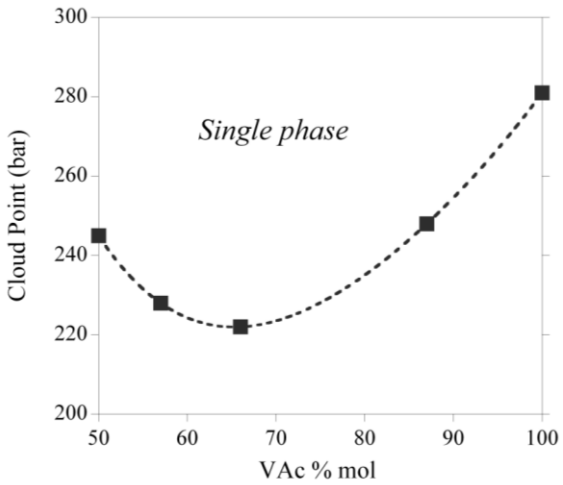

Figure III.3. Diagramme de phase de copolymères statistiques d'acétate de vinyle et d'acétate de 1-(trifluorométhyle)vinyle dans le CO_2 à 40 °C (fraction massique de 0,2 %).

Suivant la méthodologie présentée pour l'autre monomère fluoré, des calculs DFT ont été ensuite lancés pour explorer le rôle des interactions polymère-solvant. Contrairement au cas du trifluoroacetate de vinyle, la présence du groupement trifluorométhyle n'affecte que très peu la densité de charge sur l'oxygène du groupement carbonyle, principale site basique d'interactions de type Lewis dans la molécule. De même, les distances entre le carbone de la molécule de CO_2 et les oxygènes des molécules modèles sont équivalentes. Il en a donc été conclu que les interactions polymère-solvant ne pouvaient pas non plus expliquer les variations de point de trouble observées pour les copolymères riches en monomère fluoré. En s'appuyant sur les résultats expérimentaux sur la tension de surface et les interactions avec le CO_2, il a été retenu que la force motrice de ce comportement était l'entropie de mélange dont l'augmentation avec des fractions riches en monomère fluoré est caractérisée par l'augmentation des températures de transition vitreuse de 37 à 42 et 44 °C pour des fractions molaires de 33, 43 et 50 % en CF_3VAc.

Chapitre 4

Le dernier chapitre de cette thèse est consacrée à la synthèse de poly(oléfines fluorées) et à l'étude de leurs relations structure-solubilité par mesures de point de trouble et par spectroscopie infrarouge. Une étude détaillée sur l'ingénierie macromoléculaire du fluorure de vinylidène est tout d'abord présentée. Au cours de ce travail, il est démontré, pour la première fois, que la polymérisation radicalaire de ce monomère fluoré peut être contrôlée en polymérisation RAFT/MADIX, par l'intermédiaire d'un agent de type xanthate (voir Schéma IV.1).

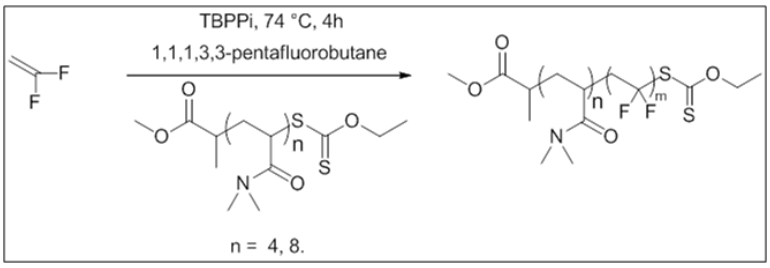

Schéma IV.1. Schéma réactionnel de la polymérisation RAFT/MADIX du fluorure de vinylidène.

De nombreuses techniques analytiques ont été utilisées pour cela, dont la chromatographie d'exclusion stérique (voir Figure IV.1), la RMN ^{19}F (voir Figure IV.2), la spectrométrie de masse MALDI-TOF (voir Figure IV.3) et la calorimétrie différentielle à balayage. La synthèse directe de copolymères à blocs avec un bloc hydrophile de type PDMA et un bloc de type poly(fluorure de vinylidène) a pu également être réalisée avec succès, ce qui constitue un avantage par rapport aux autres techniques de polymérisation radicalaire contrôlée qui nécessitent généralement des modifications post-polymérisation.

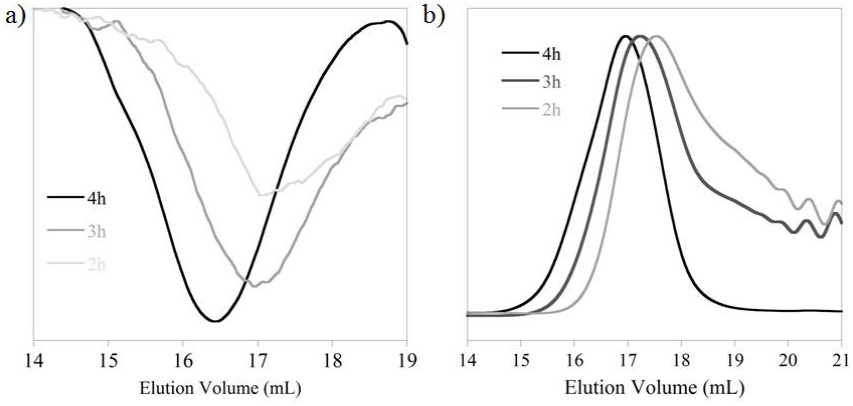

Figure IV.1. Superposition de chromatogrammes d'exclusion stérique de PVDF prélevés à différents temps, révélés par détections RI (gauche) et UV (droite).

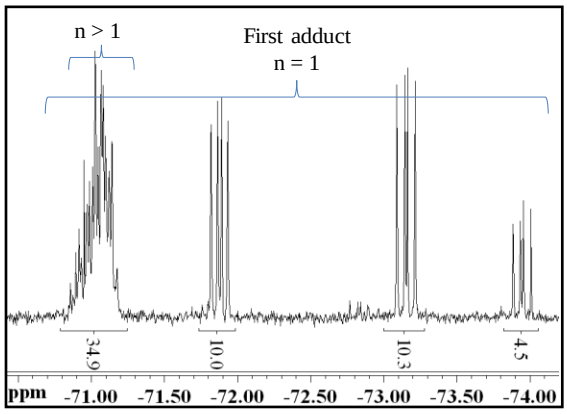

Figure IV.2. Agrandissement d'un spectre RMN ^{19}F d'un PVDF synthétisé par voie RAFT/MADIX. Le quadruplet de quadruplets est caractéristique d'une unité VDF insérée dans l'agent de transfert xanthate.

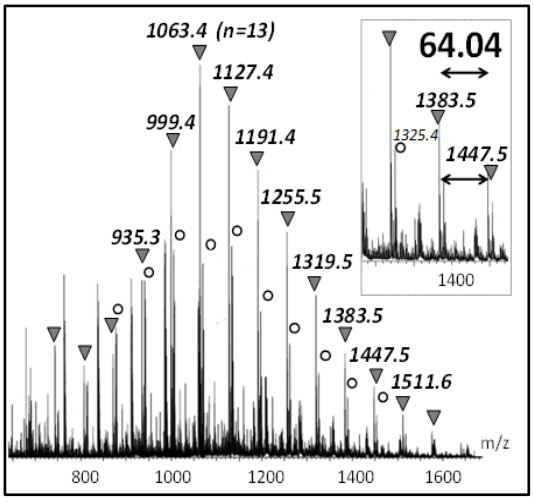

Figure IV.3. Spectre de masse MALDI-TOF d'un PVDF synthétisée par voie RAFT/MADIX. Les triangles indiquent la population principale faite d'unités de répétition VDF et des bouts de chaînes issus de la fragmentation du xanthate.

Toutefois, le caractère cristallin et les températures de fusion élevées du PVDF constituent un obstacle pour leur solubilité dans le dioxyde de carbone à des pressions inférieures à 350 bar. Afin de contourner ce problème, le fluorure de vinylidène a été copolymérisé en présence d'un monomère original, l'éther de perfluorométhyle de vinyle (PMVE) (voir Schéma IV.2).

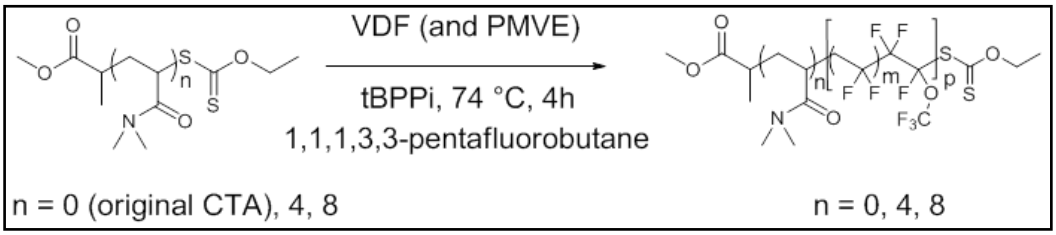

Schéma IV.2. Schéma réactionnel de la (co)polymérisation RAFT/MADIX du fluorure de vinylidène (VDF) avec le perfluorométhyle de vinyle (PMVE).

Par les mêmes moyens analytiques, il a pu être démontré un contrôle de la croissance des chaînes et des masses moléculaires finales (voir Figure IV.1).

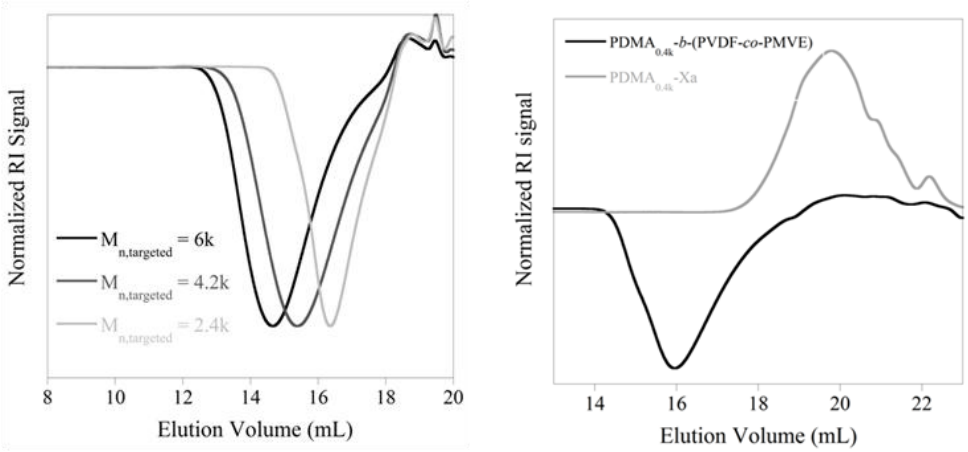

Figure IV.5. Superpositions de chromatogrammes d'exclusion stérique de copolymères statistiques P(VDF-*co*-PMVE) de longueurs de chaîne croissantes (gauche) et d'un copolymère amphiphile à blocs PDMA-*b*-P(VDF-*co*-PMVE) synthétisés par extension de chaînes d'un agent macromoléculaire RAFT/MADIX de PDMA (droite).

La solubilité des copolymères statistiques dans le dioxyde de carbone a d'abord été étudiée (voir Tableau IV.1). Les points de troubles de ces copolymères ont été observés à des pressions comparables à celles observées dans le cas de poly(perfluoropolyethers), plus connus sous le nom commercial de Krytox. Ces copolymères originaux constituent donc une nouvelle addition à la liste des copolymères CO_2-philes.

Echantillons	$M_{n,theo}$ ($g.mol^{-1}$)	$M_{n,CES}$ ($g.mol^{-1}$) [a]	Đ [a]	T_g (°C)	Point de trouble (bar) [b]	
					0.2 % wt	1 % wt
P(VDF-*co*-PMVE)$_{1.8K}$	1850	3700	1.26	-37	118 [c]	115
P(VDF-*co*-PMVE)$_{3k}$	3000	6000	1.58	-41	189	212
P(VDF-*co*-PMVE)$_{4.8K}$	4850	8900	1.63	-40	198	219

[a] Determiné par CES dans le THF. [b] Augmentation de turbidité à 40 °C. [c] Réalisé avec 0.5 % wt.

Tableau IV.1. Résultats expérimentaux portant sur la caractérisation des copolymères P(VDF-*co*-PMVE).

Leurs équivalents amphiphiles ont été ensuite évalués par mesures de point de trouble et spectroscopie infrarouge in-situ. Les quatre polymères synthétisés ont tous montré des pressions de trouble inférieures à 350 bar. Comme fait précédemment dans le chapitre 2, les effets de composition et de longueur de chaîne ont été confirmés par spectroscopie infrarouge. Ces études ont démontré l'existence d'un comportement ambivalent suivant la longueur des blocs et la composition.

Echantillons	$M_{n,theo}$ ($g.mol^{-1}$)	$M_{n,CES}$ ($g.mol^{-1}$) [a]	Đ [a]	T_g (°C)	PDMA /P(VDF-*co*-PVME) % wt	Point de trouble (bar) [b]
$PDMA_{0.4k}$-*b*-P(VDF-*co*-PMVE)$_{1.9k}$	2550	4800	1.55	-14	17	235
$PDMA_{0.4k}$-*b*-P(VDF-*co*-PMVE)$_{2.9k}$	3500	5900	1.74	-22	12	257
$PDMA_{0.8k}$-*b*-P(VDF-*co*-PMVE)$_{1.3k}$	2350	3200	1.62	14	37	347
$PDMA_{0.8k}$-*b*-P(VDF-*co*-PMVE)$_{3.3k}$	4300	7500	1.53	-4	19	295

[a] Determiné par CES dans le THF. [b] Augmentation de turbidité à 40 °C avec 1 % wt de copolymère.

Tableau IV.2. Résultats expérimentaux portant sur la caractérisation des copolymères amphiphiles à blocs de type PDMA-*b*-P(VDF-*co*-PMVE).

Conclusion

Cette thèse s'inscrit dans le cadre d'un projet visant à développer des tensioactifs macromoléculaires originaux pour le sc-CO_2. Afin d'identifier de nouveaux copolymères amphiphiles CO_2-philes, une large quantité de travail a été consacrée à développer l'outil qu'est la chimie des polymères. En particulier, des résultats encourageants ont été obtenus avec les monomères d'acétate de vinyle et de trifluoroacétate de vinyle, ce qui ouvre de nouvelles perspectives dans ce domaine. L'identification d'un monomère fluoré (de type ester vinylique) dont les polymères posséderaient une meilleure solubilité et de meilleures stabilités constitue une perspective à court terme de ce travail. Une meilleure compréhension de la polymérisation RAFT/MADIX du fluorure de vinylidène devrait également être envisagée afin d'étendre cette chimie à d'autres comonomères (oléfines fluorées ou esters de vinyle) et de nouveaux blocs hydrophiles.
À condition que les équipements nécessaires soient disponibles, l'auto-assemblage de ces copolymères amphiphiles et double-CO_2-phile devrait constituer également un vaste champ d'investigation. Enfin, les études consacrées à explorer l'activité interfaciale de ces copolymères amphiphiles constituent un prolongement naturel de ce travail. En particulier, la détermination de la tension superficielle à l'interface eau/CO_2 en présence de copolymères à blocs amphiphiles est une étape essentielle dans cette direction. L'identification d'un solvant à faible densité d'énergie cohésive et son utilisation comme solvant modèle pourrait être utile pour surmonter les difficultés liées aux mesures in situ. Une compréhension complète des relations entre la structure du polymère, les phénomènes d'auto-assemblage et la stabilisation d'émulsions pourrait être alors réalisée. L'extension de ces projets à d'autres solvants verts présentant différentes polarités et basicités devrait en outre contribuer à la généralisation de l'utilisation du CO_2 comme solvant vert pour la chimie organique et inorganique.

Etienne GIRARD

Macromolecular engineering of CO_2-philic (co)polymers through RAFT/MADIX polymerization

---

The work presented in this manuscript describes the development of original families of CO_2-philic (co)polymers in a context of an increasing promotion of green solvents such as supercritical carbon dioxide. In this respect, innovative amphiphilic block copolymers which may act as macromolecular surfactants for water/carbon dioxide emulsions are also studied.

This thesis encompasses the synthesis, the characterization and the property studies of such (co)polymers, with a particular emphasis on their solubility in supercritical CO_2. Building on RAFT/MADIX polymerization, the structure and the composition of these macromolecules were varied using vinyl acetate, fluorinated vinyl esters and fluorinated olefins as CO_2-philic monomers. The influence of macromolecular characteristics of CO_2-philic and amphiphilic copolymers including chain length, chain end group and CO_2-phobic/CO_2-philic balance on their solubility was then studied through infrared spectroscopy and cloud point measurements, in order to draw structure-property relationships.

Keywords:, RAFT/MADIX polymerization, Radical polymerization, , Fluoropolymers, Surfactants, Amphiphilic copolymers Supercritical carbon dioxide.

Etienne GIRARD

Ingénierie macromoléculaire de (co)polymères CO_2-philes par polymérisation RAFT/MADIX

Cette thèse s'inscrit dans le cadre de la recherche sur l'utilisation du dioxyde de carbone supercritique comme alternative aux solvants organiques usuels. Afin de proposer de nouveaux tensioactifs macromoléculaires stabilisants d'émulsions inverses eau/dioxyde de carbone, le travail s'est porté sur la recherche et l'étude de familles originales de (co)polymères CO_2-philes et de nouveaux copolymères à blocs amphiphiles

Les résultats présentés dans ce manuscrit de thèse incluent la synthèse, la caractérisation et les études des propriétés de ces (co)polymères, en particulier, leur solubilité dans le CO_2 supercritique. La structure et la composition de ces macromolécules ont été variées en s'appuyant sur la polymérisation RAFT/MADIX de monomères CO_2-philes tels que l'acétate de vinyle, les esters vinyliques fluorés et les oléfines fluorées. L'influence des paramètres macromoléculaires des copolymères CO_2-philes et amphiphiles sur leur solubilité, dont la longueur de chaîne, le groupe terminal et la balance hydrophile/CO_2-phile, a ensuite été étudiée par spectroscopie infrarouge et par des mesures de points de troubles, afin d'établir des relations structure-propriété.

Mots-clés : Polymérisation RAFT/MADIX, Polymérisation radicalaire, Fluoropolymères, Copolymères amphiphiles, Tensiaoctifs, Dioxyde de carbone supercritique.